ASPECTS OF A FINITE STRAIN CONSTITUTIVE MODEL FOR SEMICRYSTALLINE POLYMERS

Thesis submitted by
David William Holmes BE (Hons) JCU
in October 2007

for the degree of Doctor of Philosophy
in the School of Engineering
James Cook University

Statement of Access

I, the undersigned, author of this work, understand that James Cook University will make this thesis available for use within the University Library and, via the Australian Digital Theses network, for use elsewhere.

I understand that, as an unpublished work, a thesis has significant protection under the Copyright Act and;

I do not wish to place any further restriction on access to this work.

Signature

Date

Statement of Sources

I declare that this thesis is my own work and has not been submitted in any form for another degree or diploma at any university or other institution of tertiary education. Information derived from the published or unpublished work of others has been acknowledged in the text and a list of references is given.

Signature

Date

Electronic Copy

I, the undersigned, the author of this work, declare that the electronic copy of this thesis provided to the James Cook University Library is an accurate copy of the print thesis submitted, within the limits of the technology available.

Signature

Date

List of Publications

Throughout the progression of this research there have been several international conference presentations and international journal articles. The chapters of this thesis largely resemble these publications following the plan outline here.

Chapter 2 was presented in part at the Australian and Korean Rheology Conference, 2005 (AKRC05). The chapter has been published in largely unaltered form under the citation

> Holmes, D.W., Loughran, J.G., Suehrcke, H. (2007) Constitutive Model for Large Strain Deformation of Semicrystalline Polymers, *Mech. Time-Depend. Mater.*, **10**, 281-313, `http://dx.doi.org/10.1007/s11043-007-9023-8`.

Chapter 3 was presented at the World Congress on Computational Mechanics 2006 (WCCM VII). The chapter has been submitted for journal publication in largely unaltered form under the citation

> Holmes, D.W., Loughran, J.G. (submitted June 2007) Numerical Aspects Associated with the Implementation of a Finite Strain, Elasto-viscoelastic-viscoplastic Constitutive Theory in Principal Stretches, *Int. J. Numer. Meth. Engng.*

Chapter 4 has been submitted for journal publication in largely unaltered form under the citation

> Holmes, D.W., Loughran, J.G. (2007) Theoretical Aspects of the Testing of Elasto-viscoelastic-viscoplastic Materials, *Polym. Test.*, `http://dx.doi.org/10.1016/j.polymertesting.2007.10.002`.

Chapter 5 has been presented in part at Computational Techniques and Applications Conference 2006 (CTAC-06) and the accompanying paper has been accepted for publication in the conference proceedings under the citation

> Holmes, D.W., Loughran, J.G. (accepted March 2007) A Theory for the Isolation of the Complex Deformation Characteristics of Nonlinear Viscoelastic Materials, *ANZIAM J. (CTAC-06)*.

Statement on the Contribution of Others

I, the undersigned, declare that this thesis is my own work and acknowledge the support and contributions of the following organizations and people:

- Stipend support and research expenses were provided through an industry scholarship from Gough Plastics Pty Ltd.
- Additional research expenses were funded through the James Cook University's School of Engineering internal research allocation.
- A financial contribution toward travel expenses to the WCCM VII conference held in Los Angeles in 2006 was made by the James Cook University 'Graduate Research International Travel Awards'.
- My supervisory team of Prof. Jeffrey Loughran and Dr. Harry Suehrcke contributed towards the editorial aspects of the journal papers associated with this research (as per the indicated authorship above) and the subsequent editing of this thesis.

Signature

Date

Acknowledgements

I would like to take this opportunity to thank the many people that have made completion of this research possible.

Firstly to my principal supervisor Prof. Jeffrey Loughran, without whose initial belief, continued support and guidance, none of this would have been possible.

To my other supervisor Dr. Harry Suehrcke for sharing his wealth of practical knowledge and for the helpful input with writing.

To the administrative staff in the School of Engineering for their assistance and good humor throughout the day to day workings of university life.

To ICO Courtenay for supply of materials testing samples and to Peter Lyngcoln, Stuart Petersen and Dr. Paul Britton for assistance with preliminary experimental testing.

To my friends whose good humor and support helped maintain my sanity throughout the years of study.

And finally and most significantly to my partner Sarah Butterworth for here love, support and seemingly endless tolerance of the long nights spent writing and to our families, who made us the people we are today and continue to inspire us to learn and grow.

I thank you all

Abstract

In this thesis, the development of a constitutive model for the finite strain deformation of semicrystalline polymers is presented. It reports on the formulation and numerical implementation of the model and the theoretical aspects of the associated experimental testing and parameter estimation.

Within both academia and industry to date, there exists no single constitutive model for semicrystalline polymers that is broadly accepted as representing the general case. This is in spite of the relatively complete scientific understanding of the material's response and the increasing use of such materials where structural loading can be significant. Numerical representation of such materials conventionally involves over-simplification of response, largely necessitated by the limitations of current experimental testing methods. A complex constitutive theory is only as powerful as the experimental method from which its parameters are fit. As such, the objective of this research was to develop a complete, generalized constitutive theory for semicrystalline polymers with a corresponding testing methodology that enables its practical use within industry.

The constitutive model selected can be characterized by a parallel combination of elastic, viscoelastic and viscoplastic model elements which most closely represents the complete deformation behavior of semicrystalline polymers in the pre-necking region ($\varepsilon < 15\%$). The accompanying mathematics are formulated for 3D, finite strain and are based on thermodynamic dissipation in keeping with conventional continuum mechanics methodology. Strain hardening has been found to be of importance within the viscoplastic element. The parallel configuration of the three model elements facilitates the decoupled algorithmic treatment of each response. This has been carried out in principal space, given the assumption of isotropy, making practical both its numerical implementation and the physical determination of model parameters. A strategy analogous to classical return mapping is used for

solution of the viscoelastic evolution while a new, principal space, closest point projection return mapping algorithm has been developed for solution of the viscoplastic evolution, accounting for isotropic strain hardening. The consistent algorithmic tangential modulus is formulated to ensure quadratic convergence of the whole implicit finite element procedure.

The computational model has been verified through a series of simple finite element tests involving combinations of large strain normal and shear loadings, and large rigid body rotations. Several example problems have been solved as demonstration of the models versatility.

Using the developed model, a study using numerical simulations of uniaxial and biaxial tensile testing methods has been carried out. Through this study it has been possible to develop an experimental methodology to isolate the component stress contributions from each of the three deforming modes as well as subset separation of viscous, yield, and isotropic hardening stresses for viscoplasticity. Via conventional optimisation procedures and an additionally developed iterative procedure for the viscoelastic response, this testing methodology makes possible the full specification of the model parameter set. Verification of the testing methodology was done via comparison between the calculated test curves, and values output directly from the numerical simulations.

The model proposed in this thesis corresponds to a general account of semicrystalline polymer constitutive response, possessing capabilities not accounted for previously in theories within the literature. Perhaps the most significant outcome from this work is the experimental data processing methodology that allows such a complex model to be accurately and practically fit to real materials. Being able to better predict the loaded response of semicrystalline polymers is critical for their continued and increased use in circumstances where structural loads are possible.

Contents

List of Tables

List of Figures

Chapter 1

Introduction

1.1 Motivation

Semicrystalline polymers are used widely in everyday life. Their ease of moulding and ability to be recycled makes them a particularly attractive material for use in a multitude of different applications, including in more recent years, where high or structural loading is expected during service. When high loads and/or elevated temperatures are involved it becomes increasingly important to be able to predict the loaded response of a material so as to allow confidence in service life and informed design choice.

Empirical techniques are commonly used in industry when designing and manufacturing with semicrystalline polymers. Data from material suppliers such as Young's modulus and maximum elongation are used as benchmark values however the complex and time-dependent nature of the material means that such an overly simplified representation is commonly accompanied by an ad-hoc over-specification of material to increase confidence in the design. This is obviously undesirable from both an environmental and a business perspective.

Numerical modeling is widely used in both industry and academia to address such inadequacies with empirical methods. For semicrystalline polymers, however, to date there exists no single constitutive model that has been broadly accepted as representing the general case. Some models used in academia have possessed the correct response characteristics however have been limited to one-dimensional representation and so prove impractical for industrial application. Three-dimensional models have been used in industry however due

to the limitations of current testing methodology, so far it has only been possible to experimentally fit simplified models that approximate the desired response within a limited range of loading. An evident parallel can thus be drawn between the limitations of such a methodology and those of the aforementioned empirical methods.

There is a clear and present need for a constitutive theory that bridges this gap; correctly representing the material response and being industrially practical with respect to three-dimensional parameter estimation. The development of such a theory has been the broad aim of this research.

1.2 Objectives

While the definition of a constitutive theory generally applicable to semicrystalline polymers has so far proven illusive, significant efforts towards such a development have been documented over many years by many authors. Throughout such research, on both the microscopic and macroscopic scales, a fairly good understanding of the deformation behavior of semicrystalline polymers has been developed. In this work we will focus predominantly on the theoretical development of a suitable constitutive theory sighting the comprehensiveness of the previous research on the actual material deformation characteristics and the inadequacies of the correspondingly proposed models, as justification.

In developing a generalized constitutive theory for application to semicrystalline polymers, this thesis has three primary objectives:

1. To develop a criteria for a suitable constitutive model based on a survey of the literature and correspondingly propose a suitable new constitutive model for large strain, three-dimensional representation of semicrystalline polymers.

2. To numerically implement this model for use with a commercial finite element code.

3. To establish a three-dimensional testing procedure and data manipulation methodology that enables the generation of the full model parameter set. It is particularly important that this methodology utilize practical testing procedures that are commonly available to industry (i.e. via access to university or commercial polymer testing laboratories).

By achieving these objectives a constitutive theory can be developed that is both accurate and practical for industrial purposes.

1.3 Outline

In Chapter 2, through review of the literature and subsequent preliminary testing, a suitable constitutive model is formulated for representation of the finite strain, three-dimensional response of semicrystalline polymers. Subsequently in Chapter 3, the model is numerically implemented and preliminary numerical tests are presented to demonstrate the models performance and versatility. In Chapter 4, this numerical model is used to develop a comprehensive testing and data manipulation procedure to enable the isolation of component stress contributions from each of the relevant deformation modes, known to be of significance. In Chapter 5, a subsequent methodology is presented that uses these results to generate the model parameters through optimization techniques. Finally, conclusions are presented in Chapter 6.

Chapter 2

Constitutive Model Formulation

As will be reviewed in the sections to follow, many different types of constitutive models have been proposed for application to semicrystalline polymers with varying degrees of accuracy over a variety of different loading circumstances. To date, however, there is still no one model that is generally accepted to perform satisfactorily over a practical range of loading circumstances. This is mainly due to the complexity of the material's response to loading. As will be shown, semicrystalline polymer response comprises certain degrees of time variant and invariant response and it is the accurate account of these that has been the aim of the majority of previously proposed constitutive models. It could be argued that for the general case, this goal is yet to be achieved.

In this chapter, a review of literature associated with the development of a constitutive model for semicrystalline polymers is presented. The primary aim of this review is to establish the requirements of a generally applicable model for such materials. This review is then used as justification for the subsequent selection of a continuum mechanics model that has not previously been suggested for semicrystalline polymers. This model is theoretically compared with experimental testing on semicrystalline polymers from the literature as means of validation.

2.1 Background

In continuum mechanics there are various forms of constitutive theories that can be used for representation of the deformation behavior of materials. Perić and Owen (1998) outline

two major model types as micromechanical models and phenomenological models. Micromechanical models predict material response by simulating interactions on a molecular level. Phenomenological theories rely on macroscopic observations of representative volumes of material. Perić and Owen make note that the most powerful phenomenological theories should still take into account the *"... underlying microscopic dissipation mechanisms"* (Perić and Owen (1998): 1507). One of the most common types of phenomenological theories involves using a rheological model as the framework for a constitutive theory. Such models will be the main focus of this thesis.

Rheological models are an effective tool for understanding and representing the mechanical properties of a material. By combining simple elements such as springs and dashpots, a complicated material response to loading can be represented by a combination of easily visualized simple responses. In this form a rheological model constitutes a constitutive theory. In deformation analysis, rheological constitutive theories are widely used for two main purposes. The first of these is as a conceptual aid to help visualize the way in which a material behaves during deformation. An example of this would be to visualize the behavior of a spring when trying to understand elastic material behavior. The second is as a quantitative tool for use in predicting the loaded response of a material either manually or numerically in the form of a finite element simulation. The second of these is more pertinent to our endeavor.

When used in the form of a quantitative constitutive theory, rheological models provide the framework to which controlling constitutive mathematics are applied. Such mathematics can be either derived from the linear component expressions, such as Hooke's laws in the case of a spring, or from analogous but more complicated nonlinear theories. Such nonlinear theories can take direction from micromechanical dissipation (Perić and Owen (1998)). Where the linear constitutive expressions allow simplicity of formulation and implementation, the nonlinear theories allow for, in many cases, a more realistic representation of loaded responses where complicated load and rate dependencies are involved. The constitutive mathematics dictate the relationships between stress and strain as well as other parameters including strain-rate, time, temperature and material variables for each rheological component.

The configuration of a rheological model governs the interrelationships between each element. Different positioning of springs, dashpots, etc. in a rheological model can result in

very different model responses to deformation. The presence and timing of required forms of deformation can be controlled by the suitable selection of model configuration. It is equally important to have both a well constructed rheological framework and plausible constitutive mathematics. Choosing the correct rheological configuration accompanied by constitutive mathematics that adequately account for any required dependencies can result in a very powerful constitutive theory as will become evident.

2.2 Review of literature

The volume of published research on the constitutive behavior of semicrystalline polymers is extensive. Consequently, the review that follows reports on a representative cross-section of the constitutive models proposed in such works, on which to base conclusions about the requirements of a generally applicable model for semicrystalline polymers. This literature survey allows informed specification of the most appropriate model for such materials.

2.2.1 Direction from micromechanics

The molecular deformation mechanisms treated by micromechanical constitutive theories are generally measured explicitly during observation on molecular interactions using techniques like X-ray scattering (G'Sell et al. (1997)). Such testing is significantly more definitive in regards to recognition of the actual modes of deformation present (elasticity, viscoelasticity, etc) than the global stress-deformation measurement techniques used in macroscopic research. Correspondingly, while not the primary focus of this investigation, a brief review of micromechanics would seem beneficial.

Some of the most comprehensive work on semicrystalline polymer micromechanical modeling can be attributed to Drozdov and co workers (see for example Drozdov and Christiansen (2003) for polypropylene and Drozdov and Yuan (2003) for low density polyethylene). Like some of Drozdov's similar work with amorphous polymers (Drozdov (2001); Drozdov and Kalamkarov (1996)), this work reports on an elasto-viscoelastic-viscoplastic constitutive model that functions by mimicking molecular chain interactions to predict small strain deformation. In the small strain region, fair agreement between model prediction and experimental observation is reported.

A significant component of the research necessary to develop these types of models

is associated with the determination of the actual micromechanical mechanisms occurring during deformation. It is pertinent here to discuss some of the conclusions drawn about such mechanisms.

It is firstly important to note that semicrystalline polymers are characterized by a morphology of crystalline regions of ordered lamellae, surrounded by amorphous regions of unordered molecular chains. The amorphous regions in close proximity to, or between crystalline lamellae are noted to have greatly reduced mobility and are often regarded as a third region (Brusselle-Dupend et al. (2001); Drozdov et al. (2004); Drozdov and Christiansen (2003)). It is the interactions and behavior of these structures that account for the complex deformation behavior of semicrystalline polymers.

It is widely accepted that on the molecular level, deformation of the semicrystalline structure results from a combination of elastic, viscoelastic and viscoplastic modes (see for example Drozdov and Christiansen (2003, 2004); Drozdov and Yuan (2003)). Elasticity is associated with the stretching of molecular chains within the amorphous phase (Brusselle-Dupend et al. (2001); G'Sell et al. (1997)). A mechanism that can be compared to the behavior of purely hyperelastic materials such as rubbers and elastomers (Ogden (1984)). Drozdov and co workers (Drozdov et al. (2004); Drozdov and Christiansen (2003, 2004); Drozdov and Kalamkarov (1996)) conclude that viscoelastic response is the result of molecular chain rearrangement within the amorphous phase; primarily, the separation of chains from lamellae junctions and connection of free chains with new junctions. Thermal activation is thought responsible for these rearrangements where an increase in a molecular chain's energy enables its jump to a higher state (Drozdov et al. (2004)). The concept of viscoelastic recovery is then viewed as the progressive return of the molecular chains to their original state upon the removal of energy from the system (i.e. unloading). Viscoplastic deformation has been observed by Schrauwen et al. (2004) and also Drozdov and Christiansen (2004) to initiate in the amorphous region via inter-chain slippage[1]. At higher strains, this transitions into the crystalline phase where fine, and then coarse, lamellae sliding occurs with eventual fragmentation of the crystallites.

An explicit yield threshold is commonly observed at small strain levels far before necking (for example $\varepsilon = 2\%$ see Drozdov and Christiansen (2003)). Schrauwen et al. (2004) have

[1]Providing temperature is below the glass transition temperature such that the amorphous phase is in *glassy* state.

also observed additional yielding phenomena for strains in excess of necking (up to 200% strain). The actual mechanisms of yield are noted by Drozdov and Christiansen (2003) to be the source of some conjecture. In a general sense, the yield threshold can be related to the thermodynamic energy level necessary to induce slippage of chain-chain bonds which are most localized in the crystalline phase (see Schrauwen et al. (2004)). Strain hardening is also commonly observed. G'Sell et al. (1997) explains such phenomena to be primarily the result of lamellae fragmentation that corresponds to an increase in the restricted amorphous phase. This phase reinforces the remaining lamellae fragments and so limits further viscoplasticity. The chain density in the amorphous phase, before and after deformation, plays a key role in this phenomena (Schrauwen et al. (2004)).

For the case at hand, an unfortunate downfall of micromechanical constitutive theories arises because semicrystalline polymers have anisotropic microstructures (Drozdov et al. (2004)), while generally exhibiting isotropic deformation response on the macroscopic scale (given ideal moulding conditions). Correspondingly, extension of such theories to macroscopic applications becomes problematic and, in such cases, micromechanical models are commonly observed to perform poorly (Drozdov and Christiansen (2003); Drozdov and Yuan (2003)). This type of scaling discontinuity and the numerical cost due to the complexities associated with implementation on a practical scale, mean micromechanical models are inappropriate for the purposes of this work. The limitations of micromechanical models, however, in no way detract from the significance of actual molecular level deformation measurement. A fully general macroscopic model should account for all the deformation mechanisms observed within the microstructure, as summarized in this section.

2.2.2 Macroscopic constitutive theories

The review that follows is concerned mainly with large strain constitutive models for semicrystalline polymers. Based on the conclusions from the preceding section, our attention will be limited to models that account for some amount of elastic, viscous and plastic deformation.

Findley et al. (1976), while largely concerned with nonlinear viscoelastic integral theories, presents a simple elasto-viscoelastic-viscoplastic rheological model termed the Burgers model (Figure 2.1 (a)). While the linear Burgers model can reproduce the trends of some polymer experimental curves, it has been discounted mainly due to the fact that polymer

viscous and plastic responses are known to be nonlinear for almost all cases other than very small strain. The work of Findley et al. (1976) recognized the need to improve on the accuracy of such linear rheological models. As will be seen in what follows, more recent developments in solid mechanics have allowed the use of nonlinear constitutive relationships within rheological model frameworks, however, an additional limitation of the Burgers model is its lack of expression for an actual yield threshold such that irrecoverable deformation is present at all stages of loading.

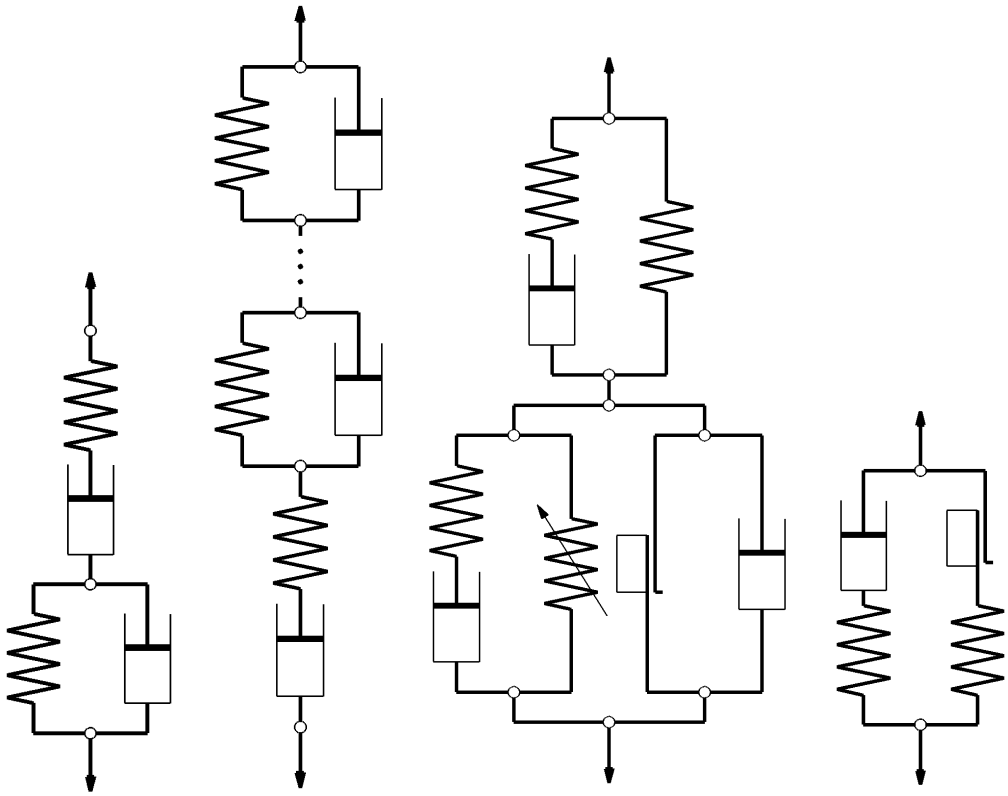

Figure 2.1: One-dimensional elasto-viscoelastic-viscoplastic rheological models used for semicrystalline polymers by (a) Findley et al. (1976), (b) Schapery (1997), (c) Brusselle-Dupend et al. (2001, 2003) and (d) Kletschkowski et al. (2004).

G'Sell and Jonas (1981), Kitagawa and co-workers (Kitagawa and Matsutani (1988); Kitagawa et al. (1989); Kitagawa and Takagi (1990)) and Schang et al. (1996) all made contributions toward validating an elasto-viscoelastic-plastic model for application to a wide range of semicrystalline polymers including polyethylene, polypropylene and polyamide 12. The model used was derived from the governing constitutive equation for a three element

viscoelastic rheological model, adding components to the expression to incorporate nonlinearity and plasticity. The addition of nonlinearity and plasticity was done mathematically and so the end model was no longer analogous to any rheological configuration. Whilst the authors of the above papers note their theory to be elasto-viscoelastic-plastic, the overall response is represented via a single governing constitutive equation. The fit of this theory to experimental data would thus account for the required components of elastic, viscous and plastic deformation automatically without explicit definition of each actual mode of deformation. This can prove to be a weakness with single expression theories derived directly from curve fitting because extrapolation outside the ranges of testing can diverge very rapidly from a reasonable prediction. This can be attributed to the nature of polynomial type fitting. In spite of this weakness, the model was tested over a variety of different loading cases and was shown to reproduce the experimental results well for all tested cases of positive strain, well into the necking region. The model was shown in all cases, however, to be inaccurate during unloading.

Lai and Bakker (1995) propose an elasto-viscoelastic-plastic integral form constitutive theory for high density polyethylene. Total strain is additively decomposed into viscoelastic and plastic components and the constitutive theory is fulfilled using data from creep and recovery tests. The theory is shown to be accurate for simulation of various creep, recovery and constant stress rate loading and unloading. Again the models performance is largely based on curve fitting while having little to do with actual molecular behavior of the material.

Schapery (1997, 1999) proposes a nonlinear elasto-viscoelastic-viscoplastic constitutive model derived from thermodynamics. While these papers are largely theoretical the first is written with the aim of representing fibre reinforced and un-reinforced plastics while the second is more generally noted to apply to several materials including semicrystalline polymers. Schapery's model is based on the theoretical rheological framework shown in Figure 2.1 (b). This model is similar to the Burgers model shown in Figure 2.1 (a) however it makes provision for any number of viscoelastic components as may be required and accounts for all constitutive relationships in a nonlinear fashion. These component constitutive relations are based on thermodynamics rather than linear rheology. Schapery discusses theories to incorporate various additional nonlinearities, as well as other possible viscoplastic theories that may also incorporate yield.

Zhang and Moore (1997a,b) report on the elasto-viscoelastic-viscoplastic behavior of high density polyethylene pipes across constant strain rate, transient strain rate, single and cyclic loading-unloading, creep, relaxation and combination tests. They then propose a nonlinear elasto-viscoelastic model derived from nonlinear rheology and an elasto-viscoplastic model derived from works by Bodner and Partom (1972, 1975) on steel, to represent observations. Both are uniaxial theories and the elasto-viscoplastic model assumes viscoplastic deformation to occur at all times and thus no yield expression is required. The two theories were compared against experimental results. It was observed that the elasto-viscoplastic theory was the superior of the two, closely predicting the majority of results seen experimentally. The nonlinear viscoelastic model was shown to be weak in predicting rapid changes in applied strain or strain rate while the only weakness with the elasto-viscoplastic model was its inability to predict strain reversal. While it would seem each of the tested models have certain advantages, it could be concluded that a more generally applicable model would incorporate both components of viscoelasticity and viscoplasticity. Other limitations with the models include the uniaxial restriction and the lack of expression for actual yield threshold or hardening in the elasto-viscoplastic model.

One of the more comprehensive testing procedures and constitutive models for semicrystalline polymers to date, was published in two parts by Brusselle-Dupend et al. (2001, 2003). They propose a uniaxial testing regime for polypropylene in the pre-necking region, designed to isolate the elastic, viscoelastic and viscoplastic components of deformation. Preliminary tests showed this pre-necking region to be within 11% strain for polypropylene. The authors proceed to use the test data to validate an elasto-viscoelastic-viscoplastic constitutive model based on the rheological framework shown in Figure 2.1 (c). The proposed model contains a viscoelastic component in series with a viscoplastic component. During testing the authors observe both kinematic and isotropic hardening and account for this in the rheological framework of the viscoplastic element. During tests at low strain, Brusselle-Dupend et al. also report a transitional zone between purely elasto-viscoelastic response and elasto-viscoelastic-viscoplastic response to occur at approximately 1.5 ± 0.3 % strain. Thus the material was seen to have a definite viscoplastic yield point which was also accounted for in the model.

The viscosity of semicrystalline polymers (dash pot coefficients, Figure 2.1 (c)) have been shown by Eyring (1936) and later Halsey et al. (1945) to evolve with varying inelastic strain

rate (the Eyring model). Brusselle-Dupend et al. (2001, 2003) found in experimentation that Eyring's expression of viscosity inadequately accounted for the viscosity of both the viscoelastic and viscoplastic responses of polypropylene. As such, new expressions were formulated with added dependencies on total strain rate. The new viscosity expressions were shown by comparison to be highly superior to the polymer viscosity models used previously.

Constitutive model validation for the Brusselle-Dupend model was carried out by comparison with experimental data and it was shown that the simulations closely reproduced the expected results for multiple cases of loading including combinations of loading, unloading, relaxation and recovery for several cases of strain rate. The work of Brusselle-Dupend and co-workers makes one of the most comprehensive attempts at accounting for the many mechanisms of semicrystalline polymers during deformation. While their model proved accurate across all cases published, there are still some important limitations. The rheological configuration is relatively complex especially the representation of strain hardening. The formulation of the model is largely phenomenological and, while accurate in application, it takes no direction from actual thermodynamics of the material continuum. Finally one of the more major limitations is that the theory is formulated for uniaxial application and would require significant work to extend the theory to account for three-dimensions.

Recently Kletschkowski et al. (2004) presented a simple rheological constitutive model to represent the response of semicrystalline polytetrafluorethylene, (Figure 2.1 (d)). From the configuration of the rheological model, it can be seen to sequentially account for viscoelasticity, then viscoplasticity within the same viscous element, the transition being governed by the state of yield. Throughout validation with experimental testing, Kletschkowski demonstrates a reasonable correlation between model predictions and the results for polytetrafluorethylene. While demonstrating some correct predictions, it could be concluded that for many cases this type of model is oversimplified. It has been indicated in many of the works reviewed above that viscoelastic and viscoplastic deformation is know to occur simultaneously, however Kletschkowski's model accounts for these modes sequentially and so can be deemed to be questionable for the general case.

Perić and Dettmer (2003) presented a finite strain constitutive theory generally applicable to most types of materials. Their model encompasses any combination of elastic,

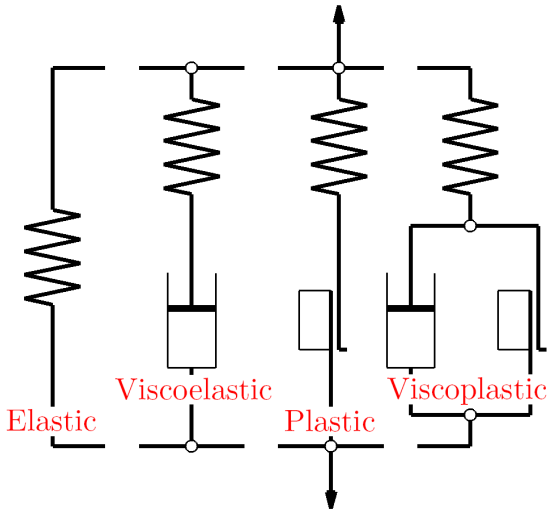

Figure 2.2: Generalized one-dimensional rheological representation of the elasto-viscoelastic-plastic-viscoplastic Perić and Dettmer (2003) model.

viscoelastic, elasto-plastic or viscoplastic response. Simultaneous account of these deformation modes is made possible by the parallel rheological framework on which the model is based. The generalized one-dimensional rheological representation is shown in Figure 2.2. The accompanying constitutive mathematics are derived from thermodynamics, allowing for both plastic and viscoplastic yield. Isotropic hardening is briefly discussed and it would be possible to extend the theory to account for kinematic hardening, following related work such as that of Simo and Hughes (2000). The technique of using continuum mechanics theories implemented over a rheological framework has found wide prior application in specific forms for large strain deformation of inelastic materials (mainly rubbers and steels) as in works by Simo (1987, 1992), Simo and Hughes (1987, 2000), Perić and Owen (1992, 1998), Reese and Govindjee (1998a) and Rosati and Valoroso (2004). Perić and Dettmer show that in a very general sense a model of this type can be widely generalized via the parallel combination of all the different types of possible elements (elastic, viscoelastic, viscoplastic and elasto-plastic). Perić and Dettmer demonstrate the model's versatility by presenting numerical simulations completed using elasto-viscoelastic and elasto-viscoelastic-plastic forms of the model, each sited as representing the response of various types of rubber[2].

The works of Nedjar (2002a,b) deal with the formulation and numerical implementation of two large strain continuum mechanics type theories for application to filled rubbers,

[2]Note, constant viscosity coefficients are used in these studies.

polymers and polymeric foams. The two different formulations are presented together and compared. The first model is based on a parallel combination of viscoelastic and viscoplastic rheological elements identical to a reduced form of the Perić and Dettmer model, Figure 2.2. The second model is based on a series rheological addition of viscoelastic and viscoplastic components, similar to that used by Brusselle-Dupend et al. (2001, 2003), shown in Figure 2.1 (c). Like the work of Perić and Dettmer, both Nedjar's models are formulated for three-dimensional large strain with constitutive mathematics developed from thermodynamics. Again, only linear viscosities are used. The second *series* model treated, involves no account of strain hardening and it would seem from the work presented that such a configuration is inappropriate for the purposes of this thesis, from both a response and implementation standpoint. The first *parallel* model, however, does incorporate isotropic hardening (and as before, kinematic hardening could be included with some development) and would seem an attractive model for semicrystalline polymers. A downfall of the specific model of Nedjar is, however, the lack of a wholly elastic component of response as was included in the Perić and Dettmer form. It will become evident in Section 2.3, that such an element is important for the response profiles observed during unloading and recovery, as observed by Brusselle-Dupend et al. (2001, 2003), and so a reduced form of the model of Perić and Dettmer would seem the more appropriate choice as will be further discussed in the next section.

2.2.3 Model selection

It has only been in the last few decades that the technology has been available to allow microscopic deformation analysis. The great majority of macroscopic constitutive theories (dating back to the 1960s) were formulated based solely on experimental observation and phenomenology, thus limiting the ability to independently distinguish actual deformation modes. This perhaps explains the length of time it has taken for this type of research to come to the conclusions that were confirmed so comparatively quickly by micromechanics.

Referring to the most recent works by Zhang and Moore (1997a,b) and Brusselle-Dupend et al. (2001, 2003), the micromechanical observations that semicrystalline polymers behave elasto-viscoelasto-viscoplastically with viscoplastic yield and strain hardening, have all been confirmed at macroscopic scale. In addition, macroscopic strain hardening has been observed to occur via both isotropic and kinematic mechanisms (Brusselle-Dupend et al.

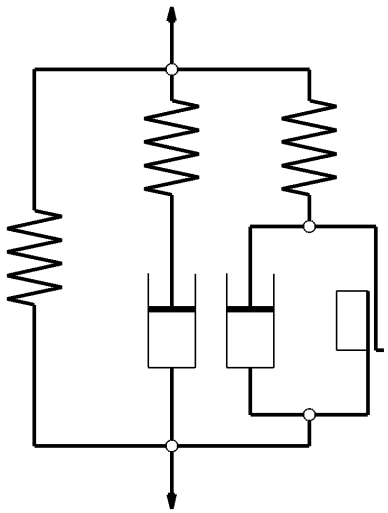

Figure 2.3: One-dimensional elasto-viscoelastic-viscoplastic rheological model.

(2001, 2003); G'Sell et al. (1997, 1999); Haward (1993); Schrauwen et al. (2004)) while a significant strain rate dependence of both the viscoelastic and viscoplastic viscosities has been observed (Brusselle-Dupend et al. (2001, 2003); Eyring (1936); Halsey et al. (1945)). No one existing model accounts for all these required behaviors and so an appropriate combination of components from existing theories will be used.

Based on the required deforming characteristics, it is proposed that a modified elasto-viscoelastic-viscoplastic form of the Perić and Dettmer model (shown in Figure 2.3) be used, incorporating both isotropic and kinematic hardening as well as nonlinear viscosity expressions comparable to those presented by Eyring (1936) and Brusselle-Dupend et al. (2001, 2003).

A major advantage of this type of model is associated with the origins of the constitutive mathematics. While not explicitly modeling the micromechanics of deformation, continuum mechanics theories such as this are based on thermodynamic laws that represent the global effect of molecular interactions. Thus, direct analogy between such theories and the mechanisms discussed in Section 2.2.1 is possible.

Firstly, hyperelastic theory is used for the elastic element where the energy of deformation is related to the thermodynamic system free energy in a similar way to that used in the micromechanical theories (Drozdov and Christiansen (2003)). For viscoelasticity, viscous

evolution is related to thermodynamic dissipation[3] and is initiated and driven via interaction with a hyperelastic element, as would be the case on the molecular level. Likewise, a hyperelastic component initiates and drives viscoplasticity whose evolution is also related to thermodynamic dissipation. Isotropic and kinematic hardening are included which represent the fragmentation and subsequent fibril reinforcing of crystalline lamellae. For deformation levels up to necking, a single yield point (well below the onset of necking) represents where microscopic yielding mechanisms become macroscopically evident.

The intimate relationship between macroscopic representation and the actual microscopic deformation mechanisms, is indicative of the value of a model such as this.

2.3 Suitability of the selected rheological form to polymers

While the Perić and Dettmer parallel model configuration (Figure 2.3) is desirable from a numerical standpoint, its explicit applicability to semicrystalline polymer response requires confirmation. A preliminary assessment of the performance of the parallel rheological configuration has been achieved using one-dimensional, linear constitutive mathematics from rheology[4]. Hooke's law (Findley et al. (1976)) was used for the elastic element constitutive relationship, i.e.

$$\sigma_e = E_e \varepsilon \tag{2.1}$$

The spring and dashpot component mathematics used for the viscoelastic element were Hooke's law and a simple newtonian evolution expression (Findley et al. (1976)) respectively

$$\sigma_{ve} = E_{ve}\left(\varepsilon - \varepsilon^i_{ve}\right), \qquad \dot{\varepsilon}^i_{ve} = \frac{1}{\eta_{ve}}\sigma_{ve} \tag{2.2}$$

A one-dimensional form of the Perzyna model was used for the viscoplastic element (refer to Appendix B for further details)

$$\sigma_{vp} = E_{vp}\left(\varepsilon - \varepsilon^i_{vp}\right), \qquad \dot{\varepsilon}^i_{vp} = \frac{\langle f \rangle}{\eta_{vp}} \frac{\partial f}{\partial \sigma_{vp}}$$

$$f = |\sigma_{vp}| - \sigma_y \tag{2.3}$$

Model parameters were chosen arbitrarily and are presented for completeness in Table 2.1.

[3] Satisfying the Clausius-Duhem form of the second law of thermodynamics (Reese and Govindjee (1998a))

[4] The actual nonlinear, three-dimensional constitutive mathematics are treated at length in Section 2.4.

Table 2.1: Arbitrarily chosen 1D linear model parameters

E_e	[MPa]	250
E_{ve}	[MPa]	1000
E_{vp}	[MPa]	1000
η_{ve}	[MPa s]	1000
η_{vp}	[MPa s]	1000
σ_y	[MPa]	1

The viscoelastic and viscoplastic evolution equations were solved using a Newton iteration scheme, analogous to that of Reese and Govindjee (1998a). A simple strain controlled computational implementation was used to generate the data presented in what follows. By showing that the parallel configuration is capable of reproducing deformation characteristics observed in the literature, the configuration is proven valid for these purposes.

2.3.1 Static loading

Some of the earliest tests on the time dependent nature of polymers were static *creep-recovery* tests (Onaran and Findley (1965), Lifshitz and Kolsky (1967) and others as summarized by Findley et al. (1976)). These tests involved maintaining a constant stress on a test sample and observing the deformation response. Load removal then results in elastic and some degree of time dependent strain recovery. This observed deformation response can be effectively reproduced by the 3 element, elasto-viscoelastic-viscoplastic model (Figure 2.3). During loading the applied stress is distributed through the three elastic springs with the viscoelastic and viscoplastic component springs driving time dependent deformation in the corresponding dashpots (providing spring stress exceeds that of yield in the case of the viscoplastic element). When an applied stress is held constant the evolution of the viscoelastic and viscoplastic dashpots proceeds while their element stresses decrease to zero and below yield respectively. The elastic element stress increases to compensate and maintain a constant total load. The increasing elastic element stress necessitates an increase in total deformation and this time dependent strain increase is referred to as *creep*. If viscoplastic yield is not reached during initial load application, the element will act as an additional elastic element with an analogous increase in stress. In this way, viscoplastic yield can either be achieved by an initially large applied stress, or as a result of increasing

creep strain, inducing increased stress in the viscoplastic spring until yield is reached. This property effectively reproduces the phenomenon of plastic residual strain being present in polymer samples following long term creep testing at stresses far below the expected yield (Findley et al. (1976)).

Release of the load results in a total model stress of zero, however due to dashpot strains the most likely stress distribution in the springs is one of tension in the elastic element and a counteracting compression in the other two. This residual element stress is what drives the creep mechanism in reverse, referred to as *recovery*. While the viscoelastic element stress will proceed to zero, that in the viscoplastic element will stop when the element stress decreases below compressive yield stress. As such a residual strain remains in the model. These results are all comparable to those observed by Onaran and Findley (1965), Lifshitz and Kolsky (1967) and Findley et al. (1976) for actual experiments on semicrystalline polymers.

Strain control tests are a powerful type of test for formulating and testing a material with simultaneous modes of deformation as is the case for semicrystalline polymers. Such testing simplifies the isolation of the parallel modes of deformation and has been used almost exclusively in more recent polymer testing. Relaxation testing is one of the earliest forms of this type of test. A relaxation test involves maintaining a constant strain on a test sample and observing the stress response (Findley et al. (1976)).

The response of the proposed model (Figure 2.3) during such stress relaxation can also be audited. The initial strain application will result in a distribution of the total stress across the three element springs driving inelastic evolution in the viscoelastic and viscoplastic elements. Subsequently holding constant some nonzero value of strain, the elastic element stress will remain constant while that in the viscoelastic and viscoplastic elements will decrease as a result of the continuing evolution of the dashpots. This progressive decrease in stress is referred to as *stress relaxation*. Again the viscoelastic stress will approach zero while the stress in the viscoplastic element will become constant when the spring stress becomes less than that of yield. This type of response is exactly as would be expected for a semicrystalline polymer as reported by Findley et al. (1976).

2.3.2 Constant strain rate loading

Constant strain rate loading is one of the most common testing methods used for the evaluation of polymer constitutive theories. A constant strain rate test involves a linear

ramp in strain over time. Figure 2.4 (a) shows a constant strain rate test simulation over time for the proposed rheological model configuration. Four graphs are shown; the top is the magnitude of strain rate over time followed by component strain vs. time response for the elastic, viscoelastic and viscoplastic elements respectively. The strain vs. time graphs show the total element strain (all three elements have equal total strain), the component of strain in the element spring and the component of strain in the dashpot is as per the key shown. Spring and dashpot strain components are a decomposition of the total strain for each element. For the viscoplastic element response, a faint horizontal line shows the spring strain corresponding to the element yield stress.

Figure 2.4 (a), (b) and (c) are representative of three different strain rates applied to the same model. It can be observed that an increase in strain rate corresponds directly to an increase in each component's level of spring strain and so total stress (through the linear relationships of equation (2.1) to (2.3)). Total model stress has been calculated and is plot against total strain in Figure 2.5 (a) for these three strain rates. Authors such as G'Sell and Jonas (1979, 1981), Kitagawa and colleagues (Kitagawa and Matsutani (1988); Kitagawa et al. (1989); Kitagawa and Takagi (1990)), Popelar et al. (1990), Duffo et al. (1995), Zhang and Moore (1997a,b) and Kontou and Farasoglou (1998) have reported on constant strain rate tensile tests of this type. Qualitative comparison between Figure 2.5 (a) and that published by Kitagawa and Takagi (1990)[5], shown in Figure 2.6 (a), indicates the proposed model's correct account of curve shape and stress response to different applied strain rates.

Tests that are often carried out in polymer research involve mid test transient jumps between constant controlled strain rates. A theoretical simulation of such a test has been carried out for the proposed rheological model. Figure 2.4 (d) shows the theoretical test strain rate, elastic, viscoelastic and viscoplastic strain components against time. It can be observed that for each element, jumps in strain rate effects each component of strain as if the *difference* in strain rate had been added to, or subtracted from, the previous response. It is also observed that the spring strains for the viscoelastic and viscoplastic elements always approach the same equilibrium value for the same applied strain rate, irrespective of strain history. Again, the total model stress response is shown against total strain in Figure 2.5 (b). The monotonic paths corresponding to each strain rate are also shown. The observed

[5]Indicative of all previously mentioned published experimental results of this type.

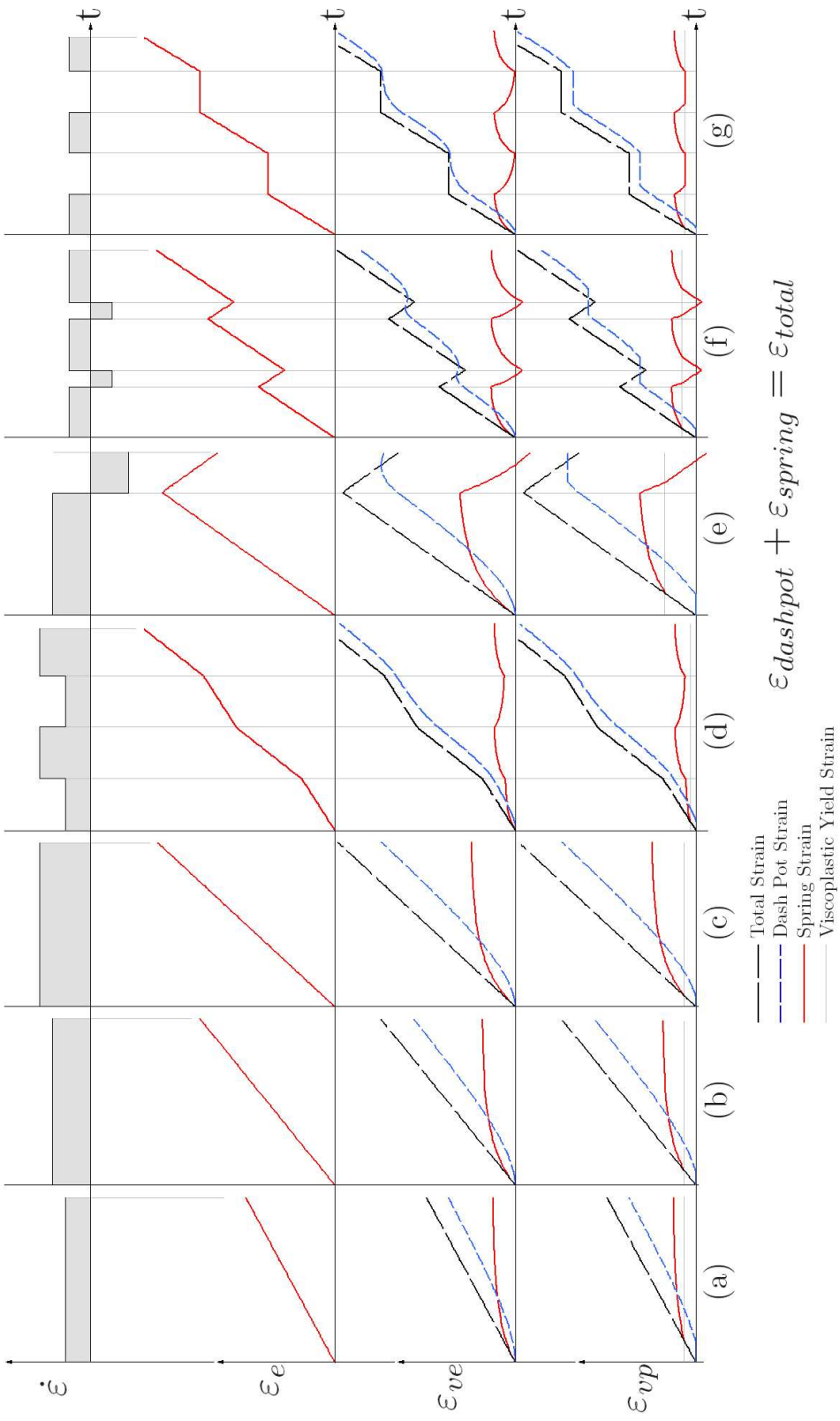

Figure 2.4: Theoretical strain curves for the proposed elasto-viscoelastic-viscoplastic rheological model showing all element components of strain for (a, b and c) constant strain rate tests, (d) changing strain rate tests, (e) loading-unloading test, (f) cyclic loading-unloading test and (g) cyclic loading-relaxation test. Figures are not drawn to scale.

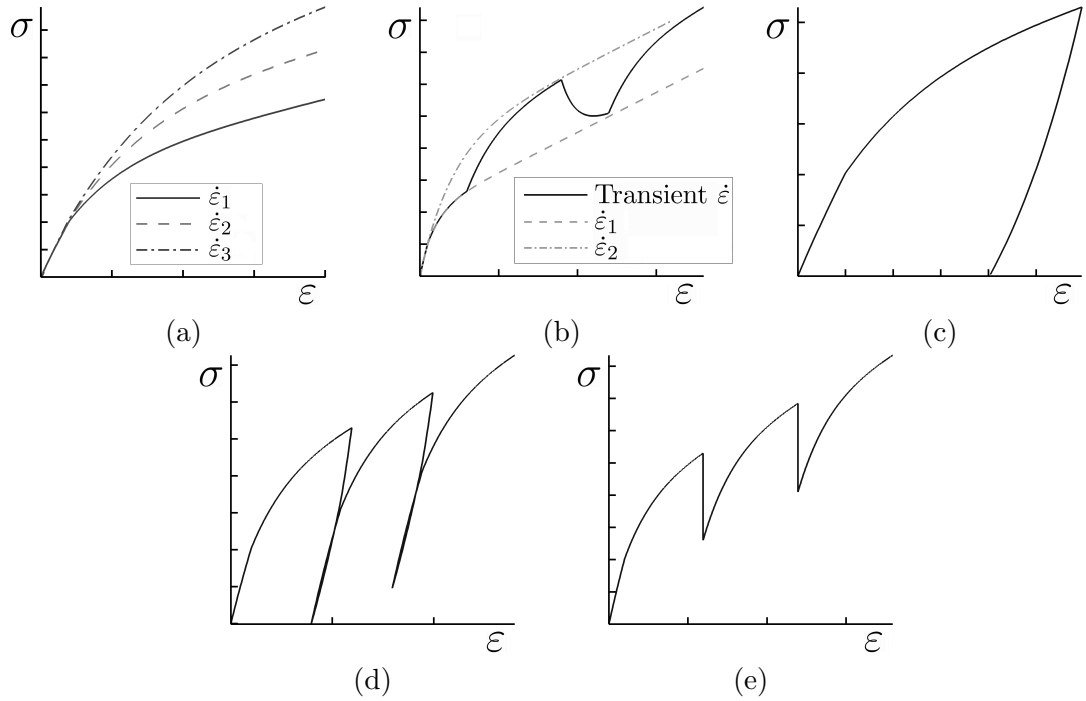

Figure 2.5: Theoretical total stress vs. total strain curves for the proposed elasto-viscoelastic-viscoplastic rheological model for (a) three constant strain rate tests, (b) changing strain rate test, (c) loading-unloading test, (d) cyclic loading-unloading test and (e) cyclic loading-relaxation test. Figures are not drawn to any scale.

path of the stress strain curve due to transient changes in strain rate, and the apparent lack of history dependence on strain rate, has been observed in experimental testing on semicrystalline polymers by G'Sell and Jonas (1981), Kitagawa and Matsutani (1988), Kitagawa et al. (1989), Kitagawa and Takagi (1990) and Zhang and Moore (1997a,b). Experimental results from Zhang and Moore (1997a) are shown in Figure 2.6 (b) for comparison.

Various other types of tests using changing states of constant strain rate have been used in the evaluation of polymer constitutive models. Kitagawa and Matsutani (1988), Popelar et al. (1990), Zhang and Moore (1997a,b), Pegoretti et al. (2000), and Brusselle-Dupend et al. (2001, 2003) have all conducted loading-unloading tests where both the loading and unloading are conducted at a constant strain rate of the same magnitude but opposite sign. Figure 2.4 (e) shows the theoretical strain component results for the proposed model . The total theoretical stress in the model has been calculated, as before, and is shown against total strain in Figure 2.5 (c). It is pertinent to note that the unloading curve has ended at a point of zero stress but nonzero strain. This property and the shape of the loading and unloading stress vs. strain curves are analogous to the observations from experiments of the

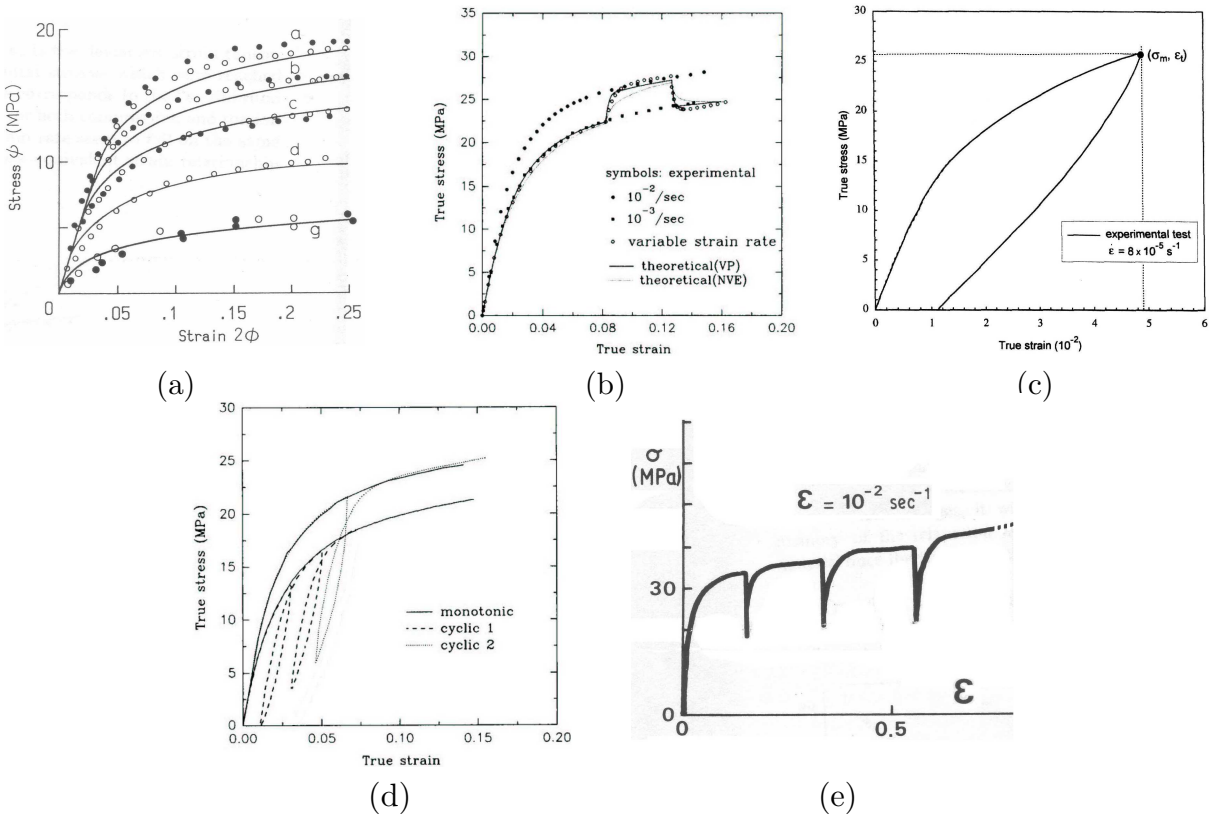

Figure 2.6: Experimental total stress vs. total strain curves taken from the literature for (a) constant strain rate tests, Kitagawa and Takagi (1990): Figure 4, p 1947, (b) changing strain rate test, Zhang and Moore (1997a): Figure 3, p 407,(c) loading-unloading test, Brusselle-Dupend et al. (2003): Figure 13, p 512, (d) cyclic loading-unloading test, Zhang and Moore (1997a): Figure 5, p 407 and (e) cyclic loading-relaxation test, G'Sell and Jonas (1981): Figure 7, p 1962.

aforementioned authors; Figure 2.6 (c) is indicative of such results for polypropylene (taken from Brusselle-Dupend et al. (2003)). Often an additional recovery period may follow such a test (Brusselle-Dupend et al. (2001, 2003)). Note that such a recovery would be driven by the residual compressive strains left in the viscoelastic and viscoplastic elements as discussed above (see Figure 2.4 (e)).

A variation of the loading-unloading test that has been used by G'Sell and Jonas (1981), Kitagawa and Matsutani (1988) and Zhang and Moore (1997a,b) involves cycling the loading-unloading procedure. The theoretical strain results for such a test are shown in Figure 2.4 (f). As was the case for the transiently changing positive strain rates in Figure 2.4 (d) and Figure 2.5 (b), the viscoelastic and viscoplastic spring strains always approach the same levels during the same strain rate. Again the total model stress has been calculated

and is shown against total strain in Figure 2.5 (d). It can be observed that upon reapplication of the loading, the stress vs. strain curve quickly approaches the path it would have traveled were no unloading to have taken place. The shape of the reloading curve does not match that of the initial loading; rather, it is steeper. Both of these properties have been observed by the authors referenced above, an example of which is provided from Zhang and Moore (1997a) in Figure 2.6 (d) for polyethylene. Another point of comparison is that the return point of stress reached by consecutive unloading periods increases with each unloading instance, observed in both Figure 2.5 (d) and Figure 2.6 (d).

Another form of cyclic test that is used during testing on semicrystalline polymers is cyclic loading-relaxation. This test loads the sample at a constant strain rate and then for a designated period of time, maintains constant strain, observing the relaxation in stress. This portion of stress relaxation is exactly the same as has been discussed above in Section 2.3.1 except that the level of strain was reached by a ramp in strain rather than a simple transient step. Component strains for a theoretical simulation with this type of loading are shown in Figure 2.4 (g). The relaxation periods are simply periods of zero strain rates as shown. The total model stress has been calculated and is shown against total strain in Figure 2.5 (e). Again, upon reapplication of the loading, the stress-strain curve quickly approaches the path it would have traveled were there no unloading. Comparison of the initial loading-relaxation curve component, can be made to that reported for polypropylene by Brusselle-Dupend et al. (2001, 2003). The results for cyclic loading-relaxation simulations are also comparable to those found during testing by G'Sell and Jonas (1981), Kitagawa and Matsutani (1988) and Kitagawa et al. (1989). A figure for comparison with actual experimental result on high density polyethylene (HDPE) is given in Figure 2.6 (e) from G'Sell and Jonas (1981).

2.3.3 Other phenomena

Another property that polymers are known to exhibit is full recovery of plastic deformation upon heat treatment. This full recovery is reported to be possible after tests of up to 20% strain in semicrystalline polymers (Pegoretti et al. (2000)) and up to 50% strain in amorphous polymers (Oleynik (1990) and Quinson et al. (1996)). Most importantly Pegoretti et al. (2000) notes that the plastic deformation in semicrystalline poly(ethylene-terephthalate) or PET resulting from tests carried up to 20% strain at room temperature,

can be fully recovered during a 6 min heat treatment at 160 $^{\circ}$C. This temperature is approximately 45 $^{\circ}$C higher than the material's glass transition temperature. The necking point of a polymer has long been known to be influenced by temperature (Brostow and Corneliussen (1986) and Budinski and Budinski (2002)) so it would be intuitive to predict that the actual viscoplastic yield would also be influenced in such a manner. With this added dependency, the proposed model would be capable of reproducing the plastic recovery observed by Pegoretti et al. (2000).

With correct expression of the temperature dependency of the viscoplastic yield stress in both tension and compression, the proposed model would be capable of total thermal plastic recovery. Referring to the earlier explanation, recovery is driven by non-zero residual element spring stresses. Following load removal, the compression in the viscoelastic component drives a full recovery of deformation. The viscoplastic element does not however recover because in most room temperature cases, the compressive yield of the material will be far greater than the residual compressive stress left in the viscoplastic component. Allowing a high enough recovery temperature to reduce the compressive yield stress toward zero, would allow free compressive evolution in the viscoplastic dashpot, comparable to that observed in the viscoelastic component. Given enough time at the elevated temperature with compressive yield stress equal to zero, the model would fully recover as is observed by Pegoretti et al. (2000) in real materials.

It is finally pertinent to note that the absence of strain hardening in the linear model presented here is an important discrepancy between the calculated curve responses and those observed in reality. Hardening is, however, taken into account in the more advanced nonlinear constitutive mathematics outlined in what follows.

2.4 Formulation of constitutive mathematics

A complete set of constitutive equations will be presented to act as a comprehensive collation of continuum mechanics constitutive theory for application to semicrystalline polymers. Perić and Dettmer (2003) provide a brief outline of constitutive equations and their foundations; these will be treated in more detail here including explicit definition of isotropic and kinematic hardening suitable for the semicrystalline polymer case. The numerical implications of incorporating strain rate dependent viscosity expressions for a three-dimensional,

large strain model will also be presented.

2.4.1 Kinematics and thermodynamics

Let us first establish some of the kinematic and thermodynamic foundations that the theory will depend on.

Of particular importance to the measurement of finite deformation is the second order *deformation gradient* tensor, $\boldsymbol{F}$ (Bonet and Wood (1997)). A key characteristic of finite deformation is the presence of rigid body motion. A consequence of this is that some arbitrary vector within the continuum of a deforming body can be described either in terms of its position in space or relative to its initial material position. These are referred to as *Eulerian* and *Lagrangian* descriptions respectively. The deformation gradient describes the final spatial configuration of such a vector with respect to its initial material configuration. The deformation gradient is evidently related to strain in both Lagrangian and Eulerian space, hence its importance to continuum mechanics.

Restriction of strain measurement into specific Lagrangian or Eulerian description results in the common measures of tensorial strain; $\boldsymbol{C} = \boldsymbol{F}^T\boldsymbol{F}$, the Lagrangian right Cauchy-Green strain tensor and $\boldsymbol{b} = \boldsymbol{F}\boldsymbol{F}^T$, the Eulerian left Cauchy-Green strain tensor. Spectral decomposition of these quantities enables the recovery of principal strain measures used widely in engineering. This decomposition is treated at length by authors such as Bonet and Wood (1997), Simo and Taylor (1991) and Itskov (2000, 2001, 2002), i.e.

$$\boldsymbol{C} = \sum_{A=1}^{3} \Lambda_A \boldsymbol{N}_A \otimes \boldsymbol{N}_A \qquad\qquad \boldsymbol{b} = \sum_{A=1}^{3} \Lambda_A \boldsymbol{n}_A \otimes \boldsymbol{n}_A \tag{2.4}$$

where $\Lambda_A,\ A = 1,2,3$ are the common eigenvalues of $\boldsymbol{C}$ and $\boldsymbol{b}$ while $\boldsymbol{N}_A$ and $\boldsymbol{n}_A$ are the Lagrangian and Eulerian eigenvector triads respectively (Bonet and Wood (1997)). Correspondingly, $\lambda_A = \sqrt{\Lambda_A}$ are the principal stretches and $\varepsilon_A = \mathbf{ln}\,(\lambda_A)$ are the logarithmic principal strains each commonly used in the experimental literature (Brusselle-Dupend et al. (2001, 2003), G'Sell and Jonas (1979), Twizell and Ogden (1983), for example).

The constitutive model treated here accounts for the parallel addition of elastic, viscoelastic and viscoplastic components (Figure 2.3). The constitutive behavior of the elastic element is associated with total deformation, however for the viscoelastic and viscoplastic elements it is necessary to separate total deformation into elastic and inelastic components.

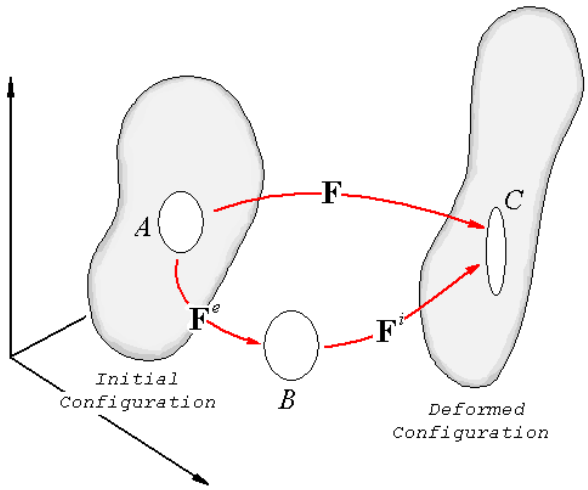

Figure 2.7: The multiplicative split of the deformation gradient into elastic and inelastic components.

In tensor space, this is facilitated via the multiplicative split of the deformation gradient, first introduced in the works of Kröner (1960) and Lee and Liu (1967) and now used widely in solid mechanics (Bonet and Wood (1997)), i.e.

$$\boldsymbol{F} = \boldsymbol{F}^e \boldsymbol{F}^i \tag{2.5}$$

This is diagrammatically represented in Figure 2.7. From the figure, where the total deformation gradient maps the initial configuration, A to its deformed configuration C, it is conceptually equivalent to allow the elastic component $\boldsymbol{F}^e$ to map A to some intermediate configuration B and correspondingly for the inelastic component $\boldsymbol{F}^i$, to map B to the final configuration C. From rearrangement of (2.5), it is convenient to establish the elastic components of right and left Cauchy-Green strain as

$$\boldsymbol{C}^e = \boldsymbol{F}^{e\,T} \boldsymbol{F}^e \qquad\qquad \boldsymbol{b}^e = \boldsymbol{F}^e \boldsymbol{F}^{e\,T} \tag{2.6}$$

Within continuum mechanics, a large part of the accurate expression of a material's constitutive behavior is associated with expression of the material's thermodynamic *free energy*, ψ (Bonet and Wood (1997); Simo and Taylor (1991)). Referring to Reese and

Govindjee (1998a), the expression of free energy can be given

$$\psi = \hat{\psi}\left(\boldsymbol{C}, \xi_1, \xi_2, ..., \xi_n\right) \tag{2.7}$$

where for some isothermal process, the free energy is a function of strain, $\boldsymbol{C}$, and some set of internal variables, ξ_i, $i = 1, 2, ..., n$. Note that because the free energy is a continuum quantity, it must be defined in terms of Lagrangian strain[6].

The strain dependence of the free energy is commonly associated with elastic mechanisms (Ogden (1984)) while the internal variables are generally associated with the inelastic response (Perić and Dettmer (2003); Simo and Hughes (2000)) which gives rise to the decoupled expression treated by Perić (1993)

$$\hat{\psi}\left(\boldsymbol{C}^e, \xi_1, \xi_2, ..., \xi_n\right) = \hat{\mathcal{W}}\left(\boldsymbol{C}^e\right) + \hat{\mathcal{H}}\left(\xi_1, \xi_2, ..., \xi_n\right) \tag{2.8}$$

where $\hat{\mathcal{W}}$ is the elastic thermodynamic potential, examples of which include the St. Venant-Kirchhoff (elastic), and Ogden (hyperelastic) models (Bonet and Wood (1997)), while the definition of $\hat{\mathcal{H}}$ clearly depends on the nature of the internal variables. Given that $\hat{\psi}$ is associated with material deformation that can be separated into elastic and inelastic components via (2.5), then $\hat{\mathcal{W}}$ is only functional on the elastic component as shown (Nedjar (2002a); Reese and Govindjee (1998a)). It follows that for a purely elastic material, $\boldsymbol{C}^e = \boldsymbol{C}$ such that

$$\hat{\psi}\left(\boldsymbol{C}\right) = \hat{\mathcal{W}}\left(\boldsymbol{C}\right) \tag{2.9}$$

where no internal variables are necessary.

Focusing on the particular case of an elasto-viscoelastic-viscoplastic constitutive theory, because of the parallel configuration (Figure 2.3), it is a common convention to define the total free energy expression via the sum of the components (Holzapfel (1996); Holzapfel and Simo (1996); Nedjar (2002a); Reese and Govindjee (1998a)) as

$$\psi = \hat{\psi}_e\left(\boldsymbol{C}\right) + \hat{\psi}_{ve}\left(\boldsymbol{C}^e_{ve}, \eta_{ve}\right) + \hat{\psi}_{vp}\left(\boldsymbol{C}^e_{vp}, \eta_{vp}, \alpha, \boldsymbol{\alpha}\right) \tag{2.10}$$

where α and $\boldsymbol{\alpha}$ are viscoplastic internal variables associated with isotropic and kinematic

[6]When a material is isotropic, the free energy can also be expressed as a function of Eulerian strain ($\boldsymbol{b}$ for example, see Reese and Govindjee (1998a)) however this is an unnecessary modification for the present development.

hardening respectively, and also, contrary to the traditional form of $\hat{\psi}_{ve}$ and $\hat{\psi}_{vp}$ (for example Reese and Govindjee (1998a); Perić and Dettmer (2003) for viscoelasticity and Perić (1993); Perić and Dettmer (2003); Simo (1992); Simo and Hughes (2000) for viscoplasticity), the viscosity terms η_{ve} and η_{vp} have been included as additional internal variables. This is due to the requirement that the viscosity terms used in any constitutive model for semicrystalline polymers, have some functionality on strain (Section 2.2.3). We will elaborate further on this point in subsequent sections.

2.4.2 Stress

To allow definition of the constitutive stress expression, it is necessary to observe that, following authors such as Holzapfel (1996), Nedjar (2002a) and Reese and Govindjee (1998a), all constitutive equations must satisfy the 2^{nd} law of thermodynamics. In Lagrangian description, this can take the form of the Clausius-Plank inequality[7]

$$\boldsymbol{S} : \tfrac{1}{2}\dot{\boldsymbol{C}} - \dot{\psi} \geq 0 \tag{2.11}$$

where $\boldsymbol{S}$ is the second Piola-Kirchhoff stress tensor. By the standard development (Nedjar (2002a); Perić and Dettmer (2003); Reese and Govindjee (1998a); Simo (1992)), implementation of (2.10) into (2.11) enables the explicit definition of the stress expression. This development is included in Appendix A.

From Appendix A, the total second Piola-Kirchhoff stress is given

$$\begin{aligned}\boldsymbol{S} &= 2\frac{\partial \hat{\psi}_e}{\partial \boldsymbol{C}} + 2\boldsymbol{F}_{ve}^{i\,-1}\frac{\partial \hat{\psi}_{ve}}{\partial \boldsymbol{C}_{ve}^{e}}\boldsymbol{F}_{ve}^{i\,-T} + 2\boldsymbol{F}_{vp}^{i\,-1}\frac{\partial \hat{\psi}_{vp}}{\partial \boldsymbol{C}_{vp}^{e}}\boldsymbol{F}_{vp}^{i\,-T} \\ &= \boldsymbol{S}_e + \boldsymbol{S}_{ve} + \boldsymbol{S}_{vp}\end{aligned} \tag{2.12}$$

In solid mechanics, while the account of the constitutive behavior of a material is inherently Lagrangian (Bonet and Wood (1997)), a commonly used implication scheme is the *Updated Lagrangian* scheme (Chen and Mizuno (1990)) which requires the stress tensor (and subsequent tangential modulus tensor, see Chapter 3) to be treated in Eulerian form. Thus it is convenient to also define the Eulerian counterpart to $\boldsymbol{S}$; the Kirchhoff stress tensor $\boldsymbol{\tau}$. Lagrangian and Eulerian quantities are related through the concepts of *push forward* and

[7] also commonly referred to as the Clausius-Duhem inequality.

pull back (Bonet and Wood (1997); Simo and Taylor (1991)) where the Kirchhoff stress can be attained from the second order push forward of $\boldsymbol{S}$ via

$$\boldsymbol{\tau} = \boldsymbol{F}\boldsymbol{S}\boldsymbol{F}^T \tag{2.13}$$

Implementing (2.13) in (2.12), then

$$\begin{aligned}\boldsymbol{\tau} &= 2\boldsymbol{F}\frac{\partial \hat{\psi}_e}{\partial \boldsymbol{C}}\boldsymbol{F}^T + 2\boldsymbol{F}^e_{ve}\frac{\partial \hat{\psi}_{ve}}{\partial \boldsymbol{C}^e_{ve}}\boldsymbol{F}^{e\,T}_{ve} + 2\boldsymbol{F}^e_{vp}\frac{\partial \hat{\psi}_{vp}}{\partial \boldsymbol{C}^e_{vp}}\boldsymbol{F}^{e\,T}_{vp} \\ &= \boldsymbol{\tau}_e + \boldsymbol{\tau}_{ve} + \boldsymbol{\tau}_{vp}\end{aligned} \tag{2.14}$$

Because of the functionality of $\boldsymbol{\tau}_{ve}$ and $\boldsymbol{\tau}_{vp}$ on the elastic component of strain, it remains to define the evolution of inelastic strain[8].

2.4.3 Viscoelastic evolution equations

Limiting our attention to the evolution of the viscoelastic response, following from Appendix A, this must satisfy the inequality

$$\boldsymbol{\tau}_{ve} : \left(-\tfrac{1}{2}\left(\mathcal{L}_v \boldsymbol{b}^e_{ve}\right)\boldsymbol{b}^{e\,-1}_{ve}\right) - \frac{\partial \hat{\psi}_{ve}}{\partial \eta_{ve}} \cdot \dot{\eta}_{ve} \geq 0 \tag{2.15}$$

The righthand $-\frac{\partial \hat{\psi}_{ve}}{\partial \eta_{ve}} \cdot \dot{\eta}_{ve}$ term is associated with the evolution of the viscosity internal variable and will be treated later. The remaining term is associated with strain evolution and is of primary interest.

Reese and Govindjee (1998a) introduce the expression

$$-\frac{1}{2}\left(\mathcal{L}_v \boldsymbol{b}^e_{ve}\right)\boldsymbol{b}^{e\,-1}_{ve} := \mathcal{V}^{-1} : \boldsymbol{\tau}_{ve} \tag{2.16}$$

such that the left hand side of (2.15) becomes

$$\boldsymbol{\tau} : \mathcal{V}^{-1} : \boldsymbol{\tau} \geq 0 \tag{2.17}$$

which is satisfied for all cases of $\boldsymbol{\tau}$ providing $\mathcal{V}^{-1}$ is positive definite.

[8]Note, tensorial elastic and inelastic deformation can be related through $\boldsymbol{C}^e = \boldsymbol{F}^{i\,-T}\boldsymbol{C}\boldsymbol{F}^{i\,-1}$, thus determining the inelastic evolution also enables resolution of $\boldsymbol{C}^e$.

The left hand term of (2.16) is related to the rate of inelastic material strain through *operator split* theory (Ortiz et al. (1983)). For the current investigation it is sufficient to draw the analogy between (2.16) and the dashpot expression, $(2.2)_2$, of the infinitesimal 1D theory where, in fourth order tensor space, $\mathcal{V}^{-1}$ represents the inverse viscosity term.

An inverse viscosity term suitable for polymers has been proposed by Reese and Govindjee (1998a) as

$$\mathcal{V}^{-1} = \frac{1}{2\eta_D}\left(\boldsymbol{I}'_4 - \tfrac{1}{3}\boldsymbol{I}\otimes\boldsymbol{I}\right) + \frac{1}{9\eta_V}\boldsymbol{I}\otimes\boldsymbol{I} \tag{2.18}$$

where η_D and η_V are deviatoric and volumetric components of viscosity respectively. The authors indicate that the viscosity terms η_D and η_V could be strain dependent but offer no further development. The terms $(\boldsymbol{I}'_4 - \frac{1}{3}\boldsymbol{I}\otimes\boldsymbol{I})$ and $\boldsymbol{I}\otimes\boldsymbol{I}$ operate through the double contraction with $\boldsymbol{\tau}_{ve}$ to isolate the deviatoric and volumetric components of stress respectively (Simo (1992)). Here $I'_{4\,ijkl} = \frac{1}{2}(\delta_{ik}\delta_{jl} + \delta_{il}\delta_{jk})$ is the supersymmetric 4th order identity tensor and $I_{ij} = \delta_{ij}$ is the 2nd order identity tensor (Bonet and Wood (1997)). Holzapfel (1996) notes that based on experimental results, the inelastic evolution of most polymeric materials is wholly deviatoric and consequently, the volumetric term from (2.18) can be ignored (i.e. $\eta_V \longrightarrow \infty$). Such a reduced form of (2.18) has been accurately implemented in the works of Perić and Dettmer (2003) and Reese and Govindjee (1998a), supporting such a restriction.

It is left to establish the actual form of viscosity expression that would allow adequate account of the strain rate dependence observed for semicrystalline polymers.

In the context of one-dimensional, finite deformation, Brusselle-Dupend et al. (2001, 2003) have proposed a viscosity expression for the viscoelastic response of semicrystalline polypropylene as

$$\eta_{ve} = \frac{h_0 - h_1 \exp\left\{h_2 \frac{|\dot{\varepsilon}^e|+3\times10^{-5}}{|\dot{\varepsilon}^i|}\right\} - h_3 \exp\left\{h_4 \frac{|\dot{\varepsilon}^e|+3\times10^{-5}}{|\dot{\varepsilon}^i|}\right\}}{(|\dot{\varepsilon}^e| + 3\times10^{-5})^{ne}} \tag{2.19}$$

where $h_{0,1,\ldots,4}$ and the exponent ne are material constants. This equation was developed due to the reported inadequacies with the conventionally used Eyring equation (Eyring (1936); Halsey et al. (1945)) when applied to semicrystalline polymer response.

For three-dimensionality, the viscosity of a material remains a scalar quantity (as per equation (2.18)) however the multidimensional dependencies of this value have not been

treated with any generality in the literature, particularly for the case at hand. It is additionally relevant to note, however, that Brusselle-Dupend et al. (2001, 2003) assumed material elasticity to be linear such that, within the current context, (2.19) may also prove overly nonlinear. It would appear that a significant amount of experimental work is needed to allow development of a three-dimensional analog[9] to (2.19).

Developing on this concept briefly, because of its strain dependence, the viscosity is considered to be an internal variable in a similar way to the strain hardening terms from plasticity. Following from Perić and Owen (1998), Reese and Govindjee (1998a) and Simo and Hughes (2000) it would be most desirable to define the constitutive behavior of internal variables via their evolution, i.e.

$$\dot{\eta}_{ve} = \hat{\eta}_{ve}\left(\boldsymbol{C}^{i}_{ve}, \eta_{ve}\right) = \hat{\eta}_{ve}\left(\boldsymbol{F}^{T}\boldsymbol{b}^{e\,-1}_{ve}\boldsymbol{F}, \eta_{ve}\right) \tag{2.20}$$

By specifying the constitutive behavior of the viscosity in this way, a numerical solution scheme such as *closest point projection*, conventionally used in plasticity (Perić (1993); Simo and Hughes (2000)), could be used for the simultaneous solution of strain, (2.16), and viscosity, (2.20). When viscosity is constant, the viscoelastic constitutive theory can be implemented via a local Newton iteration scheme (Reese and Govindjee (1998a)). Closest point projection can be interpreted as being an extension to such implementation, performing the Newton iteration for two or more mutually dependent variables.

An additional requirement of the constitutive behavior of the viscosity is that the evolution expression, (2.20), and the free energy component $\hat{\mathcal{H}}_{ve}\left(\eta_{ve}\right)$, must suitably satisfy the right hand side of the dissipation requirement, (2.15).

2.4.4 Viscoplastic evolution equations

The derivation of the constitutive equations for one-dimensional viscoplasticity with isotropic and kinematic hardening is presented for reference in Appendix B.

For three-dimensional large strain, as for viscoelasticity above, the viscoplastic constitutive equations must satisfy the thermodynamic dissipation requirement (Appendix A)

$$\boldsymbol{\tau}_{vp} : \left(-\tfrac{1}{2}\left(\mathcal{L}_{v}\boldsymbol{b}^{e}_{vp}\right)\boldsymbol{b}^{e\,-1}_{vp}\right) - \frac{\partial\hat{\psi}_{vp}}{\partial\eta_{vp}}\cdot\dot{\eta}_{vp} - \frac{\partial\hat{\psi}_{vp}}{\partial\alpha}\cdot\dot{\alpha} - \frac{\partial\hat{\psi}_{vp}}{\partial\boldsymbol{\alpha}} : \dot{\boldsymbol{\alpha}} \geq 0 \tag{2.21}$$

[9]Note, it would be possible to substitute principal vector quantities (from (2.4)) for the scalar strain rates in (2.19) however this would only be a means of preliminary conceptual implementation.

where again viscosity is implemented as a strain dependent internal variable and the scalar α, and tensorial $\boldsymbol{\alpha}$, internal variables are associated with isotropic and kinematic hardening mechanisms respectively (akin to α_{iso} and α_{kin} from the one-dimensional theory).

As was the case for the one-dimensional derivation in Appendix B, it is again pertinent to introduce the stress space conjugates to the isotropic and kinematic hardening internal variables, namely q and $\boldsymbol{q}$. By a similar argument to that which motivated the formulation of (2.8), referring to Perić (1993), Simo (1992) and Simo and Hughes (2000), the viscoplastic free energy can be expressed

$$\hat{\psi}(\boldsymbol{C}^e_{vp}, \eta_{vp}, \alpha, \boldsymbol{\alpha}) = \hat{\mathcal{W}}(\boldsymbol{C}^e_{vp}) + \hat{\mathcal{H}}^{\eta}_{vp}(\eta_{vp}) + \hat{\mathcal{H}}^{\alpha}_{vp}(\alpha) + \hat{\mathcal{H}}^{\boldsymbol{\alpha}}_{vp}(\boldsymbol{\alpha}) \tag{2.22}$$

Implementing a combined, linear isotropic/kinematic hardening law following Hughes (1984) and Simo and Hughes (2000), it can be shown that

$$\hat{\mathcal{H}}^{\alpha}_{vp} = \tfrac{1}{2}\theta\bar{\mathrm{H}}\,\alpha^2 \qquad \hat{\mathcal{H}}^{\boldsymbol{\alpha}}_{vp} = \tfrac{1}{2}\,(1-\theta)\,\bar{\mathrm{H}}\,\boldsymbol{\alpha} : \boldsymbol{\alpha} \tag{2.23}$$

$$\frac{\partial \hat{\mathcal{H}}^{\alpha}_{vp}}{\partial \alpha} = \theta\bar{\mathrm{H}}\,\alpha = -q \qquad \frac{\partial \hat{\mathcal{H}}^{\boldsymbol{\alpha}}_{vp}}{\partial \boldsymbol{\alpha}} = (1-\theta)\,\bar{\mathrm{H}}\,\boldsymbol{\alpha} = -\boldsymbol{q} \tag{2.24}$$

where $\bar{\mathrm{H}}$ is a constant parameter representing the combined hardening modulus and θ defines the proportions of isotropic and kinematic hardening; $\theta \in [0, 1]$. It follows directly from (2.24) that the *actual* hardening moduli are given

$$-\frac{\partial^2 \hat{\mathcal{H}}^{\alpha}_{vp}}{\partial \alpha^2} = -\theta\bar{\mathrm{H}} = \frac{\partial q}{\partial \alpha} \qquad -\frac{\partial^2 \hat{\mathcal{H}}^{\boldsymbol{\alpha}}_{vp}}{\partial \boldsymbol{\alpha}^2} = -\,(1-\theta)\,\bar{\mathrm{H}}\boldsymbol{I} \otimes \boldsymbol{I} = \frac{\partial \boldsymbol{q}}{\partial \boldsymbol{\alpha}} \tag{2.25}$$

These constant terms are inferred to be suitable for the current purpose however for more complex hardening characteristics, alternate specification of $\hat{\mathcal{H}}^{\alpha}_{vp}$ and $\hat{\mathcal{H}}^{\boldsymbol{\alpha}}_{vp}$ can be used.

Given the stress space hardening internal variables, it is possible to carry out a three-dimensional study of the effects of strain hardening on the yield surface as was done for the one-dimensional case (Appendix B). Following Simo (1992), Simo and Hughes (2000) and Zienkiewicz and Taylor (2003), selection of the von-Mises yield surface gives the yield function

$$f\left(\boldsymbol{\tau}_{vp} + \boldsymbol{q}, q\right) = \|\boldsymbol{\tau}_{vp} + \boldsymbol{q}\| - \sqrt{\tfrac{2}{3}}\,(\sigma_Y - q) \tag{2.26}$$

Physically $\sqrt{\frac{2}{3}}(\sigma_Y - q)$ quantifies the radius of the yield surface, while $-\boldsymbol{q}$ defines its center.

As for the viscoelastic case, inelasticity is assumed to have only deviatoric components, i.e.

$$f\left(\bar{\boldsymbol{\tau}}_{vp}+\boldsymbol{q},q\right)=\|\bar{\boldsymbol{\tau}}_{vp}+\boldsymbol{q}\|-\sqrt{\tfrac{2}{3}}\left(\sigma_Y-q\right) \tag{2.27}$$

where $\bar{\boldsymbol{\tau}}_{vp}=\mathrm{dev}[\boldsymbol{\tau}_{vp}]$ and now the internal variable $\boldsymbol{q}$ is wholly deviatoric so that $\mathrm{tr}[\boldsymbol{q}]=0$.

Following a similar development as for the one-dimensional case in Appendix B, Perzyna (1971) and subsequent authors such as Simo (1992), Simo and Hughes (2000), Perić and Owen (1992), Perić and Dettmer (2003) and Rosati and Valoroso (2004) define the evolution expression

$$-\frac{1}{2}\left(\mathcal{L}_v\boldsymbol{b}^e_{vp}\right)\boldsymbol{b}^{e\,-1}_{vp}=\frac{\langle f\left(\bar{\boldsymbol{\tau}}_{vp}+\boldsymbol{q},q\right)\rangle}{2\eta_{vp}}\frac{\partial f\left(\bar{\boldsymbol{\tau}}_{vp}+\boldsymbol{q},q\right)}{\partial\bar{\boldsymbol{\tau}}_{vp}} \tag{2.28}$$

Once again, an analogy is evident between this inelastic evolution and that reported for the one-dimensional case in Appendix B.

Referring to the explicit formulations of Simo (1992), Simo and Hughes (2000) and Zienkiewicz and Taylor (2003), the evolution of the strain space hardening internal variables in tensor space can subsequently be defined

$$\dot{\alpha}=\frac{\langle f\left(\bar{\boldsymbol{\tau}}_{vp}+\boldsymbol{q},q\right)\rangle}{2\eta_{vp}}\frac{\partial f\left(\bar{\boldsymbol{\tau}}_{vp}+\boldsymbol{q},q\right)}{\partial q} \tag{2.29}$$

$$\dot{\boldsymbol{\alpha}}=\frac{\langle f\left(\bar{\boldsymbol{\tau}}_{vp}+\boldsymbol{q},q\right)\rangle}{2\eta_{vp}}\frac{\partial f\left(\bar{\boldsymbol{\tau}}_{vp}+\boldsymbol{q},q\right)}{\partial\boldsymbol{q}} \tag{2.30}$$

Returning our attention to the dissipation requirement, (2.21), neglecting the viscosity term[10], substitution of equations (2.24), (2.27), (2.28), (2.29) and (2.30) yields with some manipulation

$$\left(\boldsymbol{\tau}_{vp}+\boldsymbol{q}\right):\frac{\langle f\rangle}{2\eta_{vp}}\frac{\left(\boldsymbol{I}'_4-\frac{1}{3}\boldsymbol{I}\otimes\boldsymbol{I}\right)}{\|\boldsymbol{\tau}_{vp}+\boldsymbol{q}\|}:\left(\boldsymbol{\tau}_{vp}+\boldsymbol{q}\right)+q\cdot\sqrt{\tfrac{2}{3}}\frac{\langle f\rangle}{2\eta_{vp}}\geq 0 \tag{2.31}$$

which is unconditionally satisfied given that from definition of the ramp function, (B.8), $\langle\cdot\rangle\geq 0$ and also from the known behavior of isotropic hardening $q\geq 0$.

The considerations regarding strain rate dependence of the viscosity for the viscoplastic case are identical in form to those presented in Section 2.4.3 for the viscoelastic case. Consequently, no further discussion is necessary within the current investigation.

[10]Satisfaction of the dissipation requirement must be considered during formulation of an expression for viscoplastic viscosity, as was the case for viscoelasticity discussed in Section 2.4.3.

Exact specification of the elastic thermodynamic potential terms, $\hat{\mathcal{W}}_e(\boldsymbol{C})$, $\hat{\mathcal{W}}_{ve}(\boldsymbol{C}^e_{ve})$ and $\hat{\mathcal{W}}_{ve}(\boldsymbol{C}^e_{vp})$, to be used within a constitutive theory for semicrystalline polymers is largely case specific. Generally any elastic or hyperelastic form of thermodynamic potential could be chosen (see Bonet and Wood (1997)). A suggestion would be to use hyperelastic Ogden potentials for the elastic (Simo and Taylor (1991)) and viscoelastic (Reese and Govindjee (1998a)) elements and an elastic type St. Venant-Kirchhoff potential for the viscoplastic element (Simo (1992)). The choice of free energy expression must be governed by experimental observation because it must represent the thermodynamic potential of the material. As such final selection of the exact free energy form requires response curves from physical tests. For a more detailed discussion of hyperelastic free energy expressions for numerical use see Simo and Taylor (1991), Simo (1992), Perić and Owen (1992), Reese and Govindjee (1998a), Simo and Hughes (2000) and Perić and Dettmer (2003).

2.5 Summary

The aim of this chapter has been to determine the most appropriate constitutive theory for semicrystalline polymers based on a review of the literature. The agreement between both microscopic and macroscopic research on the required characteristics of such a model, give strength to the model which has been selected. A preliminary study has shown the chosen parallel rheological model configuration to be suitable across a wide range of complex deformation behaviors based on comparison with experimental observations from the literature. The model's constitutive mathematics have been presented in their most general form with the objective of being broadly applicable to all semicrystalline polymers.

Chapter 3

Numerical Implementation and Verification

The numerical implementation of the constitutive theory developed in Chapter 2 is presented here. Of particular importance is the assumption of isotropy which enables the reduction of the previously defined constitutive relations into principal space. This reduction is motivated most significantly by the impracticality of fitting full tensor space model parameters to experimental data, particularly for a complex response such as this. The transition between principal constitutive representation and the tensor space stress and tangential modulus terms, critical to implicit numerical implementation, is a nontrivial aspect of such a reduction.

The numerical treatment of principal space hyperelasticity (elasticity being a subgroup) has been presented with some generality by Simo and Taylor (1991) and also Itskov (2001). Throughout the respective principal space algorithmic developments, the dependence of the explicit stress and tangential modulus tensor expressions on the conditioning of the principal stretches is fully developed. This is a key characteristic of the numerical treatment of principal stretch theories.

A suitable implementation of a finite strain viscoelastic theory in principal stretches is reported by Reese and Govindjee (1998a). The solution strategy used is akin to the operator split methodology used in plasticity (Ortiz et al. (1983)), while integration of the evolution equation is done using Newton's method. The authors report on the development of the consistent closed-form tangential modulus with some detail on the transition between

spectral and tensor quantities.

There is significant development in the literature on the numerical treatment of viscoplasticity. Simo and Hughes (2000) make note of three general classes of return mapping algorithms commonly used in plasticity. The first of these is *radial return mapping*. Simo (1992) most comprehensively treats such an algorithm for viscoplasticity including account of both isotropic and kinematic hardening. Simo's development was based on principal plane constitutive expressions, including a brief account of the reconstruction into tensor space. Radial return mapping has been applied widely within plasticity however the methodology necessitates specialized formulation for each different constitutive account of elasticity, yield, flow and hardening. An integration algorithm for the general case is the *closest point projection* method (Simo and Hughes (1987, 2000)). This methodology is mathematically more rigorous however the actual formulation is carried out independent of the specific constitutive relationships, thus enabling general application. Simo and Hughes (2000) present a closest point projection method for viscoplasticity, while most significantly, Perić and Owen (1992) and Perić (1993) report on the use of closest point projection for viscoplasticity with the addition of isotropic hardening. All three developments are presented for tensor space constitutive expressions including formulation of the consistent tangential modulus. The third class of integration algorithms is the *cutting plane algorithm* (Simo and Hughes (1987, 2000)). Such an algorithm, whilst possessing certain advantages, has been deemed to be inappropriate for the current purposes, see Simo and Hughes (1987) and the references therein for further reading on cutting plane algorithms.

The parallel addition of model elements within the chosen model (Figure 2.3) facilitates the decoupled algorithmic treatment of each response. Correspondingly, these will be treated separately in the sections that follow.

3.1 Generalized elasticity

The constitutive model outlined in Chapter 2 utilizes elastic, viscoelastic and viscoplastic deforming responses combined in parallel. Within this section, after treating preliminary kinematic and thermodynamic principals, the generalized finite strain numerical implementation of the elastic (or more correctly hyperelastic) element will be discussed. Of primary significance is the derivation of the generalized closed-form tangential modulus, expressed in

terms of principal stretches. Such an expression has been treated by Simo and Taylor (1991) and also Itskov (2001) however there still remains room for generalization, particularly in regards to the mathematical foundations of the theory.

3.1.1 Volumetric-deviatoric strain separation

The vast majority of constitutive theories used for numerical application (hyperelastic or otherwise) treat deformation as being separable into volumetric and deviatoric components. This separation has a firm basis in experimental observation (see for example Simo and Taylor (1991), Reese and Govindjee (1998a) and Holzapfel (1996)) and is a largely accepted convention in all but the most specialized of cases. The theories treated herein will adhere to this convention.

Separation of response into volumetric and deviatoric components is carried out via the multiplicative split of the deformation gradient, $\boldsymbol{F}$ as

$$\boldsymbol{F} = \boldsymbol{F}_{vol}\bar{\boldsymbol{F}} \tag{3.1}$$

where, given the scalar jacobian of $\boldsymbol{F}$, $J = \det[\boldsymbol{F}]$, the volumetric and deviatoric components of the deformation are respectively

$$\boldsymbol{F}_{vol} = J^{1/3}\boldsymbol{I} \tag{3.2}$$

$$\bar{\boldsymbol{F}} = J^{-1/3}\boldsymbol{F} \tag{3.3}$$

Recalling the right and left Cauchy-Green strain tensors introduced in Section 2.4.1 and observing this alternate split of the deformation gradient, then from equations (3.1) to (3.3)

$$\boldsymbol{C} = \boldsymbol{C}_{vol}\bar{\boldsymbol{C}} \qquad\qquad \boldsymbol{b} = \boldsymbol{b}_{vol}\bar{\boldsymbol{b}} \tag{3.4}$$

where

$$\boldsymbol{C}_{vol} = J^{2/3}\boldsymbol{I} \qquad\qquad \boldsymbol{b}_{vol} = J^{2/3}\boldsymbol{I} \tag{3.5}$$

$$\bar{\boldsymbol{C}} = J^{-2/3}\boldsymbol{C} \qquad\qquad \bar{\boldsymbol{b}} = J^{-2/3}\boldsymbol{b} \tag{3.6}$$

Because, for the current development, deformation is wholly elastic, the elastic-inelastic

multiplicative split of the deformation gradient as in (2.5) is at this stage unnecessary.

3.1.2 Thermodynamics in tensor space

As discussed in Section 2.4.1, the constitutive behavior of a purely hyperelastic material is typically represented by expression of the material's thermodynamic free energy (as in (2.9)). In view of the separability of strain into volumetric and deviatoric components, a corresponding separation of this free energy term commonly takes the form

$$\psi = \hat{\psi}\left(\boldsymbol{C}\right) = \hat{\mathcal{U}}\left(J\right) + \hat{\mathcal{W}}\left(\bar{\boldsymbol{C}}\right) \tag{3.7}$$

where the functions $\hat{\mathcal{U}}$ and $\hat{\mathcal{W}}$ describe volumetric and deviatoric components of thermodynamic potential respectively. The St. Venant-Kirchhoff (elastic), Neo-Hookean, Moony-Rivlin and Ogden models are examples of hyperelastic theories of this sort (Bonet and Wood (1997)).

Following the development of Appendix A and Section 2.4.2, the second Piola-Kirchhoff stress tensor expression for a purely hyperelastic material is given

$$\boldsymbol{S} = 2\frac{\partial\hat{\psi}\left(\boldsymbol{C}\right)}{\partial\boldsymbol{C}} \tag{3.8}$$

Implementing the chain rule in view of the separated form of (3.7) this becomes

$$\boldsymbol{S} = 2\frac{\partial\hat{\mathcal{U}}}{\partial J}\frac{\partial J}{\partial\boldsymbol{C}} + 2\frac{\partial\hat{\mathcal{W}}}{\partial\bar{\boldsymbol{C}}}\frac{\partial\bar{\boldsymbol{C}}}{\partial\boldsymbol{C}} \tag{3.9}$$

Given the push forward operation of (2.13), the separated Eulerian Kirchhoff stress term can be trivially found from manipulation of (3.9). An alternate form of Eulerian stress commonly used in solid mechanics is the Cauchy or *true* stress $\boldsymbol{\sigma}$, which is correspondingly defined

$$\boldsymbol{\sigma} = \frac{1}{J}\boldsymbol{\tau} = \frac{1}{J}\boldsymbol{F}\boldsymbol{S}\boldsymbol{F}^{T} = \frac{2}{J}\boldsymbol{F}\frac{\partial\hat{\psi}\left(\boldsymbol{C}\right)}{\partial\boldsymbol{C}}\boldsymbol{F}^{T} \tag{3.10}$$

Cauchy stress is generally the form of most interest for implicit, updated Lagrangian, stress update solution schemes.

Referring to for example Bonet and Wood (1997), following from (3.8), the Lagrangian

form of the fourth order tangential modulus tensor is defined

$$\mathbb{C} = 2\frac{\partial \boldsymbol{S}}{\partial \boldsymbol{C}} = 4\frac{\partial^2 \hat{\psi}\left(\boldsymbol{C}\right)}{\partial \boldsymbol{C}^2} \tag{3.11}$$

Again observing the separated volumetric and deviatoric components of free energy, by the chain rule

$$\mathbb{C} = \underbrace{4\frac{\partial^2 \hat{\mathcal{U}}}{\partial J^2}\frac{\partial J}{\partial \boldsymbol{C}} \otimes \frac{\partial J}{\partial \boldsymbol{C}} + 4\frac{\partial \hat{\mathcal{U}}}{\partial J}\frac{\partial^2 J}{\partial \boldsymbol{C}^2}}_{vol} + \underbrace{4\frac{\partial^2 \hat{\mathcal{W}}}{\partial \bar{\boldsymbol{C}}^2}\frac{\partial \bar{\boldsymbol{C}}}{\partial \boldsymbol{C}} \otimes \frac{\partial \bar{\boldsymbol{C}}}{\partial \boldsymbol{C}} + 4\frac{\partial \hat{\mathcal{W}}}{\partial \bar{\boldsymbol{C}}}\frac{\partial^2 \bar{\boldsymbol{C}}}{\partial \boldsymbol{C}^2}}_{dev} \tag{3.12}$$

The Eulerian tangential modulus counterpart[1] can be found via the fourth order push forward of the Lagrangian term such that

$$\boldsymbol{c} = \frac{1}{J}\boldsymbol{F}\boldsymbol{F}\mathbb{C}\boldsymbol{F}^T\boldsymbol{F}^T \tag{3.13}$$

Equation (3.12) (and its corresponding substitution in (3.13)) constitute expression of the complete closed form tangential modulus for hyperelastic materials in tensor form.

3.1.3 Spectral decomposition of strain

The assumption that the response of a material to loading is isotropic enables the reduction of constitutive representation into principal planes. A major advantage of such a representation is the significant reduction in experimental work required to fit and validate constitutive relationships, particularly in the more complex of cases. This being said, most practical numerical implementations will operate in full tensor space and so the implications of the necessary spectral reconstruction are of significant importance, as will become clearer in what follows.

[1] Note here that $\boldsymbol{c}$ is the tangential modulus corresponding to Cauchy stress

Initially recalling the tensor strain quantities from Section 2.4.1, the spectral decompositions proceed

$$\boldsymbol{C} = \sum_{A=1}^{3} \Lambda_A \boldsymbol{N}_A \otimes \boldsymbol{N}_A \qquad = \sum_{A=1}^{3} \lambda_A^2 \boldsymbol{N}_A \otimes \boldsymbol{N}_A \tag{3.14}$$

$$\boldsymbol{b} = \sum_{A=1}^{3} \Lambda_A \boldsymbol{n}_A \otimes \boldsymbol{n}_A \qquad = \sum_{A=1}^{3} \lambda_A^2 \boldsymbol{n}_A \otimes \boldsymbol{n}_A \tag{3.15}$$

$$\boldsymbol{F} = \sum_{A=1}^{3} \lambda_A \boldsymbol{n}_A \otimes \boldsymbol{N}_A \tag{3.16}$$

where now we refer to the $\boldsymbol{N}_A \otimes \boldsymbol{N}_A$ and $\boldsymbol{n}_A \otimes \boldsymbol{n}_A$ terms as the Lagrangian and Eulerian eigenvalue bases respectively. For convenience we introduce the notation $\boldsymbol{N}_A \otimes \boldsymbol{N}_A = \boldsymbol{M}_A$ and $\boldsymbol{n}_A \otimes \boldsymbol{n}_A = \boldsymbol{m}_A$.

The calculation of the eigenvalues proceeds in the conventional manner (Fitz-Gerald and Peckham (1998)) by solving the characteristic equation

$$\det\left[\boldsymbol{C} - \Lambda \boldsymbol{I}\right] = 0 \tag{3.17}$$

here for the case of the right Cauchy-Green strain tensor. Due to $\boldsymbol{C}$ being a second order, 3×3 tensor, it will have up to three distinct eigenvalues.

The determination of eigenvalue bases is wholly contingent on the presence of distinct eigenvalues. Coalescence (equality) of two or more eigenvalues means that the corresponding eigenvalue bases cannot be algebraically determined. It is this fact that necessitates the separate treatment of spectral reconstruction dependent on the exclusivity of the three eigenvalues as is done by both Simo and Taylor (1991) and Itskov (2001).

At this point it is convenient to exploit the pull back of the Eulerian eigenvalue bases, recalling the spectral decomposition of $\boldsymbol{F}$ from equation (3.16) such that

$$\boldsymbol{F}^{-1}\left(\boldsymbol{m}_A\right)\boldsymbol{F}^{-T} = \lambda_A^{-2}\boldsymbol{M}_A = \widetilde{\boldsymbol{M}}_A \tag{3.18}$$

where here we refer to $\widetilde{\boldsymbol{M}}_A$ as the modified Lagrangian eigenvalue base noting that the push forward of $\widetilde{\boldsymbol{M}}_A$ results directly in the actual Eulerian eigenvalue base $\boldsymbol{m}_A$.

Itskov (2001) provides a valuable definition of the Lagrangian eigenvalue bases $\boldsymbol{M}_A$. So as to facilitate a more straight forward transition to Eulerian description, primarily for the

further development that follows, we carry out a similar procedure for $\widetilde{\boldsymbol{M}}_A$ in Appendix C.1. The results for these modified Lagrangian eigenvalue bases for all cases of eigenvalue exclusivity are presented in the appendix. Taking the second order push forward of the expression for the case of three distinct eigenvalues[2], the Eulerian eigenvalue bases can be found via

$$\boldsymbol{m}_A = \frac{\boldsymbol{b}^2 - (\mathrm{I}_C - \Lambda_A)\,\boldsymbol{b} + \mathrm{III}_C \Lambda_A^{-1} \boldsymbol{I}}{D_A} \qquad A = 1, 2, 3 \tag{3.19}$$

A similar procedure can be performed for the other cases.

Extending the concept of spectral decomposition to the multiplicative split of $\boldsymbol{C}$ into volumetric and deviatoric components, follows directly from $(3.4)_1$, $(3.5)_1$, $(3.6)_1$ and (3.14) such that

$$\boldsymbol{C} = \boldsymbol{C}_{vol} \bar{\boldsymbol{C}} \tag{3.20}$$

$$\boldsymbol{C}_{vol} = \boldsymbol{F}_{vol}^T \boldsymbol{F}_{vol} \qquad = J^{2/3} \boldsymbol{I} \tag{3.21}$$

$$\bar{\boldsymbol{C}} = \bar{\boldsymbol{F}}^T \bar{\boldsymbol{F}} \qquad = \sum_{A=1}^{3} J^{-2/3} \lambda_A^2 \boldsymbol{N}_A \otimes \boldsymbol{N}_A \qquad = \sum_{A=1}^{3} \bar{\lambda}_A^2 \boldsymbol{N}_A \otimes \boldsymbol{N}_A \tag{3.22}$$

where in principal space $J = \lambda_1 \lambda_2 \lambda_3$ and where $\bar{\lambda}_A = J^{-1/3} \lambda_A$ are defined as the deviatoric principal stretches. An identical procedure can be carried out for the Eulerian counterpart, $\boldsymbol{b}$. It is important to note that the eigenvalue bases remain unchanged after the volumetric-deviatoric separation.

As was discussed in Section 3.1.2, the constitutive behavior of hyperelastic materials is represented by an expression of the thermodynamic free energy, equation (3.7). The reduction of this constitutive representation into principal planes requires reformulation of the free energy expression in terms of principal stretch quantities as

$$\psi = \hat{\psi}\left(\lambda_1, \lambda_2, \lambda_3\right) = \hat{\mathcal{U}}\left(J\right) + \hat{\omega}\left(\bar{\lambda}_1, \bar{\lambda}_2, \bar{\lambda}_3\right) \tag{3.23}$$

Note (3.23) is consistent with (3.7) because the deviatoric term (here $\hat{\omega}$) is now functional on the deviatoric principal stretches $\bar{\lambda}_A$.

[2]Note $\boldsymbol{F}\boldsymbol{C}\boldsymbol{F}^T = \boldsymbol{b}^2$, $\boldsymbol{F}\boldsymbol{I}\boldsymbol{F}^T = \boldsymbol{b}$ and $\boldsymbol{F}\boldsymbol{C}^{-1}\boldsymbol{F}^T = \boldsymbol{I}$

3.1.4 Stress expression in principal stretches

Equation (3.23) constitutes a reformulation of the hyperelastic constitutive theory in principal planes. It is, however, still necessary to relate this potential to tensor space stress for the majority of solid mechanics implementations. This can be achieved via the direct modification of (3.9) following the methodology presented here.

Substituting (3.23) and with further implementation of the chain rule, the second Piola-Kirchhoff stress tensor expression becomes

$$\boldsymbol{S} = 2\frac{\partial \hat{\mathcal{U}}}{\partial J}\frac{\partial J}{\partial \boldsymbol{C}} + 2\sum_{A=1}^{3}\sum_{B=1}^{3}\frac{\partial \hat{\omega}}{\partial \bar{\lambda}_B}\frac{\partial \bar{\lambda}_B}{\partial \lambda_A}\frac{\partial \lambda_A}{\partial \boldsymbol{C}} \tag{3.24}$$

For convenience here, we introduce the principal deviatoric stress term β_A such that

$$\beta_A = \sum_{B=1}^{3}\frac{\partial \hat{\omega}}{\partial \bar{\lambda}_B}\frac{\partial \bar{\lambda_B}}{\partial \lambda_A}\lambda_A = \frac{\partial \hat{\omega}}{\partial \varepsilon_A} \qquad A = 1,2,3 \tag{3.25}$$

where ε_A are the principal logarithmic strains and so the second Piola-Kirchhoff stress is then

$$\boldsymbol{S} = 2\frac{\partial \hat{\mathcal{U}}}{\partial J}\frac{\partial J}{\partial \boldsymbol{C}} + \sum_{A=1}^{3}\beta_A\left(2\lambda_A^{-1}\frac{\partial \lambda_A}{\partial \boldsymbol{C}}\right) \tag{3.26}$$

Within (3.26) it can be observed that the jacobian and principal stretch derivative terms, $\partial_{\boldsymbol{C}} J$ and $\partial_{\boldsymbol{C}}\lambda_A$, must be second order tensors and so consequently these can be viewed as driving the spectral reconstruction from principal quantities to tensor space. Once again Itskov (2001) provides a complete derivation of the eigenvalue derivatives, functional on the Lagrangian eigenvalue bases. An alternative derivation is provided in Appendices C.2 and C.3 for the principal stretch and jacobian derivatives, functional on the modified Lagrangian eigenvalue bases $\widetilde{\boldsymbol{M}}_A$.

Using the results from Appendices C.2 and C.3, the stress tensor expressions for the three different cases of eigenvalue exclusivity are defined as follows

(1) Distinct eigenvalues $\Lambda_1 \neq \Lambda_2 \neq \Lambda_3$

From (C.19) and (C.29), the second Piola-Kirchhoff stress expression becomes

$$\boldsymbol{S} = \frac{\partial \hat{\mathcal{U}}}{\partial J}J\boldsymbol{C}^{-1} + \sum_{A=1}^{3}\beta_A\widetilde{\boldsymbol{M}}_A \tag{3.27}$$

Following the push forward (3.10), the Cauchy stress tensor is given by[3]

$$\boxed{\boldsymbol{\sigma} = \frac{\partial \hat{\mathcal{U}}}{\partial J}\boldsymbol{I} + \frac{1}{J}\sum_{A=1}^{3}\beta_A \boldsymbol{m}_A} \tag{3.28}$$

(2) Double coalescence of eigenvalues $\Lambda_1 \neq \Lambda_2 = \Lambda_3 = \Lambda$

Noting that because $\lambda_2 = \lambda_3 = \lambda$, following with some development from (3.25), it can be shown that correspondingly $\beta_2 = \beta_3 = \beta$ such that

$$\boldsymbol{S} = 2\frac{\partial \hat{\mathcal{U}}}{\partial J}\frac{\partial J}{\partial \boldsymbol{C}} + \beta_1 2\lambda_1^{-1}\frac{\partial \lambda_1}{\partial \boldsymbol{C}} + \beta 2\lambda^{-1}\left(\frac{\partial \lambda_2}{\partial \boldsymbol{C}} + \frac{\partial \lambda_3}{\partial \boldsymbol{C}}\right) \tag{3.29}$$

It is now possible to substitute (C.23), (C.24) and (C.29) to yield

$$\boldsymbol{S} = \frac{\partial \hat{\mathcal{U}}}{\partial J}J\boldsymbol{C}^{-1} + \beta_1 \widetilde{\boldsymbol{M}}_1 + \beta\left(\boldsymbol{C}^{-1} - \widetilde{\boldsymbol{M}}_1\right) \tag{3.30}$$

and again following the push forward, the Cauchy stress tensor is given by

$$\boxed{\boldsymbol{\sigma} = \frac{\partial \hat{\mathcal{U}}}{\partial J}\boldsymbol{I} + \frac{1}{J}\beta\boldsymbol{I} + \frac{1}{J}\left(\beta_1 - \beta\right)\boldsymbol{m}_1} \tag{3.31}$$

(3) Triple coalescence of eigenvalues $\Lambda_1 = \Lambda_2 = \Lambda_3 = \Lambda$

Exploiting equation (3.25), it is a straightforward proof to show that when $\lambda_1 = \lambda_2 = \lambda_3 = \lambda$, then correspondingly $\beta_1 = \beta_2 = \beta_3 = \beta$. It is important, also, to observe that due to the deviatoric nature of β_A, then

$$\beta_1 + \beta_2 + \beta_3 = 0 \tag{3.32}$$

and as a consequence, the deviatoric stress term will vanish. The result that stress is wholly volumetric when all eigenvectors are equal is unsurprising. Substituting (3.32) and (C.29) into (3.26) gives

$$\boldsymbol{S} = \frac{\partial \hat{\mathcal{U}}}{\partial J}J\boldsymbol{C}^{-1} \tag{3.33}$$

[3]Note, equation boxes signify the final developed form of expressions which must be incorporated into an updated Lagrangian, implicit numerical code.

and following the push forward, the Cauchy stress tensor is given by

$$\boxed{\boldsymbol{\sigma} = \frac{\partial \hat{\mathcal{U}}}{\partial J}\boldsymbol{I}} \tag{3.34}$$

3.1.5 Closed-form tangential modulus expression in principal stretches

It remains to repeat the process of Section 3.1.4 to incorporate the principal stretch free energy expression (3.23) into the closed-form tangential modulus expression, (3.12).

In view of the principal space free energy, (3.23), the Lagrangian form of the tangential modulus expression becomes

$$\begin{aligned}\mathbb{C} = & \underbrace{4\frac{\partial^2 \hat{\mathcal{U}}}{\partial J^2}\frac{\partial J}{\partial \boldsymbol{C}} \otimes \frac{\partial J}{\partial \boldsymbol{C}} + 4\frac{\partial \hat{\mathcal{U}}}{\partial J}\frac{\partial^2 J}{\partial \boldsymbol{C}^2}}_{vol} \\ & + \underbrace{2\sum_{A=1}^{3}\sum_{B=1}^{3}\sum_{C=1}^{3}\frac{\partial \beta_A}{\partial \bar{\lambda}_C}\frac{\partial \bar{\lambda_C}}{\partial \lambda_B}\frac{\partial \lambda_B}{\partial \boldsymbol{C}} \otimes \left(2\lambda_A^{-1}\frac{\partial \lambda_A}{\partial \boldsymbol{C}}\right) + 2\sum_{A=1}^{3}\beta_A\frac{\partial}{\partial \boldsymbol{C}}\left(2\lambda_A^{-1}\frac{\partial \lambda_A}{\partial \boldsymbol{C}}\right)}_{dev} \\ = & \mathbb{C}_{vol} + \bar{\mathbb{C}}\end{aligned} \tag{3.35}$$

Again it is evident that the jacobian and principal stretch derivative terms are responsible for the spectral reconstruction from principal to tensor space. In this case, $\partial_{\boldsymbol{C}} J \otimes \partial_{\boldsymbol{C}} J$, $\partial^2_{\boldsymbol{CC}} J$, $\partial_{\boldsymbol{C}} \lambda_B \otimes \partial_{\boldsymbol{C}} \lambda_A$ and $\partial^2_{\boldsymbol{CC}} \lambda_A$ are fourth order tensors quantities that must be established.

Initially devoting our attention to the volumetric modulus term, $\mathbb{C}_{vol}$, the jacobian derivative terms $\partial_{\boldsymbol{C}} J$ and $\partial^2_{\boldsymbol{CC}} J$ have been determined in Appendix C.3 such that

$$\mathbb{C}_{vol} = J\left(\frac{\partial \hat{\mathcal{U}}}{\partial J} + J\frac{\partial^2 \hat{\mathcal{U}}}{\partial J^2}\right)\boldsymbol{C}^{-1} \otimes \boldsymbol{C}^{-1} - 2J\frac{\partial \hat{\mathcal{U}}}{\partial J}\boldsymbol{I}^{\boldsymbol{C}^{-1}} \tag{3.36}$$

Carrying out the fourth order push forward of this expression[4], the volumetric component of the Eulerian tangential modulus is now

$$\boxed{\boldsymbol{c}_{vol} = \left(\frac{\partial \hat{\mathcal{U}}}{\partial J} + J\frac{\partial^2 \hat{\mathcal{U}}}{\partial J^2}\right)\boldsymbol{I} \otimes \boldsymbol{I} - 2\frac{\partial \hat{\mathcal{U}}}{\partial J}\boldsymbol{I}'} \tag{3.37}$$

[4]Observing the specific fourth order push forward results $\boldsymbol{F}\boldsymbol{F}\left(\boldsymbol{C}^{-1} \otimes \boldsymbol{C}^{-1}\right)\boldsymbol{F}^T\boldsymbol{F}^T = (I \otimes I)_{ijkl} = \delta_{ij}\delta_{kl}$ and $\boldsymbol{F}\boldsymbol{F}(\boldsymbol{I}^{\boldsymbol{C}^{-1}})\boldsymbol{F}^T\boldsymbol{F}^T = I'_{ijkl} = \frac{1}{2}\left(\delta_{ik}\delta_{jl} + \delta_{il}\delta_{jk}\right)$.

Because the jacobian first and second derivatives are invariant to the conditions of eigenvalue exclusivity, this expression holds for all cases.

For the deviatoric tangential modulus expression, $\bar{\mathbb{C}}$, it is convenient to introduce the tangential operator term γ_{AB} such that

$$\gamma_{AB} = \sum_{C=1}^{3} \frac{\partial \beta_A}{\partial \bar{\lambda}_C} \frac{\partial \bar{\lambda_C}}{\partial \lambda_B} \lambda_B = \frac{\partial \beta_A}{\partial \varepsilon_B} \qquad A, B = 1, 2, 3 \tag{3.38}$$

where ε_B are again the principal logarithmic strains. The deviatoric tangential modulus term then reduces to

$$\bar{\mathbb{C}} = \sum_{A=1}^{3} \sum_{B=1}^{3} \gamma_{AB} \left(2\lambda_B^{-1} \frac{\partial \lambda_B}{\partial \boldsymbol{C}} \right) \otimes \left(2\lambda_A^{-1} \frac{\partial \lambda_A}{\partial \boldsymbol{C}} \right) + 2 \sum_{A=1}^{3} \beta_A \frac{\partial}{\partial \boldsymbol{C}} \left(2\lambda_A^{-1} \frac{\partial \lambda_A}{\partial \boldsymbol{C}} \right) \tag{3.39}$$

Equation (3.39) is in generalized, closed-form, applicable to all conditions of eigenvalue exclusivity. For practical implementation, explicit expression of the first and second principal stretch differentials must be input[5]. The first principal stretch differentials have been formulated in Appendix C.2. Again a modification of the methodology of Itskov (2001) is used in Appendix C.4 to establish the second principal stretch derivatives, functional on the modified Lagrangian eigenvalue bases as required.

Implementing the results from Appendices C.2 and C.4, the specific results for deviatoric tangential modulus, dependent on the different states of eigenvalue exclusivity are presented in the following

(1) Distinct eigenvalues $\Lambda_1 \neq \Lambda_2 \neq \Lambda_3$

For the case of distinct eigenvalues, all three first principal stretch differentials can be determined from (C.19), such that

$$\bar{\mathbb{C}} = \sum_{A=1}^{3} \sum_{B=1}^{3} \gamma_{AB} \widetilde{\boldsymbol{M}}_A \otimes \widetilde{\boldsymbol{M}}_B + 2 \sum_{A=1}^{3} \beta_A \partial_{\boldsymbol{C}} \widetilde{\boldsymbol{M}}_A \tag{3.40}$$

[5]Note here that often the $\partial_{\boldsymbol{C}} \left(2\lambda_A^{-1} \partial_{\boldsymbol{C}} \lambda_A \right)$ differential is carried out via $\partial_{\boldsymbol{C}} \widetilde{\boldsymbol{M}}_A$ (Itskov (2001)) with subsequent correction for eigenvalue coalescence, however for the circumstances when the eigenvalue bases are indeterminate, it would seem more accurate to carry out this derivative in the general form of (3.39). Refer to Appendix C.4.

The fourth order modified eigenvalue base derivatives, $\partial_{\boldsymbol{C}}\widetilde{\boldsymbol{M}}_A$, are found in Appendix C.4. Carrying out the fourth order push forward gives the deviatoric component of the closed-form Eulerian tangential modulus

$$\boxed{\bar{\boldsymbol{c}} = \frac{1}{J}\sum_{A=1}^{3}\sum_{B=1}^{3}\gamma_{AB}\boldsymbol{m}_A \otimes \boldsymbol{m}_B + \frac{2}{J}\sum_{A=1}^{3}\beta_A \partial_{\boldsymbol{g}}\boldsymbol{m}_A} \tag{3.41}$$

where $\partial_{\boldsymbol{g}}\boldsymbol{m}_A$ results from the fourth order push forward[6] of the modified eigenvalue base derivative expression (C.36) giving

$$\partial_{\boldsymbol{g}}\boldsymbol{m}_A = \frac{1}{D_A}\left(\boldsymbol{I}^{\boldsymbol{b}} - \sum_{B=1}^{3}\left[2\Lambda_B^2 - \left(\mathrm{I}_{\boldsymbol{C}} - \Lambda_A\right)\Lambda_B\right]\boldsymbol{m}_B \otimes \boldsymbol{m}_B - \mathrm{III}_{\boldsymbol{C}}\Lambda_A^{-1}\boldsymbol{I}'\right) \tag{3.42}$$

(2) Double coalescence of eigenvalues $\Lambda_1 \neq \Lambda_2 = \Lambda_3 = \Lambda$

The first and second principal stretch derivative terms from (3.39) for the single distinct principal stretch (Λ_1) can be determined explicitly given the results from Appendices C.2 and C.4. As such, these terms can be directly implemented as was the procedure above. For the equal principal stretches, however, the explicit first and second principal stretch derivatives remain undetermined and so further development is required.

By utilizing the combined differential terms from the Appendices, equations (C.24), (C.46) and (C.47), and by exploiting the eigenvalue equality, it is possible to express the deviatoric Lagrangian tangential modulus tensor, independent of the unknown principal stretch differentials. A full account of this procedure is provided in Appendix D.1. The resulting reduced expression is

$$\begin{aligned}\bar{\mathbb{C}} = {} & \gamma_{11}\widetilde{\boldsymbol{M}}_1 \otimes \widetilde{\boldsymbol{M}}_1 + \gamma_{22}\left(\boldsymbol{C}^{-1} - \widetilde{\boldsymbol{M}}_1\right) \otimes \left(\boldsymbol{C}^{-1} - \widetilde{\boldsymbol{M}}_1\right) \\ & + \gamma_{21}\left(\boldsymbol{C}^{-1} - \widetilde{\boldsymbol{M}}_1\right) \otimes \widetilde{\boldsymbol{M}}_1 + \gamma_{12}\widetilde{\boldsymbol{M}}_1 \otimes \left(\boldsymbol{C}^{-1} - \widetilde{\boldsymbol{M}}_1\right) \\ & - 2\beta\boldsymbol{I}^{\boldsymbol{C}^{-1}} + 2\left(\beta_1 - \beta\right)\partial_{\boldsymbol{C}}\widetilde{\boldsymbol{M}}_1\end{aligned} \tag{3.43}$$

where the single fourth order modified eigenvalue base derivative, $\partial_{\boldsymbol{C}}\widetilde{\boldsymbol{M}}_1$, is defined in Appendix C.4. Carrying out the fourth order push forward of (3.43), the deviatoric component of the closed-form Eulerian tangential modulus becomes

[6] Noting the push forward of the fourth order, symmetric identity tensor $\boldsymbol{F}\boldsymbol{F}(\boldsymbol{I}')\boldsymbol{F}^T\boldsymbol{F}^T = I^{\boldsymbol{b}}_{ijkl} = \frac{1}{2}\left(b_{ik}b_{jl} + b_{il}b_{jk}\right)$

$$\boxed{\begin{aligned}\bar{\boldsymbol{c}} &= \frac{1}{J}\gamma_{11}\boldsymbol{m}_1\otimes\boldsymbol{m}_1+\frac{1}{J}\gamma_{22}\left(\boldsymbol{I}-\boldsymbol{m}_1\right)\otimes\left(\boldsymbol{I}-\boldsymbol{m}_1\right)\\ &+ \frac{1}{J}\gamma_{21}\left(\boldsymbol{I}-\boldsymbol{m}_1\right)\otimes\boldsymbol{m}_1+\frac{1}{J}\gamma_{12}\boldsymbol{m}_1\otimes\left(\boldsymbol{I}-\boldsymbol{m}_1\right)\\ &- \frac{2}{J}\beta_2\boldsymbol{I'}+\frac{2}{J}\left(\beta_1-\beta_2\right)\partial_{\boldsymbol{g}}\boldsymbol{m}_1\end{aligned}} \tag{3.44}$$

where, as before, $\partial_{\boldsymbol{g}}\boldsymbol{m}_1$ is found from the fourth order push forward of the modified eigenvalue base derivative expression (C.45), such that

$$\partial_{\boldsymbol{g}}\boldsymbol{m}_1=\frac{1}{D_1}\left(\boldsymbol{I^b}-2\Lambda_1\left(\Lambda_1-\Lambda\right)\boldsymbol{m}_1\otimes\boldsymbol{m}_1-\mathrm{III}_{\boldsymbol{C}}\Lambda_1^{-1}\boldsymbol{I'}\right) \tag{3.45}$$

(3) Triple coalescence of eigenvalues $\Lambda_1=\Lambda_2=\Lambda_3=\Lambda$

For the triple coalescence of eigenvalues, it is not possible to explicitly define any of the first or second principal stretch derivatives. Instead, as before, the combined differential expressions from the Appendices, equations (C.25) and (C.53), can be applied along with the eigenvalue equality, to express the deviatoric Lagrangian tangential modulus tensor independent of all the principal stretch differentials.

It is, however, initially advantageous to recall (3.32) and the consequential result that when all three eigenvalues are equal, $\beta_A=0$ for all $A=1,2,3$. As a result

$$2\sum_{A=1}^{3}\beta_A\frac{\partial}{\partial\boldsymbol{C}}\left(2\lambda_A^{-1}\frac{\partial\lambda_A}{\partial\boldsymbol{C}}\right)=\boldsymbol{0} \tag{3.46}$$

and (3.39) becomes greatly simplified.

In view of (3.46), expansion and manipulation of the reduced form of (3.39) is carried out in Appendix D.2 to determine the deviatoric Lagrangian tangential modulus expression, with the result

$$\bar{\mathbb{C}}=\gamma\left(\boldsymbol{I}^{\boldsymbol{C}^{-1}}-\tfrac{1}{3}\boldsymbol{C}^{-1}\otimes\boldsymbol{C}^{-1}\right) \tag{3.47}$$

where the scalar, γ, is defined in Appendix D.2. After the fourth order push forward of this expression, the deviatoric component of the closed-form Eulerian tangential modulus for triple coalescence of eigenvalues can be given by

$$\boxed{\bar{\boldsymbol{c}}=\frac{1}{J}\gamma\left(\boldsymbol{I'}-\tfrac{1}{3}\boldsymbol{I}\otimes\boldsymbol{I}\right)} \tag{3.48}$$

Thus now the complete, closed-form tangential modulus has been defined for generalized hyperelasticity in principal space, for all possible cases of eigenvalue equality. In what follows this theory will be extended to the inelastic case.

3.2 Extension for generalized inelasticity

Developing on the formulations of Section 3.1, the generalized stress and closed-form tangential modulus expressions must be determined for the case where both elastic and inelastic deformation mechanisms are present (as for both viscoelasticity and viscoplasticity). Particular attention is again paid to the implementation of principal space constitutive theories. While a similar methodology is used to that in Section 3.1, there are some important implications associated with the introduction of inelasticity that are by and large treated unsatisfactorily within the literature. It is the objective here to address this situation for the general case.

3.2.1 Alternate treatment of the deformation gradient

For the case where material response exhibits both elastic and inelastic components, it is initially convenient to introduce two additional manipulations of the deformation gradient.

The first of these is the conventional multiplicative split of the deformation gradient into elastic and inelastic components (Kröner (1960); Lee and Liu (1967)) as was treated in Section 2.4

$$\boldsymbol{F} = \boldsymbol{F}^e \boldsymbol{F}^i \tag{3.49}$$

Recalling the earlier separation of response into volumetric and deviatoric components then it follows that

$$\boldsymbol{F} = \boldsymbol{F}^e_{vol} \boldsymbol{F}^i_{vol} \bar{\boldsymbol{F}}^e \bar{\boldsymbol{F}}^i \tag{3.50}$$

where

$$\begin{aligned} \boldsymbol{F}^e_{vol} &= J^{e\,1/3} \boldsymbol{I} & \boldsymbol{F}^i_{vol} &= J^{i\,1/3} \boldsymbol{I} \\ \bar{\boldsymbol{F}}^e &= J^{e\,-1/3} \boldsymbol{F}^e & \bar{\boldsymbol{F}}^i &= J^{i\,-1/3} \boldsymbol{F}^i \end{aligned} \tag{3.51}$$

Correspondingly, the elastic components of the right and left Cauchy-Green strain tensors

can be given by

$$\boldsymbol{C}^e = J^{e\,2/3}\bar{\boldsymbol{F}}^{e\,T}\bar{\boldsymbol{F}}^e = J^{e\,2/3}\bar{\boldsymbol{C}}^e \tag{3.52}$$

$$\boldsymbol{b}^e = J^{e\,2/3}\bar{\boldsymbol{F}}^e\bar{\boldsymbol{F}}^{e\,T} = J^{e\,2/3}\bar{\boldsymbol{b}}^e \tag{3.53}$$

The second manipulation of the deformation gradient follows the work of Reese and Govindjee (1998a). For a time discretization of the deformation history, over the time step $\Delta t_{n+1} = t_{n+1} - t_n$, the current deformation gradient can be given by

$$\boldsymbol{F}_{n+1} = \boldsymbol{F}^{e\,tr}_{n+1}\boldsymbol{F}^i_n \tag{3.54}$$

where $\boldsymbol{F}^{e\,tr}_{n+1}$ is an initial trial estimate of the current elastic component while $\boldsymbol{F}^i_n$ is the inelastic deformation at the end of the previous time step. For the remainder of this section we will omit the time subscripts from current quantities (i.e. when $t = t_{n+1}$). The actual interpretation of (3.54) will become clearer within the specific operator split algorithmic development provided later in Section 3.3. Within the context of the current development, it is sufficient to note the significance of Reese and Govindjee's observation that $\boldsymbol{F}^i_n$ is constant at current time $t = t_{n+1}$.

3.2.2 Implications for tensor space thermodynamics

The thermodynamic potential of materials exhibiting inelasticity involves additional functionality to that defined earlier for the purely hyperelastic case (Section 3.1.2). This reflects the multiple thermodynamic mechanisms at play.

Following authors such as Holzapfel (1996); Holzapfel and Simo (1996), Perić (1993), Nedjar (2002a) and Simo and Hughes (2000) and in view of equations (2.8) and (3.52), the free energy for generalized inelastic materials can be given by

$$\psi = \hat{\psi}\left(\boldsymbol{C}^e, \boldsymbol{\xi}\right) = \hat{\mathcal{U}}\left(J^e\right) + \hat{\mathcal{W}}\left(\bar{\boldsymbol{C}}^e\right) + \hat{\mathcal{H}}\left(\boldsymbol{\xi}\right) \tag{3.55}$$

where this is functional on the elastic components of material strain, and $\boldsymbol{\xi}$, some set of internal variables commonly associated with inelastic dissipation mechanisms (Simo (1992); Simo and Hughes (2000); Perić and Dettmer (2003)).

As for the hyperelastic case (Section 3.1.2), the second Piola-Kirchhoff stress expression

is attained via the manipulation of the Clausius-Duhem form of the second law of thermodynamics from Appendix A. From (2.12), for some arbitrary element with both elastic and inelastic components

$$\boldsymbol{S} = 2\frac{\partial \hat{\psi}}{\partial \boldsymbol{C}} = 2\boldsymbol{F}^{i\,-1}\frac{\partial \hat{\psi}}{\partial \boldsymbol{C}^{e}}\boldsymbol{F}^{i\,-T} \tag{3.56}$$

Incorporating the decoupled form of (3.55), using the chain rule then

$$\boldsymbol{S} = 2\boldsymbol{F}^{i\,-1}\left(\frac{\partial \hat{\mathcal{U}}}{\partial J^{e}}\frac{\partial J^{e}}{\partial \boldsymbol{C}^{e}} + \frac{\partial \hat{\mathcal{W}}}{\partial \bar{\boldsymbol{C}}^{e}}\frac{\partial \bar{\boldsymbol{C}}^{e}}{\partial \boldsymbol{C}^{e}}\right)\boldsymbol{F}^{i\,-T} \tag{3.57}$$

Following equation (3.11), the Lagrangian tangential modulus tensor for generalized inelasticity is found via the differential of (3.57)

$$\mathbb{C} = 2\frac{\partial \boldsymbol{S}}{\partial \boldsymbol{C}} = 2\frac{\partial}{\partial \boldsymbol{C}}\left\{2\boldsymbol{F}^{i\,-1}\left(\frac{\partial \hat{\mathcal{U}}}{\partial J^{e}}\frac{\partial J^{e}}{\partial \boldsymbol{C}^{e}} + \frac{\partial \hat{\mathcal{W}}}{\partial \bar{\boldsymbol{C}}^{e}}\frac{\partial \bar{\boldsymbol{C}}^{e}}{\partial \boldsymbol{C}^{e}}\right)\boldsymbol{F}^{i\,-T}\right\} \tag{3.58}$$

It is convenient to exploit the second separation of the deformation gradient (3.54), such that the right Cauchy-Green strain tensor takes the alternate form

$$\boldsymbol{C} = \boldsymbol{F}_{n}^{i\,T}\boldsymbol{F}^{e\,tr\,T}\boldsymbol{F}^{e\,tr}\boldsymbol{F}_{n}^{i} = \boldsymbol{F}_{n}^{i\,T}\boldsymbol{C}^{e\,tr}\boldsymbol{F}_{n}^{i} \tag{3.59}$$

where $\boldsymbol{C}^{e\,tr}$ is the elastic trial right Cauchy-Green strain tensor[7]. Using this expression, the separated forms of the deformation gradient (3.49) and (3.54), and observing that because $\boldsymbol{F}_{n}^{i}$ is constant at time t_{n+1}, it can be taken outside the differential, then the Lagrangian modulus term becomes

$$\mathbb{C} = 2\boldsymbol{F}_{n}^{i\,-1}\boldsymbol{F}_{n}^{i\,-1}\frac{\partial}{\partial \boldsymbol{C}^{e\,tr}}\left\{2\boldsymbol{F}^{e\,tr\,-1}\boldsymbol{F}^{e}\left(\frac{\partial \hat{\mathcal{U}}}{\partial J^{e}}\frac{\partial J^{e}}{\partial \boldsymbol{C}^{e}} + \frac{\partial \hat{\mathcal{W}}}{\partial \bar{\boldsymbol{C}}^{e}}\frac{\partial \bar{\boldsymbol{C}}^{e}}{\partial \boldsymbol{C}^{e}}\right)\boldsymbol{F}^{e\,T}\boldsymbol{F}^{e\,tr\,-T}\right\}\boldsymbol{F}_{n}^{i\,-T}\boldsymbol{F}_{n}^{i\,-T} \tag{3.60}$$

The motivation for expressing the tangential modulus expression in this way will become clearer within the principal space development that follows.

3.2.3 Spectral decomposition of elastic strain

For practical applications, as was the case for pure hyperelasticity, the assumption of isotropy within general inelasticity facilitates the reduction of constitutive representation

[7] It follows directly that the Eulerian counterpart elastic trial left Cauchy-Green strain tensor be defined by $\boldsymbol{b}^{e\,tr} = \boldsymbol{F}^{e\,tr}\boldsymbol{F}^{e\,tr\,T}$.

into principal planes.

By an identical methodology to that used for the total values in expressions (3.14) to (3.16), it is possible to spectrally decompose the elastic components of right and left Cauchy-Green stain, $\boldsymbol{C}^e$ and $\boldsymbol{b}^e$, and the deformation gradient $\boldsymbol{F}^e$. It follows that for $A = 1, 2, 3$ the elastic eigenvalues Λ^e_A, the elastic principal stretches λ^e_A, and the elastic Lagrangian and Eulerian eigenvalue bases, $\boldsymbol{N}^{(e)}_A \otimes \boldsymbol{N}^{(e)}_A = \boldsymbol{M}^{(e)}_A$ and $\boldsymbol{n}^{(e)}_A \otimes \boldsymbol{n}^{(e)}_A = \boldsymbol{m}^{(e)}_A$, can be defined. The push forward of the Eulerian eigenvalue base in elastic space gives

$$\boldsymbol{F}^{e\,-1}(\boldsymbol{m}^{(e)}_A)\boldsymbol{F}^{e\,-T} = \lambda^{e\,-2}_A \boldsymbol{M}^{(e)}_A = \widetilde{\boldsymbol{M}}^{(e)}_A \tag{3.61}$$

where $\widetilde{\boldsymbol{M}}^{(e)}_A$ are the modified elastic Lagrangian eigenvalue bases.

Because the moduli expression (3.60) involves elastic trial values also, the similar spectral decompositions of $\boldsymbol{C}^{e\,tr}$, $\boldsymbol{b}^{e\,tr}$ and $\boldsymbol{F}^{e\,tr}$ give the elastic trial eigenvalues $\Lambda^{e\,tr}_A$, the elastic trial principal stretches $\lambda^{e\,tr}_A$, and the elastic trial Lagrangian and Eulerian eigenvalue bases, $\boldsymbol{N}^{(e\,tr)}_A \otimes \boldsymbol{N}^{(e\,tr)}_A = \boldsymbol{M}^{(e\,tr)}_A$ and $\boldsymbol{n}^{(e\,tr)}_A \otimes \boldsymbol{n}^{(e\,tr)}_A = \boldsymbol{m}^{(e\,tr)}_A$. The push forward of the Eulerian eigenvalue base in elastic trial space gives

$$\boldsymbol{F}^{e\,tr\,-1}(\boldsymbol{m}^{(e\,tr)}_A)\boldsymbol{F}^{e\,tr\,-T} = \lambda^{e\,tr\,-2}_A \boldsymbol{M}^{(e\,tr)}_A = \widetilde{\boldsymbol{M}}^{(e\,tr)}_A \tag{3.62}$$

where $\widetilde{\boldsymbol{M}}^{(e\,tr)}_A$ are the modified elastic trial Lagrangian eigenvalue bases.

Referring to authors such as Simo (1992), the principal planes determined for the initial elastic trial state are equal to those for the final elastic state, i.e. $\boldsymbol{m}^{(e\,tr)}_A = \boldsymbol{m}^{(e)}_A$ and $\boldsymbol{M}^{(e\,tr)}_A = \boldsymbol{M}^{(e)}_A$. Given a similar development to that presented in Appendix C.1, the elastic Eulerian eigenvalue bases can be defined[8]

$$\boldsymbol{m}^{(e)}_A = \boldsymbol{m}^{(e\,tr)}_A = \frac{\boldsymbol{b}^{e\,tr\,2} - \left(\mathrm{I}^{e\,tr}_C - \Lambda^{e\,tr}_A\right)\boldsymbol{b}^{e\,tr} + \mathrm{III}^{e\,tr}_C \Lambda^{e\,tr\,-1}_A \boldsymbol{I}}{D^{e\,tr}_A} \qquad A = 1, 2, 3 \tag{3.63}$$

where

$$\begin{aligned} \mathrm{I}^{e\,tr}_C &= \Lambda^{e\,tr}_1 + \Lambda^{e\,tr}_2 + \Lambda^{e\,tr}_3 \\ \mathrm{II}^{e\,tr}_C &= \Lambda^{e\,tr}_1 \Lambda^{e\,tr}_2 + \Lambda^{e\,tr}_1 \Lambda^{e\,tr}_3 + \Lambda^{e\,tr}_2 \Lambda^{e\,tr}_3 \\ \mathrm{III}^{e\,tr}_C &= \Lambda^{e\,tr}_1 \Lambda^{e\,tr}_2 \Lambda^{e\,tr}_3 \end{aligned} \tag{3.64}$$

[8]Note that for the elastic case $\boldsymbol{F}^e \boldsymbol{C}^e \boldsymbol{F}^{e\,T} = \boldsymbol{b}^{e\,2}$, $\boldsymbol{F}^e \boldsymbol{I} \boldsymbol{F}^{e\,T} = \boldsymbol{b}^e$ and $\boldsymbol{F}^e \boldsymbol{C}^{e\,-1} \boldsymbol{F}^{e\,T} = \boldsymbol{I}$.

and

$$D_A^{e\,tr} = \left(\Lambda_A^{e\,tr} - \Lambda_B^{e\,tr}\right)\left(\Lambda_A^{e\,tr} - \Lambda_C^{e\,tr}\right) \qquad A \neq B \neq C \tag{3.65}$$

and where determination of $\boldsymbol{m}_A^{(e)}$ is conveniently expressed functional on the initial elastic trial values only.

It is finally pertinent to observe that, in principal space, the elastic jacobian is defined $J^e = \lambda_1^e \lambda_2^e \lambda_3^e$ and also the elastic deviatoric principal stretches are given by $\bar{\lambda}_A^e = J^{e\,-1/3}\lambda_A^e$. The free energy expression for generalized inelasticity (3.55), is thus expressed in principal planes via

$$\psi = \hat{\psi}(\lambda_1^e, \lambda_2^e, \lambda_3^e, \vec{\xi}) = \hat{\mathcal{U}}\left(J^e\right) + \hat{\omega}\left(\bar{\lambda}_1^e, \bar{\lambda}_2^e, \bar{\lambda}_3^e\right) + \hat{h}(\vec{\xi}) \tag{3.66}$$

where $\vec{\xi}$ is now some vector of principal space internal variables.

3.2.4 Stress expression in principal stretches

Extension of the stress expression to account for the principal space free energy expression (3.66), follows directly from the methodology used for the hyperelastic case in Section 3.1.4.

Given the principal space form of free energy, further implementation of the chain rule on the second Piola-Kirchhoff stress expression (3.57), gives

$$\boldsymbol{S} = 2\boldsymbol{F}^{i\,-1}\frac{\partial \hat{\mathcal{U}}}{\partial J^e}\frac{\partial J^e}{\partial \boldsymbol{C}^e}\boldsymbol{F}^{i\,-T} + 2\boldsymbol{F}^{i\,-1}\sum_{A=1}^{3}\sum_{B=1}^{3}\frac{\partial \hat{\omega}}{\partial \bar{\lambda}_B^e}\frac{\partial \bar{\lambda}_B^e}{\partial \lambda_A^e}\frac{\partial \lambda_A^e}{\partial \boldsymbol{C}^e}\boldsymbol{F}^{i\,-T} \tag{3.67}$$

We again introduce a principal deviatoric stress term, τ_A, where

$$\tau_A = \sum_{B=1}^{3}\frac{\partial \hat{\omega}}{\partial \bar{\lambda}_B^e}\frac{\partial \bar{\lambda}_B^e}{\partial \lambda_A^e}\lambda_A^e = \frac{\partial \hat{\omega}}{\partial \varepsilon_A^e} \tag{3.68}$$

and ε_A^e are the principal elastic logarithmic strains and now

$$\boldsymbol{S} = 2\boldsymbol{F}^{i\,-1}\frac{\partial \hat{\mathcal{U}}}{\partial J^e}\frac{\partial J^e}{\partial \boldsymbol{C}^e}\boldsymbol{F}^{i\,-T} + \boldsymbol{F}^{i\,-1}\sum_{A=1}^{3}\tau_A\left(2\lambda_A^{e\,-1}\frac{\partial \lambda_A^e}{\partial \boldsymbol{C}^e}\right)\boldsymbol{F}^{i\,-T} \tag{3.69}$$

The elastic jacobian and elastic principal stretch differential terms, $\partial_{\boldsymbol{C}^e} J^e$ and $\partial_{\boldsymbol{C}^e}\lambda_A^e$ can be determined via an identical methodology to that presented in Appendices C.2 and C.3 using elastic component terms. The explicit stress definitions remain dependent on the three different cases of elastic eigenvalue exclusivity.

(1) Distinct elastic eigenvalues $\Lambda_1^e \neq \Lambda_2^e \neq \Lambda_3^e$

The second Piola-Kirchhoff stress expression can be defined

$$\boldsymbol{S} = \boldsymbol{F}^{i\,-1}\frac{\partial \hat{\mathcal{U}}}{\partial J^e}J^e\boldsymbol{C}^{e\,-1}\boldsymbol{F}^{i\,-T} + \boldsymbol{F}^{i\,-1}\sum_{A=1}^{3}\tau_A\widetilde{\boldsymbol{M}}_A^{(e)}\boldsymbol{F}^{i\,-T} \tag{3.70}$$

The Cauchy stress expression is determined via the second order push forward operation defined in equation (3.10). It is pertinent to recall that authors such as Reese and Govindjee (1998a) and Holzapfel (1996) have observed the inelastic response of a variety of materials to be wholly deviatoric. Employing such a restriction $J^i = 1$, such that $J = J^e$ and recalling equations (3.49) and (3.61), the Cauchy stress is given[9]

$$\boxed{\boldsymbol{\sigma} = \frac{\partial \hat{\mathcal{U}}}{\partial J^e}\boldsymbol{I} + \frac{1}{J^e}\sum_{A=1}^{3}\tau_A\boldsymbol{m}_A^{(e)}} \tag{3.71}$$

For the cases of double and triple elastic eigenvalue coalescence, a similar modification to the stress expressions from Section 3.1.4 can be employed.

3.2.5 Closed-form tangential modulus expression in principal stretches

Following the implementation of the principal space free energy into the stress expressions in Section 3.2.4, the tangential modulus expression (3.60), can be correspondingly modified.

The Lagrangian tangential modulus expression becomes

$$\begin{aligned}\mathbb{C} = &\underbrace{2\boldsymbol{F}_n^{i-1}\boldsymbol{F}_n^{i-1}\frac{\partial}{\partial \boldsymbol{C}^{e\,tr}}\left\{2\boldsymbol{F}^{e\,tr\,-1}\boldsymbol{F}^e\frac{\partial \hat{\mathcal{U}}}{\partial J^e}\frac{\partial J^e}{\partial \boldsymbol{C}^e}\boldsymbol{F}^{e\,T}\boldsymbol{F}^{e\,tr\,-T}\right\}\boldsymbol{F}_n^{i-T}\boldsymbol{F}_n^{i-T}}_{vol} \\ &+\underbrace{2\boldsymbol{F}_n^{i-1}\boldsymbol{F}_n^{i-1}\frac{\partial}{\partial \boldsymbol{C}^{e\,tr}}\left\{2\boldsymbol{F}^{e\,tr\,-1}\boldsymbol{F}^e\sum_{A=1}^{3}\sum_{B=1}^{3}\frac{\partial \hat{\omega}}{\partial \bar{\lambda}_B^e}\frac{\partial \bar{\lambda}_B^e}{\partial \lambda_A^e}\frac{\partial \lambda_A^e}{\partial \boldsymbol{C}^e}\boldsymbol{F}^{e\,T}\boldsymbol{F}^{e\,tr\,-T}\right\}\boldsymbol{F}_n^{i-T}\boldsymbol{F}_n^{i-T}}_{dev}\end{aligned} \tag{3.72}$$

Initially focussing attention on the volumetric component of (3.72), it is beneficial to observe that via a development analogous to that in Appendix C.3, the elastic jacobian

[9] Note $\boldsymbol{F}(\boldsymbol{F}^{i\,-1}\widetilde{\boldsymbol{M}}_A^{(e)}\boldsymbol{F}^{i\,-T})\boldsymbol{F}^T = \boldsymbol{F}^e\widetilde{\boldsymbol{M}}_A^{(e)}\boldsymbol{F}^{e\,T} = \boldsymbol{m}_A^{(e)}$ from (3.61).

differential used in the preceding section is given

$$\frac{\partial J^e}{\partial \boldsymbol{C}^e} = \tfrac{1}{2} J^e \boldsymbol{C}^{e\,-1} \tag{3.73}$$

By carrying out the elastic push forward of this expression, followed by the elastic trial pull back and noting that $J = J^e = J^{e\,tr}$ because the inelastic response is wholly deviatoric, it can be shown that

$$\boldsymbol{F}^{e\,tr\,-1}\boldsymbol{F}^e \frac{\partial J^e}{\partial \boldsymbol{C}^e}\boldsymbol{F}^{e\,T}\boldsymbol{F}^{e\,tr\,-T} = \tfrac{1}{2} J^{e\,tr}\boldsymbol{C}^{e\,tr\,-1} = \frac{\partial J^{e\,tr}}{\partial \boldsymbol{C}^{e\,tr}} \tag{3.74}$$

Trivially $\partial J^e / \partial J^{e\,tr} = 1$, and so with some work, the volumetric component of the Lagrangian tangential modulus becomes

$$\begin{aligned}\mathbb{C}_{vol} &= 2\boldsymbol{F}_n^{i-1}\boldsymbol{F}_n^{i-1}\frac{\partial}{\partial \boldsymbol{C}^{e\,tr}}\left\{\frac{\partial \hat{\mathcal{U}}}{\partial J^e} J^{e\,tr}\boldsymbol{C}^{e\,tr\,-1}\right\}\boldsymbol{F}_n^{i-T}\boldsymbol{F}_n^{i-T} \\ &= \boldsymbol{F}_n^{i-1}\boldsymbol{F}_n^{i-1}\left\{J^e\left(\frac{\partial \hat{\mathcal{U}}}{\partial J^e} + J^e\frac{\partial^2 \hat{\mathcal{U}}}{\partial J^{e\,2}}\right)\boldsymbol{C}^{e\,tr\,-1}\otimes\boldsymbol{C}^{e\,tr\,-1} - 2J^e\frac{\partial \hat{\mathcal{U}}}{\partial J^e}\boldsymbol{I}^{\boldsymbol{C}^{e\,tr\,-1}}\right\}\boldsymbol{F}_n^{i-T}\boldsymbol{F}_n^{i-T}\end{aligned} \tag{3.75}$$

where $I^{\boldsymbol{C}^{e\,tr\,-1}}_{ijkl} = \frac{1}{2}(C^{e\,tr\,-1}_{ik}C^{e\,tr\,-1}_{jl} + C^{e\,tr\,-1}_{il}C^{e\,tr\,-1}_{jk})$. Carrying out the fourth order push forward[10] of (3.75) and recalling the separation of the deformation gradient given by equation (3.54), then the volumetric component of the Eulerian tangential modulus for generalized inelasticity becomes

$$\boxed{\boldsymbol{c}_{vol} = \left(\frac{\partial \hat{\mathcal{U}}}{\partial J^e} + J^e\frac{\partial^2 \hat{\mathcal{U}}}{\partial J^{e\,2}}\right)\boldsymbol{I}\otimes\boldsymbol{I} - 2\frac{\partial \hat{\mathcal{U}}}{\partial J^e}\boldsymbol{I}'} \tag{3.76}$$

for all cases of elastic eigenvalue exclusivity.

Following from the generalized stress expression (3.69), the deviatoric component of the Lagrangian tangential modulus for generalized inelasticity becomes

$$\bar{\mathbb{C}} = 2\boldsymbol{F}_n^{i\,-1}\boldsymbol{F}_n^{i-1}\frac{\partial}{\partial \boldsymbol{C}^{e\,tr}}\left\{\boldsymbol{F}^{e\,tr\,-1}\boldsymbol{F}^e\sum_{A=1}^{3}\tau_A\left(2\lambda_A^{e\,-1}\frac{\partial \lambda_A^e}{\partial \boldsymbol{C}^e}\right)\boldsymbol{F}^{e\,T}\boldsymbol{F}^{e\,tr\,-T}\right\}\boldsymbol{F}_n^{i-T}\boldsymbol{F}_n^{i-T} \tag{3.77}$$

[10] Observing that $\boldsymbol{F}^{e\,tr}\boldsymbol{F}^{e\,tr}(\boldsymbol{C}^{e\,tr\,-1}\otimes\boldsymbol{C}^{e\,tr\,-1})\boldsymbol{F}^{e\,tr\,T}\boldsymbol{F}^{e\,tr\,T} = \boldsymbol{I}\otimes\boldsymbol{I}$ and $\boldsymbol{F}^{e\,tr}\boldsymbol{F}^{e\,tr}(\boldsymbol{I}^{\boldsymbol{C}^{e\,tr\,-1}})\boldsymbol{F}^{e\,tr\,T}\boldsymbol{F}^{e\,tr\,T} = \boldsymbol{I}'$.

Via a development analogous to that in Appendix C.2, it can be shown that for the general case of three distinct elastic eigenvalues, then

$$\left(2\lambda_A^{e\,-1}\frac{\partial\lambda_A^e}{\partial\boldsymbol{C}^e}\right) = \widetilde{\boldsymbol{M}}_A^{(e)} \tag{3.78}$$

Recalling equations (3.61) and (3.62), and noting that $\boldsymbol{m}_A^{(e\,tr)} = \boldsymbol{m}_A^{(e)}$, then it can be shown that by taking the elastic push forward and subsequent elastic trial pull back of (3.78), then

$$\begin{aligned}\boldsymbol{F}^{e\,tr\,-1}\boldsymbol{F}^e\left(2\lambda_A^{e\,-1}\frac{\partial\lambda_A^e}{\partial\boldsymbol{C}^e}\right)\boldsymbol{F}^{e\,T}\boldsymbol{F}^{e\,tr\,-T} &= \boldsymbol{F}^{e\,tr\,-1}\boldsymbol{m}_A^{(e)}\boldsymbol{F}^{e\,tr\,-T} \\ &= \widetilde{\boldsymbol{M}}_A^{(e\,tr)} = \left(2\lambda_A^{e\,tr\,-1}\frac{\partial\lambda_A^{e\,tr}}{\partial\boldsymbol{C}^{e\,tr}}\right) \qquad A=1,2,3\end{aligned} \tag{3.79}$$

With substitution of this expression into (3.77), then

$$\begin{aligned}\bar{\mathbb{C}} &= 2\boldsymbol{F}_n^{i\,-1}\boldsymbol{F}_n^{i\,-1}\frac{\partial}{\partial\boldsymbol{C}^{e\,tr}}\left\{\sum_{A=1}^{3}\tau_A\left(2\lambda_A^{e\,tr\,-1}\frac{\partial\lambda_A^{e\,tr}}{\partial\boldsymbol{C}^{e\,tr}}\right)\right\}\boldsymbol{F}_n^{i\,-T}\boldsymbol{F}_n^{i\,-T} \\ &= 2\boldsymbol{F}_n^{i\,-1}\boldsymbol{F}_n^{i\,-1}\left\{\sum_{A=1}^{3}\sum_{B=1}^{3}\sum_{C=1}^{3}\sum_{D=1}^{3}\frac{\partial\tau_A}{\partial\bar{\lambda}_D^e}\frac{\partial\bar{\lambda}_D^e}{\partial\lambda_C^e}\frac{\partial\lambda_C^e}{\partial\lambda_B^{e\,tr}}\frac{\partial\lambda_B^{e\,tr}}{\partial\boldsymbol{C}^{e\,tr}}\otimes\left(2\lambda_A^{e\,tr\,-1}\frac{\partial\lambda_A^{e\,tr}}{\partial\boldsymbol{C}^{e\,tr}}\right)\right. \\ &\qquad\left.+\sum_{A=1}^{3}\tau_A\frac{\partial}{\partial\boldsymbol{C}^{e\,tr}}\left(2\lambda_A^{e\,tr\,-1}\frac{\partial\lambda_A^{e\,tr}}{\partial\boldsymbol{C}^{e\,tr}}\right)\right\}\boldsymbol{F}_n^{i\,-T}\boldsymbol{F}_n^{i\,-T}\end{aligned} \tag{3.80}$$

Use of equation (3.79) in this way circumvents the need to explicitly define any eigenvalue bases, hence the newly formed tangential modulus expression is applicable for all cases of elastic (trial) eigenvalue exclusivity.

As for hyperelasticity in Section 3.1.5, we introduce a tangential operator term, C_{AB}^{alg}, such that

$$C_{AB}^{alg} = \sum_{C=1}^{3}\sum_{D=1}^{3}\frac{\partial\tau_A}{\partial\bar{\lambda}_D^e}\frac{\partial\bar{\lambda}_D^e}{\partial\lambda_C^e}\frac{\partial\lambda_C^e}{\partial\lambda_B^{e\,tr}}\lambda_B^{e\,tr} = \frac{\partial\tau_A}{\partial\lambda_B^{e\,tr}}\lambda_B^{e\,tr} = \frac{\partial\tau_A}{\partial\varepsilon_B^{e\,tr}} \qquad A,B=1,2,3 \tag{3.81}$$

where $\varepsilon_A^{e\,tr}$ are the principal elastic trial logarithmic strains. C_{AB}^{alg} is commonly referred to as the *algorithmic tangential operator* and is treated widely in plasticity (Simo (1992); Perić (1993); Simo and Hughes (2000)). Through association with the incremental algorithmic

solution (i.e. through $\varepsilon_A^{e\,tr}$), C_{AB}^{alg} introduces *consistency* into the expression of the tangential modulus (Simo and Hughes (2000)). This concept will be treated further in Section 3.3. Correspondingly, the Lagrangian tangential modulus expression becomes

$$\bar{\mathbb{C}} = \boldsymbol{F}_n^{i\,-1}\boldsymbol{F}_n^{i\,-1}\left\{\sum_{A=1}^{3}\sum_{B=1}^{3} C_{AB}^{alg}\left(2\lambda_B^{e\,tr\,-1}\frac{\partial\lambda_B^{e\,tr}}{\partial\boldsymbol{C}^{e\,tr}}\right)\otimes\left(2\lambda_A^{e\,tr\,-1}\frac{\partial\lambda_A^{e\,tr}}{\partial\boldsymbol{C}^{e\,tr}}\right) + 2\sum_{A=1}^{3}\tau_A\frac{\partial}{\partial\boldsymbol{C}^{e\,tr}}\left(2\lambda_A^{e\,tr\,-1}\frac{\partial\lambda_A^{e\,tr}}{\partial\boldsymbol{C}^{e\,tr}}\right)\right\}\boldsymbol{F}_n^{i\,-T}\boldsymbol{F}_n^{i\,-T} \tag{3.82}$$

The first and second elastic trial principal stretch differential terms, $\partial_{\boldsymbol{C}^{e\,tr}}\lambda_A^{e\,tr}$ and $\partial^2_{\boldsymbol{C}^{e\,tr}\boldsymbol{C}^{e\,tr}}\lambda_A^{e\,tr}$, can be determined, as before, via the methodology presented in Appendices C.2 and C.4 with substitution of elastic trial strain terms. These expressions are again functional on the exclusivity of elastic trial eigenvalues.

(1) Distinct elastic trial eigenvalues $\Lambda_1^{e\,tr} \neq \Lambda_2^{e\,tr} \neq \Lambda_3^{e\,tr}$

The deviatoric component of the Lagrangian tangential modulus can be given

$$\bar{\mathbb{C}} = \boldsymbol{F}_n^{i\,-1}\boldsymbol{F}_n^{i\,-1}\left\{\sum_{A=1}^{3}\sum_{B=1}^{3} C_{AB}^{alg}\widetilde{\boldsymbol{M}}_A^{(e\,tr)}\otimes\widetilde{\boldsymbol{M}}_B^{(e\,tr)} + 2\sum_{A=1}^{3}\tau_A\partial_{\boldsymbol{C}^{e\,tr}}\widetilde{\boldsymbol{M}}_A^{(e\,tr)}\right\}\boldsymbol{F}_n^{i\,-T}\boldsymbol{F}_n^{i\,-T} \tag{3.83}$$

The Eulerian counterpart to this term is again attained via the fourth order push forward, recalling equations (3.54) and (3.62), then

$$\boxed{\bar{\boldsymbol{c}} = \frac{1}{J^e}\sum_{A=1}^{3}\sum_{B=1}^{3} C_{AB}^{alg}\boldsymbol{m}_A^{(e)}\otimes\boldsymbol{m}_B^{(e)} + \frac{2}{J^e}\sum_{A=1}^{3}\tau_A\partial_{\boldsymbol{tr}}\boldsymbol{m}_A^{(e)}} \tag{3.84}$$

where it can be shown that following the methodology of Appendix C.4

$$\partial_{\boldsymbol{tr}}\boldsymbol{m}_A^{(e)} = \frac{1}{D_A^{e\,tr}}\left(\boldsymbol{I}^{\boldsymbol{b}^{e\,tr}} - \sum_{B=1}^{3}\left[2\Lambda_B^{e\,tr\,2} - \left(\mathrm{I}_{\boldsymbol{C}}^{e\,tr} - \Lambda_A^{e\,tr}\right)\Lambda_B^{e\,tr}\right]\boldsymbol{m}_B^{(e)}\otimes\boldsymbol{m}_B^{(e)} - \mathrm{III}_{\boldsymbol{C}}^{e\,tr}\Lambda_A^{e\,tr\,-1}\boldsymbol{I}'\right) \tag{3.85}$$

where $I_{ijkl}^{\boldsymbol{b}^{e\,tr}} = \frac{1}{2}\left(b_{ik}^{e\,tr}b_{jl}^{e\,tr} + b_{il}^{e\,tr}b_{jk}^{e\,tr}\right)$.

For the cases of double and triple elastic trial eigenvalue coalescence, a similar modification to the tangential modulus expressions from Section 3.1.5 can be employed. In such cases, it is pertinent to note that, like for the purely hyperelastic case, a condition is

imposed on the algorithmic tangential operator such that for double eigenvalue coalescence

$$C_{12}^{alg} = C_{13}^{alg}, \quad C_{21}^{alg} = C_{31}^{alg}, \quad C_{22}^{alg} = C_{23}^{alg} = C_{32}^{alg} = C_{33}^{alg} \tag{3.86}$$

and for triple eigenvalue coalescence

$$C_{11}^{alg} = C_{22}^{alg} = C_{33}^{alg} = C^{alg} - \tfrac{1}{3}C^{alg}, \quad C_{12}^{alg} = C_{13}^{alg} = C_{21}^{alg} = C_{23}^{alg} = C_{31}^{alg} = C_{32}^{alg} = -\tfrac{1}{3}C^{alg} \tag{3.87}$$

Observing the chain rule expansion of C_{AB}^{alg},

$$C_{AB}^{alg} = \sum_{C=1}^{3} \frac{\partial \tau_A}{\partial \lambda_C^e} \lambda_C^e \frac{\partial \varepsilon_C^e}{\partial \varepsilon_B^{e\,tr}} \doteq \sum_{C=1}^{3} \gamma_{AC}^e \frac{\partial \varepsilon_C^e}{\partial \varepsilon_B^{e\,tr}} \tag{3.88}$$

where γ_{AB}^e can be referred to as the elastic moduli, akin to γ_{AB} from Section 3.1.5, then by a lengthy proof it can be shown that (3.86) and (3.87) are satisfied for all cases when $\partial \varepsilon_A^e / \partial \varepsilon_B^{e\,tr}$ is symmetric.

Now the complete, consistent closed-form tangential modulus has been defined for generalized inelastic materials, formulated in principal space and most significantly, invariant to the actual form of inelastic constitutive expression within the broad grouping of operator split theories. Within the context of the current investigation, this theory applies to both the viscoelastic and viscoplastic cases as will treated further in what follows.

3.3 Principal space algorithmic development of the three specific cases

Following from the results of Sections 3.1 and 3.2, it remains to determine the principal deviatoric stress terms and the tangential operator matrices for the three specific cases, i.e. the elastic, viscoelastic and viscoplastic elements. This is done via principal space algorithmic solution of the pertinent evolution equations. Following Perić and Dettmer (2003), Reese and Govindjee (1998a) and Nedjar (2002a,b), because of the parallel configuration of the total constitutive theory, the algorithmic treatment of each element may be decoupled. Thus, the elastic, viscoelastic and viscoplastic algorithms are treated separately in what follows, each requiring subsequent separate spectral reconstruction using the methodology from one of the preceding two sections.

It is important to note that within the development that follows, no provision has been made for the case of strain dependent material viscosity. As was discussed in Chapter 2, such provision would be desirable for the representation of semicrystalline polymer response, however an expression with the correct three-dimensional characteristics is yet to be developed. In the chapters that follow, an experimental and data processing methodology is outlined that makes possible the development of such an expression from future experimental work, however any further development has been outside the scope and capabilities of the current research. Constant viscosity terms are used herein as a result.

It is additionally pertinent to observe that the assumption of finite strain isotropy, which has been made to facilitate principal space treatment and practical parameter estimation, removes the ability to account for anisotropic constitutive behavior. As such, kinematic hardening cannot be accounted for within the current principal space development[11]. What follows is correspondingly limited to the inclusion of isotropic hardening.

3.3.1 Elastic element

In the absence of inelastic evolution, the majority of issues associated with the numerical implementation of a purely hyperelastic constitutive theory have been addressed in Section 3.1. It remains to discuss the principal stress and tangential operator terms and also the selected form of free energy potential.

Using a separated form of the hyperelastic free energy expression as in (3.23), the principal deviatoric stress terms β_A, $A = 1, 2, 3$ are given by (3.25). Observing (3.22), then it can be shown that

$$\frac{\partial \bar{\lambda}_B}{\partial \lambda_A} = J^{-1/3}\left(\delta_{BA} - \tfrac{1}{3}\lambda_B \lambda_A^{-1}\right) \tag{3.89}$$

and consequently (3.25) reduce to

$$\beta_A = \frac{\partial \hat{\omega}}{\partial \bar{\lambda}_A}\bar{\lambda}_A - \frac{1}{3}\sum_{B=1}^{3}\frac{\partial \hat{\omega}}{\partial \bar{\lambda}_B}\bar{\lambda}_B \tag{3.90}$$

The tangential operator matrix for pure hyperelasticity is given by expression (3.38). Exploiting equations (3.89) and (3.90), the corresponding expanded form of (3.38) can be

[11]This point highlights a fundamental flaw with a small component of the work of Simo (1992) where kinematic hardening has been incorrectly included within a principal space radial return mapping algorithm for viscoplasticity.

given

$$\gamma_{AB} = \frac{\partial \hat{\omega}}{\partial \bar{\lambda}_A}\,\delta_{AB}\bar{\lambda}_B + \frac{\partial^2 \hat{\omega}}{\partial \bar{\lambda}_A \partial \bar{\lambda}_B}\,\bar{\lambda}_A\bar{\lambda}_B + \frac{1}{9}\sum_{C=1}^{3}\sum_{D=1}^{3}\left[\frac{\partial \hat{\omega}}{\partial \bar{\lambda}_C}\,\delta_{CD}\bar{\lambda}_D + \frac{\partial^2 \hat{\omega}}{\partial \bar{\lambda}_C \partial \bar{\lambda}_D}\,\bar{\lambda}_C\bar{\lambda}_D\right] - \frac{1}{3}\sum_{C=1}^{3}\left[\frac{\partial \hat{\omega}}{\partial \bar{\lambda}_A}\,\delta_{AC}\bar{\lambda}_C + \frac{\partial \hat{\omega}}{\partial \bar{\lambda}_C}\,\delta_{CB}\bar{\lambda}_B + \frac{\partial^2 \hat{\omega}}{\partial \bar{\lambda}_A \partial \bar{\lambda}_C}\,\bar{\lambda}_A\bar{\lambda}_C + \frac{\partial^2 \hat{\omega}}{\partial \bar{\lambda}_C \partial \bar{\lambda}_B}\,\bar{\lambda}_C\bar{\lambda}_B\right] \quad (3.91)$$

The formulation to this point is general for all hyperelastic constitutive theories taking the decoupled principal space form of (3.23). For polymeric applications, it is deemed suitable here to implement a hyperelastic Ogden constitutive theory for the elastic element (Perić and Dettmer (2003); Simo and Taylor (1991); Reese and Govindjee (1998a)). The corresponding free energy expression can be given

$$\psi = \underbrace{\frac{K_{el}}{4}\left(J^2 - 2\ln J - 1\right)}_{\hat{\mathcal{U}}(J)} + \underbrace{\sum_{r=1}^{3}\frac{(\mu_{el})_r}{(\alpha_{el})_r}\left(\bar{\lambda}_1^{(\alpha_{el})_r} + \bar{\lambda}_2^{(\alpha_{el})_r} + \bar{\lambda}_3^{(\alpha_{el})_r} - 3\right)}_{\hat{\omega}(\bar{\lambda}_1,\bar{\lambda}_2,\bar{\lambda}_3)} \quad (3.92)$$

where K_{el}, $(\mu_{el})_r$ and $(\alpha_{el})_r$ are material parameters. For near incompressibility, K_{el} is given a large value (of the order of $\approx 1000(\mu_{el})_r$ following Reese and Govindjee (1998a)) which constitutes a *Lagrange multiplier* approach to incompressibility (Simo and Taylor (1991); Bonet and Wood (1997)).

It is now trivial to calculate the first and second differentials of $\hat{\mathcal{U}}$ and $\hat{\omega}$ given (3.92), for substitution into equations (3.90), (3.91) and also (3.28), (3.31), (3.34) and (3.37) to give the complete form of the hyperelastic algorithm.

3.3.2 Viscoelastic element

The principal space viscoelastic model chosen for this investigation, follows the work of Reese and Govindjee (1998a). The isolated viscoelastic element treated by these authors can be represented by the one-dimensional Maxwell model[12] shown in Figure 3.1. Here the numerical implementation of the Reese and Govindjee viscoelastic model is discussed as it applies to the general framework for inelasticity discussed in Section 3.2.

The viscoelastic element stress is related to the elastic principal strain through the expressions (3.66) and (3.68), noting that for this case of viscoelasticity, no internal variables

[12]Note that this element must be implemented in parallel with an elastic element (as in Figure 2.3) to be truly viscoelastic.

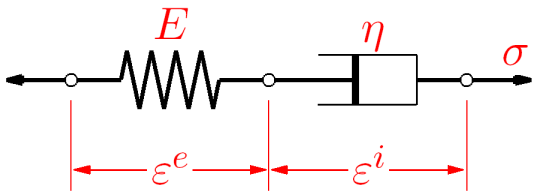

Figure 3.1: 1D rheological representation of the viscoelastic element.

are required. By a similar method to that of Section 3.3.1, the principal deviatoric stress terms τ_A, $A = 1, 2, 3$ can be defined for viscoelasticity as

$$\tau_A = \frac{\partial \hat{\omega}}{\partial \bar{\lambda}^e_A} \bar{\lambda}^e_A - \frac{1}{3} \sum_{B=1}^{3} \frac{\partial \hat{\omega}}{\partial \bar{\lambda}^e_B} \bar{\lambda}^e_B = \hat{\mathcal{T}} \left(\bar{\lambda}^e_1, \bar{\lambda}^e_2, \bar{\lambda}^e_3 \right) \tag{3.93}$$

where $\hat{\mathcal{T}}$ represents this function in later operations. The elastic strain components must be calculated via algorithmic solution of element evolution.

The constitutive expression accounting for viscoelastic evolution has been defined in Section 2.4. For the case of purely deviatoric inelastic evolution, (2.16) reduces to

$$-\frac{1}{2} \left(\mathcal{L}_v \boldsymbol{b}^e \right) \boldsymbol{b}^{e\,-1} = \frac{1}{2\eta_{ve}} \operatorname{dev} [\boldsymbol{\tau}] \tag{3.94}$$

where η_{ve} is the material viscosity, $\operatorname{dev}[\boldsymbol{\tau}] = (\boldsymbol{I}' - \frac{1}{3} \boldsymbol{I} \otimes \boldsymbol{I}) : \boldsymbol{\tau}$ is the deviatoric component of the Kirchhoff stress tensor, while $\mathcal{L}_v \boldsymbol{b}^e$ is the Lie derivative of the elastic left Cauchy-Green strain tensor as treated in Appendix A. It is convenient to note the common expansion of the Lie derivative (Perić and Dettmer (2003); Reese and Govindjee (1998a))

$$\mathcal{L}_v \boldsymbol{b}^e = \boldsymbol{F} \dot{\overline{\boldsymbol{C}^{i-1}}} \boldsymbol{F}^T = \dot{\boldsymbol{b}}^e - \boldsymbol{l}\boldsymbol{b}^e - \boldsymbol{b}^e \boldsymbol{l}^T \tag{3.95}$$

where $\boldsymbol{l} = \dot{\boldsymbol{F}} \boldsymbol{F}^{-1}$ is the spatial velocity gradient tensor.

Conventional operator split methodology of classical plasticity (Ortiz et al. (1983); Simo and Hughes (2000); Perić and Owen (1998)) is used to solve the evolution equation (3.94). Initially, over the time increment $\Delta t_{n+1} = t_{n+1} - t_n$, an elastic trial state is specified (i.e. elastic predictor) where from the rearrangement of (3.54)

$$\boldsymbol{F}^{e\,tr}_{n+1} = \boldsymbol{F}_{n+1} \boldsymbol{F}^{i-1}_n \tag{3.96}$$

Because $\boldsymbol{F}_n^i$ is assumed constant during this step, then inelastic strain rate is zero and correspondingly from (3.95), $\mathcal{L}_v \boldsymbol{b}^e = 0$; i.e. initially no inelastic evolution.

Given that inelastic flow is present (unconditional for viscoelasticity), a plastic correction step is then performed to account for any inelastic evolution that may have occurred. Over such a step, the total deformation gradient is constant, thus $\boldsymbol{l} = 0$ and correspondingly (3.94) can be reduced to

$$\dot{\boldsymbol{b}}^e = -2\frac{1}{2\eta_{ve}} \operatorname{dev}[\boldsymbol{\tau}] \cdot \boldsymbol{b}^e \tag{3.97}$$

Solution of this differential equation by conventional exponential mapping (Simo and Hughes (2000)) gives for the time step $\Delta t_{n+1} = t_{n+1} - t_n$

$$\boldsymbol{b}^e_{n+1} = \exp\left\{-2\frac{\Delta t_{n+1}}{2\eta_{ve}} \operatorname{dev}[\boldsymbol{\tau}_{n+1}]\right\} \cdot \boldsymbol{b}^{e\,tr}_{n+1} \tag{3.98}$$

Because the tensor quantities $\boldsymbol{b}^e_{n+1}$, $\boldsymbol{\tau}_{n+1}$ and $\boldsymbol{b}^{e\,tr}_{n+1}$ are know to commute for isotropic response (Reese and Govindjee (1998a); Simo (1992)), then expression (3.98) can be reduced to the principal space expression

$$\lambda^{e\,2}_{A\,n+1} = \exp\left\{-2\frac{\Delta t_{n+1}}{2\eta_{ve}} \operatorname{dev}[\tau_{A\,n+1}]\right\} \lambda^{e\,tr\,2}_{A\,n+1} \qquad A = 1,2,3 \tag{3.99}$$

where $\tau_{A\,n+1}$ are the principal deviatoric stress terms given by equation (3.93). Taking the logarithm of (3.99) and noting the vector notation $\vec{x} = [x_1, x_2, x_3]^T$, then this expression becomes

$$\vec{\varepsilon}^{\,e}_{n+1} = -\frac{\Delta t_{n+1}}{2\eta_{ve}} \vec{\tau}_{n+1} + \vec{\varepsilon}^{\,e\,tr}_{n+1} \tag{3.100}$$

Through (3.93), it is apparent that $\vec{\tau}_{n+1}$ and $\vec{\varepsilon}^{\,e}_{n+1}$ are mutually dependent and, as such, (3.100) must be solved iteratively. A suitable Newton iteration scheme is summarized in Box 1.

The algorithmic tangential operator, can be formulated following the linearization of the residual derivative term from Box 1 via

$$\Delta R_{\vec{\varepsilon}^{\,e}_{n+1}} = \underbrace{\Delta\vec{\varepsilon}^{\,e}_{n+1} + \frac{\Delta t_{n+1}}{2\eta_{ve}}\Delta\vec{\tau}_{n+1}}_{\Delta\vec{\varepsilon}^{\,e\,tr}_{n+1}} = \boldsymbol{K}_{n+1}\Delta\vec{\varepsilon}^{\,e}_{n+1} \tag{3.101}$$

Box 1: Viscoelastic algorithm

1. Initialize: $t = t_{n+1}$, $k = 0$, $\vec{\varepsilon}^{e(0)}_{n+1} = \vec{\varepsilon}^{e\,tr}_{n+1}$, $\vec{\tau}^{\,(0)}_{n+1} = \hat{\mathcal{T}}(\vec{\varepsilon}^{e(0)}_{n+1})$

2. Evaluate flow rule residual

$$R^{(k)}_{\vec{\varepsilon}^{e}_{n+1}} = \vec{\varepsilon}^{e(k)}_{n+1} + \frac{\Delta t_{n+1}}{2\eta_{ve}}\,\vec{\tau}^{\,(k)}_{n+1} - \vec{\varepsilon}^{e\,tr}_{n+1}$$

   IF: $\left|R^{(k)}_{\vec{\varepsilon}^{e}_{n+1}}\right| <$ TOL THEN: *EXIT*

3. Compute the Newton's method increment in strain

$$\frac{\partial R^{(k)}_{\vec{\varepsilon}^{e}_{n+1}}}{\partial \vec{\varepsilon}^{e(k)}_{n+1}} = \boldsymbol{I} + \frac{\Delta t_{n+1}}{2\eta_{ve}}\frac{\partial \vec{\tau}^{\,(k)}_{n+1}}{\partial \vec{\varepsilon}^{e(k)}_{n+1}} = \boldsymbol{K}^{(k)}_{n+1}$$

$$\Delta\vec{\varepsilon}^{e(k)}_{n+1} = -\left(\boldsymbol{K}^{(k)}_{n+1}\right)^{-1} R^{(k)}_{\vec{\varepsilon}^{e}_{n+1}}$$

4. Update strain and stress

$$\vec{\varepsilon}^{e(k+1)}_{n+1} = \vec{\varepsilon}^{e(k)}_{n+1} + \Delta\vec{\varepsilon}^{e(k)}_{n+1}$$

$$\vec{\tau}^{\,(k+1)}_{n+1} = \hat{\mathcal{T}}(\vec{\varepsilon}^{e(k+1)}_{n+1})$$

   Set $k \longleftarrow k+1$ and GO TO 2.

Dividing by $\partial\vec{\varepsilon}^{e}_{n+1}$, it can be shown that

$$\frac{\partial\vec{\varepsilon}^{e\,tr}_{n+1}}{\partial\vec{\varepsilon}^{e}_{n+1}} = \boldsymbol{K}_{n+1} \tag{3.102}$$

Recalling (3.81), an alternative implementation of the chain rule gives the expression

$$\boldsymbol{C}^{alg} = \frac{\partial\vec{\tau}_{n+1}}{\partial\vec{\varepsilon}^{e}_{n+1}}\frac{\partial\vec{\varepsilon}^{e}_{n+1}}{\partial\vec{\varepsilon}^{e\,tr}_{n+1}} = \frac{\partial\vec{\tau}_{n+1}}{\partial\vec{\varepsilon}^{e}_{n+1}}\boldsymbol{K}^{-1}_{n+1} \tag{3.103}$$

where the differential $\partial_{\vec{\varepsilon}^{e}_{n+1}}\vec{\tau}_{n+1}$ can be likened to an *elastic modulus* and following from (3.93), takes on an analogous form to equation (3.91) modified to be functional on elastic components of strain. Clearly $\boldsymbol{K}^{-1}_{n+1}$ is extracted from the converged algorithmic solution from Box 1.

As before, the explicit free energy potential for the viscoelastic element must be defined. Noting that no viscoelastic internal variables have been defined, then following Reese

and Govindjee (1998a) and also Perić and Dettmer (2003), a suitable choice for polymeric materials is again the Ogden model, i.e.

$$\psi = \underbrace{\frac{K_{ve}}{4}\left(J^{e\,2} - 2\ln J^e - 1\right)}_{\hat{\mathcal{U}}(J^e)} + \underbrace{\sum_{r=1}^{3} \frac{(\mu_{ve})_r}{(\alpha_{ve})_r}\left(\bar{\lambda}_1^{e\,(\alpha_{ve})_r} + \bar{\lambda}_2^{e\,(\alpha_{ve})_r} + \bar{\lambda}_3^{e\,(\alpha_{ve})_r} - 3\right)}_{\hat{\omega}(\bar{\lambda}_1^e, \bar{\lambda}_2^e, \bar{\lambda}_3^e)} \tag{3.104}$$

where K_{ve}, $(\mu_{ve})_r$ and $(\alpha_{ve})_r$ and from the evolution expressions, η_{ve} are the viscoelastic material parameters fully defining the viscoelastic constitutive behavior.

As before, all the expressions necessary for complete numerical implementation, in this case for the Reese and Govindjee viscoelastic model, have been presented. The principal deviatoric stress terms and the algorithmic tangential operator matrix, calculated with converged incremental values for elastic strain, are implemented within the generalized framework of Section 3.2 to define the full tensor space expressions for stress and *consistent*, closed-form tangential modulus.

3.3.3 Viscoplastic element

Presented here is the development of a new principal space closest point projection return mapping algorithm for viscoplasticity with isotropic hardening. A one-dimensional rheological representation of the isolated viscoplastic element is provided for illustration in Figure 3.2.

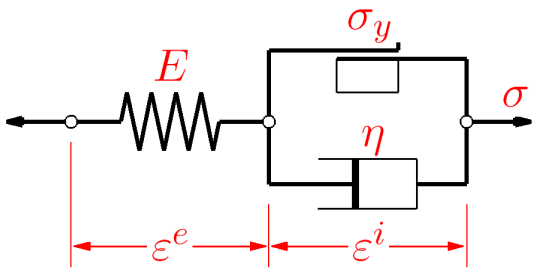

Figure 3.2: 1D rheological representation of the viscoplastic element.

As was the case for the viscoelastic element, the principal deviatoric stress vector and the corresponding elastic modulus are related to the elastic strain components via relationships

of the form

$$\vec{\tau}_{n+1} = \frac{\partial \hat{\omega}\left(\vec{\varepsilon}^{\,e}_{n+1}\right)}{\partial \vec{\varepsilon}^{\,e}_{n+1}} = \hat{\mathcal{T}}(\vec{\varepsilon}^{\,e}_{n+1}) \qquad \frac{\partial \vec{\tau}_{n+1}}{\partial \vec{\varepsilon}^{\,e}_{n+1}} = \frac{\partial^2 \hat{\omega}\left(\vec{\varepsilon}^{\,e}_{n+1}\right)}{\partial \vec{\varepsilon}^{\,e\,2}_{n+1}} = \hat{\mathbf{C}}(\vec{\varepsilon}^{\,e}_{n+1}) \tag{3.105}$$

where, given the principal space free energy expression (3.66), $\hat{\mathcal{T}}$ and $\hat{\mathbf{C}}$ are functions taking on analogous forms to equations (3.90) and (3.91) with modified functionality on elastic strain components.

Recall from Section 2.4.4 the stress space scalar internal state variable q accounting for isotropic hardening. For algorithmic treatment in principal space, because of the nature of isotropic hardening, q remains scalar. Following from equations $(2.23)_1$ and $(2.24)_1$, given a principal space free energy expression (3.66), the stress space scalar isotropic hardening internal variable and its corresponding hardening modulus can be related to its strain space scalar conjugate, α, via the functions

$$q_{n+1} = -\frac{\partial \hat{h}_{iso}(\alpha_{n+1})}{\partial \alpha_{n+1}} = \hat{\mathcal{Q}}_{iso}(\alpha_{n+1}) \qquad \frac{\partial q_{n+1}}{\partial \alpha_{n+1}} = -\frac{\partial^2 \hat{h}_{iso}(\alpha_{n+1})}{\partial \alpha^2_{n+1}} = \hat{\mathrm{K}}(\alpha_{n+1}) \tag{3.106}$$

where $\hat{\mathcal{Q}}_{iso}$ and $\hat{\mathrm{K}}$ are directly dependent on the explicit form of free energy expression (3.66) chosen.

The tensor space viscoplastic yield and evolution expressions have been defined in Section 2.4.4. Restricting these expressions to isotropic hardening

$$f = \|\mathrm{dev}[\boldsymbol{\tau}]\| - \sqrt{\tfrac{2}{3}}\,(\sigma_y - q) \tag{3.107a}$$

$$-\frac{1}{2}\left(\mathcal{L}_v \boldsymbol{b}^e\right)\boldsymbol{b}^{e-1} = \frac{\langle f \rangle}{2\eta_{vp}}\frac{\partial f}{\partial \boldsymbol{\tau}} \tag{3.107b}$$

$$\dot{\alpha} = \frac{\langle f \rangle}{2\eta_{vp}}\frac{\partial f}{\partial q} \tag{3.107c}$$

where, as before, inelastic deformation is assumed to be wholly deviatoric (see Perić and Dettmer (2003); Simo (1992)). It is pertinent to note that as a consequence of this property, it is trivially shown that $\partial_{\boldsymbol{\tau}} f = \partial_{\mathrm{dev}[\boldsymbol{\tau}]} f$.

Following an identical operator spit methodology to that discussed for viscoelasticity in Section 3.3.2, during the plastic corrector step the strain evolution expression (3.107b)

reduces to

$$\dot{\boldsymbol{b}}^{e} = -2\frac{\langle f \rangle}{2\eta_{vp}}\frac{\partial f}{\partial \boldsymbol{\tau}} \cdot \boldsymbol{b}^{e} \tag{3.108}$$

Note that if yield has not been satisfied, (3.108) reduces to zero, i.e. no inelastic evolution as expected. Solution of this differential expression by exponential mapping for the increment $\Delta t_{n+1} = t_{n+1} - t_n$ gives

$$\boldsymbol{b}^{e}_{n+1} = \exp\left\{-2\frac{\Delta t_{n+1}\,\langle f_{n+1}\rangle}{2\eta_{vp}}\frac{\partial f_{n+1}}{\partial \boldsymbol{\tau}_{n+1}}\right\} \cdot \boldsymbol{b}^{e\,tr}_{n+1} \tag{3.109}$$

As was the case during the viscoelastic development, the tensors $\boldsymbol{b}^{e}_{n+1}$, $\boldsymbol{\tau}_{n+1}$ and $\boldsymbol{b}^{e\,tr}_{n+1}$ commute due to isotropy and so the solution can be carried out in principal space

$$\lambda^{e\,2}_{A\,n+1} = \exp\left\{-2\frac{\Delta t_{n+1}\,\langle f_{n+1}\rangle}{2\eta_{vp}}\frac{\partial f_{n+1}}{\partial \tau_{A\,n+1}}\right\}\lambda^{e\,tr\,2}_{A\,n+1} \qquad A = 1,2,3 \tag{3.110}$$

where $\tau_{A\,n+1}$ are the viscoplastic deviatoric principal stress values defined by $(3.105)_1$ and now the yield function can be written in principal space

$$f_{n+1} = \hat{f}\left(\vec{\tau}_{n+1}, q_{n+1}\right) = \|\vec{\tau}_{n+1}\| - \sqrt{\tfrac{2}{3}}\left(\sigma_y - q_{n+1}\right) \tag{3.111}$$

Taking the logarithm of (3.110) gives the final expression

$$\vec{\varepsilon}^{\,e}_{n+1} = -\frac{\Delta t_{n+1}\langle f_{n+1}\rangle}{2\eta_{vp}}\frac{\partial f_{n+1}}{\partial \vec{\tau}_{n+1}} + \vec{\varepsilon}^{\,e\,tr}_{n+1} \tag{3.112}$$

For the isotropic hardening flow rule (3.107c), the scalar expression requires no modification for application in principal space. Thus, simple differential solution gives

$$\alpha_{n+1} = \frac{\Delta t_{n+1}\langle f_{n+1}\rangle}{2\eta_{vp}}\frac{\partial f_{n+1}}{\partial q_{n+1}} + \alpha_n \tag{3.113}$$

A combined iterative solution to expressions (3.112) and (3.113) is necessary because of the mutual dependence of the respective stress and strain space quantities. Solution via closest point projection can thus be likened to a generalized Newton's method solution for multiple, mutually dependent expressions. This analogy will be exploited further in Chapter 5.

Developing on the conventional closest point projection derivations of Simo and Hughes

(2000), Perić and Owen (1992) and Perić (1993), then from (3.112) and (3.113), the global flow residual array, $\boldsymbol{R}_{n+1}$, can be determined as

$$\boldsymbol{R}_{n+1} = \begin{Bmatrix} R_{\vec{\varepsilon}^{\,e}_{n+1}} \\ R_{\alpha_{n+1}} \end{Bmatrix} = \begin{Bmatrix} \vec{\varepsilon}^{\,e}_{n+1} - \vec{\varepsilon}^{\,e\,tr}_{n+1} \\ \alpha_{n+1} - \alpha_n \end{Bmatrix} + \frac{\Delta t_{n+1} \langle f_{n+1} \rangle}{2\eta_{vp}} \begin{Bmatrix} \partial_{\vec{\tau}} f_{n+1} \\ -\partial_q f_{n+1} \end{Bmatrix} \tag{3.114}$$

The two specific flow residuals $R_{\vec{\varepsilon}^{\,e}_{n+1}}$ and $R_{\alpha_{n+1}}$ can now be differentiated with respect to their corresponding stress space terms. For the strain residual, $R_{\vec{\varepsilon}^{\,e}_{n+1}}$, noting that $\vec{\varepsilon}^{\,e\,tr}_{n+1}$ is constant over the return mapping, this differential is given

$$\begin{aligned} \frac{\partial R_{\vec{\varepsilon}^{\,e}_{n+1}}}{\partial \vec{\tau}_{n+1}} = \frac{\partial \vec{\varepsilon}^{\,e}_{n+1}}{\partial \vec{\tau}_{n+1}} + \frac{\Delta t_{n+1}}{2\eta_{vp}}\, \partial_{\vec{\tau}} f_{n+1} \otimes \partial_{\vec{\tau}} f_{n+1} + \frac{\Delta t_{n+1} \langle f_{n+1} \rangle}{2\eta_{vp}}\, \partial^2_{\vec{\tau}\vec{\tau}} f_{n+1} \\ + \frac{\Delta t_{n+1}}{2\eta_{vp}}\, \partial_q f_{n+1} \partial_{\vec{\tau}} f_{n+1} \otimes \frac{\partial q_{n+1}}{\partial \vec{\tau}_{n+1}} + \frac{\Delta t_{n+1} \langle f_{n+1} \rangle}{2\eta_{vp}}\, \partial^2_{\vec{\tau}q} f_{n+1} \otimes \frac{\partial q_{n+1}}{\partial \vec{\tau}_{n+1}} \end{aligned} \tag{3.115}$$

Linearizing (3.115), recalling $(3.105)_2$ and observing that it is the objective of the Newton increment to enforce $R_{\vec{\varepsilon}^{\,e}_{n+1}} + \Delta R_{\vec{\varepsilon}^{\,e}_{n+1}} \longrightarrow 0$ then it can be shown

$$\begin{aligned} -R_{\vec{\varepsilon}^{\,e}_{n+1}} = \left[\hat{\mathbf{C}}(\vec{\varepsilon}^{\,e}_{n+1})^{-1} + \frac{\Delta t_{n+1}}{2\eta_{vp}}\, \partial_{\vec{\tau}} f_{n+1} \otimes \partial_{\vec{\tau}} f_{n+1} + \frac{\Delta t_{n+1} \langle f_{n+1} \rangle}{2\eta_{vp}}\, \partial^2_{\vec{\tau}\vec{\tau}} f_{n+1} \right] \Delta \vec{\tau}_{n+1} \\ + \left[\frac{\Delta t_{n+1}}{2\eta_{vp}}\, \partial_q f_{n+1} \partial_{\vec{\tau}} f_{n+1} + \frac{\Delta t_{n+1} \langle f_{n+1} \rangle}{2\eta_{vp}}\, \partial^2_{\vec{\tau}q} f_{n+1} \right] \Delta q_{n+1} \end{aligned} \tag{3.116}$$

By repeating an identical procedure for the isotropic hardening residual term and combining the two results into matrix form, it becomes possible to rearrange for the two incremental values $\Delta \vec{\tau}_{n+1}$ and Δq_{n+1}. This is presented in Box 2 describing the full iterative algorithmic solution over the time step $\Delta t_{n+1} = t_{n+1} - t_n$.

Following primarily the work of Perić (1993), determination of the algorithmic tangential operator matrix is facilitated via the direct linearization of the algorithm in Box 2. As for the viscoelastic case, it can be shown that over the increment $\Delta t_{n+1} = t_{n+1} - t_n$, then $-\boldsymbol{R}_{n+1} = \Delta \boldsymbol{R}_{n+1} = [\Delta \vec{\varepsilon}^{\,e\,tr}_{n+1}, \Delta \alpha_n]^T$ such that manipulation of the matrix incremental update expression from Box 2 gives

$$\begin{bmatrix} \Xi^{\vec{\tau}\vec{\tau}}_{n+1} & \Xi^{\vec{\tau}q}_{n+1} \\ \Xi^{q\vec{\tau}}_{n+1} & \Xi^{qq}_{n+1} \end{bmatrix} \begin{Bmatrix} \partial \vec{\tau}^{(k)}_{n+1} \\ \partial q^{(k)}_{n+1} \end{Bmatrix} = \begin{Bmatrix} \partial \vec{\varepsilon}^{\,e\,tr}_{n+1} \\ \partial \alpha_n \end{Bmatrix} \tag{3.117}$$

Box 2: Viscoplastic algorithm

1. Initialize: $t = t_{n+1}$, $k = 0$, $\vec{\varepsilon}^{e(0)}_{n+1} = \vec{\varepsilon}^{e\,tr}_{n+1}$, $\alpha^{(0)}_{n+1} = \alpha_n$, $\vec{\tau}^{(0)}_{n+1} = \hat{\mathcal{T}}(\vec{\varepsilon}^{e(0)}_{n+1})$ and $q^{(0)}_{n+1} = \hat{\mathcal{Q}}_{iso}(\alpha^{(0)}_{n+1})$.

2. Evaluate yield and flow rule residual

$$f^{(k)}_{n+1} = \hat{f}\big(\vec{\tau}^{(k)}_{n+1}, q^{(k)}_{n+1}\big); \quad \boldsymbol{R}^{(k)}_{n+1} = \begin{Bmatrix} \vec{\varepsilon}^{e\,(k)}_{n+1} - \vec{\varepsilon}^{e\,tr}_{n+1} \\ \alpha^{(k)}_{n+1} - \alpha_n \end{Bmatrix} + \frac{\Delta t_{n+1}\big\langle f^{(k)}_{n+1}\big\rangle}{2\eta_{vp}} \begin{Bmatrix} \partial_{\vec{\tau}} f^{(k)}_{n+1} \\ -\partial_q f^{(k)}_{n+1} \end{Bmatrix}$$

   IF: $\big\|\boldsymbol{R}^{(k)}_{n+1}\big\| < \text{TOL}$ THEN: *EXIT*, ELSE:

3. Calculate the complete *algorithmic* modulus

$$\boldsymbol{\Xi}^{(k)-1}_{n+1} = \begin{bmatrix} \Xi^{\vec{\tau}\vec{\tau}\,(k)}_{n+1} & \Xi^{\vec{\tau}q\,(k)}_{n+1} \\ \Xi^{q\vec{\tau}\,(k)}_{n+1} & \Xi^{qq\,(k)}_{n+1} \end{bmatrix}^{-1}$$

   where

$$\begin{aligned}
\Xi^{\vec{\tau}\vec{\tau}\,(k)}_{n+1} &= \hat{\mathbf{C}}^{(k)-1}_{n+1} + \tfrac{\Delta t_{n+1}}{2\eta_{vp}} \partial_{\vec{\tau}} f^{(k)}_{n+1} \otimes \partial_{\vec{\tau}} f^{(k)}_{n+1} + \tfrac{\Delta t_{n+1}\langle f^{(k)}_{n+1}\rangle}{2\eta_{vp}} \partial^2_{\vec{\tau}\vec{\tau}} f^{(k)}_{n+1} \\
\Xi^{\vec{\tau}q\,(k)}_{n+1} &= \tfrac{\Delta t_{n+1}}{2\eta_{vp}} \partial_q f^{(k)}_{n+1} \partial_{\vec{\tau}} f^{(k)}_{n+1} + \tfrac{\Delta t_{n+1}\langle f^{(k)}_{n+1}\rangle}{2\eta_{vp}} \partial^2_{\vec{\tau}q} f^{(k)}_{n+1} \\
\Xi^{q\vec{\tau}\,(k)}_{n+1} &= -\tfrac{\Delta t_{n+1}}{2\eta_{vp}} \partial_q f^{(k)}_{n+1} \partial_{\vec{\tau}} f^{(k)}_{n+1} - \tfrac{\Delta t_{n+1}\langle f^{(k)}_{n+1}\rangle}{2\eta_{vp}} \partial^2_{q\vec{\tau}} f^{(k)}_{n+1} \\
\Xi^{qq\,(k)}_{n+1} &= \hat{\mathrm{K}}^{(k)-1}_{n+1} - \tfrac{\Delta t_{n+1}}{2\eta_{vp}} \partial_q f^{(k)}_{n+1} \partial_q f^{(k)}_{n+1} - \tfrac{\Delta t_{n+1}\langle f^{(k)}_{n+1}\rangle}{2\eta_{vp}} \partial^2_{qq} f^{(k)}_{n+1}
\end{aligned}$$

4. Compute the incremental update of stress space quantities

$$\begin{Bmatrix} \Delta\vec{\tau}^{(k)}_{n+1} \\ \Delta q^{(k)}_{n+1} \end{Bmatrix} = -\boldsymbol{\Xi}^{(k)-1}_{n+1} \cdot \boldsymbol{R}^{(k)}_{n+1}$$

5. Update stress, strain and hardening terms

$$\begin{Bmatrix} \vec{\tau}^{(k+1)}_{n+1} \\ q^{(k+1)}_{n+1} \end{Bmatrix} = \begin{Bmatrix} \vec{\tau}^{(k)}_{n+1} \\ q^{(k)}_{n+1} \end{Bmatrix} + \begin{Bmatrix} \Delta\vec{\tau}^{(k)}_{n+1} \\ \Delta q^{(k)}_{n+1} \end{Bmatrix} \quad \longrightarrow \quad \begin{Bmatrix} \vec{\varepsilon}^{e\,(k+1)}_{n+1} \\ \alpha^{(k+1)}_{n+1} \end{Bmatrix} = \begin{Bmatrix} \vec{\varepsilon}^{e\,(k)}_{n+1} \\ \alpha^{(k)}_{n+1} \end{Bmatrix} + \begin{Bmatrix} \hat{\mathbf{C}}^{(k)-1}_{n+1} \cdot \Delta\vec{\tau}^{(k)}_{n+1} \\ \hat{\mathrm{K}}^{(k)-1}_{n+1} \Delta q^{(k)}_{n+1} \end{Bmatrix}$$

   Set $k \longleftarrow k+1$ and GO TO 2.

Expanding and dividing by $\partial \vec{\varepsilon}^{\,e\,tr}_{n+1}$ it can be shown that

$$\Xi^{\vec{\tau}\vec{\tau}}_{n+1} \frac{\partial \vec{\tau}_{n+1}}{\partial \vec{\varepsilon}^{\,e\,tr}_{n+1}} + \Xi^{\vec{\tau}q}_{n+1} \otimes \frac{\partial q_{n+1}}{\partial \vec{\varepsilon}^{\,e\,tr}_{n+1}} = \boldsymbol{I} \tag{3.118a}$$

$$\Xi^{q\vec{\tau}}_{n+1} \cdot \frac{\partial \vec{\tau}_{n+1}}{\partial \vec{\varepsilon}^{\,e\,tr}_{n+1}} + \Xi^{qq}_{n+1} \frac{\partial q_{n+1}}{\partial \vec{\varepsilon}^{\,e\,tr}_{n+1}} = \vec{0} \tag{3.118b}$$

This system of equations has two unknowns, $\partial_{\vec{\varepsilon}^{\,tr}_{n+1}} \vec{\tau}_{n+1}$ and $\partial_{\vec{\varepsilon}^{\,tr}_{n+1}} q_{n+1}$. Simultaneous solution for $\partial_{\vec{\varepsilon}^{\,tr}_{n+1}} \vec{\tau}_{n+1}$ then gives with some manipulation, the algorithmic tangential operator matrix

$$\boldsymbol{C}^{alg} = \frac{\partial \vec{\tau}_{n+1}}{\partial \vec{\varepsilon}^{\,e\,tr}_{n+1}} = \left[\Xi^{\vec{\tau}\vec{\tau}}_{n+1} - \left(\Xi^{qq}_{n+1}\right)^{-1} \Xi^{\vec{\tau}q}_{n+1} \Xi^{q\vec{\tau}}_{n+1} \right]^{-1} \tag{3.119}$$

It remains to specify the exact free energy expression that governs the elastic and hardening relationships within expressions (3.105) and (3.106). The generalized form of the free energy expression (3.66), becomes for isotropic hardening

$$\psi = \hat{\psi}(\lambda^e_1, \lambda^e_2, \lambda^e_3, \alpha) = \hat{\mathcal{U}}\left(J^e\right) + \hat{\omega}\left(\bar{\lambda}^e_1, \bar{\lambda}^e_2, \bar{\lambda}^e_3\right) + \hat{h}_{iso}(\alpha) \tag{3.120}$$

Once again implementing an Ogden potential for the elastic components of (3.120) then

$$\hat{\mathcal{U}}(J^e) = \frac{K_{vp}}{4}\left(J^{e\,2} - 2\ln J^e - 1\right) \tag{3.121}$$

$$\hat{\omega}(\bar{\lambda}^e_1, \bar{\lambda}^e_2, \bar{\lambda}^e_3) = \sum_{r=1}^{3} \frac{(\mu_{vp})_r}{(\alpha_{vp})_r}\left(\bar{\lambda}_1^{e\,(\alpha_{vp})_r} + \bar{\lambda}_2^{e\,(\alpha_{vp})_r} + \bar{\lambda}_3^{e\,(\alpha_{vp})_r} - 3\right) \tag{3.122}$$

The remaining term of (3.120) is chosen here as a simple linear isotropic hardening law analogous to that from Section 2.4.4 (Hughes (1984); Simo and Hughes (2000)), i.e.

$$\hat{h}_{iso}(\alpha) = \tfrac{1}{2}\,\bar{\mathrm{K}}\,\alpha^2 \tag{3.123}$$

where $\bar{\mathrm{K}}$ is the scalar isotropic hardening modulus. Now K_{vp}, $(\mu_{vp})_r$, $(\alpha_{vp})_r$, $\bar{\mathrm{K}}$ and, from the evolution expressions, η_{vp} are the viscoplastic material parameters fully defining the viscoplastic constitutive behavior.

Selection of a linear isotropic hardening relationship is done largely for numerical simplicity and also for the significant reductions in experimental work required to fulfill the hardening parameter when compared to more complex, nonlinear theories. It would be, however, equally applicable to implement a more complex hardening relationship were there

a need to do so. This is a prime example of the power of closest point projection return mapping algorithms.

The principal deviatoric stress terms and the algorithmic tangential operator matrix for the viscoplastic case, calculated with converged incremental values for elastic strain, are again implemented within the generalized framework of Section 3.2 to define the full tensor space expressions for stress and *consistent*, closed-form tangential modulus.

3.4 Numerical verification

The performance of the numerical model treated in the preceding sections is demonstrated here through several verification finite element models. The developed elasto-viscoelastic-viscoplastic material model has been implemented in the form of a user material subroutine (UMAT) for use with the commercial finite element package ABAQUS. The examples presented in what follows provide evidence of the robust nature of the formulation and demonstrate the industrial applicability of the model. Because the results presented represent model testing, the model parameters have been selected qualitatively during the initial testing stages to best demonstrate the performance of the model.

3.4.1 Single element normal tests

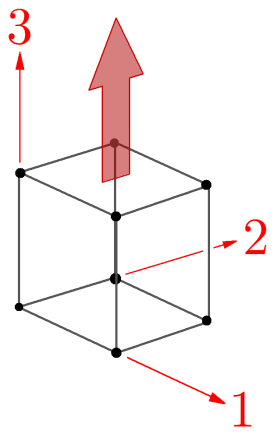

Figure 3.3: Single element geometry for normal testing.

The simplest verification tests involve normal loading of a single element such as the 8-node brick element in Figure 3.3. Loading of this type means the principal planes and global axes coincide and so many of the spectral implications associated with principal

stretch constitutive treatment in tensor space (see Sections 3.1 and 3.2) are negated. Correspondingly, such tests assess, primarily, the performance of the principal space algorithmic aspects treated in Section 3.3.

Taking direction from the types of testing performed on real materials (see for example G'Sell et al. (1992); Zhang and Moore (1997a,b); Brusselle-Dupend et al. (2001, 2003)) uniaxial and biaxial tests incorporating various combinations of loading, unloading, relaxation, recovery and creep were performed to test the implemented material model. Specific examples of these types of tests have formed the basis for the development of the testing methodology outlined in Chapter 4. For actual results from testing of this type, refer to Chapter 4.

3.4.2 Simple shear tests

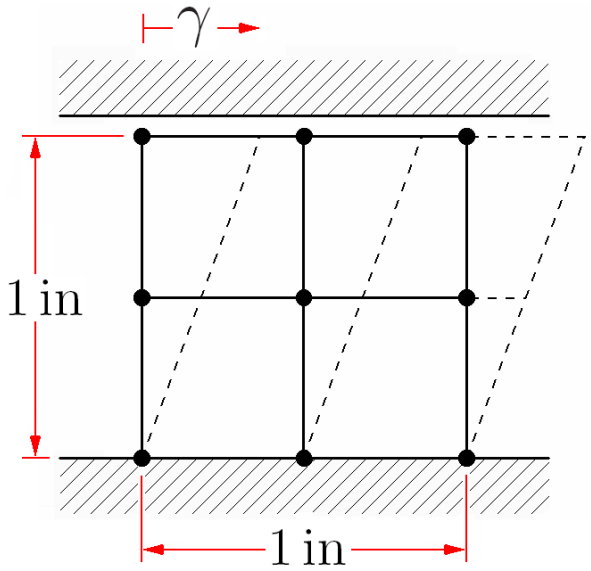

Figure 3.4: Four element simple shear test geometry (figure based on that of Reese and Govindjee (1998a)).

The geometry and simple finite element mesh for the second numerical example is shown in Figure 3.4. This plane strain, simple shear example has been used previously by Reese and Govindjee (1998a) for verification of an elasto-viscoelastic constitutive model. The goal of this numerical simulation is to assess the performance of the treated principal space elasto-viscoelastic-viscoplastic model during a fully three-dimensional problem where rotation of the principal axes is significant. The selected material parameters are provided in Table 3.1.

Table 3.1: Elasto-viscoelastic-viscoplastic material parameters for simple shear testing; the subscript $n = el, ve, vp$ for the elastic, viscoelastic and viscoplastic elements respectively.

Parameter	Units	Elastic	Viscoelastic	Viscoplastic
K_n	[psi]	1×10^5	1×10^5	1×10^5
$(\mu_n)_1$	[psi]	20	51.4	20
$(\mu_n)_2$	[psi]	-7	-18	-
$(\mu_n)_3$	[psi]	1.5	3.86	-
$(\alpha_n)_1$		1.8	1.8	2
$(\alpha_n)_2$		-2	-2	-
$(\alpha_n)_3$		7	7	-
η_n	[psi s]	-	1360.975	1360.975
σ_y	[psi]	-	-	5
$\bar{K}$	[psi]	-	-	250

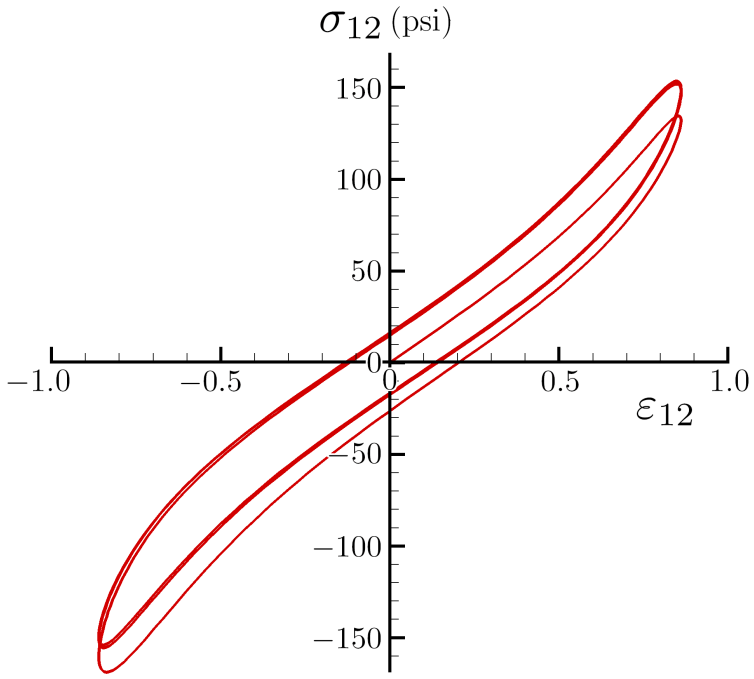

Figure 3.5: In-plane Cauchy shear stress vs shear logarithmic strain for sinusoidal simple shear test.

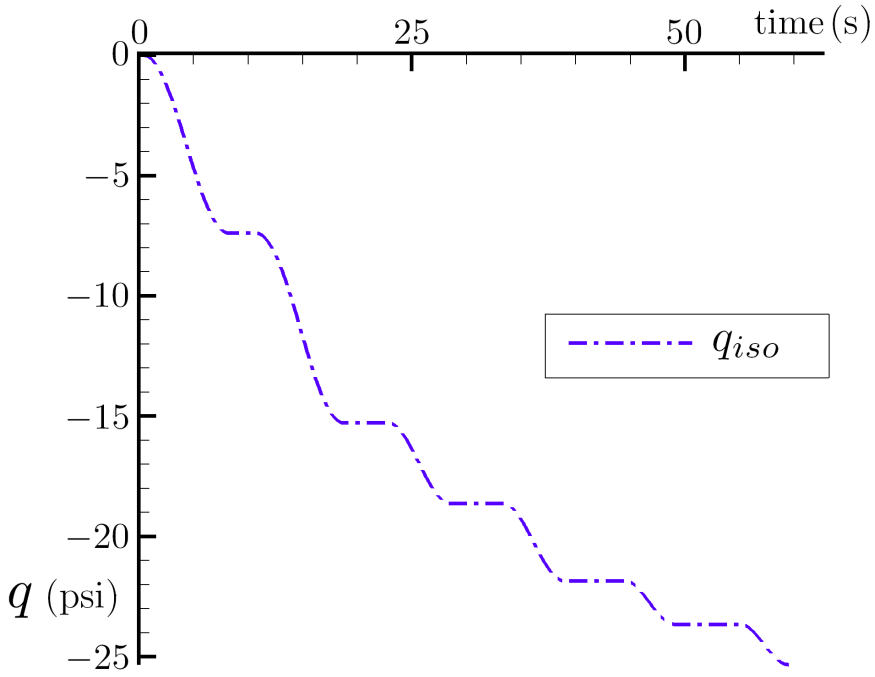

Figure 3.6: Stress space isotropic hardening internal variable during cyclic simple shear test.

A prescribed horizontal displacement was applied to the top edge of the test square sinusoidally such that $\gamma = \sin(0.3\,t)$. This top edge was constrained in the vertical dimension while the three bottom nodes were pinned. In what follows the results from three full sinusoidal cycles are presented ($t = 0 \longrightarrow 62.83\,\mathrm{s}$).

The in-plane Cauchy shear stress is plot against logarithmic shear strain in Figure 3.5 for the sinusoidal simple shear simulation. The plot shows a relatively rapid approach toward cyclic equilibrium.

Of particular importance for the principal plane formulation treated in the preceding sections is the correct spectral treatment of the internal state variables during rotation such as that during simple shear. The sinusoidal testing in this section demonstrates a combination of finite strain, finite rotation and load reversal. Provided in Figure 3.6 is a plot of the stress space isotropic hardening internal variable which shows that the numerical implementation being verified, performs as required from both a rotation and load reversal standpoint.

3.4.3 Simply supported beam: Creep

In the third numerical example, the creep response of a three-dimensional elasto-viscoelastic-viscoplastic simply supported beam during a constantly applied distributed top load was observed (see Figure 3.7). This is a more practical example with creep response being commonly observed when semicrystalline polymers have been used in such circumstances in the past. The material parameters used for this example are the same as for the previous example provided in Table 3.1.

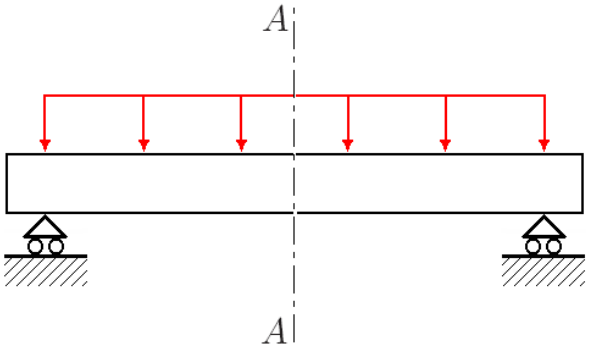

Figure 3.7: Distributed load applied to simply supported beam during creep test.

The beam geometry used for the numerical simulation was 200 in × 20 in × 10 in (Length × Height × Width) and a plane of symmetry $A - A$ (see Figure 3.7) was subsequently observed. 375 8-node brick elements were used to discretize the beam half. A distributed pressure of 0.05 psi was applied to the top surface. This surface load was initially ramped up to 0.05 psi over 10 s and was then held constant for a creep period of 400 s. The deflection of the center section $A - A$ during this period was of most significance. This deflection (δ_{A-A}) is plot against time in Figure 3.8 (note the initial 10 s ramping of the load).

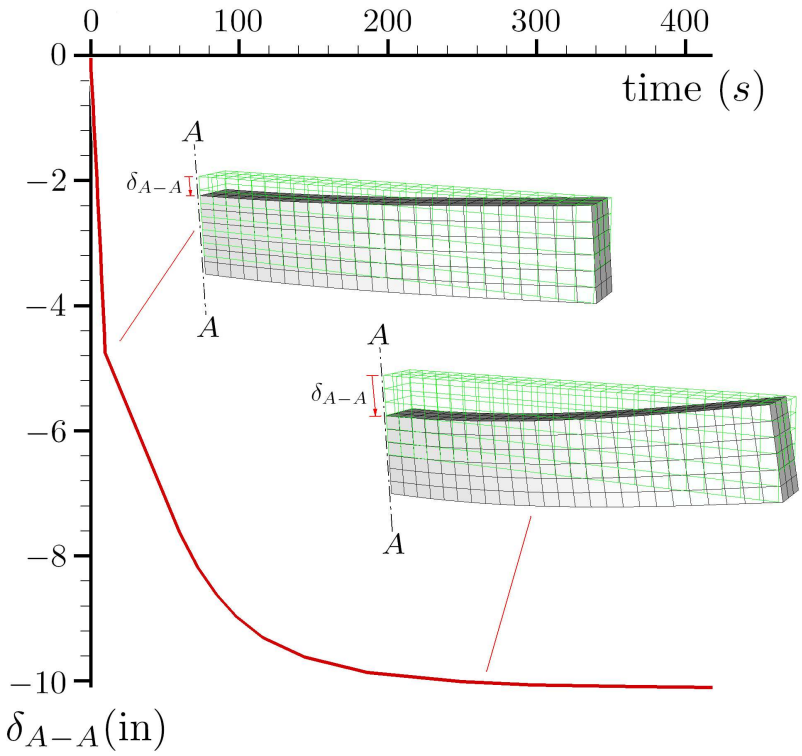

Figure 3.8: Diagram showing the deflection (creep) over time of the simply supported beam following an initially ramped application of the loading; deflection corresponds to a section at the beams center.

3.4.4 Simply supported beam: Relaxation

The final example presented here is an alternate form of the simply supported beam example from Section 3.4.3 above. In this example the center section of the beam $A-A$ was loaded with a prescribed deflection (Figure 3.9) and the relaxation of the axial stress component was observed. The geometry and material model parameters are the same as those used in Section 3.4.3.

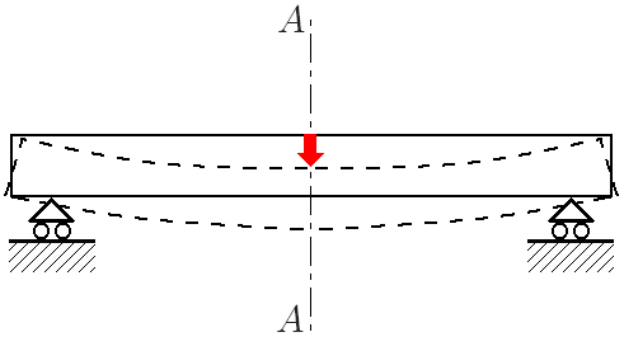

Figure 3.9: Prescribed displacement, applied to the center section of a simply supported beam during relaxation test.

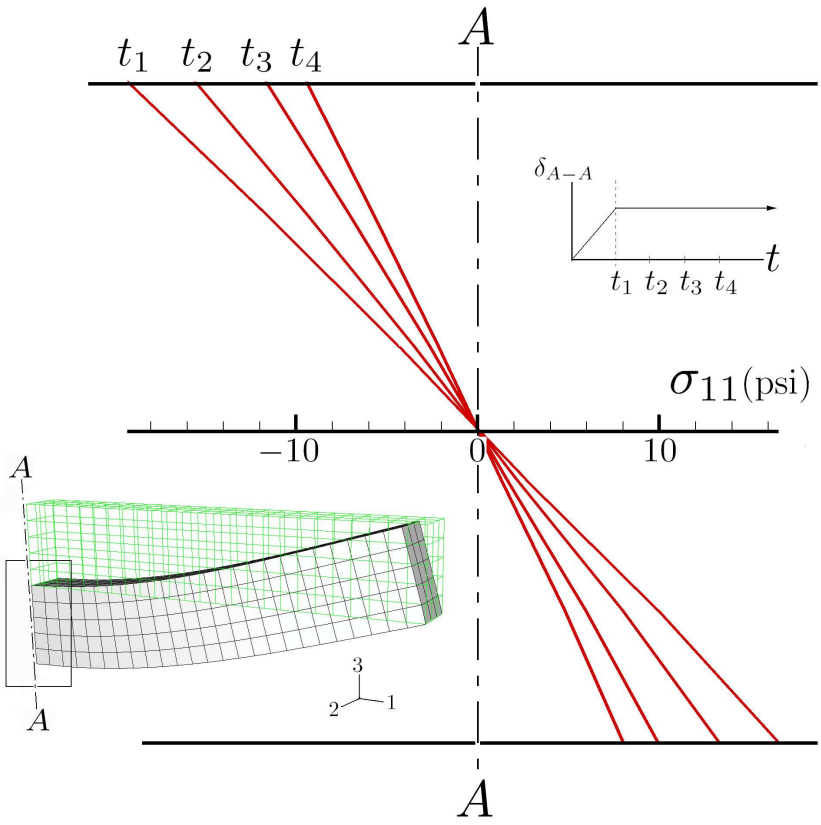

Figure 3.10: Relaxation of the center section axial stress components of the simply supported beam over time. $t_1, t_2, ...t_4$ correspond to arbitrary times during the period of relaxation.

An initial prescribed vertical displacement of -20 in was applied to section $A - A$, ramped over a period of 10 s as before. This displacement was then held for a period of 1000 s and the relaxation of the axial component of stress (σ_{11}) across the whole central

section was observed. A diagram of this axial stress relaxation across the section $A - A$ is provided in Figure 3.10. As would be expected, the axial stress can be seen to reduce or *relax* over time.

3.5 Summary

The objective of this chapter has been to present the principal space numerical implementation of the developed constitutive theory. The form of the implementation generally accommodates possible constitutive variabilities that may arise between polymer classes, provided that they can be broadly classified as being elasto-viscoelastic-viscoplastic. Tensorial expressions for stress and consistent closed-form tangential modulus have been developed for the generalized principal space cases of hyperelasticity and inelasticity. This was done to enable the subsequent algorithmic developments for the three model elements, to be carried out wholly in principal space. Most significantly, a new principal space closest point projection algorithm has been developed for viscoplasticity accommodating isotropic hardening. Numerical examples have been presented as illustration of the implemented model and as a demonstration of the models reproduction of deforming phenomena observed in real situations.

Chapter 4

Development of Testing Methodology

A complex deformation response such as that of semicrystalline polymers results in significant difficulty in generating the parameters for a correspondingly complex constitutive theory such as that developed in this research. This has greatly limited the industrial applicability of similar models in the past. This chapter presents a new testing methodology for isolating the relative elastic, viscoelastic and viscoplastic stress contributions of such materials. By isolating the individual modes of deformation, the task of accurately estimating the model parameters becomes greatly simplified as is subsequently treated in Chapter 5. The testing methodology proposed has been developed using the computational model of Chapter 3. Simulations of real uniaxial testing procedures were used with arbitrarily chosen material parameters. All graphics in this chapter are taken from the numerical results[1]. The major advantage of using such a process to develop a testing regime was the ability to extract the actual component stress values from the program for comparison and validation. This insight allows confidence in the accuracy of the method.

The experimental interrogation and constitutive modeling of semicrystalline polymers has been the focus of many research publications. Authors such as G'Sell and Jonas (1981) pioneered constant strain rate testing of these types of materials using stress relaxation and transient strain rate jumps between loadings to help understand time-dependence and

[1]Note numerical simulations use *self consistent* units; that is, the system of units used for the material parameters gives results in the same unit system. SI units have been used arbitrarily within our simulations however this is a wholly inconsequential specification. All presented graphical results have unspecified units in view of this generality.

plasticity. Similar techniques were adopted by Kitagawa and co workers (Kitagawa and Matsutani (1988); Kitagawa et al. (1989)). A more traditional technique to study viscoelasticity involves using creep and relaxation (Findley et al. (1976)). More recently, creep tests have been used by Zhang and Moore (1997a,b) in combination with constant strain rate testing to phenomenologically fit elasto-viscoelastic and viscoplastic models to polyethylene. In spite of the significant body of research on fitting models to experimental results, the methodology has been predominantly to fit models to *total* stress-strain data, until a two part publication by Brusselle-Dupend et al. (2001, 2003) on polypropylene. Brusselle-Dupend utilized a variety of loading, relaxation, unloading and recovery type tests to partially isolate specific deformation modes, thus allowing insight into the actual behavior of the material. Three-dimensionality was, however, not treated and viscoplasticity was not incorporated in parallel so significant further development of the testing procedure is required for such a method to suit the current theory.

A one-dimensional rheological representation of elasto-viscoelasto-viscoplasticity has been shown in Figure 2.3. Some of the major difficulties with component response separation can immediately be observed from this figure. Firstly there are three independent expressions of elasticity (springs). Distinction between each of these is particularly important to the behavior of each component; however the contribution of each may not be easily discernable during testing. Also, there are two viscous or *time-dependent* components (dashpots) whose separate contributions to time evolution may also not be immediately obvious. These difficulties are compounded by the presence of viscoplastic yield and strain hardening. It was the aim when developing the methodology presented in what follows, to circumvent such limitations.

4.1 3D results from uniaxial testing

Of critical importance to accurate measurement of material response is correct interpretation of tensile test results. One of the most widely used and available methods of testing is the uniaxial tensile test (G'Sell and Jonas (1981); Brusselle-Dupend et al. (2001, 2003); G'Sell and Jonas (1979)). For polymeric, large strain applications, the most desirable format of such a test incorporates closed loop strain control (G'Sell and Jonas (1979)) in the

tensile direction as well as instantaneous measurement of strain in the lateral direction(s)[2]. This can be done using mechanical, laser or video extensometry (G'Sell et al. (1992); Kontou and Farasoglou (1998); Michaeli and Glißmann (2000); Hung and Voloshin (2003)). Instantaneous lateral strain measurement allows for true tensile stress calculations throughout the testing and is also important for the three-dimensional interpretation of the data which follows.

Many research papers treat the results of uniaxial experiments as being one-dimensional in nature (see for example G'Sell and Jonas (1981); Brusselle-Dupend et al. (2001, 2003); Twizell and Ogden (1983)). This may be an inaccurate assumption and could be a major contributor in the inability of such results to be extended to account for three-dimensionality, particularly for large strain. Referring to Figure 4.1 (a) it is evident that because the uniaxial tensile specimen is unconstrained in the lateral dimensions during testing (axis 1 and 2), *total* corresponding lateral stress is zero. Lateral strain is however nonzero and providing the material is reasonably isotropic in nature, some lateral compressive stress component must result. Explanation for this discrepancy comes from the fact that all material deformation invokes a hydrostatic pressure on the deforming material (Bonet and Wood (1997)). For tensile loading, this pressure acts to increase the volume and so a correspondingly positive volumetric stress acts equally in all material directions. In the uniaxial test case, this stress balances the lateral compressive stresses. Total stress can thus be separated into *volumetric* (directionally invariant) and *deviatoric* (directionally dependent) components, a procedure treated at length in the computational mechanics literature (Simo and Hughes (2000); Reese and Govindjee (1998a); Simo (1992); Simo and Taylor (1991); Flory (1961)).

The governing equations for principal volumetric/deviatoric stress separation are

$$\sigma_A = \sigma_{vol} + \mathrm{dev}\,[\sigma_A] \tag{4.1}$$

$$\sigma_{vol} = \frac{\sigma_1 + \sigma_2 + \sigma_3}{3} \tag{4.2}$$

$$\mathrm{dev}\,[\sigma_A] = \bar{\sigma}_A = \sigma_A - \frac{\sigma_1 + \sigma_2 + \sigma_3}{3} \tag{4.3}$$

for $A = 1, 2, 3$, the principal directions. The separation of principal logarithmic strain into volumetric and deviatoric components takes the same form with substitution of ε for σ in

[2]For cylindrical test specimens a single radial strain measurement is needed while for rectangular test samples, measurement of width and thickness strain is necessary.

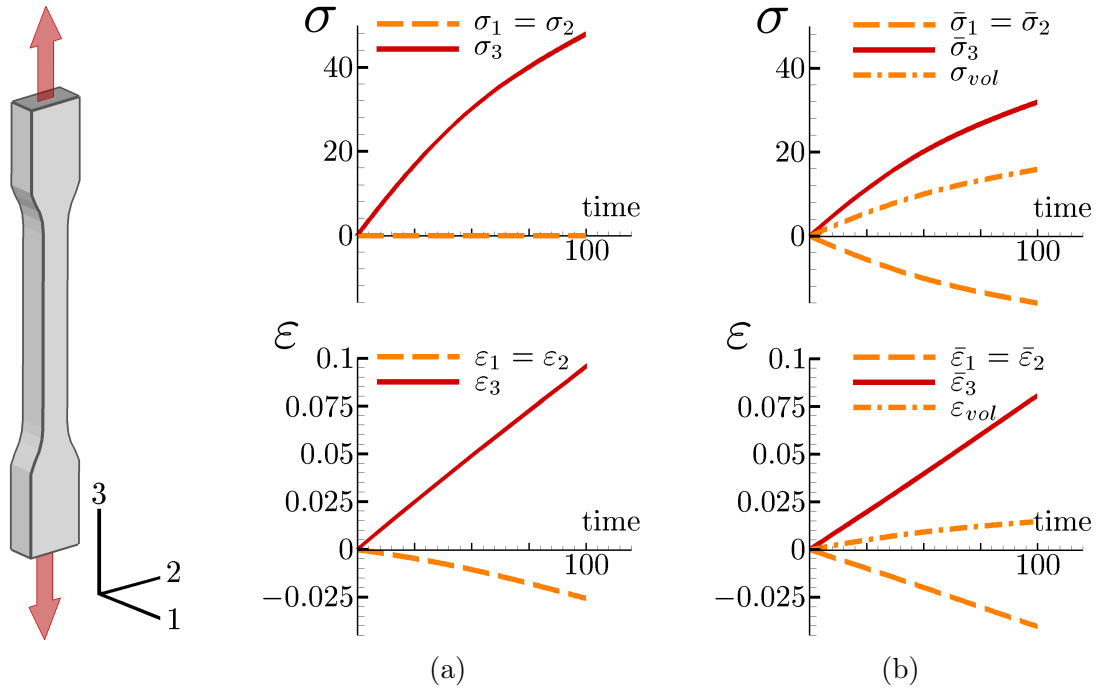

Figure 4.1: Square cross-sectioned uniaxial tensile test sample showing corresponding (a) total stress-time and logarithmic stain-time response, and (b) stress-time and logarithmic strain-time with separated volumetric and deviatoric components.

equations (4.1), (4.2) and (4.3). The resulting separated stress-time and strain-time curves are given in Figure 4.1 (b).

By calculating the volumetric and deviatoric stress and strain components from uniaxial testing, non-zero three-dimensional stress/strain data can be attained using common uniaxial testing equipment. Continuum mechanics constitutive theories are most commonly expressed in terms of separated volumetric and deviatoric relationships (Perić and Dettmer (2003); Simo and Hughes (2000); Reese and Govindjee (1998a); Simo (1992); Simo and Taylor (1991)) and each of these is able to be fit from the uniaxial test results. When parallel deformation modes are present, a volumetric and deviatoric constitutive relationship must be found for each mode. A common practice in computational mechanics is to treat all volumetric response as elastic and thus account for all time-dependence and plasticity within the deviatoric constitutive relationships (Perić and Dettmer (2003); Simo (1992)). Correspondingly, only the deviatoric data set will be treated in what follows, however if inelasticity is present in the volumetric response, this procedure can identically be applied to the volumetric data set. Note also that for the sake of clarity, the methodology discussed

herein deals with only one of the three deviatoric principal stress directions. The procedure presented is intended to be repeated for all other principal directions to fulfill the true three-dimensional data set.

4.2 Isolation of viscoelastic component stress

The measurement of viscoelastic contribution to total deforming stress has been treated in detail by Brusselle-Dupend et al. (2001, 2003) for polypropylene. Their procedure works on the premise that when conducting a constant strain rate loading test up to some specified ultimate strain ε_{ult}, viscoelastic component stress will develop which will wholly relax if that strain were then held constant for some *relaxation* period. By measuring the relaxed stress for a variety of ε_{ult} values, up to some maximum, the relaxed stress data points will lie on the isolated viscoelastic component stress curve.

For materials with parallel elastic, viscoelastic and viscoplastic modes of deformation (Figure 2.3), the accuracy of Brusselle-Dupend's method relies on i) the elementary assumption that elastic component stress remains constant during a period of constant total strain and ii) a rather less elementary assumption that there is also no (or negligible) viscoplastic relaxation. This second assumption is however not necessarily consistent with what is known about viscoplasticity from metals research whereby viscoplastic relaxation has been experimentally observed (see for example Yang et al. (2004)). The amount of this relaxation is largely influenced by the degree of strain hardening and is often non-negligible when compared to that of the viscoelastic element. This fact has been further confirmed during our numerical experiments. Consequently, modification of the method of Brusselle-Dupend to isolate viscoelastic stress is required for it to be more representative in the presence of a simultaneous viscoplastic contribution.

Viscoplastic relaxation will be negligible generally only when strain hardening is sufficient to immobilize viscous evolution, either prior to, or as an instantaneous result of initiating reverse loading (i.e. relaxation). For monotonic loading, this is the case for pre-yield, but generally not for loading after the onset of plasticity. It is possible, however, to condition a material such that hardening is sufficiently high.

Cyclic loading is often used in plasticity research to develop and test strain hardening (Ortiz et al. (1983); Perić and Dettmer (2003)). Here, isotropic hardening increases with

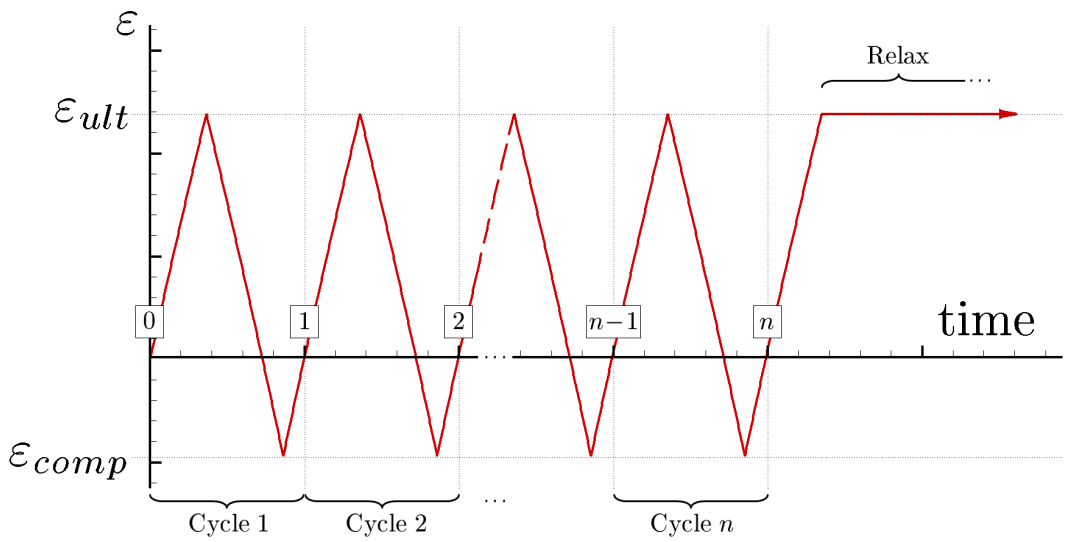

Figure 4.2: Total logarithmic strain control profile for cyclic load-unload test ending with a stress relaxation period.

each cycle, ultimately to a point where all subsequent element response is elastic. The strain-time profile of a cyclic stress conditioning prior to a relaxation test is shown in Figure 4.2. Strain is applied cyclicly between ε_{ult} in tension and some compressive strain ε_{comp}. By cycle $n-1$, viscoplastic strain hardening has increased to the level that for subsequent cycle n, the viscoplastic element behaves elastically and so after subsequent reloading, relaxation will be wholly viscoelastic. Of critical importance to this method is that the viscoelastic stress profile follows exactly the same path for each cycle. Because viscoelastic stress begins at zero (point 0, Figure 4.2), viscoelastic stress must return to zero at the end of each cycle (points $1, 2, ..., n$). This can be achieved via the correct selection of ε_{comp}.

To find ε_{comp}, several trials may need to be carried out. Referring to Figure 4.3, one cycle follows the path a, b, c, d. The specification of ε_{comp} defines the position of c and d. The aim is for there to be zero viscoelastic stress at the end of the loop (point d) which can be confirmed by conducting a relaxation period at zero total strain at this point[3]. If viscoelastic stress is zero as required, then stress will remain constant during relaxation[4]. Too small a value of ε_{comp} will result in positive relaxation and too large a ε_{comp} will result in negative relaxation as is illustrated in the figure. Hence, a suitably close value for ε_{comp} can be found using relatively few trial estimates.

[3]The viscoplastic element is assumed elastic and so will have no contribution to this relaxation, providing total stress at d is small.

[4]Total stress may be nonzero at this point because of plasticity.

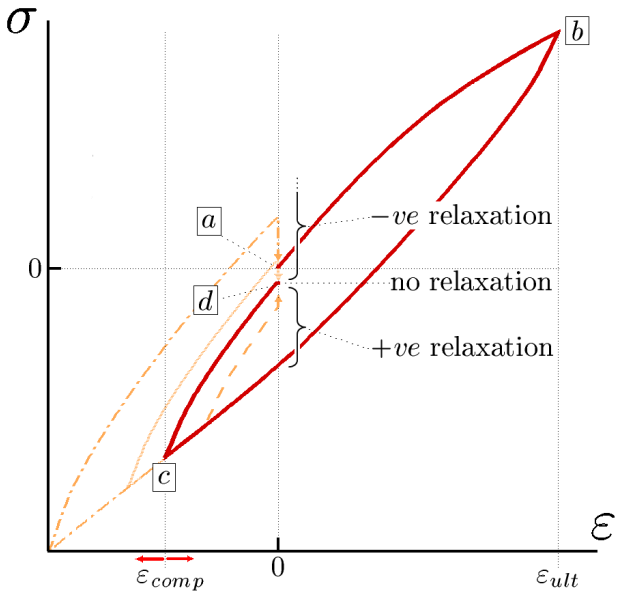

Figure 4.3: Total stress, total logarithmic strain curve for a single conditioning loop to calculate ε_{comp}.

With a suitable ε_{comp} value, cyclic conditioning prior to relaxation can be carried out with no alteration of the initial viscoelastic stress path. An example of the resulting stress strain data (deviatoric) is shown in Figure 4.4. A sufficient number of cycles are performed when consecutive maximum stress values, corresponding to ε_{ult}, are within a suitable tolerance of one another. The subsequent relaxation stress can then be used in an analogous manner to that by Brusselle-Dupend et al. (2001, 2003).

An important consideration in the interpretation of data, such as from Figure 4.4, is in regards to the form of strain measured. Ideally, uniaxial deviatoric strain should be controlled during testing. Unfortunately, deviatoric strain is a function of all principal directions of the test specimen as has been discussed in Section 4.1. The resulting strain control would thus need to be functional on all three dimensions of strain readings, a largely impractical requirement. Instead, careful treatment of *total* uniaxial strain control data can assure accuracy. The most significant implication of this, is in regards to relaxation. Referring to Figure 4.4, while the total uniaxial strain is held constant during the relaxation period, clearly deviatoric strain increases (for tension). By splitting the response into viscoelastic (ve) and combined elastic and viscoplastic ($e + vp$) components (Figure 4.5), it can be seen that this increase in deviatoric strain results in an increase in $\bar{\sigma}_{e+vp}$, meaning

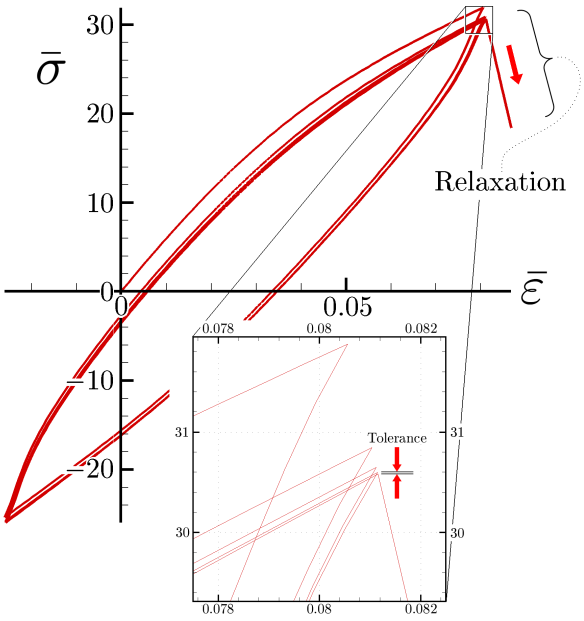

Figure 4.4: Example of deviatoric stress, deviatoric logarithmic strain curve for a cyclic conditioning test to isolate the viscoelastic component of stress.

the relaxed stress or $\bar{\sigma}_{ve(apparent)}$ underestimates the actual viscoelastic stress, $\bar{\sigma}_{ve}$ corresponding to $\bar{\varepsilon}_{ult}$. While this is the case, the end point of the relaxation at $(\bar{\varepsilon}_{relax}, \bar{\sigma}_{relax})$ remains on the combined $e + vp$ curve. By developing a set of stress *and* strain data points on this curve, the result can be subtracted from the total response curve to give the *correct* viscoelastic stress component.

The discontinuity between total strain control during testing and the actual deviatoric strain result has an effect on various other conventions of traditional testing including the accuracy of constant applied strain rate. This is however outside the scope of this research. For completeness, is it worthwhile to note that this behavior also affects relaxation at zero strain as in Figure 4.3, however this affect has been observed to be negligible in all numerical test cases to date and so no correction has been treated here.

4.3 Separation of elastic and viscoplastic component stresses

There is significant difficulty associated with the separation of elastic and viscoplastic components of stress. Direct isolation is theoretically possible in the absence of strain hardening using infinitely low strain rate testing, however this is not the case when hardening is present. Unlike in the viscoelastic case, viscoplastic evolution results from a complex combination

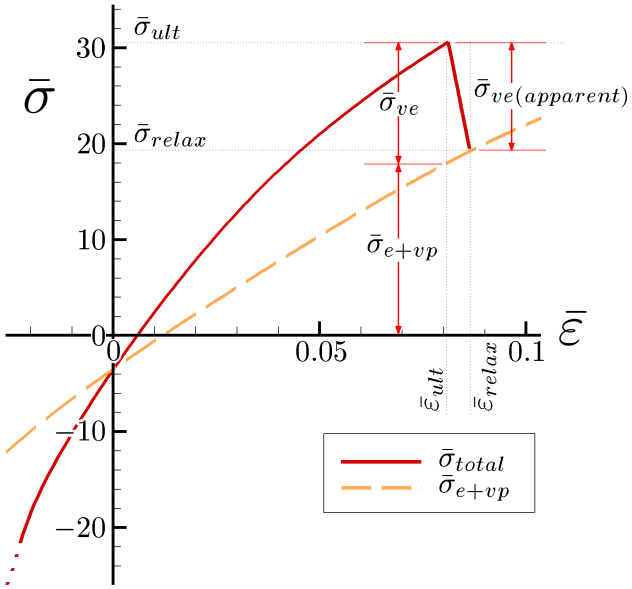

Figure 4.5: Interpretation of relaxation test data accounting for the slip in deviatoric logarithmic strain resulting from the use of total, uniaxial strain control.

of viscous, yield and hardening stress contributions and as such its direct distinction from the elastic component of stress is impossible. Measurement of the exact contributions of each deformation mode is particularly important if a constitutive representation is to reproduce phenomena like unloading and recovery accurately. This section presents a method using realistic testing procedures and iterative data manipulation to separate the elastic and viscoplastic components of stress.

The procedure that follows is made possible by the assumption that the viscoplastic element elastic potential is linear[5]. This is a common convention in computational mechanics (Simo (1992); Perić and Dettmer (2003)). Any deviations of the total elasticity from linearity can be accounted for in the potentials of the elastic or viscoelastic elements. Such deviations are, however, inferred to be small for polymeric materials in the ranges of strain being treated here (pre-necking region, see Twizell and Ogden (1983); Brusselle-Dupend et al. (2001, 2003)). As such, very little loss of generality is predicted to result from the assumption.

[5]Note, this has no effect on the nonlinearity of the viscous evolution or hardening potentials of the viscoplastic element, only that the 'spring' component of the element has a linear stress-strain relationship (such as the St. Venant-Kirchhoff potential, Bonet and Wood (1997))

4.3.1 Initial elastic stress estimate

The first step in the procedure is to get an initial, plausible range estimate for the elastic component of stress. It is an elementary conclusion that the elastic stress curve must lie somewhere within the combined elastic and viscoplastic forward loading curve, $\bar{\sigma}_{e+vp}$ (Section 4.2). Further refinement can be achieved by finding the curvature of the elastic stress-strain curve.

It has been commonly observed in the literature (see for example Dickson et al. (1984) and Feaugas (1999) for plasticity and Neu et al. (2000) and Brusselle-Dupend et al. (2001, 2003) for viscoplasticity) that a linear region exists in the unloading curve of purely plastic materials. For viscoplastic materials the bounds of this linear region correspond to where forward viscous evolution ends and where backward viscous evolution begins. Within the linear region, the viscoplastic element behaves elastically. The implication for materials with simultaneous viscoelastic and viscoplastic response is that within this elastic region of viscoplastic unloading, any stress relaxation becomes wholly viscoelastic. Because it is the linear region that is of interest here, points on the $\bar{\sigma}_{e+vp}$ curve in this region can then be generated using load-unload-recovery tests as in Section 4.2 but without the need for cyclic conditioning. The linear region of viscoplastic unloading will result in a quasi-linear region on this combined elastic and viscoplastic curve. Any deviation from linearity in this section can be wholly attributed to the curvature of the elastic response curve. This curvature can be measured as a vertical difference from a line tangential to the quasi-linear region at its origin. This will be the same vertical difference as between the elastic response curve and a tangent to it at the same strain. Using geometric techniques, this deviation can be combined with that from one or more similar tests, taken to different levels of ultimate strain, to generate the curvature of the complete elastic curve[6]. While the angle of any tangent to the elastic curve is unknown, the evident limitations on it will result in a reduced elastic range.

Referring to Figure 4.6 (a), for the case where the elastic curve has decreasing slope, the maximum limit of the elastic range will not exceed the $\bar{\sigma}_{e+vp}$ curve at any point and the minimum limit will have a positive slope at all points. It can be seen from the figure

[6]Note here that the elastic unloading stress-strain curvature is found and due to the nature of elasticity, this is identical to its forward loading counterpart. Consequently, the forward loading elastic curvature can be determined.

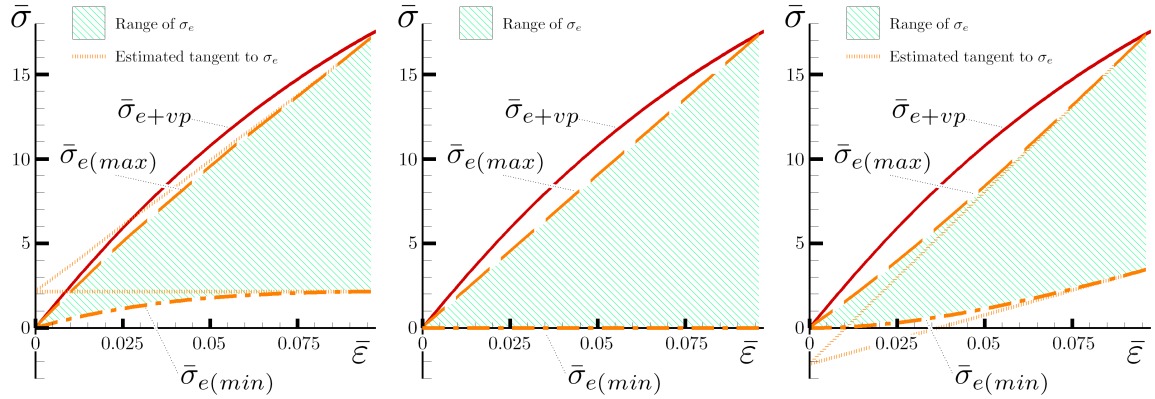

Figure 4.6: Reduced elastic range utilizing measured curvature and the limits on it for an elastic curve of (a) decreasing slope, (b) constant slope and (c) increasing slope.

that these two limitations, reduce the range of possible elastic stress values from that known initially. Figure 4.6 (b) and (c) indicate two other possibilities for elastic response curvature for the linear case and the case of increasing slope respectively. The refinement of the elastic stress curve range and the explicit specification of its curvature are useful for what follows.

4.3.2 Testing regime

Two additional types of experimental tests are required for the isolation of elastic and viscoplastic stress components. The first of these is a loading-unloading-recovery test. Referring to Figure 4.7, loading (up to some specified $\bar{\varepsilon}_{ult}$) and unloading is carried out at the same constant strain rate magnitude. Unloading proceeds until zero total stress is observed at which point that stress is held at zero for a period of recovery. The strain measurements before and after recovery ($\bar{\varepsilon}_a$ and $\bar{\varepsilon}_b$, Figure 4.7) are of particular importance. This type of test must be repeated for multiple $\bar{\varepsilon}_{ult}$ values up to the maximum strain required. The number and spacing of these tests must be adequate to gain sufficient resolution on the desired isolated stress curves as will become apparent.

There are several possible implementations of the second test required. The aim of this test is to provide the combined elastic and viscoplastic unloading curve stress component, $\bar{\sigma}_{e+vp}$, corresponding to the strain at the onset of recovery, $\bar{\varepsilon}_a$ (i.e. $\bar{\sigma}_{e+vp}(\bar{\varepsilon}_a)$, see Figure 4.8). In almost all conceivable cases of strain in the pre-necking region, kinematic hardening will be small enough for the viscoplastic element deformation to be in the elastic range when

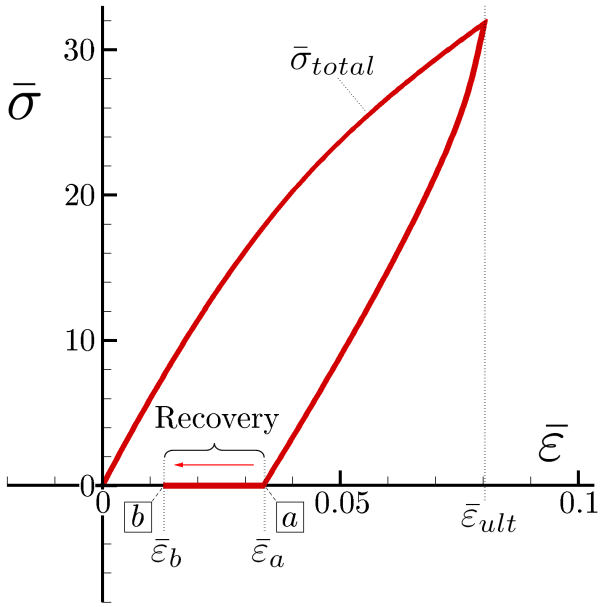

Figure 4.7: Load-unload-recovery testing.

total stress returns to zero. As a result, monotonic load-unload-relaxation testing can be used to locate $\bar{\sigma}_{e+vp}$ points in analogous form to that discussed in Section 4.3.1. Specification of the exact point where relaxation should be initiated is made difficult by the previously discussed shift in deviatoric strain during total strain control, stress relaxation. The most direct account for this is achieved by carrying out several tests with relaxation periods defining points on the $\bar{\sigma}_{e+vp}$ curve either side of that required. Interpolation between the points will then provide the exact stress measurement required ('Direct method', Figure 4.8).

Carrying out several relaxation tests for each recovery strain corresponds to a significant number of experiments. A more efficient alternative involves carrying out a single load-unload-relaxation test for each recovery test, beginning the relaxation period at or near the initial point of zero stress (point a). An approximation for $\bar{\sigma}_{e+vp}$ ($\bar{\varepsilon}_a$) can then be made based on the nature of recovery. At $\bar{\varepsilon}_a$, while total stress is zero, component stresses need not be. During recovery, non-zero viscoelastic stress drives its relaxation such that ultimately only elastic and viscoplastic stress components are left. Component stress redistribution during this process drives strain recovery. Because only elastic and viscoplastic stresses are present at the end of recovery, it is known to be a point on the $\bar{\sigma}_{e+vp}$ curve (i.e. $\bar{\sigma}_{e+vp} = 0$). By tracing a line from this point, b, through the point of relaxation from a, an approximation to

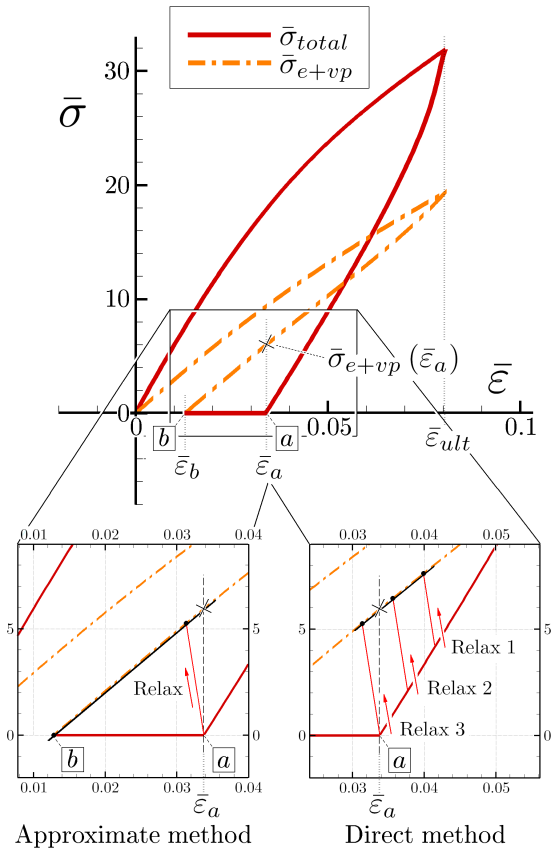

Figure 4.8: Combined elastic and viscoplastic component of stress at the beginning of recovery and the *Approximate* and *Direct* methods of its calculation.

the required stress data point will exist where the line intersects $\bar{\varepsilon}_a$; 'Approximate method', Figure 4.8. Any error with this approximation will relate to the curvature of the elastic stress (see Section 4.3.1). This too could be incorporated into the calculations for a totally accurate result however the error involved will in most cases be small.

Each of these methods should yield sufficiently accurate value for $\bar{\sigma}_{e+vp}\,(\bar{\varepsilon}_a)$. In the case where the elastic stress curve is highly nonlinear, the direct method may be superior, in most other cases the approximate method will suffice.

4.3.3 The viscoplastic element modulus

It is the processing of the data acquired in Section 4.3.2 above that enables the explicit elastic and viscoplastic stress components to be attained. For clarity, the methodology that follows is presented as a graphical technique however development of an algebraic or numerical analogue is a trivial extension.

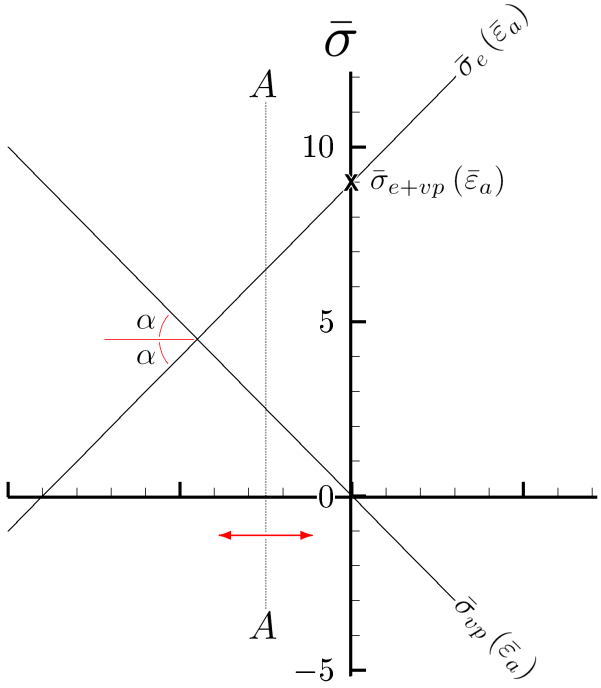

Figure 4.9: X diagram representation of (4.4).

Initially choosing a single recovery test set ($\bar{\varepsilon}_a$, $\bar{\varepsilon}_b$ and $\bar{\sigma}_{e+vp}(\bar{\varepsilon}_a)$) it can be seen that

$$\bar{\sigma}_{e+vp}(\bar{\varepsilon}_a) = \bar{\sigma}_e(\bar{\varepsilon}_a) + \bar{\sigma}_{vp}(\bar{\varepsilon}_a) \tag{4.4}$$

This relationship can be represented graphically as in Figure 4.9 where any vertical section $A - A$ will satisfy (4.4). For convenience, we will refer to this diagram as an X diagram. Algebraically, $\bar{\sigma}_e(\bar{\varepsilon}_a)$ and $\bar{\sigma}_{vp}(\bar{\varepsilon}_a)$ are functional on one another but are unknown and so have an infinite range. Suppose that the elastic stress curve is known, then for any $\bar{\sigma}_e(\bar{\varepsilon}_a)$ stress component, the X diagram can be used to calculate the companion viscoplastic stress component, $\bar{\sigma}_{vp}(\bar{\varepsilon}_a)$. This is demonstrated in Figure 4.10 where for some strain $\bar{\varepsilon}_a$, the $\bar{\sigma}_{e+vp}(\bar{\varepsilon}_a)$ and $\bar{\sigma}_e(\bar{\varepsilon}_a)$ values are projected from the stress-strain curve (a), onto the X diagram (b), the corresponding viscoplastic value is found and returned to the stress-strain plot.

Using the arbitrarily chosen elastic stress curve from Figure 4.10 (a), the strains before and after recovery are known ($\bar{\varepsilon}_a$ and $\bar{\varepsilon}_b$), therefore the change in elastic stress, $\Delta\bar{\sigma}_e(\Delta\bar{\varepsilon})$, during relaxation is also known, Figure 4.11 (a). As was done for the single data point in Figure 4.10, here both stress points can be projected onto the X diagram (Figure 4.11 (b))

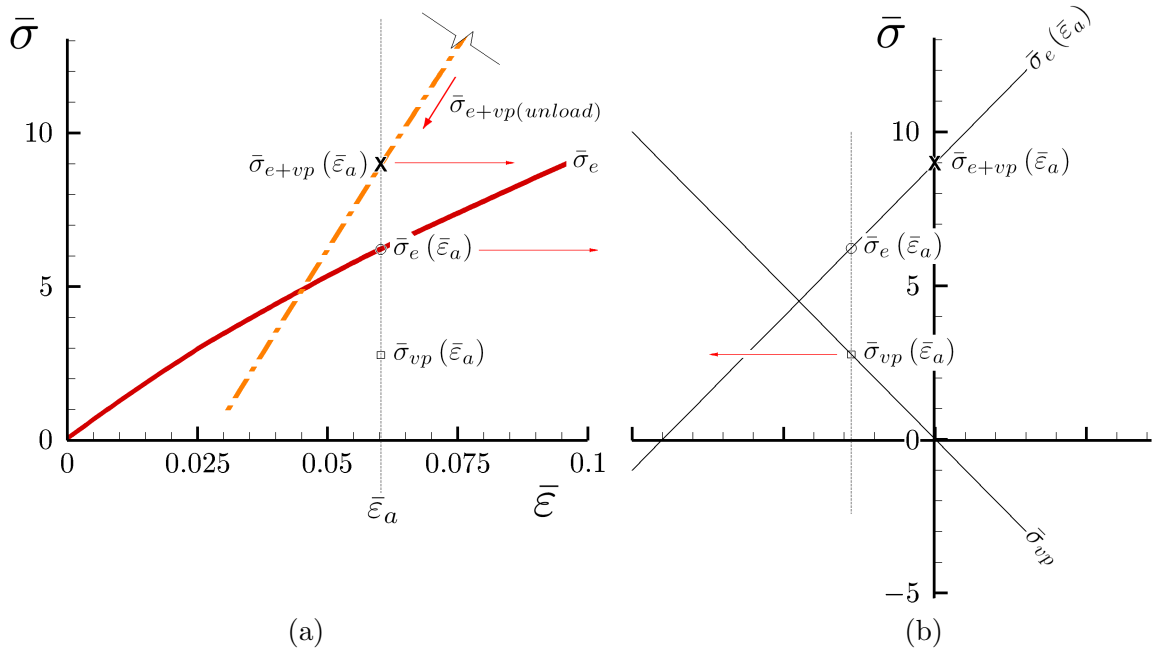

Figure 4.10: Calculation of the viscoplastic stress component corresponding to a known elastic stress component via projection between (a) the stress-logarithmic strain curve and (b) the X diagram.

to calculate the corresponding change in viscoplastic stress during relaxation, $\Delta\bar{\sigma}_{vp}(\Delta\bar{\varepsilon})$. It is important to note that the elastic stress corresponding to the end of recovery, $\bar{\sigma}_e(\bar{\varepsilon}_b)$, is projected onto the $\bar{\sigma}_{e+vp}(\bar{\varepsilon}_b) = 0$ line on the X diagram because, as noted previously, the combined elastic and viscoplastic stress curve is always zero at the end of recovery.

The most important step here is to recall that the viscoplastic element behaves elastically during the entire recovery period. Consequently, the change in the elastic component of viscoplastic strain during the recovery will be equal to the change in total strain, i.e.

$$\Delta\bar{\varepsilon}^e_{vp} = \Delta\bar{\varepsilon} \tag{4.5}$$

Because the elastic potential of the viscoplastic element has been assumed linear, the corresponding elastic modulus, E_{vp}, will be constant and thus can be defined from any and all $i = 1, 2, ..., n$ recovery test sets as

$$E_{vp} = \left.\frac{\Delta\bar{\sigma}_{vp}}{\Delta\bar{\varepsilon}^e_{vp}}\right|_{i=1,2,...,n} = \left.\frac{\Delta\bar{\sigma}_{vp}}{\Delta\bar{\varepsilon}}\right|_{i=1,2,...,n} \tag{4.6}$$

Carrying out the procedure from Figure 4.11 to calculate E_{vp} for $i = 1, 2, ..., n$ sets of

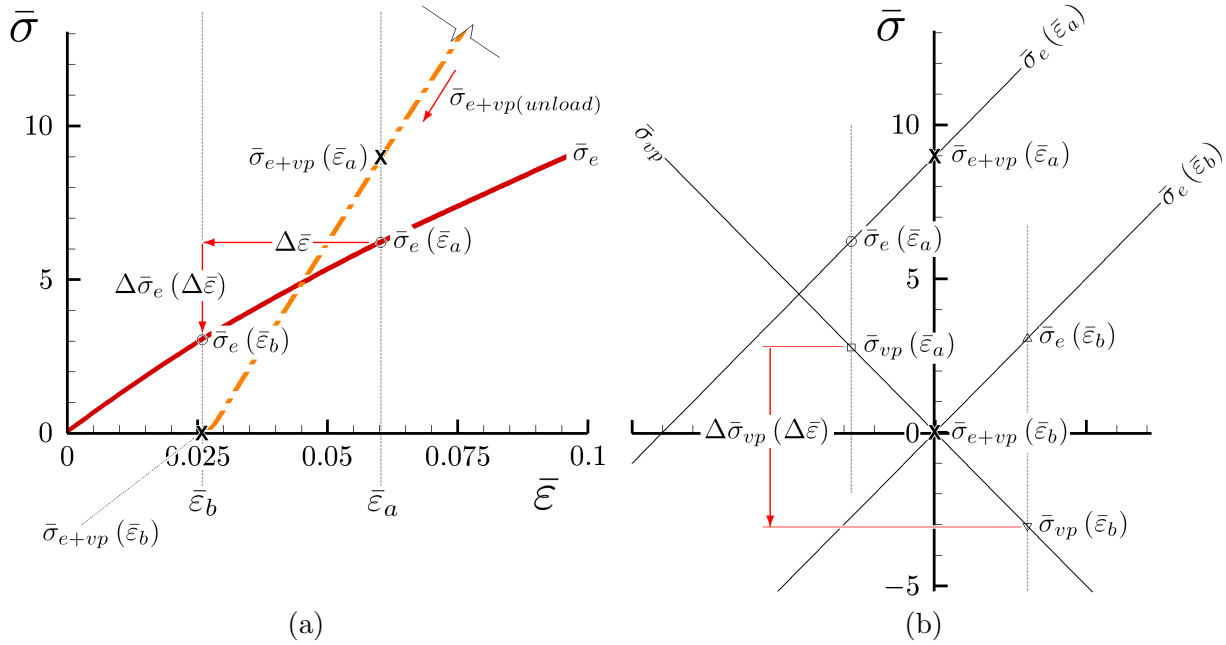

Figure 4.11: Calculation of the change in viscoplastic stress corresponding to the change in elastic stress during relaxation via projection between (a) the stress-logarithmic strain curve and (b) the X diagram.

data, an average value for the viscoplastic modulus can be attained that is representative of the entire range of strain of interest. This process is carried out in Figure 4.12. Graphically, the average E_{vp} value can be attained by plotting $\Delta\bar{\sigma}_{vp}(\Delta\bar{\varepsilon})|_i$, against $\Delta\bar{\varepsilon}|_i$ and calculating the slope of a linear trend-line (Figure 4.13). It is pertinent to note that because the viscoplastic modulus is equal for all magnitudes of strain, its value is solely dependent on the elastic stress curve that was initially chosen. This functionality is denoted by $E_{vp}(\bar{\sigma}_e)$. It is this relationship that can be exploited to establish the explicit components of elastic and viscoplastic stress, as presented in the next section.

4.3.4 Elastic and viscoplastic stress and strain components

The previous section has established the relationship between an arbitrarily chosen elastic stress curve and the viscoplastic modulus. Because the viscoplastic potential is linear, this can be extended to calculate the elastic and plastic components of viscoplastic strain during loading via

$$\bar{\varepsilon}^e_{vp} = \frac{\bar{\sigma}_{e+vp} - \bar{\sigma}_e}{E_{vp}} \tag{4.7}$$

$$\bar{\varepsilon}^p_{vp} = \bar{\varepsilon} - \bar{\varepsilon}^e_{vp} \tag{4.8}$$

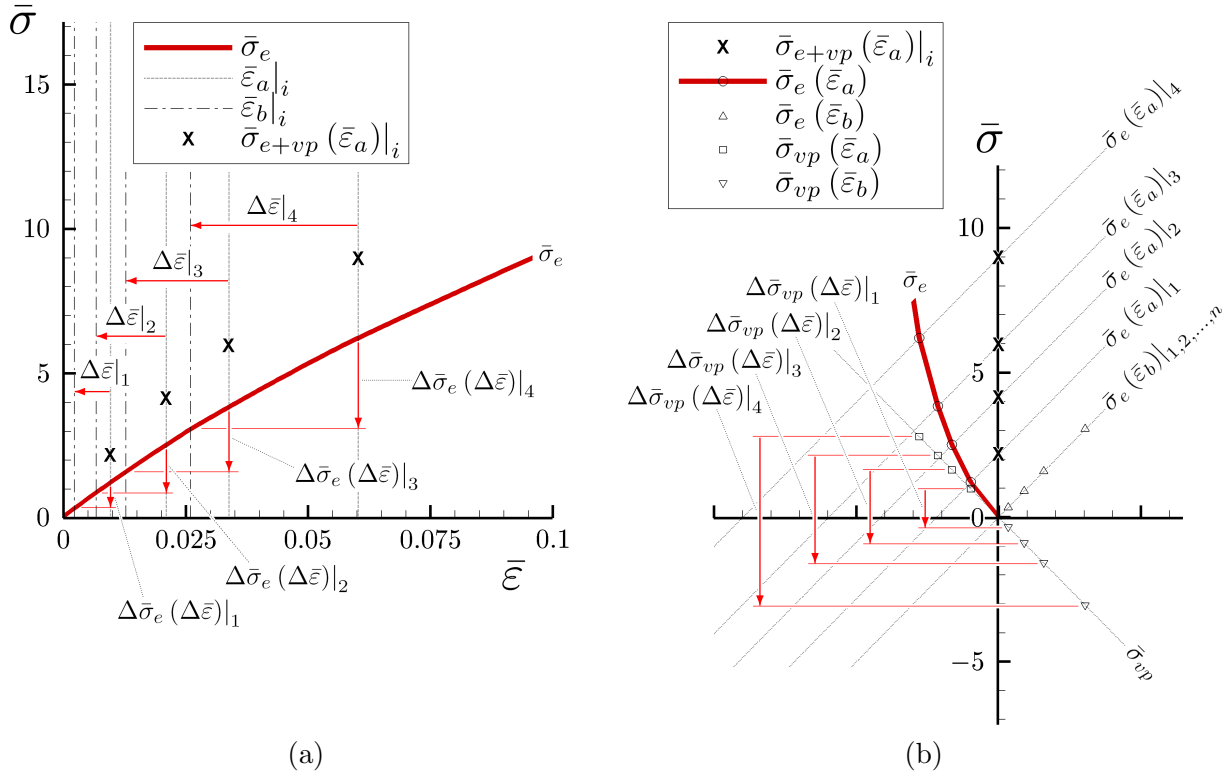

Figure 4.12: Calculation of the change in viscoplastic stress for all $n = 4$ sets of experimental data via projection between (a) the stress-logarithmic strain curve and (b) the X diagram.

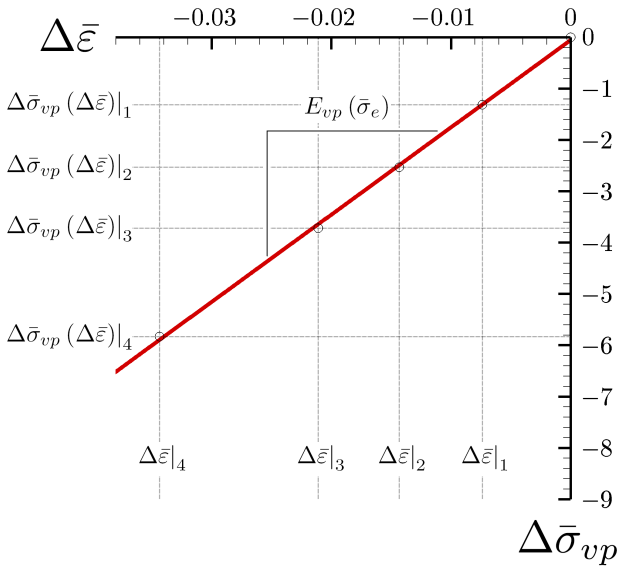

Figure 4.13: Change in viscoplastic stress during recovery against change in total logarithmic strain during recovery showing the subsequently calculated average E_{vp}.

where all values correspond to that from forward loading.

Conventionally it has been assumed that the residual strain in an elasto-viscoelastic-viscoplastic material after recovery ($\bar{\varepsilon}_b$ in Section 4.3.2) is equivalent to the maximum plastic strain developed during loading (i.e. that accumulated at $\bar{\varepsilon}_{ult}$, see Brusselle-Dupend et al. (2001, 2003)). From (4.8) however, it can be inferred that the accuracy of such an assumption would be offset by any elastic component of viscoplastic strain present after recovery (non-zero if $\bar{\varepsilon}_b \neq 0$). In all numerical test cases to date, however, such an offset has been observed to become significant only in the later stages of plastic evolution. Within the initial stages of plastic deformation (within pre-necking region), the assumption that residual recovery strain is equivalent to the generated plastic component of viscoplastic strain is accurate.

Knowing the value of $\bar{\varepsilon}^p_{vp}$ at the early stages of viscoplastic evolution and knowing the subsequent relationships back to E_{vp} and $\bar{\sigma}_e$ from equations (4.7) and (4.8), and Section 4.3.3, it is possible to define the explicit values for elastic and viscoplastic stress components as required. This will be done graphically using the most basic form of trial estimate and correction however it is conceivable that a numerical analogue may also be possible.

In Section 4.3.1, a range for the elastic stress curve was developed and its actual curvature was determined. Using the known curvature of the elastic stress, it is possible to discretize this range into multiple possible curves between the maximum and minimum known limits. An example of such a discretization is illustrated in Figure 4.14 (a). Proceeding with the X diagram method (Figure 4.14(b)[7]) to determine the various possible viscoplastic modulus values (Figure 4.14(c)), equations (4.7) and (4.8) are then used to determine the corresponding $\bar{\varepsilon}^p_{vp}$ curves, Figure 4.14(d).

Superimposed on Figure 4.14(d), are the residual strain values left after recovery. As noted before, these points approximate the plastic component of viscoplastic strain generated during forward loading and as such are ploted against the time to maximum forward strain ($\bar{\varepsilon}_{ult}$). It is evident from the figure that the approximate plastic strain curve, $\bar{\varepsilon}^p_{vp(approximate)}$, lies between the *second* and *third* trial curves. Thus

$$\bar{\varepsilon}^p_{vp}\left(E_{vp}\left(\bar{\sigma}_{e(2)}\right)\right) > \bar{\varepsilon}^p_{vp} > \bar{\varepsilon}^p_{vp}\left(E_{vp}\left(\bar{\sigma}_{e(3)}\right)\right) \tag{4.9}$$

[7]Only the elastic stress curves corresponding to $\bar{\varepsilon}_a|_i$, $i = 1, 2, ..., n$ have been shown. The other points have been generated as in Section 4.3.3 but are omitted from the figure for clarity.

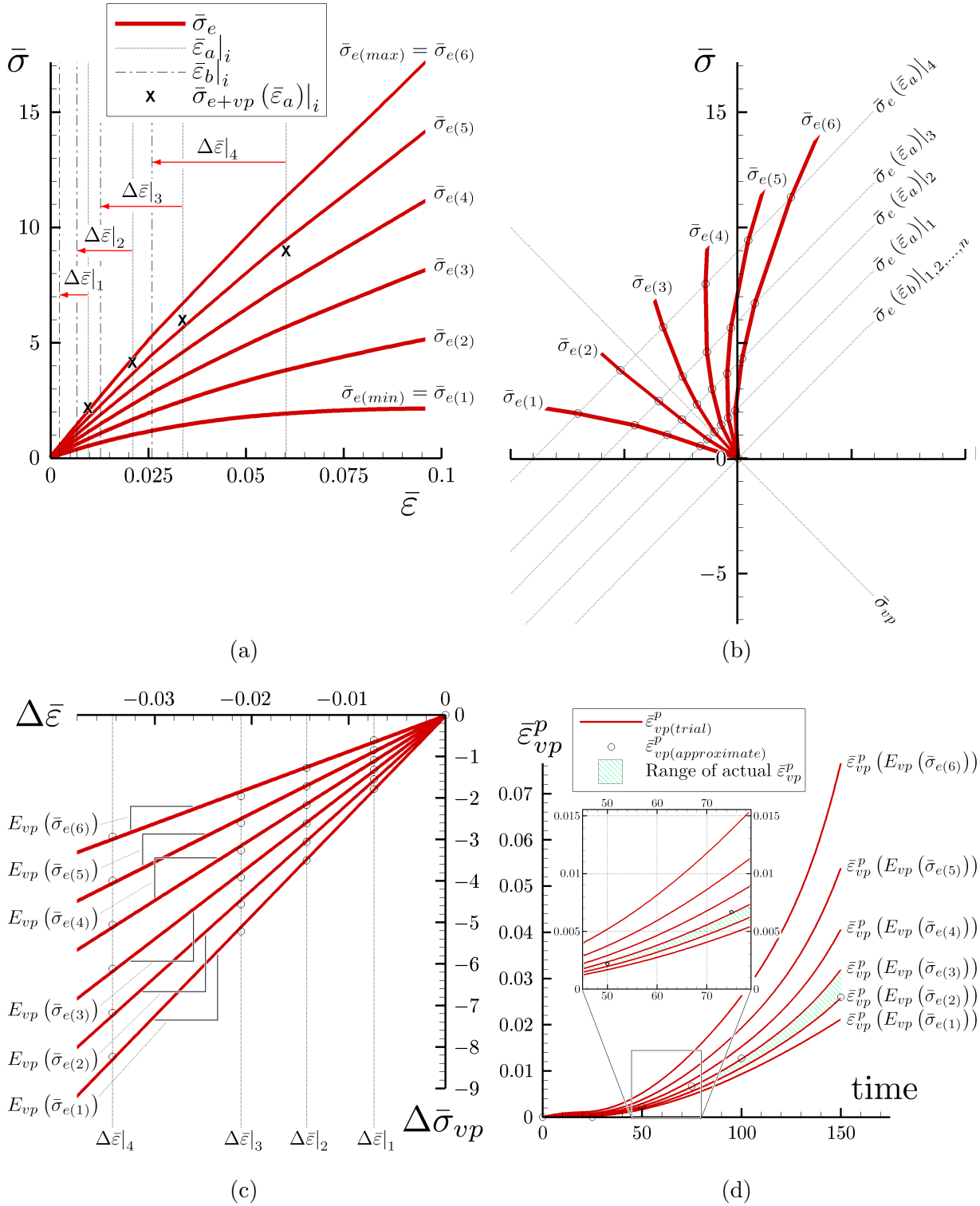

Figure 4.14: Calculation of the plastic component of viscoplastic logarithmic strain using X diagram methodology showing the relative (a) stress-logarithmic strain curves, (b) the X diagram, (c) the resulting viscoplastic modulus curves and (d) the calculated plastic component of viscoplastic logarithmic strain vs time.

and correspondingly

$$\bar{\sigma}_{e(2)} < \bar{\sigma}_e < \bar{\sigma}_{e(3)} \tag{4.10}$$

Clearly, the range for $\bar{\sigma}_e$ has been significantly reduced during this process. If necessary, $\bar{\sigma}_{e(2)}$ and $\bar{\sigma}_{e(3)}$ can be used as the updated minimum and maximum elastic stress curves and the process can be repeated with subsequent iterations converging toward more accurate values for $\bar{\sigma}_e$, E_{vp} and $\bar{\varepsilon}^p_{vp}$. As has been the case for the example shown here, the variability of the approximation $\bar{\varepsilon}_b \simeq \bar{\varepsilon}^p_{vp}$ may limit this type of further refinement. The most practical way to circumvent this is to carry out this procedure at two or more strain rates (generally the maximum and minimum rates of interest) and take average values for $\bar{\sigma}_e$ within where the two calculated end ranges intersect. This will give exact values for $\bar{\sigma}_e$ and subsequently E_{vp} and $\bar{\varepsilon}^p_{vp}$.

Recalling from Section 4.2 that the combined elastic and viscoplastic loading curve, $\bar{\sigma}_{e+vp}$ is known then

$$\bar{\sigma}_{vp} = \bar{\sigma}_{e+vp} - \bar{\sigma}_e \tag{4.11}$$

and all required stress components have been isolated.

The accuracy of the isolated stress components found using the presented methodology is evident from comparison with the actual values output from the numerical simulation, Figure 4.15. Relatively few assumptions were required to arrive at this outcome with the result being a more comprehensive account of the deforming behavior of such materials than has been possible in previous research of this nature (Brusselle-Dupend et al. (2001, 2003)).

4.4 Measurement of subset viscoplastic viscous, yield and hardening stresses

There exists a significant amount of published research concerned with the isolation of subset stress components for plastic and viscoplastic materials (see for example Brusselle-Dupend et al. (2001, 2003); Dickson et al. (1984); Feaugas (1999); Neu et al. (2000)). In plasticity these subset stresses are commonly referred to as *back* and *effective* stress, referring to the translation and radius of the yield surface respectively (Feaugas (1999)). From a continuum mechanics standpoint, back stress is associated with kinematic hardening, while effective

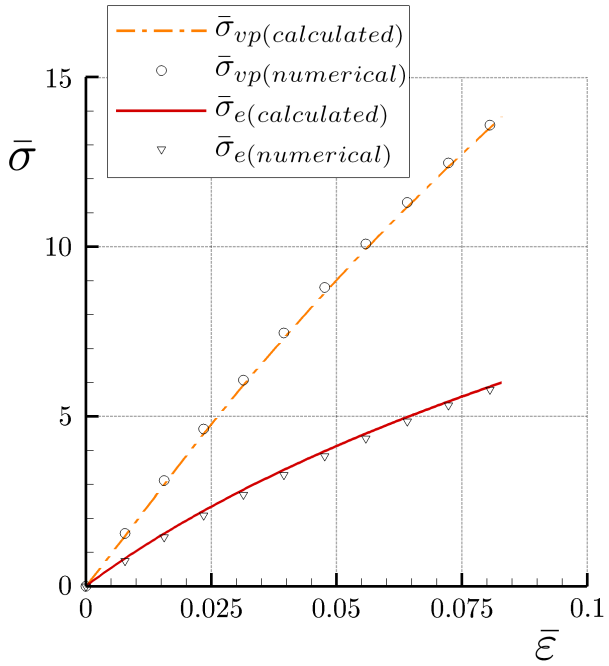

Figure 4.15: Comparison of the isolated elastic and viscoplastic forward loading stress components found using the X diagram methodology with the actual values output from the numerical analysis.

stress refers to the combined measures of yield stress and isotropic hardening. In viscoplasticity, a fourth stress component is present, accounting for viscous evolution. The explicit separation of viscoplastic stress into four components; yield stress ($\bar{\sigma}_y$), kinematic hardening stress ($\bar{\sigma}_{kin}$), isotropic hardening stress ($\bar{\sigma}_{iso}$) and viscous or dashpot stress ($\bar{\sigma}_{d-p}$), is a largely theoretical convenience as, from a micro-mechanical perspective, it is more common to think of yield and hardening as being one entity. To spite this fact, the constitutive behaviors of each are indeed independent (or at least separate) and so individual measurement is quite valuable. Back-stress type isolation methodology is modified to this end in what follows, noting that while kinematic hardening was neglected within the numerical model of Chapter 3, here it has been retained for generality (see Simo and Hughes (2000) for more on the components of viscoplasticity).

As was the case in the previous section, data from numerical simulations was used to gain insight into the actual mechanism of the isolation testing method. From a load-unload test, the viscoplastic stress and the relative subset stress components ($\bar{\sigma}_y$, $\bar{\sigma}_{kin}$, $\bar{\sigma}_{iso}$ and $\bar{\sigma}_{d-p}$)[8] are shown in Figure 4.16. From the methodology presented in previous sections it

[8]The inclusion of kinematic hardening within these numerical simulations was done on an ad-hoc basis, justified by the uniaxial nature of the tests.

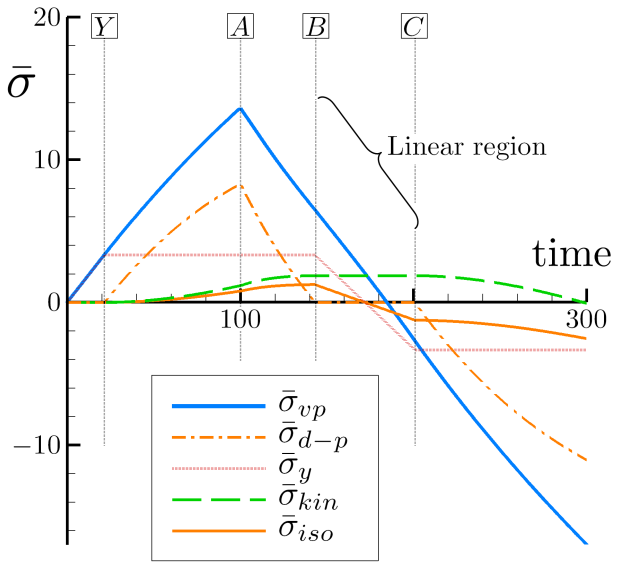

Figure 4.16: Components of viscoplastic stress during a load-unload simulation showing regions of importance for back-stress isolation technique.

is possible to define the following values from such a test:

1. the value of viscoplastic stress at yield, Y
2. the whole viscoplastic loading curve, 0 to A, and
3. the linear section of unloading stress and correspondingly its bounds, B and C.

It is the aim of the back-stress isolation methodology to calculate the subset viscoplastic components at the end of loading (A). By carrying out such tests across a range of peak stress values (strain controlled), data points on each component stress curve can be defined. Because the values of viscoplastic stress ($\bar{\sigma}_{vp}$) at Y, A, B and C can be measured from tests, these values can be used to calculate the required component values.

Conventional back-stress isolation methodology applied to this circumstance exploits the following observations

$$\bar{\sigma}_{vp}|_Y = \bar{\sigma}_y \tag{4.12}$$

$$\bar{\sigma}_{vp}|_A = \bar{\sigma}_{d-p} + \bar{\sigma}_y + \bar{\sigma}_{iso} + \bar{\sigma}_{kin} \tag{4.13}$$

$$\bar{\sigma}_{vp}|_B = \bar{\sigma}_y + \bar{\sigma}_{iso} + \bar{\sigma}_{kin} \tag{4.14}$$

$$\bar{\sigma}_{vp}|_C = -\bar{\sigma}_y - \bar{\sigma}_{iso} + \bar{\sigma}_{kin} \tag{4.15}$$

Simultaneous solution of equations (4.12) to (4.15) enables the calculation of the four unknown subset stress components.

There is an evident discrepancy with equations (4.12) to (4.15) whereby for the method to calculate the component stresses at A, $\bar{\sigma}_y$, $\bar{\sigma}_{iso}$ and $\bar{\sigma}_{kin}$ must all remain constant during initial unloading (A to B). Clearly from the figure this is not the case. In the early stages of unloading, while steadily decreasing in magnitude, forward viscous plastic evolution continues until B. As a consequence, the strain hardening quantities $\bar{\sigma}_{iso}$ and $\bar{\sigma}_{kin}$, correspondingly continue to increase until the end of forward plastic strain evolution. Assuming $\bar{\sigma}_{iso}$ and $\bar{\sigma}_{kin}$ to be constant over this period results in significant error; in the case of Figure 4.16, this error is of the order of 50%.

Amending equations (4.12) to (4.15) to account for the change in $\bar{\sigma}_{iso}$ and $\bar{\sigma}_{kin}$ from A to B

$$\bar{\sigma}_{vp}|_Y = \bar{\sigma}_y \tag{4.16}$$

$$\bar{\sigma}_{vp}|_A = \bar{\sigma}_{d-p} + \bar{\sigma}_y + \bar{\sigma}_{iso} + \bar{\sigma}_{kin} \tag{4.17}$$

$$\bar{\sigma}_{vp}|_B = \bar{\sigma}_y + \bar{\sigma}_{iso} + \Delta\bar{\sigma}_{iso} + \bar{\sigma}_{kin} + \Delta\bar{\sigma}_{kin} \tag{4.18}$$

$$\bar{\sigma}_{vp}|_C = -\bar{\sigma}_y - \bar{\sigma}_{iso} - \Delta\bar{\sigma}_{iso} + \bar{\sigma}_{kin} + \Delta\bar{\sigma}_{kin} \tag{4.19}$$

where $\bar{\sigma}_y$, $\bar{\sigma}_{kin}$, $\bar{\sigma}_{iso}$ and $\bar{\sigma}_{d-p}$ are the true values at A and where $\Delta\bar{\sigma}_{iso} = \bar{\sigma}_{iso}|_B - \bar{\sigma}_{iso}|_A$ and $\Delta\bar{\sigma}_{kin} = \bar{\sigma}_{kin}|_B - \bar{\sigma}_{kin}|_A$.

We now have six unknown values with only four equations and hence a unique solution cannot be achieved. This deficiency can be resolved by exploiting the useful outcome from Section 4.3.4 that, given the viscoplastic stress and elastic relationship, the elastic and plastic components of viscoplastic strain can be found, i.e.

$$\bar{\varepsilon}^e_{vp} = \frac{\bar{\sigma}_{vp}}{E_{vp}} \tag{4.20}$$

$$\bar{\varepsilon}^p_{vp} = \bar{\varepsilon} - \bar{\varepsilon}^e_{vp} \tag{4.21}$$

Thus, the plastic components of viscoplastic strain at A and B (i.e. $\bar{\varepsilon}^p_{vp}|_A$ and $\bar{\varepsilon}^p_{vp}|_B$) can be calculated. A common convention in computational plasticity is to assume the relationship between kinematic and isotropic hardening stresses and the plastic component of viscoplastic strain to be linear (Simo and Hughes (2000); Hughes (1984)). Here a similar

assumption will be adopted as a means of achieving the objective. This assumption can be implemented as follows

$$\frac{\bar{\varepsilon}^p_{vp}|_A}{\bar{\varepsilon}^p_{vp}|_B} = \frac{\bar{\sigma}_{iso}|_A}{\bar{\sigma}_{iso}|_B} = \frac{\bar{\sigma}_{iso}}{\bar{\sigma}_{iso} + \Delta\bar{\sigma}_{iso}} \tag{4.22}$$

and likewise

$$\frac{\bar{\varepsilon}^p_{vp}|_A}{\bar{\varepsilon}^p_{vp}|_B} = \frac{\bar{\sigma}_{kin}|_A}{\bar{\sigma}_{kin}|_B} = \frac{\bar{\sigma}_{kin}}{\bar{\sigma}_{kin} + \Delta\bar{\sigma}_{kin}} \tag{4.23}$$

Because the plastic strain components at A and B are known, equations (4.22) and (4.23) can be solved simultaneously with equations (4.16) to (4.19) to result in a unique solutions for the four subset stress components at A.

A weakness with the theory proposed here is that the hardening moduli are assumed linear when this may not be the case for real materials. This being said, within the range of strains being discussed, there is only a small likelihood that nonlinearity would be severe enough to affect the result significantly. Given the degree of error associated with the conventional back-stress method, any correction, linear or otherwise, would result in a considerable increase in accuracy to that used previously and so is worthwhile.

4.5 Summary

The testing and data manipulation methodology presented in this chapter, makes possible the total isolation of the elastic, viscoelastic and viscoplastic stress components of semicrystalline polymer response, as well as the subset viscoplastic element stress components. Isolating the respective deformation response characteristics greatly simplifies the determination of material model parameters as will become evident in the following chapter. The performance of the developed testing methodology has been compared against the results from numerical simulations with known stress components. The result of this comparison has demonstrated the developed method to be highly accurate.

Chapter 5

Parameter Estimation

In this chapter, the theoretical aspects of the parameter estimation for the developed elasto-viscoelastic-viscoplastic constitutive model are presented. This methodology is intended for use with experimental data of the type treated in Chapter 4. The work presented here, represents the bridging between the theoretical model and physical experimentation and is critical for the meaningful implementation of a constitutive theory such as that developed in the earlier chapters of this thesis. The difficulties associated with parameter estimation have been a major contributing factor toward the inadequacies of existing constitutive theories with comparable levels of complexity. It has been the aim of the testing methodology of Chapter 4 and the techniques presented in what follows, to circumvent many of these difficulties.

For hyperelastic materials such as rubbers, relatively standardized parameter determination techniques have been developed using least squares optimization algorithms such as that commonly attributed to Levenberg and Marquardt (Levenberg (1944); Marquardt (1963)). This methodology and others such as the Gauss-Newton and various quasi-Newton methods (Gill and Murray (1978); Nocedal and Wright (1999)) have found wide implementation within many commercial curve fitting software packages. It is a major advantage of the methodology presented in Chapter 4, that the majority of material parameters required for the constitutive theory developed here can be calculated using such conventional optimization methods.

For the viscoelastic element, however, it is not possible to distinguish between the elastic and inelastic components of strain during testing. Consequently, because of the complex

nature of the constitutive relationships ((2.14), (2.16) and (2.18)), the standard curve fitting approach is insufficient to fully develop the viscoelastic parameter set. A modification on the methodology of Levenberg and Marquardt is presented in Section 5.2 assuming a constant viscoelastic viscosity coefficient. As will be discussed, the formal derivation of this methodology can easily be extended to the case where the viscoelastic constitutive relationship incorporates a strain(rate) dependent viscosity, such as that discussed in Section 2.4.3. Such an extension is, at this stage, left to the reader, however the benefits of such a generalized approach to parameter estimation for future research in this area, are self-evident.

As has been the case in the preceding chapters of this thesis, the parallel configuration of material response enables the parameter estimation techniques for each corresponding model element to be treated separately in the sections that follow.

5.1 Levenberg-Marquardt optimization for hyperelasticity

Various authors such as Twizell and Ogden (1983), Benjeddou et al. (1993) and Ogden et al. (2004) have reported on the implementation of Levenberg-Marquardt optimization for the estimation of hyperelastic constitutive model parameters. Through the experimental methods of Chapter 4, the elastic element stress component can be isolated from the total response and so such optimization techniques can be used in the conventional manner to generate the corresponding elastic element parameters. An alternate derivation of the Levenberg-Marquardt method is developed here, firstly to enable the implementation of fully three-dimensional data of the type discussed in Section 4.1 and secondly as a prelude to the more complex development that is required for the viscoelastic element.

The elastic element constitutive relationship is assumed to be best fit by an Ogden thermodynamic potential of the type given in equation (3.92). Fit of the linear volumetric component of this expression, $\hat{\mathcal{U}}(J)$, is a trivial procedure and need not be treated further here. The highly nonlinear deviatoric component is our primary focus in what follows. Substitution of equation (3.92) in (3.90) for $k = 1, K$ experimental data points, gives the three-dimensional principal deviatoric stress expression

$$\beta_{A\,k} = \sum_{r=1}^{3} (\mu_{el})_r \left[\bar{\lambda}_{A\,k}^{(\alpha_{el})_r} - \frac{1}{3} \sum_{B=1}^{3} \bar{\lambda}_{B\,k}^{(\alpha_{el})_r} \right] \qquad A = 1, 2, 3 \tag{5.1}$$

The deviatoric principal stresses $\beta_{A\,k}$ and deviatoric principal stretches $\bar{\lambda}_{A\,k}$ are obtained directly from the experimental testing, while the model parameters $(\mu_{el})_r$ and $(\alpha_{el})_r$, $r = 1, 2, 3$ are conventionally determined through the least squares optimization of (5.1).

From (5.1) a straight forward development obtains the residual function

$$R_{\beta_A\,k} = \beta_{A\,k} - \sum_{r=1}^{3}(\mu_{el})_r \left[\bar{\lambda}_{A\,k}^{(\alpha_{el})_r} - \frac{1}{3}\sum_{B=1}^{3}\bar{\lambda}_{B\,k}^{(\alpha_{el})_r}\right] \qquad A = 1, 2, 3 \tag{5.2}$$

which must be minimized over the whole data set (i.e. $k = 1, K$ experimental data points). In a least squares sense, we require the minimization of a least squares criterion S, i.e.

$$S = \hat{S}(\vec{\mu}_{el}, \vec{\alpha}_{el}) = \sum_{k=1}^{K} R_{\vec{\beta}\,k} \cdot R_{\vec{\beta}\,k} \tag{5.3}$$

where $R_{\vec{\beta}\,k}$ is the vector notation of the residuals and likewise, the two Ogden parameter sets are denoted by the vectors

$$\vec{\mu}_{el} = ((\mu_{el})_1, (\mu_{el})_2, (\mu_{el})_3)^T \quad \text{and} \quad \vec{\alpha}_{el} = ((\alpha_{el})_1, (\alpha_{el})_2, (\alpha_{el})_3)^T \tag{5.4}$$

Departing from the conventional derivation of Levenberg (1944) and Marquardt (1963), it is convenient to regard (5.2) in a similar way to the viscoplastic residual functions of Section 3.3.3. Using differential techniques taken from closest point projection, and initially focusing on the formulation for a single data point, i.e. $k = 1$, the differentiation of $R_{\vec{\beta}}$ with respect to $\vec{\mu}_{el}$[1] can proceed

$$\begin{aligned}\frac{\partial R_{\beta_A}}{\partial(\mu_{el})_B} = &\left(-\bar{\lambda}_A^{(\alpha_{el})_B} + \frac{1}{3}\sum_{C=1}^{3}\bar{\lambda}_C^{(\alpha_{el})_B}\right) \\ &+ \sum_{C=1}^{3}\left(-(\mu_{el})_C\left[\bar{\lambda}_A^{(\alpha_{el})_C}\ln\bar{\lambda}_A^{(\alpha_{el})_C} - \frac{1}{3}\sum_{D=1}^{3}\bar{\lambda}_D^{(\alpha_{el})_C}\ln\bar{\lambda}_D^{(\alpha_{el})_C}\right]\right)\frac{\partial(\alpha_{el})_C}{\partial(\mu_{el})_B} \\ &A, B = 1, 2, 3\end{aligned} \tag{5.5}$$

linearizing around $\partial\vec{\mu}_{el}$ and noting that by the standard argument, an incremental correction

[1] As will become evident, the arbitrary initial selection of $\partial\vec{\mu}_{el}$ or $\partial\vec{\alpha}_{el}$ here, has no effect on the final outcome of the development

of the residual should enforce $R_{\vec{\beta}} + \partial R_{\vec{\beta}} \longrightarrow 0$, then

$$
\begin{aligned}
-R_{\beta_A} = &\sum_{B=1}^{3}\left(-\bar{\lambda}_A^{(\alpha_{el})_B} + \frac{1}{3}\sum_{C=1}^{3}\bar{\lambda}_C^{(\alpha_{el})_B}\right)\partial(\mu_{el})_B \\
&+ \sum_{B=1}^{3}\left(-(\mu_{el})_B\left[\bar{\lambda}_A^{(\alpha_{el})_B}\ln\bar{\lambda}_A^{(\alpha_{el})_B} - \frac{1}{3}\sum_{C=1}^{3}\bar{\lambda}_C^{(\alpha_{el})_B}\ln\bar{\lambda}_C^{(\alpha_{el})_B}\right]\right)\partial(\alpha_{el})_B \\
&\qquad\qquad\qquad\qquad\qquad\qquad\qquad\qquad\qquad\qquad A = 1,2,3 \quad (5.6)
\end{aligned}
$$

which is nonspecific to the initial choice of derivative denominator.

Following the convention of closest point projection, (5.6) can be represented by the matrix form

$$
-R_{\vec{\beta}} = -\begin{Bmatrix} R_{\beta_1} \\ R_{\beta_2} \\ R_{\beta_3} \end{Bmatrix} = \begin{bmatrix} & \\ \boldsymbol{\Xi}^{(\mu_{el})} & \boldsymbol{\Xi}^{(\alpha_{el})} \\ & \end{bmatrix} \begin{Bmatrix} \Delta(\mu_{el})_1 \\ \Delta(\mu_{el})_2 \\ \Delta(\mu_{el})_3 \\ \Delta(\alpha_{el})_1 \\ \Delta(\alpha_{el})_2 \\ \Delta(\alpha_{el})_3 \end{Bmatrix} \qquad (5.7)
$$

where

$$
\begin{aligned}
\Xi_{AB}^{(\mu_{el})} &= -\bar{\lambda}_A^{(\alpha_{el})_B} + \frac{1}{3}\sum_{C=1}^{3}\bar{\lambda}_C^{(\alpha_{el})_B} \\
\Xi_{AB}^{(\alpha_{el})} &= -(\mu_{el})_B\left[\bar{\lambda}_A^{(\alpha_{el})_B}\ln\bar{\lambda}_A^{(\alpha_{el})_B} - \frac{1}{3}\sum_{C=1}^{3}\bar{\lambda}_C^{(\alpha_{el})_B}\ln\bar{\lambda}_C^{(\alpha_{el})_B}\right] \\
&\qquad\qquad\qquad\qquad\qquad\qquad A, B = 1,2,3 \qquad (5.8)
\end{aligned}
$$

and where $\Delta(\mu_{el})_A$ and $\Delta(\alpha_{el})_A$, $A = 1,2,3$, correspond to incremental updates of the Ogden parameters within some iterative solution scheme.

It can be seen that the composite system of equations (5.7), are presently insufficient to allow exclusive pointwise determination of the incremental update terms $\Delta(\mu_{el})_A$ and $\Delta(\alpha_{el})_A$. For the general case, the matrix expression (5.7) can be formulated for each of $k = 1, K$ data points. Combining these array sets together, noting that $\vec{\mu}_{el}$ and $\vec{\alpha}_{el}$ are constant parameters over the whole data set, then we find that one, *overdeterminate* system of equations is the result (i.e. there are multiple solution possibilities). A least squares

solution becomes necessary. For $k = 1, K$ data points, the composite matrix expression can be given

$$-\begin{Bmatrix} R_{\vec{\beta}\,1} \\ R_{\vec{\beta}\,1} \\ \vdots \\ R_{\vec{\beta}\,K} \end{Bmatrix} = \begin{bmatrix} \Xi_1^{(\mu_{el})} & \Xi_1^{(\alpha_{el})} \\ \Xi_2^{(\mu_{el})} & \Xi_2^{(\alpha_{el})} \\ \vdots & \vdots \\ \Xi_K^{(\mu_{el})} & \Xi_K^{(\alpha_{el})} \end{bmatrix} \begin{Bmatrix} \Delta(\mu_{el})_1 \\ \Delta(\mu_{el})_2 \\ \Delta(\mu_{el})_3 \\ \Delta(\alpha_{el})_1 \\ \Delta(\alpha_{el})_2 \\ \Delta(\alpha_{el})_3 \end{Bmatrix} \quad \longrightarrow \quad -\boldsymbol{R}_{\vec{\beta}} = \boldsymbol{\Xi}\,\boldsymbol{\Delta} \tag{5.9}$$

where $\boldsymbol{\Xi}$ is commonly referred to as the *Jacobian* matrix.

The mechanisms of the Levenberg-Marquardt method begin to become clearer when considering the solution to (5.9) using Moore-Penrose pseudoinverse techniques (Ben-Israel and Greville (1974)). For some rectangular matrix A_{mn}, where a conventional matrix inverse may remain indeterminant for reasons of rank deficiency or because $m \neq n$, Moore (1935) and Penrose (1954) are first credited as showing that a *quasi* or *pseudo* inverse, denoted by $A_{nm}^{\dagger}$, can still be determined that provides a solution to some system of equations $A_{mn}x_n = b_m$, i.e. $x_n = A_{nm}^{\dagger}b_m$. Given the circumstance where $m > n$, as in (5.9), such a solution is not unique; rather, it corresponds to a set of solutions which satisfy some least squares type criteria. Authors such as Bjerhammar (1951a,b) and then Penrose (1954) first recognized this link between pseudoinverse methodology and least squares optimization.

Following the development summarized by Ben-Israel and Greville (1974), a suitable form of pseudoinverse solution for an overdetermined system with the general expression $\boldsymbol{A}\,\vec{x} = \vec{b}$, can be defined

$$\vec{x} = \left[\boldsymbol{A}^T\boldsymbol{A} + \gamma\boldsymbol{I}\right]^{-1}\boldsymbol{A}^T\,\vec{b} \tag{5.10}$$

where $\boldsymbol{I}$ denotes a suitably scaled, square identity matrix (i.e. if $\boldsymbol{A} = A_{mn}$ then $\boldsymbol{I} = I_{nn}$), and where the scalar γ, arbitrarily accounts for all possible solutions for $\vec{x}$. Equation (5.10) corresponds to a set of generalized minimizations of the Euclidean vector norm

$$\left\|\vec{b} - \boldsymbol{A}\,\vec{x}\right\| \tag{5.11}$$

in a least squares sense.

Neglecting for a moment that, as yet, a unique solution to $\vec{x}$ in (5.10) has not been

determined; implementing this procedure for the parameter estimation case being treated, the generalized solution to (5.9) at some arbitrary increment, j, becomes

$$\boldsymbol{\Delta}^{(j)} = -\left[(\boldsymbol{\Xi}^{(j)})^T\,\boldsymbol{\Xi}^{(j)} + \gamma^{(j)}\boldsymbol{I}\right]^{-1}(\boldsymbol{\Xi}^{(j)})^T\,\boldsymbol{R}_{\vec{\beta}}^{(j)} \tag{5.12}$$

The incremental update for the Ogden parameters is correspondingly

$$\begin{Bmatrix}\vec{\mu}_{el}\\ \vec{\alpha}_{el}\end{Bmatrix}^{(j+1)} = \begin{Bmatrix}\vec{\mu}_{el}\\ \vec{\alpha}_{el}\end{Bmatrix}^{(j)} + \boldsymbol{\Delta}^{(j)} \tag{5.13}$$

On closer inspection, it becomes apparent that expressions (5.12) and (5.13) exactly recover the classical form of the Levenberg-Marquardt update expression for the determination of hyperelastic constitutive parameters as treated by authors such as Twizell and Ogden (1983) and Benjeddou et al. (1993).

The determination of a unique value for the scalar term γ is necessary to allow an exclusive solution to (5.12). Marquardt (1963) is generally cited as having been first to propose a specific convergence based searching algorithm for γ which is often compared to *line search* type methodology (see Nocedal and Wright (1999) for more on line search methods). Numerous modifications and reformulations of such algorithms have been subsequently published (see for example Benjeddou et al. (1993), Fan and Yuan (2005) and Nocedal and Wright (1999)) with the intention of improving efficiency, stability and/or convergence. The objective of all such algorithms is to determine a value for γ, known to exist for all possible cases (Marquardt (1963)), such that for successive increments, say $j \longrightarrow j+1$, reduction of the initially determined least squares criterion, S, is enforced, i.e.

$$S^{(j+1)} < S^{(j)} \tag{5.14}$$

As was the case for (5.10), when given some arbitrary $\gamma \in \mathbb{R}$ within (5.12), the minimization of the corresponding Euclidean vector norm, $\|\boldsymbol{R}_{\vec{\beta}} - \boldsymbol{\Xi}\,\boldsymbol{\Delta}\|$, is satisfied in a non-unique fashion. Implementation of a convergence based searching algorithm for γ, enforces the necessary additional, *specific*, minimization of the stress residual, in a least squares sense and over the whole data set (i.e. through (5.3)). Thus, the determination of successive suitable values for the increment, $\boldsymbol{\Delta}^{(j)}$, is made possible that will result in iterative convergence

Box 3: Searching algorithm for Levenberg-Marquardt parameter

Initialize: $j = 0$; estimate trial values for $\vec{\mu}_{el}^{(0)}$ and $\vec{\alpha}_{el}^{(0)}$ and correspondingly calculate $S^{(0)}$

Provide initial estimate of the Levenberg-Marquardt parameter, γ, and a suitable scaling factor, u, i.e. $\gamma^{(0)} = 0.01$, $u = 10$

1. Calculate the least squares criterion

$$S^{(j+1)} = \left\| \boldsymbol{R}_{\vec{\beta}}^{(j+1)} \left(\boldsymbol{\Delta}^{(j)} \left(\gamma^{(j)} \right) \right) \right\|$$

for the cases of $\gamma^{(j)} = \gamma^{(j)}$ and $\gamma^{(j)} = \gamma^{(j)}/u$, i.e. $S^{(j+1)}\left(\gamma^{(j)}\right)$ and $S^{(j+1)}\left(\gamma^{(j)}/u\right)$

2. IF: $S^{(j+1)}\left(\gamma^{(j)}/u\right) \leq S^{(j)}$ THEN: $\gamma^{(j+1)} = \gamma^{(j)}/u$;
IF: $S^{(j+1)}\left(\gamma^{(j)}/u\right) > S^{(j)} \geq S^{(j+1)}\left(\gamma^{(j)}\right)$ THEN: $\gamma^{(j+1)} = \gamma^{(j)}$;
IF: $S^{(j+1)}\left(\gamma^{(j)}/u\right) > S^{(j)} < S^{(j+1)}\left(\gamma^{(j)}\right)$ THEN: multiply $\gamma^{(j)}$ by u successively until $S^{(j+1)}\left(\gamma^{(j)}u^n\right) \leq S^{(j)}$; Let $\gamma^{(j+1)} = \gamma^{(j)}u^n$

3. Check for convergence
IF: $S^{(j+1)}\left(\gamma^{(j+1)}\right) <$ TOL THEN: *EXIT*
ELSE: Set $j \longleftarrow j + 1$ and GO TO 1.

toward appropriate, *unique*, least squares approximations to $\vec{\mu}_{el}$ and $\vec{\alpha}_{el}$ (i.e. as a result of successive decreases in S).

The searching algorithm for the incremental determination of γ, originally proposed by Marquardt (1963), is outlined in Box 3 as an example of such methods. The particular choice to use a more modern, improved method is left at the discretion of the reader, noting that most commercial Levenberg-Marquardt numerical algorithms will perform sufficiently well in the majority of cases.

5.2 A modified Levenberg-Marquardt technique for nonlinear viscoelasticity

The alternate manner by which the classical Levenberg-Marquardt expression has been derived in Section 5.1, has some key advantages for the determination of such an expression when multiple constitutive expressions are to be fit (as with viscoelasticity). Most significantly, by conducting the residual differentiation using closest point projection techniques,

it becomes possible to develop the jacobian matrix from multiple residual functions (recall the operations of Section 3.3.3). Correspondingly, only one optimization algorithm needs to be solved to establish the least squares solution. There are several benefits associated with such an approach as will become clearer in what follows.

The specific viscoelastic constitutive theory that has been treated in this work follows that of Reese and Govindjee (1998a), as outlined in Sections 2.4.3 and 3.3.2. Again limiting attention to the nonlinear deviatoric response, substituting the Ogden hyperelastic potential (3.104) into the principal deviatoric stress expression (3.93) and also utilizing a modified form of the principal space evolution equation (3.99), then the two governing constitutive equations to be optimized become

$$\tau_{A\,k} = \sum_{r=1}^{3} (\mu_{ve})_r \left[\bar{\lambda}_{A\,k}^{e\,(\alpha_{ve})_r} - \frac{1}{3} \sum_{B=1}^{3} \bar{\lambda}_{B\,k}^{e\,(\alpha_{ve})_r} \right] \qquad A = 1,2,3 \tag{5.15}$$

$$\bar{\lambda}_{A\,k}^{e} = \exp\left\{ \frac{-\Delta t_k}{2\,\eta_{ve}} \tau_{A\,k} \right\} \bar{\lambda}_{A\,k}^{e\,tr} \qquad A = 1,2,3 \tag{5.16}$$

For some arbitrary data point k, $\tau_{A\,k}$ denote the viscoelastic principal deviatoric stress components, $\bar{\lambda}_{A\,k}^{e}$ are the elastic components of the principal deviatoric stretches, $\Delta t_k = t_k - t_{k-1}$ is the time increment between successive data points and $\bar{\lambda}_{A\,k}^{e\,tr}$ is the trial elastic deviatoric principal stretch (see Section 3.2.3).

For the viscoelastic case, the form of (5.15) and (5.16) suggest that the model parameters $\vec{\mu}_{ve}$, $\vec{\alpha}_{ve}$ and η_{ve} should ideally be fit to stress and elastic strain data. As has already been noted, however, the elastic components of strain cannot be determined during testing. As such, in what follows we include $\bar{\lambda}_{A\,k}^{e}$ as an undetermined set of parameters to be additionally fit to stress and *total* strain data. This capability is one of the main motivations for the use of closest point projection style differentiation.

The residual forms of equations (5.15) and (5.16) are trivially determined as

$$R_{\tau_A} = \tau_{A\,k} - \sum_{r=1}^{3} (\mu_{ve})_r \left[\bar{\lambda}_{A\,k}^{e\,(\alpha_{ve})_r} - \frac{1}{3} \sum_{B=1}^{3} \bar{\lambda}_{B\,k}^{e\,(\alpha_{ve})_r} \right] \qquad A = 1,2,3 \tag{5.17}$$

$$R_{\lambda_A} = \bar{\lambda}_{A\,k}^{e} - \exp\left\{ \frac{-\Delta t_k}{2\eta_{ve}} \tau_{A\,k} \right\} \bar{\lambda}_{A\,k}^{e\,tr} \qquad A = 1,2,3 \tag{5.18}$$

As before, we initially limit attention to a single arbitrary data point (i.e. $k = 1$) such

that the residual differential functions are given[2]

$$\frac{\partial R_{\tau_A}}{\partial \bar{\lambda}^e_B} = \sum_{C=1}^{3}\left(-\bar{\lambda}_A^{e\,(\alpha_{ve})_C} + \frac{1}{3}\sum_{D=1}^{3}\bar{\lambda}_D^{e\,(\alpha_{ve})_C}\right)\frac{\partial(\mu_{ve})_C}{\partial \bar{\lambda}^e_B} + \sum_{C=1}^{3}\left(-(\mu_{ve})_C\left[\bar{\lambda}_A^{e\,(\alpha_{ve})_C}\ln\bar{\lambda}_A^{e\,(\alpha_{ve})_C} - \frac{1}{3}\sum_{D=1}^{3}\bar{\lambda}_D^{e\,(\alpha_{ve})_C}\ln\bar{\lambda}_D^{e\,(\alpha_{ve})_C}\right]\right)\frac{\partial(\alpha_{ve})_C}{\partial \bar{\lambda}^e_B} + \left(0_A\right)\frac{\partial \eta_{ve}}{\partial \bar{\lambda}^e_B} + \left(-\sum_{r=1}^{3}(\mu_{ve})_r(\alpha_{ve})_r\left[\bar{\lambda}_A^{e\,[(\alpha_{ve})_r-1]}\delta_{AB} - \frac{1}{3}\bar{\lambda}_B^{e\,[(\alpha_{ve})_r-1]}\right]\right)$$

$$A, B = 1, 2, 3 \quad (5.19)$$

$$\frac{\partial R_{\lambda_A}}{\partial \eta_{ve}} = \sum_{B=1}^{3}\left(0_{AB}\right)\frac{\partial(\mu_{ve})_B}{\partial \eta_{ve}} + \sum_{B=1}^{3}\left(0_{AB}\right)\frac{\partial(\alpha_{ve})_B}{\partial \eta_{ve}} + \left(-\frac{\Delta t}{2\,\eta_{ve}^2}\,\tau_A \exp\left\{-\frac{\Delta t}{2\,\eta_{ve}}\,\tau_A\right\}\bar{\lambda}_A^{e\,tr}\right) + \sum_{B=1}^{3}\left(\delta_{AB}\right)\frac{\partial \bar{\lambda}^e_B}{\partial \eta_{ve}}$$

$$A = 1, 2, 3 \quad (5.20)$$

where $0_A = 0$ and $0_{AB} = 0$ for $A, B = 1, 2, 3$ which represent a null vector and null matrix respectively. Linearizing each equation around its respective differential base and noting that over the update increment the aim is to now enforce $R_{\vec{\tau}} + \partial R_{\vec{\tau}} \longrightarrow 0$ and $R_{\vec{\lambda}} + \partial R_{\vec{\lambda}} \longrightarrow 0$, then

$$-R_{\tau_A} = \sum_{B=1}^{3}\left(-\bar{\lambda}_A^{e\,(\alpha_{ve})_B} + \frac{1}{3}\sum_{C=1}^{3}\bar{\lambda}_C^{e\,(\alpha_{ve})_B}\right)\partial(\mu_{ve})_B + \sum_{B=1}^{3}\left(-(\mu_{ve})_B\left[\bar{\lambda}_A^{e\,(\alpha_{ve})_B}\ln\bar{\lambda}_A^{e\,(\alpha_{ve})_B} - \frac{1}{3}\sum_{C=1}^{3}\bar{\lambda}_C^{e\,(\alpha_{ve})_B}\ln\bar{\lambda}_C^{e\,(\alpha_{ve})_B}\right]\right)\partial(\alpha_{ve})_B + \left(0_A\right)\partial\eta_{ve} + \sum_{B=1}^{3}\left(-\sum_{r=1}^{3}(\mu_{ve})_r(\alpha_{ve})_r\left[\bar{\lambda}_A^{e\,[(\alpha_{ve})_r-1]}\delta_{AB} - \frac{1}{3}\bar{\lambda}_B^{e\,[(\alpha_{ve})_r-1]}\right]\right)\partial\bar{\lambda}^e_B$$

$$A = 1, 2, 3 \quad (5.21)$$

[2]Note that, again, the selection of the differential denominator terms are wholly arbitrary within the context of the current development.

$$
\begin{aligned}
-R_{\lambda_A} = &\sum_{B=1}^{3}\left(0_{AB}\right)\partial(\mu_{ve})_B + \sum_{B=1}^{3}\left(0_{AB}\right)\partial(\alpha_{ve})_B \\
&+\left(-\frac{\Delta t}{2\,\eta_{ve}^2}\,\tau_A \exp\left\{-\frac{\Delta t}{2\,\eta_{ve}}\,\tau_A\right\}\bar{\lambda}_A^{e\,tr}\right)\partial\eta_{ve} + \sum_{B=1}^{3}\left(\delta_{AB}\right)\partial\bar{\lambda}_B^e \\
& \qquad\qquad\qquad\qquad\qquad\qquad\qquad\qquad\qquad\qquad A = 1,2,3 \quad (5.22)
\end{aligned}
$$

Equations (5.21) and (5.22) can once again be composed into matrix form via

$$
-\begin{Bmatrix} R_{\vec{\tau}} \\ R_{\vec{\lambda}} \end{Bmatrix} = -\begin{Bmatrix} R_{\tau_1} \\ R_{\tau_2} \\ R_{\tau_3} \\ R_{\lambda_1} \\ R_{\lambda_2} \\ R_{\lambda_3} \end{Bmatrix} = \begin{bmatrix} & & & \\ \boldsymbol{\Xi}^{\tau\mu} & \boldsymbol{\Xi}^{\tau\alpha} & \vec{0} & \boldsymbol{\Xi}^{\tau\lambda} \\ \mathbf{0} & \mathbf{0} & \vec{\Xi}^{\lambda\eta} & \boldsymbol{I} \\ & & & \end{bmatrix} \begin{Bmatrix} \Delta(\mu_{ve})_1 \\ \Delta(\mu_{ve})_2 \\ \Delta(\mu_{ve})_3 \\ \Delta(\alpha_{ve})_1 \\ \Delta(\alpha_{ve})_2 \\ \Delta(\alpha_{ve})_3 \\ \Delta\eta_{ve} \\ \Delta\bar{\lambda}_1^e \\ \Delta\bar{\lambda}_2^e \\ \Delta\bar{\lambda}_3^e \end{Bmatrix} \tag{5.23}
$$

where

$$
\begin{aligned}
\Xi_{AB}^{\tau\mu} &= -\bar{\lambda}_A^{e\,(\alpha_{el})_B} + \frac{1}{3}\sum_{C=1}^{3}\bar{\lambda}_C^{e\,(\alpha_{el})_B} \\
\Xi_{AB}^{\tau\alpha} &= -(\mu_{el})_B\left[\bar{\lambda}_A^{e\,(\alpha_{el})_B}\ln\bar{\lambda}_A^{e\,(\alpha_{el})_B} - \frac{1}{3}\sum_{C=1}^{3}\bar{\lambda}_C^{e\,(\alpha_{el})_B}\ln\bar{\lambda}_C^{e\,(\alpha_{el})_B}\right] \\
\Xi_{AB}^{\tau\lambda} &= -\sum_{r=1}^{3}(\mu_{ve})_r(\alpha_{ve})_r\left[\bar{\lambda}_A^{e\,[(\alpha_{ve})_r-1]}\delta_{AB} - \frac{1}{3}\bar{\lambda}_B^{e\,[(\alpha_{ve})_r-1]}\right] \\
\Xi_A^{\lambda\eta} &= -\frac{\Delta t}{2\,\eta_{ve}^2}\,\tau_A \exp\left\{-\frac{\Delta t}{2\,\eta_{ve}}\,\tau_A\right\}\bar{\lambda}_A^{e\,tr} \\
& \qquad\qquad\qquad\qquad A, B = 1,2,3 \qquad (5.24)
\end{aligned}
$$

and where $\Delta(\mu_{ve})_A$, $\Delta(\alpha_{ve})_A$, $\Delta\eta_{ve}$ and $\Delta\bar{\lambda}_A^e$, $A = 1,2,3$, correspond to incremental updates of the viscoelastic parameters and elastic strains within some iterative solution scheme. Note also that the null arrays have been denoted here using standard matrix notation, i.e. $\vec{0} \rightarrow 0_A$

Table 5.1: Effect on the nature of the optimization equation set as subsequent data points are included in the calculations

Number of data points	Number of equations	Number of parameters
1	6	10
2	12	13
3	18	16
4	24	19
⋮	⋮	⋮

and $\mathbf{0} \rightarrow 0_{AB}$, $A, B = 1, 2, 3$.

As before, the system of equations represented by (5.23) is indeterminate for any single data point. Following the procedure of Section 5.1, a combined form of (5.23) is incorporated for $k = 1, K$ data points. Where the number of undetermined parameters remaind constant throughout such an expansion for the hyperelastic case, here the parameter set will have both constant and variable components such that the parameter array will now expand with the residual and jacobian arrays as data points are added. Table 5.1 illustrates the nature of the equation set as subsequent data points are included in the optimization.

It can be seen from Table 5.1, that the system of equations becomes overdeterminate when 3 or more data points are used. In such circumstances a least squares solution is possible, as desired.

The matrix expansion of (5.23) over $k = 1, K$ data points can be carried out using the following structure

$$-\begin{Bmatrix} R_{\vec{\tau}\,1} \\ R_{\vec{\lambda}\,1} \\ R_{\vec{\tau}\,2} \\ R_{\vec{\lambda}\,2} \\ \vdots \\ R_{\vec{\tau}\,K} \\ R_{\vec{\lambda}\,K} \end{Bmatrix} = \begin{bmatrix} \boldsymbol{\Xi}_1^{\tau\mu} & \boldsymbol{\Xi}_1^{\tau\alpha} & \vec{0} & \boldsymbol{\Xi}_1^{\tau\lambda} & \mathbf{0} & & \mathbf{0} \\ \mathbf{0} & \mathbf{0} & \vec{\Xi}_1^{\lambda\eta} & \boldsymbol{I} & \mathbf{0} & \dots & \mathbf{0} \\ \boldsymbol{\Xi}_2^{\tau\mu} & \boldsymbol{\Xi}_2^{\tau\alpha} & \vec{0} & \mathbf{0} & \boldsymbol{\Xi}_2^{\tau\lambda} & & \mathbf{0} \\ \mathbf{0} & \mathbf{0} & \vec{\Xi}_2^{\lambda\eta} & \mathbf{0} & \boldsymbol{I} & & \mathbf{0} \\ & & \vdots & & & \ddots & \vdots \\ \boldsymbol{\Xi}_K^{\tau\mu} & \boldsymbol{\Xi}_K^{\tau\alpha} & \vec{0} & \mathbf{0} & \mathbf{0} & \dots & \boldsymbol{\Xi}_K^{\tau\lambda} \\ \mathbf{0} & \mathbf{0} & \vec{\Xi}_K^{\lambda\eta} & \mathbf{0} & \mathbf{0} & & \boldsymbol{I} \end{bmatrix} \begin{Bmatrix} \Delta(\vec{\mu}_{ve}) \\ \Delta(\vec{\alpha}_{ve}) \\ \Delta\eta_{ve} \\ \Delta\vec{\lambda}_1^e \\ \Delta\vec{\lambda}_2^e \\ \vdots \\ \Delta\vec{\lambda}_K^e \end{Bmatrix} \tag{5.25}$$

Denoting the jacobian by the indexed form $\boldsymbol{\Xi}_{mn}$, then for each subsequent data point

added, the result on the indices follows $m = m + 6$ and $n = n + 3$. For the general case, the matrix expression dimensions can be given as $-\boldsymbol{R}_{(6K)} = \boldsymbol{\Xi}_{(6K)(7+3K)}\boldsymbol{\Delta}_{(7+3K)}$ which is comparable to the results of Table 5.1.

By iteratively solving (5.25) within the Levenberg-Marquardt scheme of (5.12) and using the γ searching algorithm of Box 3 (or an equivalent method) the full viscoelastic parameter set can be determined, as well as the elastic components of strain, over the whole set of data. This is carried out simultaneously within the one least squares operation. It is pertinent to note that because the update expression presented, does not differ in theoretical form from that seen in most commercial software packages, only minor modification of an existing numerical Levenberg-Marquardt algorithm would be necessary for full numerical implementation. Also, as a result of this, it can be inferred that such an algorithm would also retain the convergence qualities of the conventional Levenberg-Marquardt implementations; a particularly beneficial result.

5.3 Estimation of viscoplastic element parameters

Estimation of the viscoplastic component parameters proves to be a relatively trivial procedure in comparison to the viscoelastic case treated above. This can be attributed to the rather comprehensive nature of the testing methodology presented in Chapter 4. This testing methodology facilitates the full isolation of the element subset stress and strain components and so the corresponding constitutive relationships can be fit independently of one another with relative ease.

While the specific parameter estimation operations are straight forward, we still must convert the results from the testing of Chapter 4 to a specific form which is appropriate for use within an optimization of the viscoplastic constitutive theory (theory outlined in Sections 2.4.4 and 3.3.3). From Section 3.3.3, the principal space strain evolution expression (3.112) can be rewritten

$$\vec{\varepsilon}^{\,i} = \frac{\langle f \rangle}{2\eta_{vp}} \frac{\partial f}{\partial \vec{\tau}} \tag{5.26}$$

Substituting the explicit yield function (3.111) and observing the relevant differentiation rules outlined by authors such as Simo (1992) and Itskov (2007), then this expression can

be expanded such that

$$\vec{\varepsilon}^{\,i} = \frac{1}{2\eta_{vp}} \frac{\vec{\tau}}{\| \vec{\tau} \|} \left(\| \vec{\tau} \| - \sqrt{\tfrac{2}{3}} \left(\sigma_y - q \right) \right) \tag{5.27}$$

and rearranging

$$2\eta_{vp}\, \vec{\varepsilon}^{\,i} = \vec{\tau} - \sqrt{\tfrac{2}{3}} \frac{\vec{\tau}}{\| \vec{\tau} \|}\, \sigma_y + \sqrt{\tfrac{2}{3}} \frac{\vec{\tau}}{\| \vec{\tau} \|}\, q \tag{5.28}$$

Recalling from Section 2.3 the standard constitutive equation governing dashpot evolution, $(2.2)_2$, then with some manipulation, we attain an expression for total viscoplastic stress, functional on the three subset stress components as

$$\vec{\tau} = \vec{\tau}_{d-p} + \sqrt{\tfrac{2}{3}} \frac{\vec{\tau}}{\| \vec{\tau} \|}\, \sigma_y - \sqrt{\tfrac{2}{3}} \frac{\vec{\tau}}{\| \vec{\tau} \|}\, q \tag{5.29}$$

where $\vec{\tau}_{d-p}$ represents the principal components of stress in the theoretical viscoplastic dashpot and the other two terms are the three dimensional stress contributions of the yield and isotropic hardening respectively.

From Chapter 4, Figure 4.16, it has been shown that the viscoplastic element subset stress components can be separately determined from experimentation. Correspondingly, the total deviatoric principal Cauchy stress can be written as a function of the four calculated components via (4.17), i.e.

$$\bar{\sigma}_{vp}|_A = \bar{\sigma}_{d-p}\,|_A + \bar{\sigma}_{kin}|_A + \bar{\sigma}_y|_A + \bar{\sigma}_{iso}|_A \qquad A = 1, 2, 3 \tag{5.30}$$

For the numerical model of Chapter 3, kinematic hardening is neglected and so the kinematic hardening stress component, $\bar{\sigma}_{kin}|_A$, is assumed to be zero, thus

$$\bar{\sigma}_{vp}|_A = \bar{\sigma}_{d-p}\,|_A + \bar{\sigma}_y|_A + \bar{\sigma}_{iso}|_A \qquad A = 1, 2, 3 \tag{5.31}$$

Paying careful attention to that fact that (5.29) refers to principal deviatoric Kirchhoff stress while (5.31) refers to principal deviatoric Cauchy stress, then these two expressions are related via

$$\bar{\sigma}_{vp}|_A = \frac{1}{J}\, \tau_A \qquad A = 1, 2, 3 \tag{5.32}$$

Also, because $\vec{\tau}$ remains deviatoric across the whole range of data, then for the case of

uniaxial tension in, for example, the $A = 1$ direction, then

$$\sqrt{\tfrac{2}{3}}\,\frac{\vec{\tau}}{\|\,\vec{\tau}\,\|} = (\,2/3, -1/3, -1/3\,)^T \tag{5.33}$$

which is constant for all $\vec{\tau}$ during the tensile test.

Through substitution of (5.29) and (5.31) into (5.32), and by observing (5.33), then it becomes possible to develop functional relationships between the three constitutive model stress terms, and the corresponding three experimentally determined stress terms. The component relationships are

$$\tau_{d-p}|_A = J\,\bar{\sigma}_{vp}|_A \qquad\qquad A = 1,2,3 \tag{5.34a}$$

$$\sigma_y = 1\tfrac{1}{2}\,J\,\bar{\sigma}_y|_1 = -3\,J\,\bar{\sigma}_y|_2 = -3\,J\,\bar{\sigma}_y|_3 \tag{5.34b}$$

$$q = -1\tfrac{1}{2}\,J\,\bar{\sigma}_y|_1 = 3\,J\,\bar{\sigma}_y|_2 = 3\,J\,\bar{\sigma}_y|_3 \tag{5.34c}$$

In addition, it has also been shown that the principal inelastic logarithmic strain components, $\vec{\varepsilon}^{\,i}$, can be determined from the experimental testing. Observing the relationship of this strain to the strain space conjugate of the isotropic hardening internal variable (see Appendix B), then through the rate equality

$$\dot{\alpha} = \left|\dot{\vec{\varepsilon}}^{\,i}\right| \tag{5.35}$$

the strain space isotropic hardening internal variable may also be determined from the experimental results.

Now, having determined an association between the form of the experimental data and that of the variable terms used within the viscoplastic constitutive theory, it is a direct development to determine estimates for the pertinent model parameters using conventional curve fitting operations. The viscosity coefficient can be directly related to inelastic strain rate and the dashpot stress component through the three-dimensional analogue of $(2.2)_2$, while the isotropic hardening parameter can be fit via the direct solution of equation (3.106) (with substitution of (3.123)). The viscoplastic yield criterion is directly output from (5.34b) and the element elastic relationship (Ogden or otherwise) can be determined through the exact methodology of Section 5.1 using the total deviatoric viscoplastic stress and elastic

strain component vectors within the optimization.

It is worthwhile to note that while a constant viscosity and hardening coefficient have been used within this work, from a parameter estimation perspective, it would be a simple extension to implement nonlinear relationships for these terms. Because all element stress and strain components are discernable from the experimental tests, such expressions could easily be fit using analogous optimization procedures to that used in Section 5.1.

5.4 Generalization of the modified Levenberg-Marquardt method

Section 5.2 has outlined the application of the modified Levenberg-Marquardt method to the specific case of a viscoelastic constitutive theory with constant viscosity coefficient. Where the conventional Levenberg-Marquardt formulation is generally applicable to any single expression optimization procedure[3], the developed modification has a more generalized applicability to parameter estimation situations, allowing for multiple constitutive relationships and additional unknown terms that can span and vary across the whole range of data. Such a method is potentially applicable to a wide variety of complex solid mechanics optimization problems where conventional optimization techniques may be inappropriate. Here we will briefly treat the generalized implementation of the new method and discuss its advantages from a materials research perspective, specifically in regards to the inclusion of a strain(rate) dependent viscosity term within the viscoelastic constitutive expressions (an important component of semicrystalline polymer response, see Chapter 2).

A primary consideration for the generalized formulation of the modified Levenberg-Marquardt method is that any equation system to be numerically fit using the method must satisfy the condition

$$N_{eq} > N_{par(var)} \tag{5.36}$$

where N_{eq} is the number of equations per data point[4] while $N_{par(var)}$ is the number of variable parameters per data point[5]. This condition is critical to the least squares solvability of a system of equations as it ensures that the system will become overdeterminate at some

[3]'Single expression' refers to a single algebraic relationship, be it between scalars, vectors or tensors.

[4]Note that for the principal space example of Section 5.2, a single data point from 3D testing corresponds to a set of principal stress and strain vectors whose components are related through a system of 6 equations, i.e. $N_{eq} = 6$.

[5]Variable parameters are those which change across the data set, i.e. elastic strain components in Section 5.2, $N_{par(var)} = 3$.

stage during the successive inclusion of test data points.

The number of data points above which the system will become overdeterminant, provides an insight into the minimum frequency of data records required during experimental testing so as to fully resolve the least squares solution. This criterion can be defined as

$$N_{data(min)} > \frac{N_{par(const)}}{N_{eq} - N_{par(var)}} \tag{5.37}$$

where $N_{data(min)}$ is the minimum number of data points required, while $N_{par(const)}$ is the number of parameters which remain constant across the whole data set (the constant parameters in Section 5.2 were $\vec{\mu}_{ve}$, $\vec{\alpha}_{ve}$ and η_{ve}, such that in that case $N_{par(const)} = 7$). For the development in Section 5.2, Table 5.1 provides a manual demonstration of this concept, where

$$N_{data(min)} = 3 > \frac{7}{6-3} \tag{5.38}$$

such that in that example, any experimental test result sets need more than 3 data points to enable a least squares solution.

For the general case, any system of interdependent equations to be optimized should converge toward a least squares solution providing the system satisfies (5.36) and that it is possible to generate significantly more actual experimental data points (denoted by N_{data}) than the minimum number required for the system to become overdeterminant, i.e.

$$N_{data} \gg N_{data(min)} \tag{5.39}$$

Few other theoretical restrictions on general application of the developed optimization technique have been encountered within the scope of applicability outlined already.

For the viscoelastic behavior of semicrystalline polymers, the optimization method developed in this chapter represents a powerful research tool for possible future extensions. While the viscosity coefficient of these materials has been shown to posses strain(rate) dependence (Brusselle-Dupend et al. (2001, 2003)), what little treatment there is in the literature on such a functionality is largely inappropriate for the case of three-dimensional response and particularly when a nonlinear elastic relationship is also taken into consideration. The developed model reported on in this thesis has retained a simpler, constant viscosity coefficient as a necessary approximation, however it would be highly desirable to

facilitate the inclusion of a nonlinear term for future work.

The nonlinear behavior of the viscosity coefficient can be directly determined with a single modification to the method of Section 5.2. By including the viscosity term as an additional variable parameter (like the elastic strain components), (5.36) is still satisfied and the whole system can be optimized prior to any specific definition of a viscosity function. Once the behavior of viscosity over the test range is determined, a suitably representative expression can be developed 'after the fact'. In such a way, the modified Levenberg-Marquardt method has additional capabilities as a response isolation tool, enabling research on a materials constitutive behavior without the limitation of needing a pre-formulated expression.

5.5 Summary

In this chapter, techniques have been developed to determine the explicit material model parameters from experimental test results of the type outlined in Chapter 4. A modification to conventional Levenberg-Marquardt optimization has been developed that enables generation of both the hyperelastic and viscoelastic element parameters. Determination of the viscoplastic model parameters has been subsequently treated; a trivial process due to the full isolation of stress results from the testing methods of Section 4.4. The generalization of the modified Levenberg-Marquardt method has briefly been discussed to facilitate the future extension of this work to incorporate additional nonlinearity, particularly within expression of material viscosity. Using the testing methodology of Chapter 4 and the optimization and parameter generation methods presented in this chapter, the full parameter set for the proposed elasto-viscoelastic-viscoplastic model can be determined.

Chapter 6

Conclusions

In this chapter the implications and importance of the work presented in this thesis are discussed with the intention of bringing the various treated theoretical facets into practical context. An objective assessment of the associated limitations is presented, as is a brief outline of the most important directions in which future work in this area should proceed.

6.1 Discussions on the proposed theories

The constitutive theory developed in this work, has been formulated using conventional continuum mechanics techniques. The suitability of this class of constitutive theory for the representation of semicrystalline polymers has been inferred from the accuracy of such theories when used for the constitutive representation of other complex materials such as rubbers and metals. A key advantage of using a continuum mechanics constitutive theory is the inherent suitability of such theories to three-dimensional numerical implementation.

In spite of the wide prior implementation of continuum mechanics constitutive theories, the theoretical implications of experimentally fitting such models, particularly the more complex nonlinear forms, are addressed rather poorly within the literature. In the early stages of this work it became obvious that, while physical experimentation is critically important for any implemented theory, the major void in published knowledge is associated with the theoretical aspects of such testing methodologies and the meaning of the subsequent results in regards to constitutive behavior. As a result, the experimental components of this thesis have remained largely theoretical in nature in an attempt to develop an insight into the actual constitutive functionality of the material, something which cannot be easily

achieved using just phenomenological experimental testing.

While this work has been largely theoretical in nature, care has been taken to ensure the theoretical components retain strong foundations in reality. Through an extensive review of semicrystalline polymer literature, it has become clear that, in spite of the inadequacies of existing constitutive representation, there is significant agreement on the actual response characteristics of the material. Using this information within the model development, it has been possible to make an informed judgement on the most appropriate model characteristics without the need to carry out additional testing. Also, the developed model and the subsequent theoretical testing and parameter estimation methodologies, have been developed so as to be *self consistent*. That is; the testing and, to a lesser extent, the parameter estimation methodologies have been developed and verified using the results from the developed numerical model. Thus, providing the initial lemma associated with the selection of suitable response characteristics is proven correct, then the subsequent testing and parameter estimation methodologies will also hold up to scrutiny. Given the strength of the conclusions drawn about material deformation characteristics from the literature review, there can be considerable confidence in the accuracy and the physical applicability of the theories that have been proposed.

A priority has been placed on industrial practicality, in this thesis, and there are several important aspects which illustrate this. Firstly, within the numerical model implementation, an emphasis has been placed on the flexibility of the actual subset constitutive relationships. While the broad classification of these materials as being elasto-viscoelastic-viscoplastic is verified widely in the literature, the variability of specific subset response characteristics such as element elastic relationships and an explicit hardening rule can be dependent on things like polymer type, grade and moulding conditions. The implementation that has been presented, has accounted for all these subset constitutive components in a general fashion and so can be generally applied for the majority of semicrystalline polymer situations with very little modification needed between different grades etc. Secondly, while the proposed experimental testing methodology is extensive, the actual tests it requires can be easily carried out using no more specialized testing apparatus than would be available in most commercial or university structural laboratories. The advantage of such features, from an industrial point of view, is the versatility that results, firstly with respect to the flexibility of materials which can be represented and secondly with respect to the ability of someone

in industry to determine their own model parameters for a given design situation. The work in this thesis, through the generalized theoretical approach taken, can correspondingly be seen to be applicable to a wider audience than may have been the case had a single specific material been the focus.

6.2 Critiques and limitations

Throughout the chapters of this thesis, the various working assumptions and simplifications that have been used, have been clearly outlined. As such, the majority of these need not be repeated here. It is, however, pertinent to briefly discuss some additional limiting implications, associated with this work.

One of the more fundamental restrictions to the general use of the developed numerical model, stems from the assumption of material isotropy. Here, material isotropy refers to the isotropic nature of the deformation properties of the material, i.e. model parameters are equal in each direction. While in most industrial circumstances this is a sound assumption, poor moulding or fabrication practices can adversely affect the material properties and cause anisotropy. The material's properties can vary significantly due to factors such as molecular orientation and degree of crystallinity (Sharples (1966)). As such, care must be taken when using the developed numerical model in industrial and design circumstances, that the corresponding moulding and fabrication conditions promote isotropic material properties, necessary for this assumption to remain valid. It should be said that a priority is generally placed on such moulding and fabrication conditions within modern industry already, regardless of the implications to numerical modeling.

A further restriction resulting from the isotropic assumption has been the consequential limitations imposed on the inclusion of strain hardening within the numerical model. While it could be argued that the inclusion of isotropic hardening allows a general account of strain hardening mechanisms, authors such as Brusselle-Dupend et al. (2001, 2003) have indicated the additional importance of kinematic hardening within semicrystalline polymer response. Also, shear strain softening has been observed under certain conditions in semicrystalline polypropylene by G'Sell et al. (1997). For circumstances where inclusion of these additional anisotropic hardening behaviors is deemed important, an involved, full tensor space numerical implementation becomes necessary. Such a development has, however, fallen outside

the scope of the current research.

It is additionally important to note that the developed numerical model neglects possible variations in temperature that may occur in real loading circumstances (i.e. assumes an isothermal deformation environment). Extension of this work to account for temperature effects is possible using techniques such as those outlined by Reese and Govindjee (1998b), however this too has been outside the scope of this thesis.

Within the developed testing methodology, an assumption has been made that the viscoplastic element elastic relationship is linear. This may prove limiting for particularly nonlinear materials, however due to the restricted range of strain ($< 15\%$) being treated, it would be rare that such an assumption would cause significant error.

Throughout the progression of this research, a major emphasis has been placed on limiting the number of simplifications and assumptions. The intention has been to represent the behavior of semicrystalline polymers as closely as possible without many of the simplifications that have restricted the accuracy and applicability of such previous models. It is hoped that the result is a practical theory that performs accurately for the general case of response.

6.3 Future directions

Within this work, it has not been possible to carry out the physical experimental testing needed for final model verification, due to the obvious time and scope restrictions on doctoral research. This aspect is perhaps the most important future direction for subsequent research to progress in, so as to confirm the results discussed in this work. Within such experimental research, further study on possible nonlinear viscosity and hardening relationships should also be pursued, making use of the research techniques discussed in the preceding chapters. The inclusion of such nonlinear functions would have important implications for the numerical model implementation, thus necessitating additional careful consideration.

6.4 Conclusion

It was the aim of this work to develop a constitutive theory that would be both accurate and practical for use within industry. A new constitutive model has been developed for the

representation of semicrystalline polymer response in the pre-necking region of finite strain. A generalized numerical model has been developed to enable finite element analysis using the model, while a testing and parameter estimation methodology has been proposed which enables the determination of the full model parameter set.

Bibliography

Ben-Israel, A. and Greville, T. N. E. (1974) *Generalized inverses: Theory and applications*. Cambridge University Press, Sydney.

Benjeddou, A., Jankovich, E. and Hadhri, T. (1993) Determination of the parameters of Ogden's law using biaxial data and Levenberg-Marquardt-Fletcher algorithm. *J. Elastomers and Plastics*, **25**, 224–248.

Bjerhammar, A. (1951a) Rectanglular reciprocal matrices, with special reference to geodetic calculations. *Bulletin Géodésique*, **52**, 188–220.

Bjerhammar, A. (1951b) Applications of calculus of matrices to method of least squares; with special reference to geodetic calculations. *Trans. Roy. Inst. Tech. Stockholm*, **49**, 1–86.

Bodner, S. R. and Partom, Y. (1972) A large deformation elastic-viscoplastic analysis of a thick-walled spherical shell. *J. Appl. Mech.*, **39**, 751–757.

Bodner, S. R. and Partom, Y. (1975) Constitutive equations for elastic-viscoplastic strain-hardening materials. *J. Appl. Mech.*, **42**, 385–389.

Bonet, J. and Wood, R. D. (1997) *Nonlinear continuum mechanics for finite element analysis*. Cambridge University Press, Melbourne.

Brostow, W. and Corneliussen, R. D. (eds.) (1986) *Failure of Plastics*. Hanser Publishers, New York.

Brusselle-Dupend, N., Lai, D., Feaugas, X., Guigon, M. and Clavel, M. (2001) Mechanical behavior of a semicrystalline polymer before necking. Part I: Characterization of uniaxial behavior. *Polym. Eng. Sci.*, **41**, 66–76.

Brusselle-Dupend, N., Lai, D., Feaugas, X., Guigon, M. and Clavel, M. (2003) Mechanical behavior of a semicrystalline polymer before necking. Part II: Modeling of uniaxial behavior. *Polym. Eng. Sci.*, **43**, 501–518.

Budinski, K. G. and Budinski, M. K. (2002) *Engineering Materials: Properties and Selection*. Prentice Hall, Sydney.

Chen, W. F. and Mizuno, E. (1990) *Nonlinear analysis in soil mechanics*. Elsevier, New York.

Crisfield, M. A. (1997) *Advanced Topics*, vol. 2 of *Non-linear finite element analysis of solids and structures*. John Wiley and Sons Ltd, Brisbane.

Dickson, J. I., Boutin, J. and Handfield, L. (1984) A comparison of two simple methods for measuring cyclic internal and effective stresses. *Mater. Sci. Eng.*, **64**, L7–L11.

Drozdov, A. D. (2001) Modeling the viscoelastoplastic behavior of amorphous glassy polymers. *Polym. Eng. Sci.*, **41**, 1762–1770.

Drozdov, A. D., Agarwal, S. and Gupta, R. K. (2004) The effect of temperature on the viscoelastic behavior of linear low-density polyethylene. *Archive Appl. Mech.*, **73**, 591–614.

Drozdov, A. D. and Christiansen, J. C. (2003) Model for the viscoelastic and viscoplastic responses of semicrystalline polymers. *J. Appl. Polym. Sci.*, **88**, 1438–1450.

Drozdov, A. D. and Christiansen, J. C. (2004) Constitutive equations for the viscoplastic response of isotactic polypropylene in cyclic tests: The effect of strain rate. *Polym. Eng. Sci.*, **44**, 548–556.

Drozdov, A. D. and Kalamkarov, A. L. (1996) A constitutive model for nonlinear viscoelastic behavior of polymers. *Polym. Eng. Sci.*, **36**, 1907–1919.

Drozdov, A. D. and Yuan, Q. (2003) Effect of annealing on the viscoelastic and viscoplastic responses of low-density polyethylene. *J. Polym. Sci., Part B: Polym. Phys.*, **41**, 1638–1655.

Duffo, P., Monasse, B., Haudin, J. M., G'Sell, C. and Dahoun, A. (1995) Rheology of polypropylene in the solid state. *J. Mater. Sci.*, **30**, 701–711.

Eyring, H. (1936) Viscosity, plasticity, and diffusion as examples of absolute reaction rates. *J. Chem. Phys.*, **4**, 283–291.

Fan, J. and Yuan, Y. (2005) On the quadratic convergence of the levenberg-marquardt method without nonsingularity assumption. *Computing*, **74**, 23–39.

Feaugas, X. (1999) On the origin of the tensile flow stress in the stainless steel aisi 316l at 300k: Back stess and effective stress. *Acta mater.*, **47**, 3617–3632.

Findley, W. N., Lai, J. S. and Onaran, K. (1976) *Creep and relaxation of nonlinear viscoelastic materials*. Dover Publications, Inc., New York.

Fitz-Gerald, G. F. and Peckham, I. A. (1998) *Mathematical methods for engineers and scientists*. Prentice Hall, Sydney.

Flory, P. J. (1961) Thermodynamic relations for highly elastic materials. *Trans. Faraday. Soc.*, **57**, 829–838.

Gill, P. E. and Murray, W. (1978) Algorithms for the solution of the nonlinear least-squares problem. *SIAM J. Numer. Anal.*, **15**, 977–992.

G'Sell, C., Dahoun, A., Favier, V., Hiver, J. M., Philippe, M. J. and Canova, G. R. (1997) Microstructure transformation and stress-strain bahavior of isotactic polypropylene under large plastic deformation. *Polym. Eng. Sci.*, **37**, 1702–1711.

G'Sell, C., Dahoun, A., Royer, F. X. and Philippe, M. J. (1999) The influence of the amorphous matrix on the plastic hardening at large strain of semicrystalline polymers. *Modelling Simul. Mater. Sci. Eng.*, **7**, 817–828.

G'Sell, C., Hiver, J. M., Dahoun, A. and Souahi, A. (1992) Video-controlled tensile testing of polymers and metals beyond the necking point. *J. Mater. Sci.*, **27**, 5031–5039.

G'Sell, C. and Jonas, J. J. (1979) Determination of the plastic behaviour of solid polymers at constant true strain rate. *J. Mater. Sci.*, **14**, 583–591.

G'Sell, C. and Jonas, J. J. (1981) Yield and transient effects during the plastic deformation of solid polymers. *J. Mater. Sci.*, **16**, 1956–1974.

Halsey, G., Jr., H. J. W. and Eyring, H. (1945) Mechanical properties of textiles. *I. Text. Res. J.*, **15**, 295–311.

Haward, R. N. (1993) Strain hardening of thermoplastics. *Macromolecules*, **26**, 5860–5869.

Holzapfel, G. A. (1996) On large strain viscoelasticity: Continuum formulation and finite element applications to elastomeric structures. *Int. J. Numer. Meth. Engng.*, **39**, 3903–3926.

Holzapfel, G. A. and Simo, J. C. (1996) A new viscoelastic constitutive model for continuous media at finite thermomechanical changes. *Int. J. Solids Struct.*, **33**, 3019–3034.

Hughes, T. J. R. (1984) Numerical implementation of constitutive models: Rate-independent deviatoric plasticity. In S. Nemat-Nasser, R. Asaro and G. Hegemier (eds.), *Theoretical foundations for large scale computations of nonlinear material behaviour*, pages 29–57, Martinus Nijhoff Publishers, Dordrecht.

Hung, P. C. and Voloshin, A. S. (2003) In-plane strain measurement by digital image correlation. *J. Braz. Soc. Mech. Sci. & Eng.*, **25**, 215–221.

Itskov, M. (2000) On the theory of fourth-order tensors and their applications in computational mechanics. *Comput. Methods Appl. Mech. Engrg.*, **189**, 419–438.

Itskov, M. (2001) A generalized orthotropic hyperelastic material model with application to incompressible shells. *Int. J. Numer. Meth. Engng.*, **50**, 1777–1799.

Itskov, M. (2002) The derivative with respect to a tensor: some theoretical aspects and applications. *Z. Angew. Math. Mech.*, **82**, 535–544.

Itskov, M. (2007) *Tensor algebra and tensor analysis for engineers: With applications to continuum mechanics*. Springer, New York.

Kintzel, O. (2005) Fourth-order tensors - tensor differentiation with applications to continuum mechanics. Part II: Tensor analysis on manifolds. *Z. Angew. Math. Mech.*, **85**, 1–23.

Kitagawa, M. and Matsutani, T. (1988) Effect of time and temperature on nonlinear constitutive equation in polypropylene. *J. Mater. Sci.*, **23**, 4085–4090.

Kitagawa, M., Mori, T. and Matsutani, T. (1989) Rate-dependent nonlinear constitutive equation for polypropylene. *J. Polym. Sci., Part B: Polym. Phys.*, **27**, 85–95.

Kitagawa, M. and Takagi, H. (1990) Nonlinear constitutive equation for polyethylene under combined tension and torsion. *J. Polym. Sci., Part B: Polym. Phys.*, **28**, 1943–1953.

Kletschkowski, T., Schomburg, U. and Bertram, A. (2004) An endochronic viscoplastic approach for materials with different behavior in tension and compression. *Mech. Time-Depend. Mat.*, **8**, 119–135.

Kontou, E. and Farasoglou, P. (1998) Determination of the true stress-strain behaviour of polypropylene. *J. Mater. Sci.*, **33**, 147–153.

Kröner, E. (1960) Allgemeine kontinuumstheorie der versetzungen und eigenspannungen. *Arch. Rational Mech. Anal.*, **4**, 273–334.

Lai, J. and Bakker, A. (1995) An integral constitutive equation for nonlinear plasto-viscoelastic behavior of high-density polyethylene. *Polym. Eng. Sci.*, **35**, 1339–1347.

Lee, E. H. and Liu, D. T. (1967) Finite-strain elastic-plastic theory with application to plane-wave analysis. *J. Appl. Phys.*, **38**, 19–27.

Levenberg, K. (1944) A method for the solution of certain non-linear problems in least squares. *Quart. Appl. Math.*, **2**, 164–168.

Lifshitz, J. M. and Kolsky, H. (1967) Non-linear viscoelastic behaviour of polyethylene. *Int. J. Solids Structures*, **3**, 383–397.

Marquardt, D. W. (1963) An algorithm for least-squares estimation of nonlinear parameters. *SIAM J. Appl. Math.*, **11**, 431–441.

Michaeli, W. and Glißmann, M. (2000) Investigation and measurement of the true stress/strain behaviour of semi-crystalline thermoplastics. *Macromol. Mater. Eng.*, **284/285**, 19–24.

Moore, E. H. (1935) General analysis. *Memoirs Amer. Philos. Soc.*, **1**, 147–209.

Nedjar, B. (2002a) Frameworks for finite strain viscoelastic-plasticity based on multiplicative decompositions. part i: Continuum formulations. *Comput. Methods Appl. Mech. Engng.*, **191**, 1541–1562.

Nedjar, B. (2002b) Frameworks for finite strain viscoelastic-plasticity based on multiplicative decompositions. part ii: Computational aspects. *Comput. Methods Appl. Mech. Engng.*, **191**, 1563–1593.

Neu, R. W., Scott, D. T. and Woodmansee, M. W. (2000) Measurement and modeling of back stress at intermediate to high homologous temperatures. *Int. J. Plasticity*, **16**, 283–301.

Nocedal, J. and Wright, S. J. (1999) *Numerical optimization*. Springer-Verlag, New York.

Ogden, R. W. (1984) *Non-linear elastic deformations*. Dover Publications, Inc., New York.

Ogden, R. W., Saccomandi, G. and Sgura, I. (2004) Fitting hyperelastic models to experimental data. *Compute. Mech.*, **34**, 484–502.

Oleynik, E. F. (1990) In E. Baer and A. Moet (eds.), *High performance polymers: structure, properties, composites, fibres*, page 79, Hanser, Munich.

Onaran, K. and Findley, W. N. (1965) Combined stress-creep experiments on a nonlinear viscoelastic material to determine the kernel functions for a multiple integral representation of creep. *Trans., Soc. Rheol.*, **9**, 299–327.

Ortiz, M., Pinsky, P. M. and Taylor, R. L. (1983) Operator split methods for the numerical solution of the elastoplastic dynamic problem. *Comput. Methods Appl. Mech. Engrg.*, **39**, 137–157.

Owen, D. R. J. and Hinton, E. (1986) *Finite elements in plasticity: Theory and practice*. Pineridge Press Ltd, Swansea.

Pegoretti, A., Guardini, A., Migliaresi, C. and Ricco, T. (2000) Recovery of post-yielding deformations in semicrystalline poly(ethylene-terephthalate). *Polymer*, **41**, 1857–1864.

Penrose, R. (1954) A generalized inverse for matrices. *Proc. Cambridge Philos. Soc.*, **51**, 406–413.

Perić, D. (1993) On a class of consitutive equations in viscoplasticity: Formulation and computational issues. *Int. J. Numer. Meth. Engng.*, **36**, 1365–1393.

Perić, D. and Dettmer, W. (2003) A computational model for generalized inelastic materials at finite strains combining elastic, viscoelastic and plastic material behaviour. *Engng. Comp.*, **20**, 768–787.

Perić, D. and Owen, D. R. J. (1992) A model for large deformations of elasto-viscoplastic solids at finite strain: Computational issues. In D. Besdo and E. Stein (eds.), *Finite inelastic deformations: Theory and applications*, pages 299–312, Springer-Verlag, Berlin.

Perić, D. and Owen, D. R. J. (1998) Finite-element applications to the nonlinear mechanics of solids. *Rep. Prog. Phys.*, **61**, 1495–1574.

Perzyna, P. (1971) Thermodynamic theory of viscoplasticity. In C.-S. Yih (ed.), *Advances in applied mechanics*, vol. 11, pages 313–354, Academic Press, New York.

Popelar, C. F., Popelar, C. H. and Kenner, V. H. (1990) Viscoelastic material characterization and modeling for polyethylene. *Polym. Eng. Sci.*, **30**, 577–586.

Quinson, R., Perez, J., Rink, M. and Pavan, A. (1996) Components of non-elastic deformation in amorphous glassy polymers. *J. Mater. Sci.*, **31**, 4387–4394.

Reese, S. and Govindjee, S. (1998a) A theory of finite viscoelasticity and numerical aspects. *Int. J. Solids Structures*, **35**, 3455–3482.

Reese, S. and Govindjee, S. (1998b) Theoretical and numerical aspects in the thermo-viscoelastic material behavior of rubber-like polymers. *Mech. Time-Depend. Mater.*, **1**, 357–396.

Rosati, L. and Valoroso, N. (2004) A return map algorithm for general isotropic elasto/visco-plastic materials in principal space. *Int. J. Numer. Meth. Engng.*, **60**, 461–498.

Schang, O., Billon, N., Muracciole, J. M. and Fernagut, F. (1996) Mechanical behavior of a ductile polyamide 12 during impact. *Polym. Eng. Sci.*, **36**, 541–550.

Schapery, R. A. (1997) Nonlinear viscoelastic and viscoplastic constitutive equations based on thermodynamics. *Mech. of Time-Depend. Mat. 1*, pages 209–240.

Schapery, R. A. (1999) Nonlinear viscoelastic and viscoplastic constitutive equations with growing damage. *Int. J. Fracture.*, **97**, 33–66.

Schrauwen, B. A. G., Janssen, R. P. M., Govaert, L. E. and Meijer, H. E. H. (2004) Intrinsic deformation behaviour of semicrystalline polymers. *Macromolecules*, **37**, 6069–6078.

Sharples, A. (1966) *Polymer crystallization*. Edward Arnold (publishers) Ltd, London.

Simo, J. C. (1987) On a fully three-dimensional finite-strain viscoelastic damage model: Formulation and computational aspects. *Comput. Methods Appl. Mech. Engrg.*, **60**, 153–173.

Simo, J. C. (1992) Algorithms for static and dynamic multiplicative plasticity that preserve the classical return mapping schemes of the infinitesimal theory. *Comput. Methods Appl. Mech. Engrg.*, **99**, 61–112.

Simo, J. C. and Hughes, T. J. R. (1987) General return mapping algorithms for rate-independent plasticity. In C. S. Desai (ed.), *Constitutive laws for engineering materials: Theory and applications*, pages 221–231, Elsevier, New York.

Simo, J. C. and Hughes, T. J. R. (2000) *Computational Inelasticity*. Springer, New York.

Simo, J. C. and Taylor, R. L. (1991) Quasi-incompressible finite elasticity in principal stretches. continuum basis and numerical algorithms. *Comput. Methods Appl. Mech. Engrg.*, **85**, 273–310.

Twizell, E. H. and Ogden, R. W. (1983) Non-linear optimization of the material constants in Ogden's stress-deformation function for incompressible isotropic elastic materials. *J. Austral. Math. Soc. Ser. B*, **24**, 424–434.

Yang, X. J., Chow, C. L. and Lau, K. J. (2004) A unified viscoplastic description of 63sn-37pb solder alloy under cyclic straining and stressing. *Proc. Instn Mech. Engrs*, **218**, 909–920.

Zhang, C. and Moore, I. D. (1997a) Nonlinear mechanical response of high density polyethylene. Part I: Experimental investigation and model evaluation. *Polym. Eng. Sci.*, **37**, 404–413.

Zhang, C. and Moore, I. D. (1997b) Nonlinear mechanical response of high density polyethylene. Part II: Uniaxial constitutive modeling. *Polym. Eng. Sci.*, **37**, 414–420.

Zienkiewicz, O. C. and Taylor, R. L. (2003) *Solid Mechanics*, vol. 2 of *The finite element method*. Butterworth Heinemann, Sydney, 5 edn.

Appendix A

Derivation of the dissipation requirement

For a constant temperature process, the Clausius-Plank form of the 2nd law of thermodynamics is expressed in Lagrangian form via

$$\boldsymbol{S} : \tfrac{1}{2}\dot{\boldsymbol{C}} - \dot{\psi} \geq 0 \tag{A.1}$$

where $\dot{\boldsymbol{C}}$ is the time differential of the right Cauchy-Green strain tensor, : denotes the tensor double contraction (see Bonet and Wood (1997)) and $\dot{\psi}$ is the time derivative of the free energy expression. The free energy expression ψ is expressed in terms of elastic, viscoelastic and viscoplastic components as

$$\psi = \hat{\psi}_e\left(\boldsymbol{C}\right) + \hat{\psi}_{ve}\left(\boldsymbol{C}^e_{ve}, \eta_{ve}\right) + \hat{\psi}_{vp}\left(\boldsymbol{C}^e_{vp}, \eta_{vp}, \alpha, \boldsymbol{\alpha}\right) \tag{A.2}$$

Note here that for the semicrystalline polymer application, the viscosity terms η_{ve} and η_{vp} have become internal variables because of their functionality on strain (rate). Recalling the definition $\boldsymbol{C} = \boldsymbol{F}^T\boldsymbol{F}$ and the multiplicative split of the deformation gradient, (2.6), it is convenient to substitute the relationships

$$\boldsymbol{C}^e_{ve} = \boldsymbol{F}^{i\,-T}_{ve}\boldsymbol{C}\boldsymbol{F}^{i\,-1}_{ve} \quad \text{and} \quad \boldsymbol{C}^e_{vp} = \boldsymbol{F}^{i\,-T}_{vp}\boldsymbol{C}\boldsymbol{F}^{i\,-1}_{vp} \tag{A.3}$$

such that now

$$\psi = \hat{\psi}_e\left(\boldsymbol{C}\right) + \hat{\psi}_{ve}\left(\boldsymbol{F}_{ve}^{i\,-T}\boldsymbol{C}\boldsymbol{F}_{ve}^{i\,-1}, \eta_{ve}\right) + \hat{\psi}_{vp}\left(\boldsymbol{F}_{vp}^{i\,-T}\boldsymbol{C}\boldsymbol{F}_{vp}^{i\,-1}, \eta_{vp}, \alpha, \boldsymbol{\alpha}\right) \tag{A.4}$$

Following Reese and Govindjee (1998a) and Nedjar (2002a), taking the chain rule differential of (A.4) with respect to time gives

$$\begin{aligned}\dot{\psi} = &\frac{\partial\hat{\psi}_e}{\partial\boldsymbol{C}} : \dot{\boldsymbol{C}} + \frac{\partial\hat{\psi}_{ve}}{\partial\boldsymbol{C}_{ve}^e} : \frac{\partial\boldsymbol{C}_{ve}^e}{\partial\boldsymbol{C}} : \dot{\boldsymbol{C}} + \frac{\partial\hat{\psi}_{ve}}{\partial\boldsymbol{C}_{ve}^e} : \frac{\partial\boldsymbol{C}_{ve}^e}{\partial\boldsymbol{F}_{ve}^i} : \dot{\boldsymbol{F}}_{ve}^{i} \\ &+ \frac{\partial\hat{\psi}_{vp}}{\partial\boldsymbol{C}_{vp}^e} : \frac{\partial\boldsymbol{C}_{vp}^e}{\partial\boldsymbol{C}} : \dot{\boldsymbol{C}} + \frac{\partial\hat{\psi}_{vp}}{\partial\boldsymbol{C}_{vp}^e} : \frac{\partial\boldsymbol{C}_{vp}^e}{\partial\boldsymbol{F}_{vp}^i} : \dot{\boldsymbol{F}}_{vp}^{i} \\ &+ \frac{\partial\hat{\psi}_{ve}}{\partial\eta_{ve}} \cdot \dot{\eta}_{ve} + \frac{\partial\hat{\psi}_{vp}}{\partial\eta_{vp}} \cdot \dot{\eta}_{vp} + \frac{\partial\hat{\psi}_{vp}}{\partial\alpha} \cdot \dot{\alpha} + \frac{\partial\hat{\psi}_{vp}}{\partial\boldsymbol{\alpha}} : \dot{\boldsymbol{\alpha}}\end{aligned} \tag{A.5}$$

Separately evaluating specific terms from within (A.5), for the $\dot{\boldsymbol{C}}$ terms, where the subscript $n = ve, vp$

$$\begin{aligned}\frac{\partial\hat{\psi}_n}{\partial\boldsymbol{C}_n^e} : \frac{\partial\boldsymbol{C}_n^e}{\partial\boldsymbol{C}} : \dot{\boldsymbol{C}} &= \frac{\partial\hat{\psi}_n}{\partial\boldsymbol{C}_n^e} : \frac{\partial\left(\boldsymbol{F}_n^{i\,-T}\boldsymbol{C}\boldsymbol{F}_n^{i\,-1}\right)}{\partial\boldsymbol{C}} : \dot{\boldsymbol{C}} \\ &= \frac{\partial\hat{\psi}_n}{\partial\boldsymbol{C}_n^e} : \boldsymbol{F}_n^{i\,-T}\boldsymbol{I}_4\boldsymbol{F}_n^{i\,-1} : \dot{\boldsymbol{C}}\end{aligned}$$

where from Itskov (2000, 2002) and Kintzel (2005), the derivative of some second order tensor A_{ij} with respect to its self is given by $\partial A_{ij}/\partial A_{kl} = I_{4\,ijkl} = \delta_{ij}\delta_{kl}$, the fourth order identity tensor. Also, a useful identity used by Reese and Govindjee (1998a) associated with the double tensor contraction is $\boldsymbol{A} : \boldsymbol{B} = \boldsymbol{C}^{-1}\boldsymbol{A}\boldsymbol{D}^{-1} : \boldsymbol{D}\boldsymbol{B}\boldsymbol{C}$. Correspondingly

$$= 2\boldsymbol{F}_n^{i\,-1}\frac{\partial\hat{\psi}_n}{\partial\boldsymbol{C}_n^e}\boldsymbol{F}_n^{i\,-T} : \tfrac{1}{2}\dot{\boldsymbol{C}} \tag{A.6}$$

For the $\dot{\boldsymbol{F}}_n^{i}$ terms

$$\begin{aligned}\frac{\partial\hat{\psi}_n}{\partial\boldsymbol{C}_n^e} : \frac{\partial\boldsymbol{C}_n^e}{\partial\boldsymbol{F}_n^i} : \dot{\boldsymbol{F}}_n^{i} &= \frac{\partial\hat{\psi}_n}{\partial\boldsymbol{C}_n^e} : \frac{\partial\left(\boldsymbol{F}_n^{i\,-T}\boldsymbol{C}\boldsymbol{F}_n^{i\,-1}\right)}{\partial\boldsymbol{F}_n^i} : \dot{\boldsymbol{F}}_n^{i} \\ &= \frac{\partial\hat{\psi}_n}{\partial\boldsymbol{C}_n^e} : \left(\frac{\partial\boldsymbol{F}_n^{i\,-T}}{\partial\boldsymbol{F}_n^{i\,T}}\boldsymbol{C}\boldsymbol{F}_n^{i\,-1} : \dot{\boldsymbol{F}}_n^{i\,T} + \partial\boldsymbol{F}_n^{i\,-T}\boldsymbol{C}\frac{\partial\boldsymbol{F}_n^{i\,-1}}{\partial\boldsymbol{F}_n^i} : \dot{\boldsymbol{F}}_n^{i}\right)\end{aligned}$$

From Itskov (2000, 2002), for second order tensors $\partial\boldsymbol{A}^{-1}/\partial\boldsymbol{A} = -\boldsymbol{A}^{-1}\otimes\boldsymbol{A}^{-1}$ and also $\boldsymbol{A}\otimes\boldsymbol{B} : \boldsymbol{C} = \boldsymbol{A}\boldsymbol{C}\boldsymbol{B}$. Using these properties and the double contraction identity used in

(A.6) then with some development

$$= \boldsymbol{F}_n^{i\,-1} \frac{\partial \hat{\psi}_n}{\partial \boldsymbol{C}_n^e} \boldsymbol{F}_n^{i\,-T} : \left(-\dot{\boldsymbol{F}}_n^{i\,T} \boldsymbol{F}_n^{i\,-T} \boldsymbol{C} - \boldsymbol{C} \boldsymbol{F}_n^{i\,-1} \dot{\boldsymbol{F}}_n^{i} \right) \tag{A.7}$$

Using (A.6) and (A.7) in (A.5) and substituting this for the free energy time differential term in (A.1) gives the new form of the Clausius-Plank inequality for the semicrystalline polymers as

$$\begin{aligned}
&\left(\boldsymbol{S} - 2\frac{\partial \hat{\psi}_e}{\partial \boldsymbol{C}} - 2\boldsymbol{F}_{ve}^{i\,-1} \frac{\partial \hat{\psi}_{ve}}{\partial \boldsymbol{C}_{ve}^e} \boldsymbol{F}_{ve}^{i\,-T} - 2\boldsymbol{F}_{vp}^{i\,-1} \frac{\partial \hat{\psi}_{vp}}{\partial \boldsymbol{C}_{vp}^e} \boldsymbol{F}_{vp}^{i\,-T} \right) : \tfrac{1}{2}\dot{\boldsymbol{C}} \\
&+ \boldsymbol{F}_{ve}^{i\,-1} \frac{\partial \hat{\psi}_{ve}}{\partial \boldsymbol{C}_{ve}^e} \boldsymbol{F}_{ve}^{i\,-T} : \left(\dot{\boldsymbol{F}}_{ve}^{i\,T} \boldsymbol{F}_{ve}^{i\,-T} \boldsymbol{C} + \boldsymbol{C} \boldsymbol{F}_{ve}^{i\,-1} \dot{\boldsymbol{F}}_{ve}^{i} \right) \\
&+ \boldsymbol{F}_{vp}^{i\,-1} \frac{\partial \hat{\psi}_{vp}}{\partial \boldsymbol{C}_{vp}^e} \boldsymbol{F}_{vp}^{i\,-T} : \left(\dot{\boldsymbol{F}}_{vp}^{i\,T} \boldsymbol{F}_{vp}^{i\,-T} \boldsymbol{C} + \boldsymbol{C} \boldsymbol{F}_{vp}^{i\,-1} \dot{\boldsymbol{F}}_{vp}^{i} \right) \\
&- \frac{\partial \hat{\psi}_{ve}}{\partial \eta_{ve}} \cdot \dot{\eta}_{ve} - \frac{\partial \hat{\psi}_{vp}}{\partial \eta_{vp}} \cdot \dot{\eta}_{vp} - \frac{\partial \hat{\psi}_{vp}}{\partial \alpha} \cdot \dot{\alpha} - \frac{\partial \hat{\psi}_{vp}}{\partial \boldsymbol{\alpha}} : \dot{\boldsymbol{\alpha}} \geq 0
\end{aligned} \tag{A.8}$$

By the standard argument treated by authors such as Simo (1992), Reese and Govindjee (1998a), Perić and Owen (1998), Nedjar (2002a,b) and Perić and Dettmer (2003), the first term of (A.8) is equated to zero such that

$$\begin{aligned}
\boldsymbol{S} &= 2\frac{\partial \hat{\psi}_e}{\partial \boldsymbol{C}} + 2\boldsymbol{F}_{ve}^{i\,-1} \frac{\partial \hat{\psi}_{ve}}{\partial \boldsymbol{C}_{ve}^e} \boldsymbol{F}_{ve}^{i\,-T} + 2\boldsymbol{F}_{vp}^{i\,-1} \frac{\partial \hat{\psi}_{vp}}{\partial \boldsymbol{C}_{vp}^e} \boldsymbol{F}_{vp}^{i\,-T} \\
&= \boldsymbol{S}_e + \boldsymbol{S}_{ve} + \boldsymbol{S}_{vp}
\end{aligned} \tag{A.9}$$

Also, the Eulerian counterpart, the Kirchhoff stress tensor, can be attained via the second order *push forward* of (A.9) (Bonet and Wood (1997); Simo and Taylor (1991)) such that

$$\begin{aligned}
\boldsymbol{\tau} &= 2\boldsymbol{F} \frac{\partial \hat{\psi}_e}{\partial \boldsymbol{C}} \boldsymbol{F}^T + 2\boldsymbol{F}_{ve}^e \frac{\partial \hat{\psi}_{ve}}{\partial \boldsymbol{C}_{ve}^e} \boldsymbol{F}_{ve}^{e\,T} + 2\boldsymbol{F}_{vp}^e \frac{\partial \hat{\psi}_{vp}}{\partial \boldsymbol{C}_{vp}^e} \boldsymbol{F}_{vp}^{e\,T} \\
&= \boldsymbol{\tau}_e + \boldsymbol{\tau}_{ve} + \boldsymbol{\tau}_{vp}
\end{aligned} \tag{A.10}$$

Using (A.10) it is now possible to further develop (A.7). Firstly exploiting the symmetric nature of $\boldsymbol{C}$, then

$$\frac{\partial \hat{\psi}_n}{\partial \boldsymbol{C}_n^e} : \frac{\partial \boldsymbol{C}_n^e}{\partial \boldsymbol{F}_n^i} : \dot{\boldsymbol{F}}_n^i = 2\boldsymbol{F}_n^{i\,-1} \frac{\partial \hat{\psi}_n}{\partial \boldsymbol{C}_n^e} \boldsymbol{F}_n^{i\,-T} : -\boldsymbol{C} \boldsymbol{F}_n^{i\,-1} \dot{\boldsymbol{F}}_n^i$$

Using the previously noted double contraction identity

$$= -2\boldsymbol{F}^e_n \frac{\partial \hat{\psi}_n}{\partial \boldsymbol{C}^e_n} \boldsymbol{F}^{eT}_n : \boldsymbol{F}^{-T} \boldsymbol{C} \boldsymbol{F}^{i\,-1}_n \dot{\boldsymbol{F}}^i_n \boldsymbol{F}^{-1}$$

Substituting the result from (A.10) and exploiting the multiplicative split of the deformation gradient, (2.6), then with some development

$$= -\boldsymbol{\tau}_n : \boldsymbol{F}^e_n \dot{\boldsymbol{F}}^i_n \boldsymbol{F}^{i\,-1}_n \boldsymbol{F}^{e\,-1}_n \tag{A.11}$$

It is convenient here to introduce the Lie derivative of the elastic left Cauchy-Green strain tensor, $\mathcal{L}_v \boldsymbol{b}^e_n$ where from Bonet and Wood (1997), Perić and Owen (1998), Simo and Hughes (2000), Itskov (2000), Perić and Dettmer (2003) and Kintzel (2005)

$$\mathcal{L}_v \boldsymbol{b}^e_n = \boldsymbol{F} \dot{\overline{\left(\boldsymbol{F}^{-1} \boldsymbol{b}^e_n \boldsymbol{F}^{-T}\right)}} \boldsymbol{F}^T = \dot{\boldsymbol{b}}^e_n - \boldsymbol{l}\boldsymbol{b}^e_n - \boldsymbol{b}^e_n \boldsymbol{l}^T \tag{A.12}$$

where $\boldsymbol{l}$ is the spatial velocity gradient given by $\boldsymbol{l} = \dot{\boldsymbol{F}}\boldsymbol{F}^{-1}$ (Reese and Govindjee (1998a); Perić and Dettmer (2003)). Making further use of (2.6), and noting that $\boldsymbol{b}^e_n = \boldsymbol{F}^e_n \boldsymbol{F}^{e\,T}_n$ then after some development

$$\mathcal{L}_v \boldsymbol{b}^e_n = -\boldsymbol{F}^e_n \dot{\boldsymbol{F}}^i_n \boldsymbol{F}^{i\,-1}_n \boldsymbol{F}^{e\,-1}_n \boldsymbol{b}^e_n - \boldsymbol{b}^e_n \boldsymbol{F}^{e\,-T}_n \boldsymbol{F}^{i\,-T}_n \dot{\boldsymbol{F}}^{i\,T}_n \boldsymbol{F}^{e\,T}_n \tag{A.13}$$

Observing the symmetry of $\boldsymbol{b}^e_n$, rearranging gives

$$\boldsymbol{F}^e_n \dot{\boldsymbol{F}}^i_n \boldsymbol{F}^{i\,-1}_n \boldsymbol{F}^{e\,-1}_n = -\tfrac{1}{2} \left(\mathcal{L}_v \boldsymbol{b}^e_n\right) \boldsymbol{b}^{e\,-1}_n \tag{A.14}$$

such that now (A.11) becomes

$$\frac{\partial \hat{\psi}_n}{\partial \boldsymbol{C}^e_n} : \frac{\partial \boldsymbol{C}^e_n}{\partial \boldsymbol{F}^i_n} : \dot{\boldsymbol{F}}^i_n = \boldsymbol{\tau}_n : \tfrac{1}{2} \left(\mathcal{L}_v \boldsymbol{b}^e_n\right) \boldsymbol{b}^{e\,-1}_n \tag{A.15}$$

In view of (A.9) and (A.15) it is a direct development to show that the Clausius-Plank

inequality, (A.8), takes the final form

$$\begin{aligned}&\boldsymbol{\tau}_{ve} : \left(-\tfrac{1}{2}\left(\mathcal{L}_v \boldsymbol{b}^e_{ve}\right)\boldsymbol{b}^{e\,-1}_{ve}\right) + \boldsymbol{\tau}_{vp} : \left(-\tfrac{1}{2}\left(\mathcal{L}_v \boldsymbol{b}^e_{vp}\right)\boldsymbol{b}^{e\,-1}_{vp}\right)\\ &- \frac{\partial \hat{\psi}_{ve}}{\partial \eta_{ve}} \cdot \dot{\eta}_{ve} - \frac{\partial \hat{\psi}_{vp}}{\partial \eta_{vp}} \cdot \dot{\eta}_{vp} - \frac{\partial \hat{\psi}_{vp}}{\partial \alpha} \cdot \dot{\alpha} - \frac{\partial \hat{\psi}_{vp}}{\partial \boldsymbol{\alpha}} : \dot{\boldsymbol{\alpha}} \geq 0\end{aligned} \tag{A.16}$$

Appendix B

Viscoplastic constitutive equations in 1D

The one dimensional viscoplastic rheological element discussed here is comparable to that treated by Simo and Hughes (2000), Owen and Hinton (1986) and Zienkiewicz and Taylor (2003). The 1D rheological form is provided in Figure B.1.

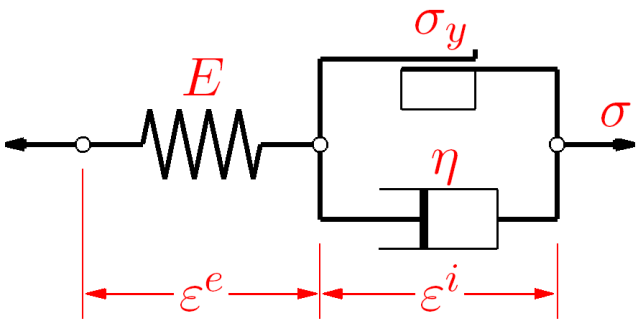

Figure B.1: One-dimensional elasto-viscoplastic rheological element (based on figure supplied by Simo and Hughes (2000)).

From the figure it can be observed that the total element strain is the sum of the elastic and inelastic components

$$\varepsilon = \varepsilon^e + \varepsilon^i \tag{B.1}$$

The spring element accounts for the instantaneous elastic behavior where total element stress is related to elastic strain via Hooke's law

$$\sigma = E\varepsilon^e = E\left(\varepsilon - \varepsilon^i\right) \tag{B.2}$$

Within the inelastic element, firstly from time independent plasticity (Owen and Hinton (1986); Simo and Hughes (2000)), the friction slider is known to be only capable of carrying stress levels up to and including its yield threshold (σ_y in the case of perfect plasticity). Inelastic evolution is only possible when $\sigma = \pm\sigma_y$. In the case of viscoplasticity as in Figure B.1, the parallel inclusion of the dashpot enables the element to carry more stress than that of the yield limit with the *extra* stress above σ_y being taken up in the dashpot and consequently governing inelastic evolution. The extra stress, σ_{ex}, can be defined by

$$\sigma_{ex} = \begin{cases} \sigma - \sigma_y & \text{if} \quad \sigma \geq \sigma_y \\ \sigma + \sigma_y & \text{if} \quad \sigma \leq -\sigma_y \\ 0 & \text{if} \quad \sigma \in (-\sigma_y, \sigma_y) \end{cases} \tag{B.3}$$

For the case of nonzero extra stress, it can be shown that

$$\sigma_{ex} = (|\sigma| - \sigma_y)\,\text{sign}\,(\sigma) \tag{B.4}$$

where $|\cdot| = \sqrt{(\cdot)^2}$ denotes the scalar magnitude and where $\text{sign}\,(\cdot)$ is a commonly used operator adequately defined by Simo and Hughes (2000) as

$$\text{sign}\,(x) = \begin{cases} x & \text{if} \quad x > 0 \\ -x & \text{if} \quad x < 0 \end{cases} \tag{B.5}$$

From (B.3), σ_{ex} is nonzero only if

$$f\,(\sigma) = |\sigma| - \sigma_y > 0 \tag{B.6}$$

where $f\,(\sigma)$ is referred to as the yield function. To allow σ_{ex} to be defined for all cases of $f\,(\sigma)$, following the work of Perić and Dettmer (2003), Simo (1992), Simo and Hughes (2000), Zienkiewicz and Taylor (2003) and Crisfield (1997), a *ramp* function, $\langle\cdot\rangle$, is introduced such that

$$\sigma_{ex} = \langle f\,(\sigma)\rangle \frac{\partial f\,(\sigma)}{\partial \sigma} \tag{B.7}$$

where

$$\langle x \rangle = \frac{(x + |x|)}{2} = \begin{cases} x & \text{if} \quad x > 0 \\ 0 & \text{if} \quad x \leq 0 \end{cases} \tag{B.8}$$

and also it was convenient to exploit the differential of (B.6) where

$$\frac{\partial}{\partial \sigma} \left(f \left(\sigma \right) \right) = \frac{\partial}{\partial \sigma} \left(\sqrt{\sigma^2} - \sigma_y \right) = \frac{\sigma}{\sqrt{\sigma^2}} = \text{sign} \left(\sigma \right) \tag{B.9}$$

Now (B.7) is consistent with (B.3).

Observing that the inelastic evolution of a dashpot is governed by the newtonian evolution equation similar to equation (2.2) (Findley et al. (1976); Owen and Hinton (1986); Simo and Hughes (2000)), then for the viscoplastic element

$$\dot{\varepsilon}^i = \frac{1}{\eta} \sigma_{ex} = \frac{\langle f \left(\sigma \right) \rangle}{\eta} \frac{\partial f \left(\sigma \right)}{\partial \sigma}$$

$$f \left(\sigma \right) = |\sigma| - \sigma_y \tag{B.10}$$

A viscoplastic constitutive relationship in the form of (B.10) was first proposed by Perzyna (1971).

The one-dimensional viscoplastic constitutive theory presented so far has dealt with *perfect viscoplasticity* in the sense that strain hardening of the plastic element (friction slider) has not been accounted for. Both isotropic and kinematic hardening have been shown to be important properties for semicrystalline polymers and so further development is necessary.

Firstly, the elastic limit, $\mathbb{E}_\sigma$, for the case of perfect plasticity is diagrammatically represented in Figure B.2. When stress is within the elastic limit, $|\sigma| - \sigma_y \leq 0$, deformation is wholly elastic. For stresses exceeding the elastic range, (B.6) is satisfied and there is inelastic evolution governed by (B.10).

When strain hardening is present, the internal variables α_{iso} and α_{kin} are introduced (Simo and Hughes (2000)) which are related to the inelastic strain evolution by

$$\dot{\alpha}_{iso} = \left| \dot{\varepsilon}^i \right|$$

$$\dot{\alpha}_{kin} = \dot{\varepsilon}^i \tag{B.11}$$

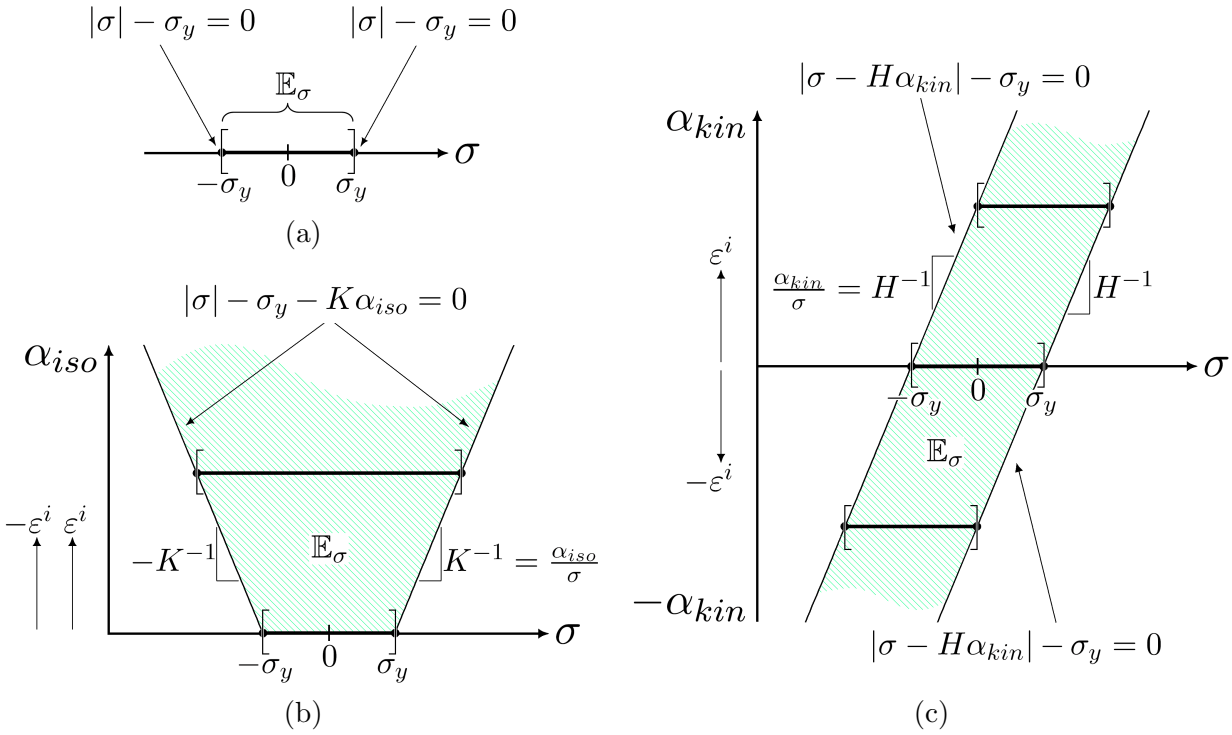

Figure B.2: Diagrammatical representation of the elastic limit for (a) perfect plasticity, (b) isotropic hardening (developed from Simo and Hughes (2000), Figure 1.6, page 13) and (c) kinematic hardening.

Graphical representation of the effect of isotropic and kinematic hardening on the elastic range in response to inelastic strain evolution is provided in Figures B.2 (b) and (c) respectively. The strain space internal variables α_{iso} and α_{kin} are related to the stress space elastic range through the isotropic and kinematic hardening moduli, K and H.

Combining the boundary expressions of the elastic range from Figure B.2 (b) and (c) for the combined case of isotropic and kinematic hardening gives the new expression for yield function

$$f\left(\sigma, \alpha_{iso}, \alpha_{kin}\right) = |\sigma - H\alpha_{kin}| - (\sigma_y + K\alpha_{iso}) \tag{B.12}$$

Because (B.12) is expressed in a combination of stress and strain space terms, it is convenient from a numerical standpoint to introduce the stress space conjugates to the internal variables, q_{iso} and q_{kin}, where

$$\begin{aligned} q_{iso} &= -K\alpha_{iso} \\ q_{kin} &= -H\alpha_{kin} \end{aligned} \tag{B.13}$$

such that now

$$f\left(\sigma + q_{kin}, q_{iso}\right) = \left|\sigma + q_{kin}\right| - \left(\sigma_y - q_{iso}\right) \tag{B.14}$$

An identical procedure to that carried out for the perfect viscoplastic case above then leads us to the result

$$\varepsilon^i = \frac{\langle f\left(\sigma + q_{kin}, q_{iso}\right)\rangle}{\eta} \frac{\partial f\left(\sigma + q_{kin}, q_{iso}\right)}{\partial \sigma} \tag{B.15}$$

where now

$$\frac{\partial f\left(\sigma + q_{kin}, q_{iso}\right)}{\partial \sigma} = \frac{\sigma + q_{kin}}{\left|\sigma + q_{kin}\right|} = \operatorname{sign}\left(\sigma + q_{kin}\right) \tag{B.16}$$

It is a useful result to derive (B.14) with respect to q_{iso} and q_{kin} such that

$$\frac{\partial f\left(\sigma + q_{kin}, q_{iso}\right)}{\partial q_{iso}} = 1 \tag{B.17}$$

$$\frac{\partial f\left(\sigma + q_{kin}, q_{iso}\right)}{\partial q_{kin}} = \frac{\sigma + q_{kin}}{\left|\sigma + q_{kin}\right|} = \frac{\partial f\left(\sigma + q_{kin}, q_{iso}\right)}{\partial \sigma} \tag{B.18}$$

Now using (B.11), (B.17) and (B.18) and noting that $\left|\frac{x}{\sqrt{x^2}}\right| = 1$, with some development the evolution of internal hardening variables can be defined by

$$\dot{\alpha}_{iso} = \frac{\langle f\left(\sigma + q_{kin}, q_{iso}\right)\rangle}{\eta} \frac{\partial f\left(\sigma + q_{kin}, q_{iso}\right)}{\partial q_{iso}} \tag{B.19}$$

and

$$\dot{\alpha}_{kin} = \frac{\langle f\left(\sigma + q_{kin}, q_{iso}\right)\rangle}{\eta} \frac{\partial f\left(\sigma + q_{kin}, q_{iso}\right)}{\partial q_{kin}} \tag{B.20}$$

A numerical solution strategy such as *radial return mapping* or *closest point projection* (Simo and Hughes (2000)) can be used to solve for the mutually dependent plastic evolution equations, (B.15), (B.19) and (B.20). Equations (B.2), (B.14), (B.15), (B.19) and (B.20) constitute a complete constitutive equation set for one-dimensional viscoplasticity accounting for isotropic and kinematic hardening.

Appendix C

Principal Space Differentials

C.1 Modified Lagrangian eigenvalue base definition

From the definition of the modified Lagrangian eigenvalue base, equation (3.18), it can be shown that

$$\widetilde{\boldsymbol{M}}_1 + \widetilde{\boldsymbol{M}}_2 + \widetilde{\boldsymbol{M}}_3 = \boldsymbol{C}^{-1} \tag{C.1}$$

$$\Lambda_1\widetilde{\boldsymbol{M}}_1 + \Lambda_2\widetilde{\boldsymbol{M}}_2 + \Lambda_3\widetilde{\boldsymbol{M}}_3 = \boldsymbol{I} \tag{C.2}$$

$$\Lambda_1^2\widetilde{\boldsymbol{M}}_1 + \Lambda_2^2\widetilde{\boldsymbol{M}}_2 + \Lambda_3^2\widetilde{\boldsymbol{M}}_3 = \boldsymbol{C} \tag{C.3}$$

(1) Distinct eigenvalues $\Lambda_1 \neq \Lambda_2 \neq \Lambda_3$

Solving the system of equation (C.1) to (C.3) yields

$$\widetilde{\boldsymbol{M}}_A = \frac{\boldsymbol{C} - (\mathrm{I}_C - \Lambda_A)\,\boldsymbol{I} + \mathrm{III}_C\Lambda_A^{-1}\boldsymbol{C}^{-1}}{D_A} \qquad A = 1,2,3 \tag{C.4}$$

where

$$D_A = (\Lambda_A - \Lambda_B)\,(\Lambda_A - \Lambda_C) \qquad A \neq B \neq C \tag{C.5}$$

and the well known first and third principal invariants I_C and III_C have been exploited where

$$\mathrm{I}_C = \Lambda_1 + \Lambda_2 + \Lambda_3 \qquad \mathrm{II}_C = \Lambda_1\Lambda_2 + \Lambda_1\Lambda_3 + \Lambda_2\Lambda_3 \qquad \mathrm{III}_C = \Lambda_1\Lambda_2\Lambda_3 \tag{C.6}$$

Note that this is an identical result to that found by Simo and Taylor (1991).

(2) Double coalescence of eigenvalues $\Lambda_1 \neq \Lambda_2 = \Lambda_3 = \Lambda$

From standard algebra, it can be shown that for the case when $\Lambda_2 = \Lambda_3$, the corresponding modified eigenvalue bases remain undetermined given only equations (C.1) to (C.3). To account for this (C.1) and (C.2) can take the modified form

$$\widetilde{\boldsymbol{M}}_1 + \left(\widetilde{\boldsymbol{M}}_2 + \widetilde{\boldsymbol{M}}_3\right) = \boldsymbol{C}^{-1} \tag{C.7}$$

$$\Lambda_1\widetilde{\boldsymbol{M}}_1 + \Lambda\left(\widetilde{\boldsymbol{M}}_2 + \widetilde{\boldsymbol{M}}_3\right) = \boldsymbol{I} \tag{C.8}$$

Here now the modified eigenvalue base corresponding to the single distinct eigenvalue Λ_1 can be determined as can the combined $\left(\widetilde{\boldsymbol{M}}_2 + \widetilde{\boldsymbol{M}}_3\right)$ contribution as

$$\widetilde{\boldsymbol{M}}_1 = \frac{\boldsymbol{I} - \Lambda\boldsymbol{C}^{-1}}{\Lambda_1 - \Lambda} \tag{C.9}$$

$$\left(\widetilde{\boldsymbol{M}}_2 + \widetilde{\boldsymbol{M}}_3\right) = \boldsymbol{C}^{-1} - \widetilde{\boldsymbol{M}}_1 \tag{C.10}$$

Although Simo and Taylor (1991) do not present an alternative definition such as this for the case of double eigenvalue coalescence, it can be trivially shown that (C.4) reduces to (C.9) in such circumstances and so there would be no loss in generality to use only equation (C.4) in both cases.

(3) Triple coalescence of eigenvalues $\Lambda_1 = \Lambda_2 = \Lambda_3 = \Lambda$

For the case of triple coalescence of eigenvalues, from equations (C.1) to (C.3) the modified eigenvalue bases are all algebraically indeterminate. In this case, (C.1) is of sole importance to the corresponding spectral reconstruction.

C.2 First principal stretch differentials

Recalling the three principal invariants, equations (C.6), by exploiting the traditional tensor forms of these invariants (Bonet and Wood (1997)) (functional on the right Cauchy-Greens

strain), (C.6) become

$$\mathrm{tr}\left[\boldsymbol{C}\right] = \Lambda_1 + \Lambda_2 + \Lambda_3 \tag{C.11}$$

$$\tfrac{1}{2}\left(\mathrm{tr}\left[\boldsymbol{C}\right]^2 + \mathrm{tr}\left[\boldsymbol{C}^2\right]\right) = \Lambda_1\Lambda_2 + \Lambda_1\Lambda_3 + \Lambda_2\Lambda_3 \tag{C.12}$$

$$\det\left[\boldsymbol{C}\right] = \Lambda_1\Lambda_2\Lambda_3 \tag{C.13}$$

Differentiating equations (C.11) to (C.13) with respect to $\boldsymbol{C}$ gives after manipulation

$$\boldsymbol{I} = \partial_{\boldsymbol{C}}\Lambda_1 + \partial_{\boldsymbol{C}}\Lambda_2 + \partial_{\boldsymbol{C}}\Lambda_3 \tag{C.14}$$

$$\boldsymbol{C} = \mathrm{I}_{\boldsymbol{C}}\boldsymbol{I} - (\Lambda_2 + \Lambda_3)\,\partial_{\boldsymbol{C}}\Lambda_1 - (\Lambda_1 + \Lambda_3)\,\partial_{\boldsymbol{C}}\Lambda_2 - (\Lambda_1 + \Lambda_2)\,\partial_{\boldsymbol{C}}\Lambda_3 \tag{C.15}$$

$$\mathrm{III}_{\boldsymbol{C}}\boldsymbol{C}^{-1} = \Lambda_2\Lambda_3\partial_{\boldsymbol{C}}\Lambda_1 + \Lambda_1\Lambda_3\partial_{\boldsymbol{C}}\Lambda_2 + \Lambda_1\Lambda_2\partial_{\boldsymbol{C}}\Lambda_3 \tag{C.16}$$

(1) Distinct eigenvalues $\Lambda_1 \neq \Lambda_2 \neq \Lambda_3$

Appendix C.1 provided definition of the modified eigenvalue bases, $\widetilde{\boldsymbol{M}}_A$, $A = 1, 2, 3$ functional on the eigenvalues and $\boldsymbol{C}$, $\boldsymbol{I}$ and $\mathrm{III}_{\boldsymbol{C}}\boldsymbol{C}^{-1}$. Equations (C.14) to (C.16) can be substituted into (C.4) and following straight forward manipulation

$$\partial_{\boldsymbol{C}}\Lambda_A = \Lambda_A\widetilde{\boldsymbol{M}}_A, \qquad A = 1, 2, 3 \tag{C.17}$$

Recalling the relationship $\lambda_A = \sqrt{\Lambda_A}$, the corresponding principal stretch derivatives can be found via the chain rule expansion

$$\begin{aligned}\frac{\partial\lambda_A}{\partial\boldsymbol{C}} &= \sum_{B=1}^{3}\frac{\partial\lambda_A}{\partial\Lambda_B}\frac{\partial\Lambda_B}{\partial\boldsymbol{C}} \\ &= \frac{1}{2}\lambda_A^{-1}\frac{\partial\Lambda_A}{\partial\boldsymbol{C}}\end{aligned} \tag{C.18}$$

such that now

$$\boxed{\partial_{\boldsymbol{C}}\lambda_A = \tfrac{1}{2}\lambda_A\widetilde{\boldsymbol{M}}_A, \qquad A = 1, 2, 3} \tag{C.19}$$

(2) Double coalescence of eigenvalues $\Lambda_1 \neq \Lambda_2 = \Lambda_3 = \Lambda$

For the case of double eigenvalue coalescence, again substituting equations (C.14) to (C.16) into the modified eigenvalue base expression (C.9), yields

$$\partial_{\boldsymbol{C}} \Lambda_1 = \Lambda_1 \widetilde{\boldsymbol{M}}_1 \tag{C.20}$$

Rearranging (C.16), such that

$$\boldsymbol{C}^{-1} = \Lambda_1^{-1} \partial_{\boldsymbol{C}} \Lambda_1 + \Lambda_2^{-1} \partial_{\boldsymbol{C}} \Lambda_2 + \Lambda_3^{-1} \partial_{\boldsymbol{C}} \Lambda_3 \tag{C.21}$$

then exploiting (C.20) it can be shown

$$\partial_{\boldsymbol{C}} (\Lambda_2 + \Lambda_3) = \Lambda \left(\boldsymbol{C}^{-1} - \widetilde{\boldsymbol{M}}_1 \right) \tag{C.22}$$

Again implementing equation (C.18), the principal stretch derivatives for double eigenvalue coalescence become

$$\boxed{\begin{aligned} \partial_{\boldsymbol{C}} \lambda_1 &= \tfrac{1}{2} \lambda_1 \widetilde{\boldsymbol{M}}_1 && \text{(C.23)} \\ \partial_{\boldsymbol{C}} (\lambda_2 + \lambda_3) &= \tfrac{1}{2} \lambda \left(\boldsymbol{C}^{-1} - \widetilde{\boldsymbol{M}}_1 \right) && \text{(C.24)} \end{aligned}}$$

(3) Triple coalescence of eigenvalues $\Lambda_1 = \Lambda_2 = \Lambda_3 = \Lambda$

Because the eigenvalue bases remain undetermined in the case of triple coalescence of eigenvalues, no distinct principal stretch derivatives can be found, however utilizing equations (C.18) and (C.21) it can be shown that

$$\boxed{\partial_{\boldsymbol{C}} (\lambda_1 + \lambda_2 + \lambda_3) = \tfrac{1}{2} \lambda \boldsymbol{C}^{-1}} \tag{C.25}$$

which is a useful result.

C.3 First and second jacobian differentials

Noting the definition of the jacobian, J, in principal space as $J = \lambda_1\lambda_2\lambda_3$, then using the chain rule, its derivative with respect to the right Cauchy-Green strain tensor becomes

$$\frac{\partial J}{\partial \boldsymbol{C}} = \sum_{A=1}^{3} \frac{\partial J}{\partial \lambda_A}\frac{\partial \lambda_A}{\partial \boldsymbol{C}} \tag{C.26}$$

Observing

$$\frac{\partial J}{\partial \lambda_A} = \lambda_B\lambda_C, \qquad A \neq B \neq C \tag{C.27}$$

and assuming the case of distinct eigenvalues, then equations (C.19) and (C.27) can be substituted into (C.26) to give

$$\frac{\partial J}{\partial \boldsymbol{C}} = \frac{1}{2}J\widetilde{\boldsymbol{M}}_1 + \frac{1}{2}J\widetilde{\boldsymbol{M}}_2 + \frac{1}{2}J\widetilde{\boldsymbol{M}}_3 \tag{C.28}$$

Finally, recalling (C.1), then

$$\boxed{\partial_{\boldsymbol{C}} J = \tfrac{1}{2}J\boldsymbol{C}^{-1}} \tag{C.29}$$

Equation (C.29) is identical to that used by Simo and Taylor (1991). It is worthwhile to note that similarly, this process can be repeated for the cases of double and triple eigenvalue coalescence yielding, with some manipulation, the same expression. This result clearly demonstrates the invariance of the volumetric terms to dimensionally variant strain as expected.

The second differential of the jacobian, $\partial^2_{\boldsymbol{CC}} J$ can be found via the straightforward differential of equation (C.29). From the chain rule

$$\begin{aligned}\frac{\partial^2 J}{\partial \boldsymbol{C}^2} &= \frac{\partial}{\partial \boldsymbol{C}}\left(\tfrac{1}{2}J\boldsymbol{C}^{-1}\right) \\ &= \frac{1}{2}\frac{\partial J}{\partial \boldsymbol{C}}\boldsymbol{C}^{-1} + \frac{1}{2}J\frac{\partial \boldsymbol{C}^{-1}}{\partial \boldsymbol{C}}\end{aligned} \tag{C.30}$$

Simo and Taylor (1991) represent the differential, $\partial_{\boldsymbol{C}}\boldsymbol{C}^{-1}$, by the fourth order tensor $-\boldsymbol{I}^{\boldsymbol{C}^{-1}}$ where it can be shown that

$$\frac{\partial C^{-1}_{ij}}{\partial C_{kl}} = -I^{\boldsymbol{C}^{-1}}_{ijkl} = -\frac{1}{2}\left(C^{-1}_{ik}C^{-1}_{jl} + C^{-1}_{il}C^{-1}_{jk}\right) \tag{C.31}$$

Using this and with further implementation of (C.29), the second differential of the jacobian (C.30), becomes

$$\boxed{\partial^2_{\boldsymbol{CC}} J = \tfrac{1}{4} J \boldsymbol{C}^{-1} \otimes \boldsymbol{C}^{-1} - \tfrac{1}{2} J \boldsymbol{I}^{\boldsymbol{C}^{-1}}} \tag{C.32}$$

C.4 Second principal stretch differentials

The different treatment of the first principal stretch differentials dependent on eigenvalue equalities in Appendix C.2, necessitates the analogous separation of the second principal stretch differentials as follows.

(1) Distinct eigenvalues $\Lambda_1 \neq \Lambda_2 \neq \Lambda_3$

Because all eigenvalue bases are independently discernable for distinct eigenvalues, the second principal stretch derivative terms reduce to first modified eigenvalue base derivatives as has been noted in Section 3.1.5. Taking the derivative of equations (C.1) to (C.3) with respect to the right Cauchy-Green strain tensor yields

$$\partial_{\boldsymbol{C}} \widetilde{\boldsymbol{M}}_1 + \partial_{\boldsymbol{C}} \widetilde{\boldsymbol{M}}_2 + \partial_{\boldsymbol{C}} \widetilde{\boldsymbol{M}}_3 = -\boldsymbol{I}^{\boldsymbol{C}^{-1}} \tag{C.33}$$

$$\Lambda_1 \partial_{\boldsymbol{C}} \widetilde{\boldsymbol{M}}_1 + \Lambda_2 \partial_{\boldsymbol{C}} \widetilde{\boldsymbol{M}}_2 + \Lambda_3 \partial_{\boldsymbol{C}} \widetilde{\boldsymbol{M}}_3 = -\sum_{A=1}^{3} \Lambda_A \widetilde{\boldsymbol{M}}_A \otimes \widetilde{\boldsymbol{M}}_A \tag{C.34}$$

$$\Lambda_1^2 \partial_{\boldsymbol{C}} \widetilde{\boldsymbol{M}}_1 + \Lambda_2^2 \partial_{\boldsymbol{C}} \widetilde{\boldsymbol{M}}_2 + \Lambda_3^2 \partial_{\boldsymbol{C}} \widetilde{\boldsymbol{M}}_3 = \boldsymbol{I}' - 2 \sum_{A=1}^{3} \Lambda_A^2 \widetilde{\boldsymbol{M}}_A \otimes \widetilde{\boldsymbol{M}}_A \tag{C.35}$$

having used the relationship $\partial_{\boldsymbol{C}} \Lambda_A = \Lambda_A \widetilde{\boldsymbol{M}}_A$ from (C.17). By simultaneous solution and subsequent algebraic manipulation of equation (C.33) to (C.35) it can be shown that the modified Lagrangian eigenvalue base derivatives are given by

$$\partial_{\boldsymbol{C}} \widetilde{\boldsymbol{M}}_A = \frac{1}{D_A} \left(\boldsymbol{I}' - \sum_{B=1}^{3} \left[2\Lambda_B^2 - (\mathrm{I}_{\boldsymbol{C}} - \Lambda_A) \Lambda_B \right] \widetilde{\boldsymbol{M}}_B \otimes \widetilde{\boldsymbol{M}}_B - \mathrm{III}_{\boldsymbol{C}} \Lambda_A^{-1} \boldsymbol{I}^{\boldsymbol{C}^{-1}} \right)$$

$$A = 1, 2, 3 \tag{C.36}$$

(2) Double coalescence of eigenvalues $\Lambda_1 \neq \Lambda_2 = \Lambda_3 = \Lambda$

When two eigenvalues are equal, only the other distinct eigenvalue has an explicitly defined eigenvalue base. Consequently, it would be inconsistent to replace the second derivatives

of the non-unique principal stretches with the first derivatives of undetermined eigenvalue bases as was possible when all the eigenvalues were distinct. An alternate methodology will be used such that the second differential terms are functional on the determined eigenvalue base only.

Recalling equation (C.10)

$$\boldsymbol{C}^{-1} - \widetilde{\boldsymbol{M}}_1 = \widetilde{\boldsymbol{M}}_2 + \widetilde{\boldsymbol{M}}_3 \tag{C.37}$$

Substitution of this expression into (C.22) gives

$$\widetilde{\boldsymbol{M}}_2 + \widetilde{\boldsymbol{M}}_3 = \Lambda^{-1}\partial_{\boldsymbol{C}}\left(\Lambda_2 + \Lambda_3\right) \tag{C.38}$$

Using this expression, the system of equations (C.1) to (C.3) are modified

$$\widetilde{\boldsymbol{M}}_1 + \Lambda^{-1}\partial_{\boldsymbol{C}}\left(\Lambda_2 + \Lambda_3\right) = \boldsymbol{C}^{-1} \tag{C.39}$$

$$\Lambda_1\widetilde{\boldsymbol{M}}_1 + \partial_{\boldsymbol{C}}\left(\Lambda_2 + \Lambda_3\right) = \boldsymbol{I} \tag{C.40}$$

$$\Lambda_1^2\widetilde{\boldsymbol{M}}_1 + \Lambda\partial_{\boldsymbol{C}}\left(\Lambda_2 + \Lambda_3\right) = \boldsymbol{C} \tag{C.41}$$

Now taking the differential of the modified expressions (C.39) to (C.41), with respect to the right Cauchy-Green strain tensor gives

$$\partial_{\boldsymbol{C}}\widetilde{\boldsymbol{M}}_1 + \Lambda^{-1}\partial^2_{\boldsymbol{CC}}\left(\Lambda_2 + \Lambda_3\right) - \Lambda^{-2}\left(\partial_{\boldsymbol{C}}\Lambda_2 \otimes \partial_{\boldsymbol{C}}\Lambda_2 + \partial_{\boldsymbol{C}}\Lambda_3 \otimes \partial_{\boldsymbol{C}}\Lambda_3\right) = -\boldsymbol{I}^{\boldsymbol{C}^{-1}} \tag{C.42}$$

$$\Lambda_1\partial_{\boldsymbol{C}}\widetilde{\boldsymbol{M}}_1 + \partial^2_{\boldsymbol{CC}}\left(\Lambda_2 + \Lambda_3\right) = -\Lambda_1\widetilde{\boldsymbol{M}}_1 \otimes \widetilde{\boldsymbol{M}}_1 \tag{C.43}$$

$$\Lambda_1^2\partial_{\boldsymbol{C}}\widetilde{\boldsymbol{M}}_1 + \Lambda\partial^2_{\boldsymbol{CC}}\left(\Lambda_2 + \Lambda_3\right) + \left(\partial_{\boldsymbol{C}}\Lambda_2 \otimes \partial_{\boldsymbol{C}}\Lambda_2 + \partial_{\boldsymbol{C}}\Lambda_3 \otimes \partial_{\boldsymbol{C}}\Lambda_3\right) = \boldsymbol{I}' - 2\Lambda_1^2\widetilde{\boldsymbol{M}}_1 \otimes \widetilde{\boldsymbol{M}}_1 \tag{C.44}$$

Within the new system of equations (C.42) to (C.44), there are three unknowns; $\partial_{\boldsymbol{C}}\widetilde{\boldsymbol{M}}_1$, $\partial^2_{\boldsymbol{CC}}\left(\Lambda_2 + \Lambda_3\right)$ and $\left(\partial_{\boldsymbol{C}}\Lambda_2 \otimes \partial_{\boldsymbol{C}}\Lambda_2 + \partial_{\boldsymbol{C}}\Lambda_3 \otimes \partial_{\boldsymbol{C}}\Lambda_3\right)$. Simultaneous solution for the modified Lagrangian eigenvalue base derivative $\partial_{\boldsymbol{C}}\widetilde{\boldsymbol{M}}_1$ gives

$$\partial_{\boldsymbol{C}}\widetilde{\boldsymbol{M}}_1 = \frac{1}{D_1}\left(\boldsymbol{I}' - 2\Lambda_1\left(\Lambda_1 - \Lambda\right)\widetilde{\boldsymbol{M}}_1 \otimes \widetilde{\boldsymbol{M}}_1 - \mathrm{III}_{\boldsymbol{C}}\Lambda_1^{-1}\boldsymbol{I}'\right) \tag{C.45}$$

Correspondingly, the second and third unknown terms can be given by the functions

$$\partial^2_{\boldsymbol{CC}}\left(\Lambda_2 + \Lambda_3\right) = -\Lambda_1\widetilde{\boldsymbol{M}}_1 \otimes \widetilde{\boldsymbol{M}}_1 - \Lambda_1\partial_{\boldsymbol{C}}\widetilde{\boldsymbol{M}}_1 \tag{C.46}$$

$$(\partial_{\boldsymbol{C}}\Lambda_2 \otimes \partial_{\boldsymbol{C}}\Lambda_2 + \partial_{\boldsymbol{C}}\Lambda_3 \otimes \partial_{\boldsymbol{C}}\Lambda_3) = -\Lambda_1\Lambda\widetilde{\boldsymbol{M}}_1 \otimes \widetilde{\boldsymbol{M}}_1 + \mathrm{III}_{\boldsymbol{C}}\Lambda_1^{-1}\boldsymbol{I}^{\boldsymbol{C}^{-1}} - \Lambda\left(\Lambda_1 - \Lambda\right)\partial_{\boldsymbol{C}}\widetilde{\boldsymbol{M}}_1 \tag{C.47}$$

where (C.46) and (C.47) are expressed wholly in terms of the known modified eigenvalue base and its derivative as desired.

(3) Triple coalescence of eigenvalues $\Lambda_1 = \Lambda_2 = \Lambda_3 = \Lambda$

As was the case for the first principal strain differentials, when $\Lambda_1 = \Lambda_2 = \Lambda_3 = \Lambda$, the second differentials are also all exclusively indeterminate. This being said, a useful result can be attained via a procedure similar to that used above for the case of double eigenvalue coalescence.

From equations (C.1) and (C.21)

$$\widetilde{\boldsymbol{M}}_1 + \widetilde{\boldsymbol{M}}_2 + \widetilde{\boldsymbol{M}}_3 = \Lambda^{-1}\partial_{\boldsymbol{C}}\left(\Lambda_1 + \Lambda_2 + \Lambda_3\right) \tag{C.48}$$

Substitution of this term into equations (C.1) and (C.2) gives the modified equation system

$$\Lambda^{-1}\partial_{\boldsymbol{C}}\left(\Lambda_1 + \Lambda_2 + \Lambda_3\right) = \boldsymbol{C}^{-1} \tag{C.49}$$

$$\partial_{\boldsymbol{C}}\left(\Lambda_1 + \Lambda_2 + \Lambda_3\right) = \boldsymbol{I} \tag{C.50}$$

Differentiation with respect to the right Cauchy-Green strain tensor gives

$$\Lambda^{-1}\partial^2_{\boldsymbol{C}\boldsymbol{C}}\left(\Lambda_1 + \Lambda_2 + \Lambda_3\right) - \Lambda^{-2}\left(\partial_{\boldsymbol{C}}\Lambda_1 \otimes \partial_{\boldsymbol{C}}\Lambda_1 + \partial_{\boldsymbol{C}}\Lambda_2 \otimes \partial_{\boldsymbol{C}}\Lambda_2 + \partial_{\boldsymbol{C}}\Lambda_3 \otimes \partial_{\boldsymbol{C}}\Lambda_3\right) = -\boldsymbol{I}^{\boldsymbol{C}^{-1}} \tag{C.51}$$

$$\partial^2_{\boldsymbol{C}\boldsymbol{C}}\left(\Lambda_1 + \Lambda_2 + \Lambda_3\right) = \boldsymbol{0} \tag{C.52}$$

and by trivial simultaneous solution,

$$(\partial_{\boldsymbol{C}}\Lambda_1 \otimes \partial_{\boldsymbol{C}}\Lambda_1 + \partial_{\boldsymbol{C}}\Lambda_2 \otimes \partial_{\boldsymbol{C}}\Lambda_2 + \partial_{\boldsymbol{C}}\Lambda_3 \otimes \partial_{\boldsymbol{C}}\Lambda_3) = \Lambda^2\boldsymbol{I}^{\boldsymbol{C}^{-1}} \tag{C.53}$$

Appendix D

Expansions of $\bar{\mathbb{C}}$

D.1 Expansion of $\bar{\mathbb{C}}$ for double coalescence of eigenvalues

Due to the nature of the results for first and second principal stretch derivatives from Appendices C.2 and C.4 when two eigenvalues coalesce, expression of the specific deviatoric component of the closed-form tangential modulus is only possible after expansion of equation (3.39).

Recalling that the derivative of the single exclusive eigenvalue is know from (C.23), then the expansion of the deviatoric tangential modulus proceeds

$$\begin{aligned}
\bar{\mathbb{C}} = \quad & \gamma_{11}\widetilde{\boldsymbol{M}}_1 \otimes \widetilde{\boldsymbol{M}}_1 + && \gamma_{12}\widetilde{\boldsymbol{M}}_1 \otimes \left(2\lambda_2^{-1}\frac{\partial \lambda_2}{\partial \boldsymbol{C}}\right) + && \gamma_{13}\widetilde{\boldsymbol{M}}_1 \otimes \left(2\lambda_3^{-1}\frac{\partial \lambda_3}{\partial \boldsymbol{C}}\right) \\
+ \quad & \gamma_{21}\left(2\lambda_2^{-1}\frac{\partial \lambda_2}{\partial \boldsymbol{C}}\right) \otimes \widetilde{\boldsymbol{M}}_1 + && \gamma_{22}\left(2\lambda_2^{-1}\frac{\partial \lambda_2}{\partial \boldsymbol{C}}\right) \otimes \left(2\lambda_2^{-1}\frac{\partial \lambda_2}{\partial \boldsymbol{C}}\right) + && \gamma_{23}\left(2\lambda_2^{-1}\frac{\partial \lambda_2}{\partial \boldsymbol{C}}\right) \otimes \left(2\lambda_3^{-1}\frac{\partial \lambda_3}{\partial \boldsymbol{C}}\right) \\
+ \quad & \gamma_{31}\left(2\lambda_3^{-1}\frac{\partial \lambda_3}{\partial \boldsymbol{C}}\right) \otimes \widetilde{\boldsymbol{M}}_1 + && \gamma_{32}\left(2\lambda_3^{-1}\frac{\partial \lambda_3}{\partial \boldsymbol{C}}\right) \otimes \left(2\lambda_2^{-1}\frac{\partial \lambda_2}{\partial \boldsymbol{C}}\right) + && \gamma_{33}\left(2\lambda_3^{-1}\frac{\partial \lambda_3}{\partial \boldsymbol{C}}\right) \otimes \left(2\lambda_3^{-1}\frac{\partial \lambda_3}{\partial \boldsymbol{C}}\right) \\
+ \quad & 2\beta_1 \partial_{\boldsymbol{C}}\widetilde{\boldsymbol{M}}_1 + && 2\beta_2 \frac{\partial}{\partial \boldsymbol{C}}\left(2\lambda_2^{-1}\frac{\partial \lambda_2}{\partial \boldsymbol{C}}\right) + && 2\beta_3 \frac{\partial}{\partial \boldsymbol{C}}\left(2\lambda_3^{-1}\frac{\partial \lambda_3}{\partial \boldsymbol{C}}\right)
\end{aligned} \tag{D.1}$$

Of particular importance to the reduction of this expression is the observation that when $\Lambda_2 = \Lambda_3 = \Lambda$, then via algebraic manipulation of equation (3.38) it can be shown that

$$\gamma_{12} = \gamma_{13}, \qquad \gamma_{21} = \gamma_{31}, \qquad \gamma_{22} = \gamma_{23} = \gamma_{32} = \gamma_{33} \tag{D.2}$$

Also, recalling equation (C.18), it is convenient to use the eigenvalue form of the second

principal stretch derivatives via

$$\frac{\partial}{\partial \boldsymbol{C}}\left(2\lambda_A^{-1}\frac{\partial \lambda_A}{\partial \boldsymbol{C}}\right) = \frac{\partial}{\partial \boldsymbol{C}}\left(\Lambda_A^{-1}\frac{\partial \Lambda_A}{\partial \boldsymbol{C}}\right) \tag{D.3}$$

such that now (D.1) reduces to

$$\begin{aligned}\bar{\mathbb{C}} = {} & \gamma_{11}\widetilde{\boldsymbol{M}}_1 \otimes \widetilde{\boldsymbol{M}}_1 + \gamma_{12}\widetilde{\boldsymbol{M}}_1 \otimes \left[2\lambda^{-1}\partial_{\boldsymbol{C}}\left(\lambda_2+\lambda_3\right)\right] \\ & + \gamma_{21}\left[2\lambda^{-1}\partial_{\boldsymbol{C}}\left(\lambda_2+\lambda_3\right)\right] \otimes \widetilde{\boldsymbol{M}}_1 + \gamma_{22}\left[2\lambda^{-1}\partial_{\boldsymbol{C}}\left(\lambda_2+\lambda_3\right)\right] \otimes \left[2\lambda^{-1}\partial_{\boldsymbol{C}}\left(\lambda_2+\lambda_3\right)\right] \\ & + 2\beta_1\partial_{\boldsymbol{C}}\widetilde{\boldsymbol{M}}_1 + 2\beta\Lambda^{-1}\partial^2_{\boldsymbol{C}\boldsymbol{C}}\left(\Lambda_2+\Lambda_3\right) - 2\beta\Lambda^{-2}\left(\partial_{\boldsymbol{C}}\lambda_2 \otimes \partial_{\boldsymbol{C}}\lambda_2 + \partial_{\boldsymbol{C}}\lambda_3 \otimes \partial_{\boldsymbol{C}}\lambda_3\right)\end{aligned} \tag{D.4}$$

With substitution of equations (C.24), (C.46) and (C.47), following some development the deviatoric component of the specific Lagrangian tangential modulus for double coalescence of eigenvalues becomes

$$\begin{aligned}\bar{\mathbb{C}} = {} & \gamma_{11}\widetilde{\boldsymbol{M}}_1 \otimes \widetilde{\boldsymbol{M}}_1 + \gamma_{22}\left(\boldsymbol{C}^{-1} - \widetilde{\boldsymbol{M}}_1\right) \otimes \left(\boldsymbol{C}^{-1} - \widetilde{\boldsymbol{M}}_1\right) \\ & + \gamma_{21}\left(\boldsymbol{C}^{-1} - \widetilde{\boldsymbol{M}}_1\right) \otimes \widetilde{\boldsymbol{M}}_1 + \gamma_{12}\widetilde{\boldsymbol{M}}_1 \otimes \left(\boldsymbol{C}^{-1} - \widetilde{\boldsymbol{M}}_1\right) \\ & - 2\beta\boldsymbol{I}^{\boldsymbol{C}^{-1}} + 2\left(\beta_1 - \beta\right)\partial_{\boldsymbol{C}}\widetilde{\boldsymbol{M}}_1\end{aligned} \tag{D.5}$$

This expression is now formulated invariant to the unknown eigenvalue bases and their respective unknown derivatives and so can be directly numerically implemented.

D.2 Expansion of $\bar{\mathbb{C}}$ for triple coalescence of eigenvalues

Expansion of the reduced form of expression (3.39), due to (3.46), enables definition of the deviatoric tangential modulus, invariant to the unknown principal stretch derivative. Expressing the differential terms in eigenvalue form as per (C.18), then

$$\begin{aligned}\bar{\mathbb{C}} = {} & \gamma_{11}\left(\Lambda_1^{-1}\frac{\partial \Lambda_1}{\partial \boldsymbol{C}}\right) \otimes \left(\Lambda_1^{-1}\frac{\partial \Lambda_1}{\partial \boldsymbol{C}}\right) + \gamma_{12}\left(\Lambda_1^{-1}\frac{\partial \Lambda_1}{\partial \boldsymbol{C}}\right) \otimes \left(\Lambda_2^{-1}\frac{\partial \Lambda_2}{\partial \boldsymbol{C}}\right) + \gamma_{13}\left(\Lambda_1^{-1}\frac{\partial \Lambda_1}{\partial \boldsymbol{C}}\right) \otimes \left(\Lambda_3^{-1}\frac{\partial \Lambda_3}{\partial \boldsymbol{C}}\right) \\ + {} & \gamma_{21}\left(\Lambda_2^{-1}\frac{\partial \Lambda_2}{\partial \boldsymbol{C}}\right) \otimes \left(\Lambda_1^{-1}\frac{\partial \Lambda_1}{\partial \boldsymbol{C}}\right) + \gamma_{22}\left(\Lambda_2^{-1}\frac{\partial \Lambda_2}{\partial \boldsymbol{C}}\right) \otimes \left(\Lambda_2^{-1}\frac{\partial \Lambda_2}{\partial \boldsymbol{C}}\right) + \gamma_{23}\left(\Lambda_2^{-1}\frac{\partial \Lambda_2}{\partial \boldsymbol{C}}\right) \otimes \left(\Lambda_3^{-1}\frac{\partial \Lambda_3}{\partial \boldsymbol{C}}\right) \\ + {} & \gamma_{31}\left(\Lambda_3^{-1}\frac{\partial \Lambda_3}{\partial \boldsymbol{C}}\right) \otimes \left(\Lambda_1^{-1}\frac{\partial \Lambda_1}{\partial \boldsymbol{C}}\right) + \gamma_{32}\left(\Lambda_3^{-1}\frac{\partial \Lambda_3}{\partial \boldsymbol{C}}\right) \otimes \left(\Lambda_2^{-1}\frac{\partial \Lambda_2}{\partial \boldsymbol{C}}\right) + \gamma_{33}\left(\Lambda_3^{-1}\frac{\partial \Lambda_3}{\partial \boldsymbol{C}}\right) \otimes \left(\Lambda_3^{-1}\frac{\partial \Lambda_3}{\partial \boldsymbol{C}}\right)\end{aligned} \tag{D.6}$$

Again exploiting the eigenvalue equality $\Lambda_1 = \Lambda_2 = \Lambda_3 = \Lambda$, from direct development of (3.38) it can be shown that

$$\gamma_{11} = \gamma_{22} = \gamma_{33} = \gamma - \tfrac{1}{3}\gamma, \qquad \gamma_{12} = \gamma_{13} = \gamma_{21} = \gamma_{23} = \gamma_{31} = \gamma_{32} = -\tfrac{1}{3}\gamma \tag{D.7}$$

where the scalar term, γ, is introduced for convenience. It follows that now

$$\begin{aligned}\bar{\mathbb{C}} = \gamma \left[\Lambda^{-2} \left(\partial_{\boldsymbol{C}}\Lambda_1 \otimes \partial_{\boldsymbol{C}}\Lambda_1 + \partial_{\boldsymbol{C}}\Lambda_2 \otimes \partial_{\boldsymbol{C}}\Lambda_2 + \partial_{\boldsymbol{C}}\Lambda_3 \otimes \partial_{\boldsymbol{C}}\Lambda_3\right)\right] \\ -\tfrac{1}{3}\gamma \left[\Lambda^{-2} \left(\partial_{\boldsymbol{C}}\Lambda_1 \otimes \partial_{\boldsymbol{C}}\Lambda_1 + \partial_{\boldsymbol{C}}\Lambda_1 \otimes \partial_{\boldsymbol{C}}\Lambda_2 + \partial_{\boldsymbol{C}}\Lambda_1 \otimes \partial_{\boldsymbol{C}}\Lambda_3\right.\right. \\ \partial_{\boldsymbol{C}}\Lambda_2 \otimes \partial_{\boldsymbol{C}}\Lambda_1 + \partial_{\boldsymbol{C}}\Lambda_2 \otimes \partial_{\boldsymbol{C}}\Lambda_2 + \partial_{\boldsymbol{C}}\Lambda_2 \otimes \partial_{\boldsymbol{C}}\Lambda_3 \\ \left.\left.\partial_{\boldsymbol{C}}\Lambda_3 \otimes \partial_{\boldsymbol{C}}\Lambda_1 + \partial_{\boldsymbol{C}}\Lambda_3 \otimes \partial_{\boldsymbol{C}}\Lambda_2 + \partial_{\boldsymbol{C}}\Lambda_3 \otimes \partial_{\boldsymbol{C}}\Lambda_3\right)\right]\end{aligned} \tag{D.8}$$

The term in the second round brackets can be factored to $\partial_{\boldsymbol{C}}\left(\Lambda_1 + \Lambda_2 + \Lambda_3\right) \otimes \partial_{\boldsymbol{C}}\left(\Lambda_1 + \Lambda_2 + \Lambda_3\right)$ so, with substitution of equations (C.21) and (C.53), the modulus term becomes

$$\bar{\mathbb{C}} = \gamma \left(\boldsymbol{I}^{\boldsymbol{C}^{-1}} - \tfrac{1}{3}\boldsymbol{C}^{-1} \otimes \boldsymbol{C}^{-1}\right) \tag{D.9}$$

which is again invariant to the unknown eigenvalue bases and their respective unknown derivatives as required.